

# Foundations of Visible Light Communication Circuits

Lih Chieh Png and Kiat Seng Yeo

February 28, 2016



# Preface



**Figure 1** At *The University of Manchester*, UK, 2002.



**Figure 2** Taken at Princes Mall while working at *Burton's*, Edinburgh, 2004.

In about 20 years' time, the success of IBM/Intel's optical processor will kickstart a revolution in the computer industry. If all the Pentium chips were to be replaced by optical chips, we should see an emergence of a whole new generation of optical I/O ports on the PC. Together, with the arrival of the age of LEDs, PCs can be connected to LED lamps to transmit information using these optical ports. Ethernet and USB are expected to transform in order to be compatible with visible light communication (VLC).

The potential for visible light communication is huge. Not far away from now, data communication would be available just at the touch of a switch. LEDs would take over as the primary light source in homes and offices, meaning that Internet, audio and video entertainment would be instant - that is, the moment you switch on the lights.

The primary motivation for this book is to introduce visible light communication to engineering students through practical circuits and simple applications.



**Figure 3** In a bookstore in Shanghai, 2013.

The second motivation is due to the fact that we find no other book in the world that teaches the practical construction of VLC circuits and systems. To curious researchers and project students, we hope you would find this book useful - one which would inspire you to develop your own ideas for next-generation wireless communications.

This e-book is a compilation of our papers for your convenience. I have thought of a good title for this book and changed it. The previous title of this book is *Visibilis Luminis Communicatione (Version 3)*.



**Figure 4** In Hefei, China, 2016.

Ethan LC Png

Nanyang Technological University, Singapore.

Singapore University of Technology and Design, Singapore.

*M. Sc. Computation (UMIST, UK), Adv. Dip. Computer and Communication Systems (Ngee Ann Polytechnic, SG), B. A. English Language and Literature (The Open University, UK), Dip. Mechanical Engineering (Singapore Polytechnic, SG)*

# Contents

Chapter 1 Simple Audio VLC Transceivers	1
1.1 Single 741 Design	1
1.2 Stereo Designs using 741 and 386	1
1.3 Pulse-Width Modulated Transceiver for Voice	1
1.4 Muxing and Demuxing of Audio Signals for VLC	1
Chapter 2 White-LED Transceiver Designs for Data Communications	15
2.1 Abstract	15
2.2 Introduction	15
2.3 Hardware Description	16
2.3.1 Prototype 1	16
2.3.2 Prototype 2	18
2.3.3 Prototype 3	18
2.3.4 Prototype 4	18
2.3.5 Prototype 5	18
2.4 LED and Photodiodes	19
2.5 Concentrators	20
2.6 Experimental Setup for Performance Test	20
2.7 Performance	20
2.8 Conclusion	21
Chapter 3 Designs of Audio VLC Transceiver Circuits on Commercial Airliners	33
3.1 Abstract	33
3.2 Introduction	33

3.3	OPA2134	34
3.4	LM833	35
3.5	LME49860	35
3.6	Tone Control	35
3.7	Photodiodes	35
3.8	Conclusion	36
<b>Chapter 4 Designs of VLC Mass-Storage Transceiver for SD-Card File Transfer</b>		41
4.1	Abstract	41
4.2	Introduction	41
4.3	Prototype 1: Circuit Description	42
4.3.1	Transmitter Operation: SD-Card Side	42
4.3.2	Receiver Operation: PC Side	43
4.4	Prototype 2: Circuit Description	43
4.5	Software Description	43
4.6	Performance	44
4.7	Reducing the Number of Components	44
4.8	12 MHz Design: White-LED Mass Storage Transceivers	44
4.9	Conclusion	45
<b>Chapter 5 Audio, Video, and Data VLC Transceiver Design for Smartphones and Tablets</b>		55
5.1	Abstract	55
5.2	Introduction	56
5.3	VLC Audio Circuit	57
5.3.1	VLC Audio Transmitter: Hardware Description	57
5.3.2	VLC Audio Receiver: Hardware Description	58
5.4	VLC Video Circuit	61
5.5	A Multimedia System: Integrating Video and Audio Signals	62
5.6	USB-Android Bridge to UART Interface	62
5.7	The VLC Transceiver	63
5.8	Conclusion	63
<b>Chapter 6 Early Tsunami Forecasting Using Deep-Sea Visible-Light LEDs</b>		71
6.1	Abstract	71
6.2	Introduction	71
6.3	Operational Theory: Beer's Law	72
6.4	Proposed Design of the Prototype	73

6.4.1	Receiver Circuit	73
6.5	Conclusion	73
Chapter 7	MIMO-Diversity Switching Techniques in Visible Light Communication	77
7.1	Abstract	77
7.2	Introduction	78
7.3	Concept Formulation	79
7.4	Method 1: A 4 by 4 MIMO-Diversity Auto-Switchable Transceiver	79
7.4.1	Transmitter Description: MIMO Scheme Circuitry	80
7.4.2	Transmitter Description: Diversity Scheme Circuitry	80
7.4.3	Receiver Description	80
7.4.4	Test Setup and Experiment	81
7.5	Method 2: MIMO-Diversity Software-Controlled COM Port Switching	81
7.5.1	Test Setup and Experiment	82
7.6	Analyses	83
7.7	Optics: Focusing Gap	84
7.8	Test Setup and Experiment	85
7.8.1	Range of the Focusing Gap	85
7.8.2	Received Power Measurement	86
7.9	Modification of the Channel Gain Equation	87
7.10	Conclusion	88
Chapter 8	Optical Infrastructure for VLC for Public Housing and Commercial Buildings	99
8.1	Abstract	99
8.2	Introduction	99
8.3	Spider-Web Metropolitan Area Network	100
8.4	Inter-Building and Intra-Building Wiring	103
8.5	WOPCOM in Operation	106
8.6	WOPCOM Devices	109
8.6.1	Optical Control Panel (OCP)	109
8.6.2	WOP Ceiling Transmitter	110
8.6.3	WOP Strip	110
8.7	Conclusion	112
Chapter 9	Designs of VLC LAN Transceivers	119

9.1 Choosing the LAN Connector	119
9.2 Transformer Circuit	120
9.3 Conclusion	121
Chapter 10 VLC Designs for Audio-Video Streaming, Ethernet Connectivity and Indoor Positioning	
10.1 Abstract	131
10.2 Introduction	131
10.3 Stereo Audio and Composite Video VLC Transmission Cir- cuits	133
10.4 10Mbps Ethernet VLC Circuit	133
10.5 16-Channel MIMO: VLC Transmitter Design	134
10.6 16-Channel MIMO: VLC Receiver Design	134
10.7 Receiver Integration with Notebooks and PCs	135
10.8 VLC UART Transceiver Shield	137
10.9 VLC IPS Android App	137
10.10 Conclusion	138
Chapter 11 Designs of VLC Video and Audio Transceivers for Desktop HDMI Applications	
11.1 How It Works	157
11.2 Room for Improvements	159
11.3 Conclusion	159
Chapter 12 VLC System Design for Position Detection	
12.1 Abstract	165
12.2 Introduction	165
12.3 Ultrasound and VLC: How It Works	167
12.4 Obtaining the Position for Indoor Environment	167
12.5 Transmitter Hardware	168
12.6 Arduino Codes for Transmitter	169
12.7 Receiver Hardware	170
12.8 Arduino Codes for Receiver	170
12.8.1 *.ino Codes for Arduino Uno	171
12.8.2 *.ino Codes for Arduino Mega	173
12.9 Simple Version	175
12.9.1 Codes	175
12.10 Difference between GPS and IPS	176
12.11 MATLAB	178

12.12Conclusion	181
Chapter 13Hybrids: Fusion of Visible Light and RF Channels	193
13.1 Abstract	193
13.2 Introduction	194
13.3 Visible Light Communication Channel	195
13.4 Radio Frequency Communication Channel	197
13.5 Parallel Gaussian Channel	198
13.6 Modeling Wireless Indoor Channel Condition	199
13.7 Total Received Power	200
13.8 Simulation and Analyses	201
13.9 Comparison between Indoor and Outdoor RF Channels	204
13.10Conclusion	204
Chapter 14Fusion of VLC and Plasmonics for Clinical Diagnostics	209
14.1 Abstract	209
14.2 Introduction	209
14.3 Surface Plasmon Resonance and DVD	210
14.3.1 SPR DVD-R - How It Works	211
14.4 DVD-R Experiment on the Lab Spectrometer	213
14.5 Portable POC Device Design	215
14.5.1 Calculation of Absorbance	216
14.6 Conclusion	217



# **Chapter 1**

## **Simple Audio VLC Transceivers**

To begin, I would like you to try out these basic circuits by yourself or with your classmates. Audio signals are low in frequency (20 Hz to 21 kHz). This allows you to understand the workings of optical transmitters and receivers easier. For this chapter I will not be explaining and describing the circuits. It is good for you to try out and discover things by yourself.

### **1.1 SINGLE 741 DESIGN**

### **1.2 STEREO DESIGNS USING 741 AND 386**

### **1.3 PULSE-WIDTH MODULATED TRANSCEIVER FOR VOICE**

### **1.4 MUXING AND DEMUXING OF AUDIO SIGNALS FOR VLC**

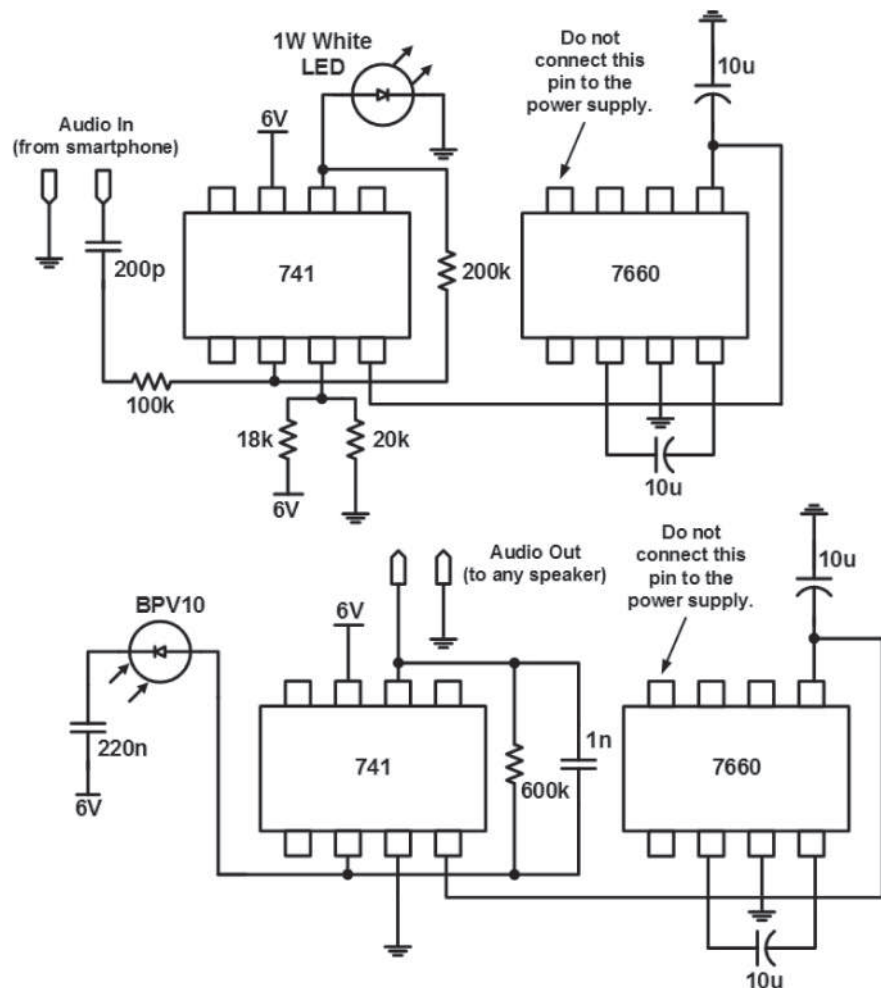


**Figure 1.1** The ICL7660 is optional if you are running on a tight budget. It is just to isolate the ground for noise reduction.

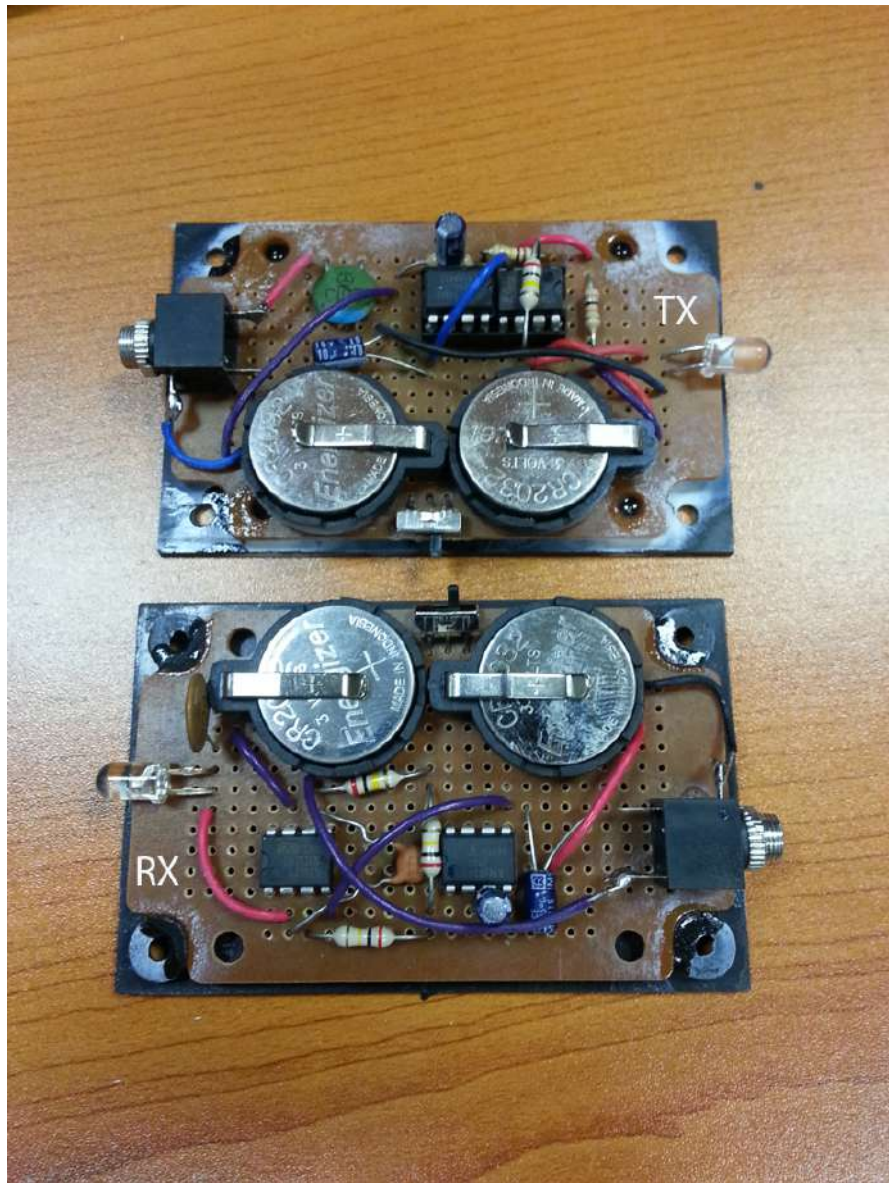


**Figure 1.2** Prototype picture.

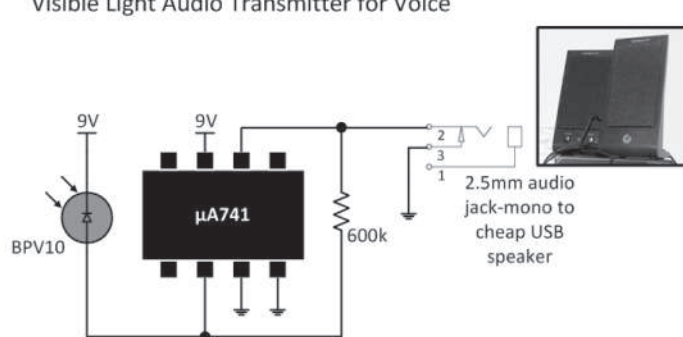
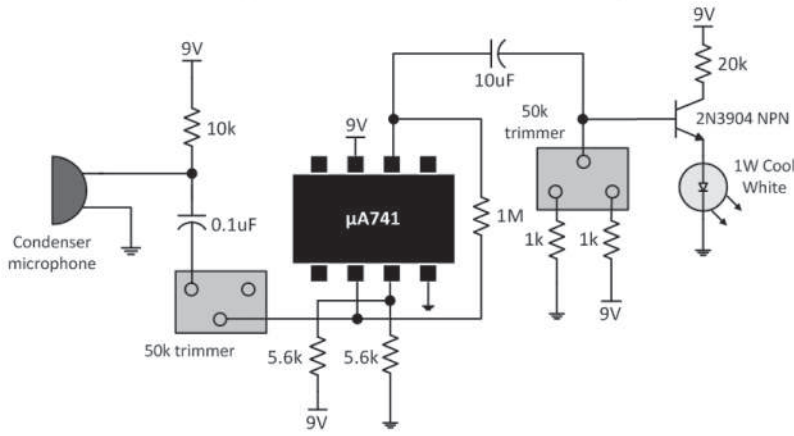
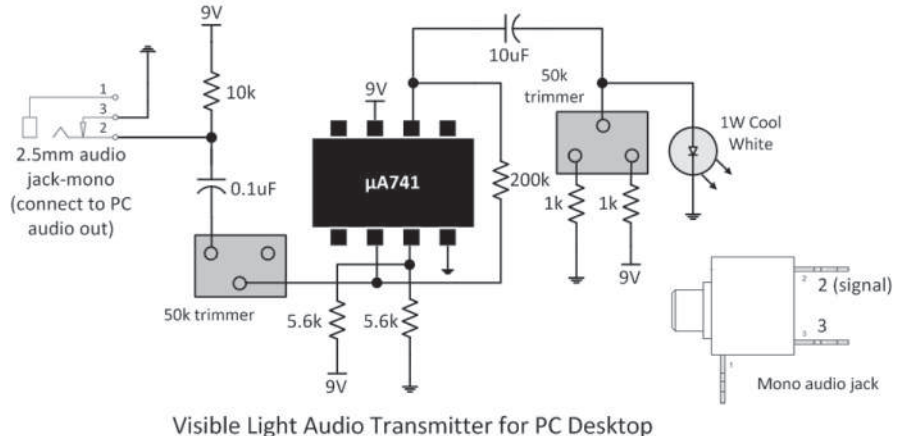


**Figure 1.3** Observe the differences between circuits for music and voice.

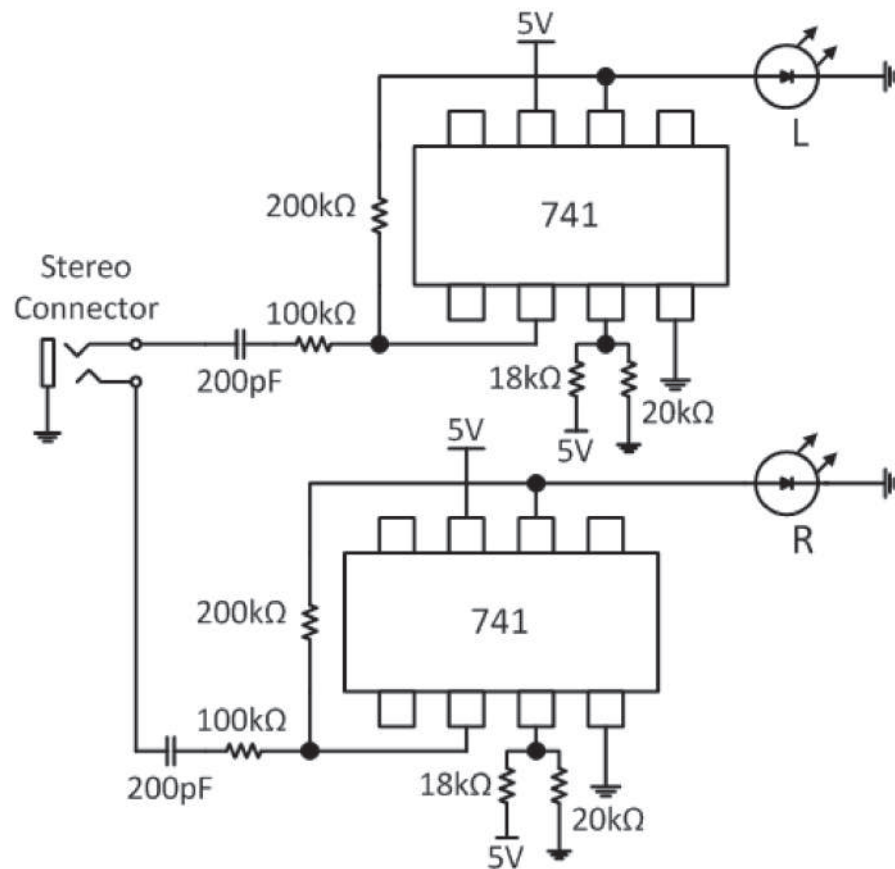


Figure 1.4 VLC stereo transmitter.

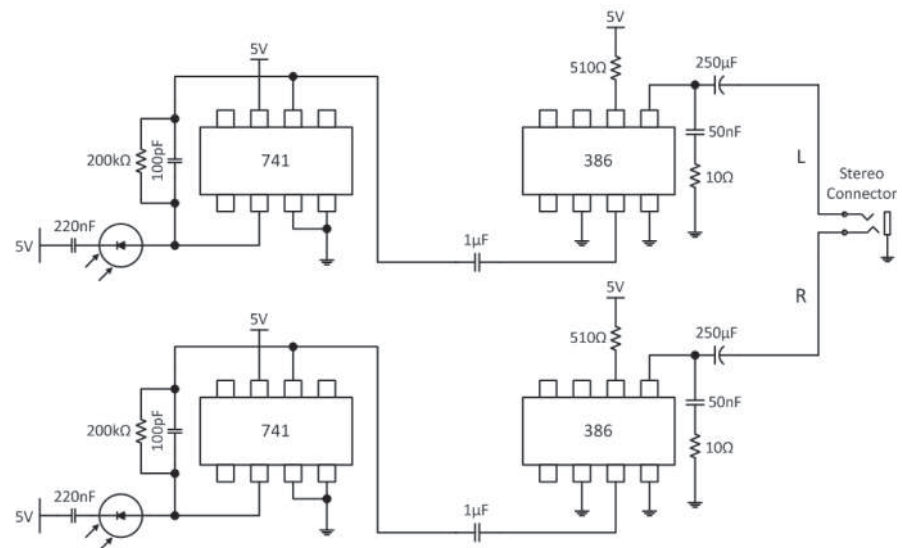


Figure 1.5 VLC stereo receiver.

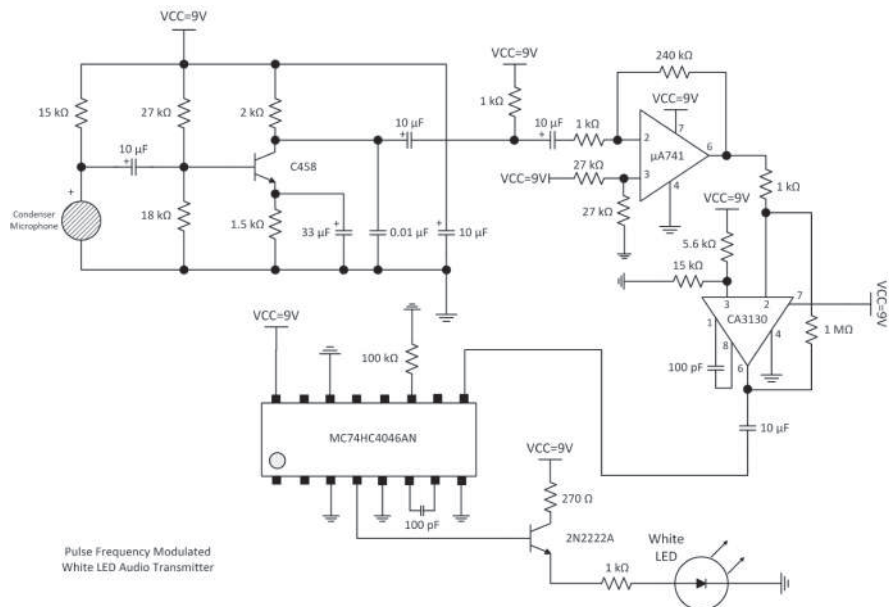


Figure 1.6 PWM VLC audio transmitter circuit.

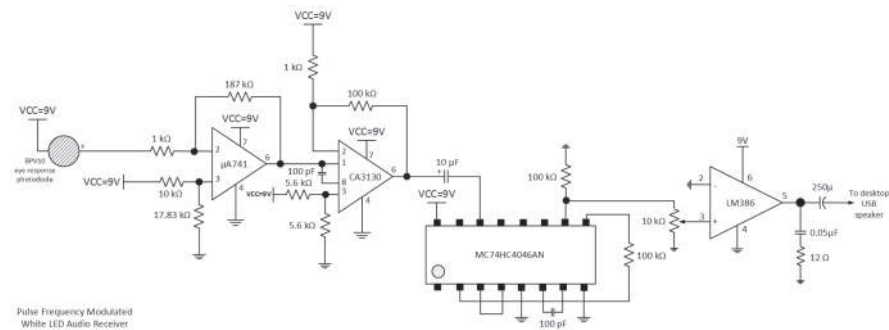
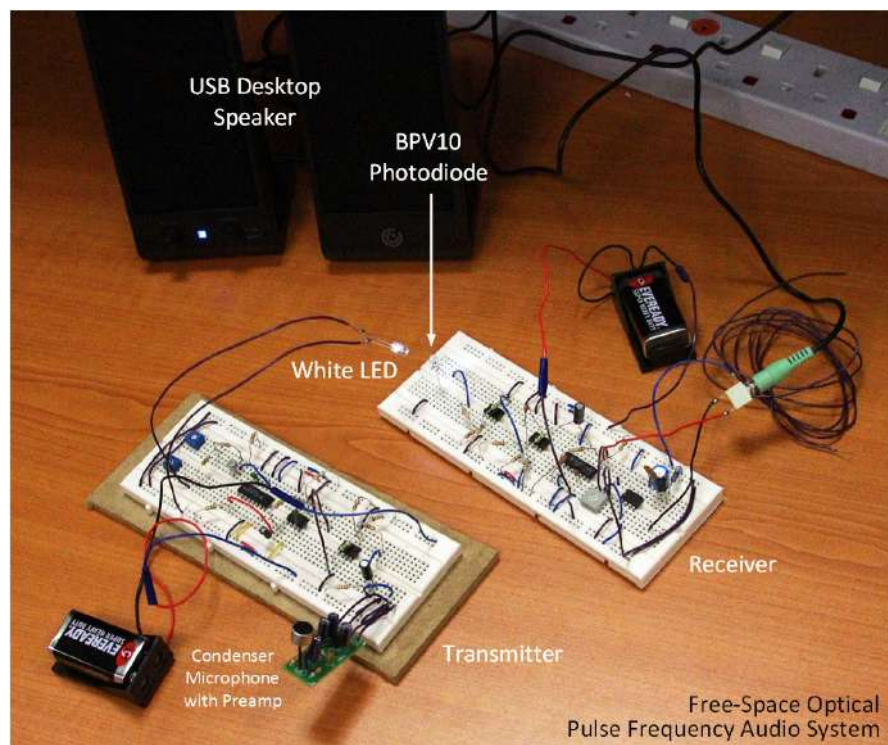
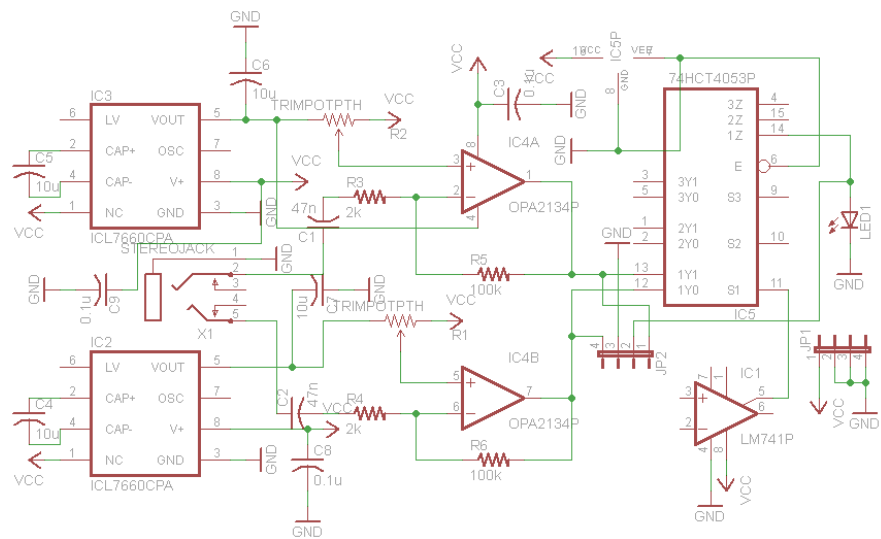


Figure 1.7 PWM VLC audio receiver circuit.



**Figure 1.8** Photo: PWM VLC audio TX and RX circuits.



**Figure 1.9** Schematic: stereo audio transmitter with multiplexing.

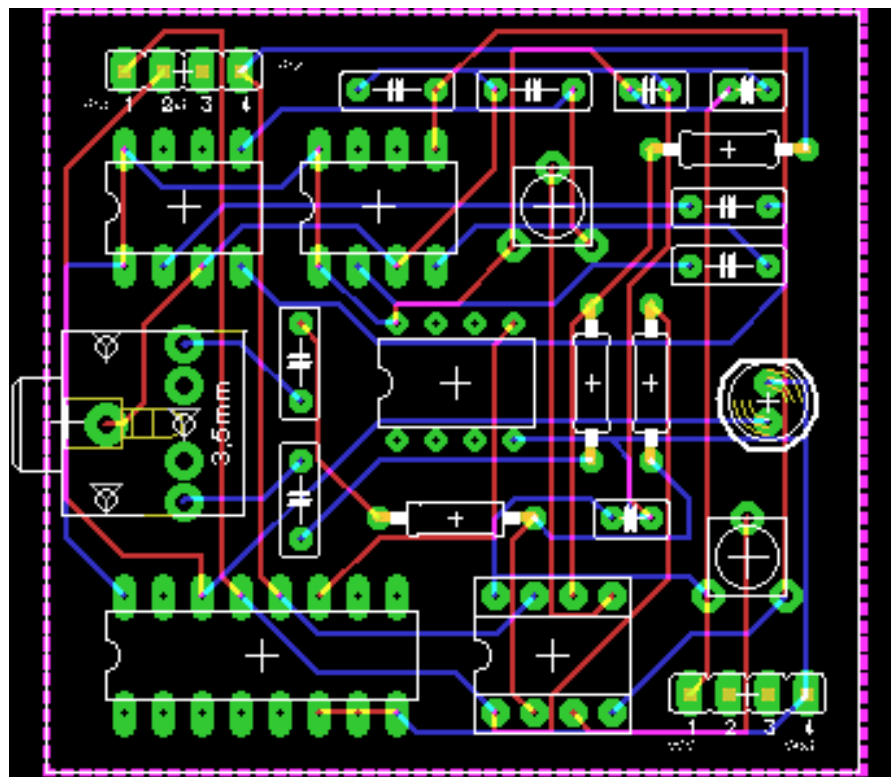


**Figure 1.10** Board layout: stereo audio transmitter with multiplexing.

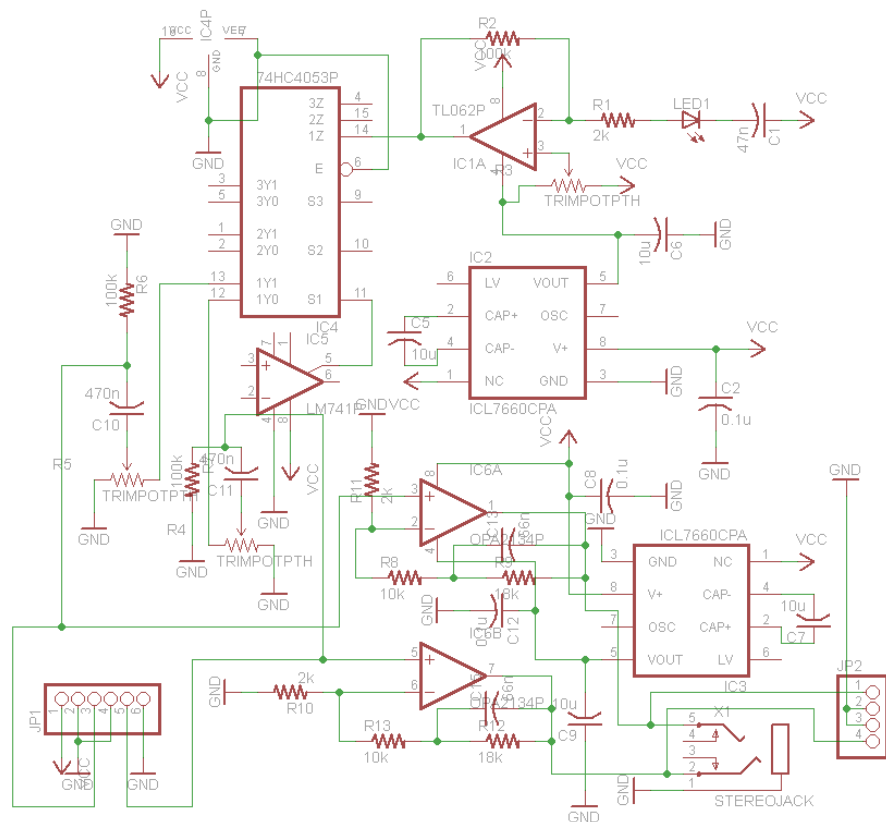


**Figure 1.11** Schematic: stereo audio receiver with demultiplexing.

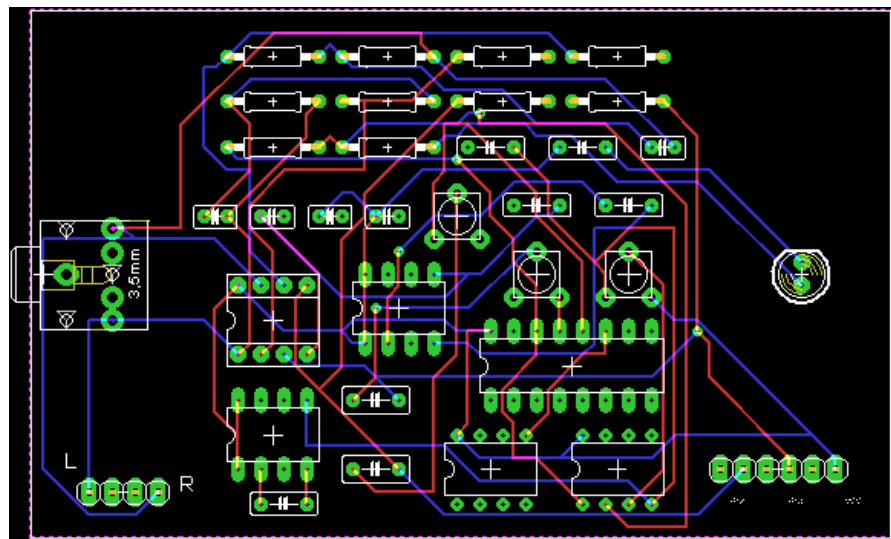


**Figure 1.12** Board layout: stereo audio receiver with demultiplexing.

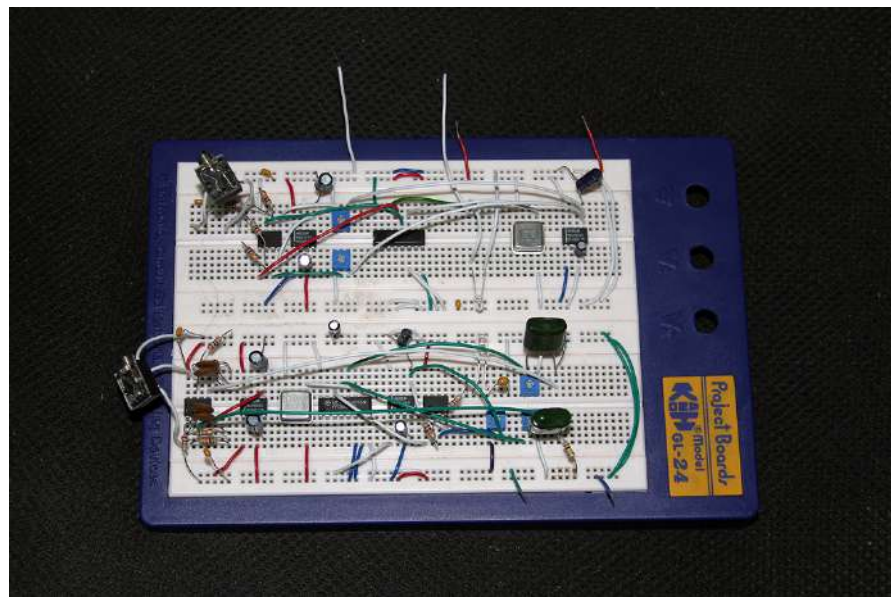


**Figure 1.13** Breadboard testbed.

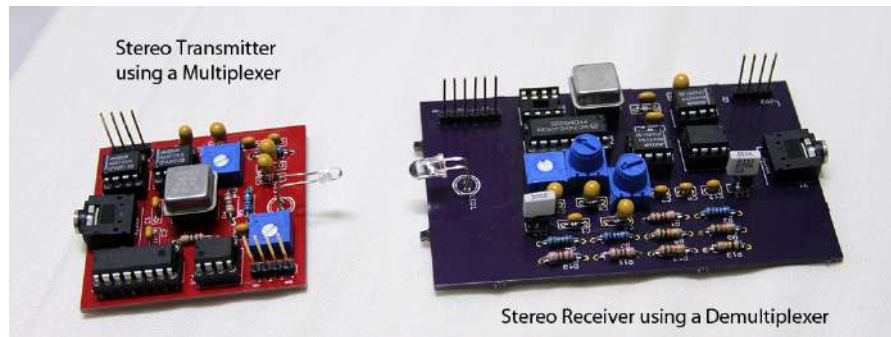


**Figure 1.14** Full consumer product pcb.



# **Chapter 2**

## **White-LED Transceiver Designs for Data Communications**

### **2.1 ABSTRACT**

Wireless optical communication using visible light is one of the emerging green technologies that has not been fully utilized. Many versions of white-LED transceivers have been built, but mainly due to the high cost of good photodiodes and the existing popularity of fluorescent lamps, visible-light communication (VLC) only receives luke-warm attention to date. In this paper, we introduce five low-cost and efficient transceiver circuit designs that can be constructed using on-the-market components. They can be applied in moderate-speed data communications such as smart phones and tablets for ad-hoc transmission of photos and files. The potentials for these designs are wide if we are able to scale down the circuits to tiny PCBs or manufacture them at IC level.

### **2.2 INTRODUCTION**

LED is a very green technology. Since very little heat is produced, it can reduce interior temperatures by 1 to 2 degrees, thus lowering air-conditioning costs and  $CO_2$  emissions. LED lighting is also much safer for the living and working environment because it is mercury free and does not produce IR or UV rays which can be harmful to human eyes and skin [1].

White LED communication uses light in the visible spectrum as the carrier medium. The functional duality of LEDs - both as a light source and a communication medium - creates many new and interesting applications [2]-[19] based on the fast-switching characteristic of LEDs and the ability to modulate lightwave for free-space communications. In this kind of technology, it is possible to achieve high-speed data transmission for high data loads with low implementation complexity. Also, lightwave cannot penetrate walls, thus making it easy to secure transmissions against casual eavesdropping. Furthermore, unlike radio frequencies, the visible-light spectrum does not need licensing.

Given the strengths of LEDs [10]: long lifetime, high tolerance to humidity, small size, and low power consumption, a white-LED communication system is therefore potentially feasible for indoor wireless networks. VLC is somewhere between Bluetooth and WLAN, but in the near future, it will replace these two technologies if the transceiver circuit can be fabricated with LED and photodiode together on a single chip. We should expect a sudden burst of popularity in white-LED communication in the next generation of personal computers after IBM and Intel have successfully fabricated and tested their new optical core processors. Optical I/O ports would most probably replace our LAN and USB interfaces. These ports would be able to connect to ceiling lights, wall lights, or desk lamps via a repeating adaptor.

In the following section, five types of transceiver circuit prototypes are introduced. The design principle in this work is based on cost cutting, simplicity, and the most common electronic components on the market. The intended application is serial peer-to-peer, ad-hoc communication. The schematic in Fig. 2.1 is the simplest serial data transceiver one can build.

## 2.3 HARDWARE DESCRIPTION

### 2.3.1 Prototype 1

The components of Prototype 1 (Fig. 2.3) consist mainly of a microcontroller, a repeater, and a USB-RS232 converter. The transmitter consists of the microcontroller PIC12F508, which is used for the modulation of the TX signal from the  $\mu$ USB-MB5 (USB-RS232 converter). When the TX pin transits from logic low to logic high, the 12F508 generates a 40 kHz carrier. During low periods, the carrier is suppressed. After the modulation of the signal, the output of the microcontroller is passed to an NPN darlington transistor to drive the white LEDs.

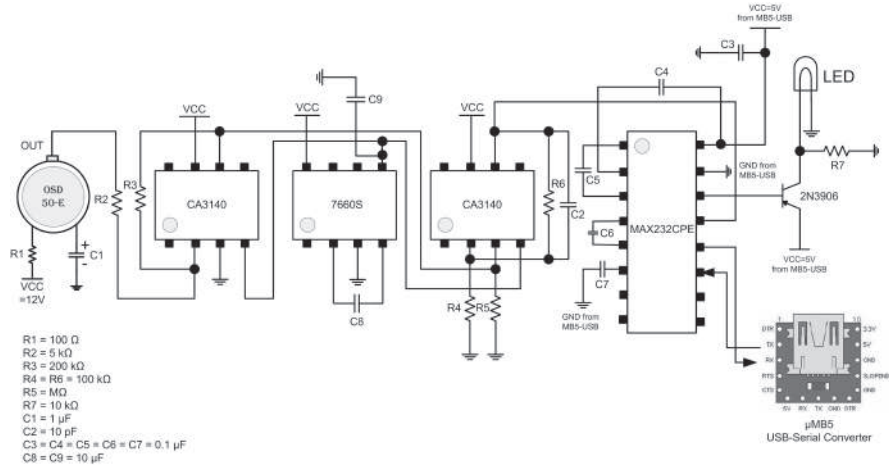


**Figure 2.1** The simplest VLC serial circuit.

The repeater receives white-light signals using the BS520 eye-response photodiode and retransmits them at a higher power. Signals received by the BS520 is usually weak and easily affected by ambient light. The repeater circuit is used to shape and boost the received signal from the photodiode before passing it to the IR transmitter. The other use of the repeater is to fine-tune the signal to the correct frequency so that it can be readily accepted by the IR receiver. The path between the IR transmitter and the IR receiver must be enclosed to ensure that the receiver does not receive reflected signals from the transmitter. Alternatively, an optoisolator IC (e.g. 4N25) can also be used in place of the IR transmitter and receiver.

After the IR receiver receives signals from the repeater and demodulates them, the demodulated signals are sent to the RX pin of the  $\mu$ USB-MB5, which then passes the converted signals back to the computer. The  $\mu$ USB-MB5 RS232-to-USB converter is one of the more expensive items in the transceiver (USD\$58), but there should be less expensive serial converters out there in the market.

The design of Prototype 1 is based on the established IR technology by creating a hybrid combination (Fig. 2.4) of IR and visible-light devices. The components are cheap and widely available.

### 2.3.2 Prototype 2

In Prototype 2 (Fig. 2.5), a PIC12F508 microcontroller is used to generate a 40 kHz clock which is passed to the one-shot IC DM74121N. The TX signal from the  $\mu$ USB-MB5 is then pulse-position modulated (PPM) by the one-shot device 74121 before being transmitted out through the LEDs.

The receiver consists of a Centronic OSD50-E eye-response photodiode, a preamplifier KA2181, a phase-locked loop MM74HC4046N, and an inverter 74LS04. Light signals received by the photodiode is preamplified and shaped by the preamplifier before being demodulated by the phase-locked loop. For the KA2181 circuit, the user must find its optimal inductor value which determines the receiver's sensitivity.

### 2.3.3 Prototype 3

Prototype 3 (Fig. 2.6) has no modulation and demodulation scheme, thus it is able to transmit and receive at a higher baud rate. The circuit consists of two operational amplifiers CA3140E. The first functions as a preamplifier and buffer, while the second functions as a comparator as well as a low-pass filter. CA3140E is a BiMOS operational amplifier with MOSFET input and bipolar output. It has a good speed performance up to 4.5 Mhz.

The D flip-flop accepts data and clock signals (from the resonant oscillator circuit) to generate state-triggered signals for transmission. Without the clock oscillator, there will be no continuous light. The MAX232CPE IC is used to convert signal levels between RS232 and TTL.

### 2.3.4 Prototype 4

The design of Prototype 4 (Fig. 2.8) is a little different from that of Prototype 3. Here, we multiplex the clock and data with an AND gate 74LS08 and demultiplex the received signal with a negative edge-triggered JK flip-flop 74LS112. Prototype 3 does not transmit the carrier.

### 2.3.5 Prototype 5

Prototype 5 (Fig. 2.9) is a PPM transceiver. Its transmitter modulates by triggering on the negative and positive transitions of the data signal and then *OR*ing them together. The receiver demodulates by passing the signal through a JK flip-flop.

This circuit configuration has a wide data range from 2400 bps to 115200 bps in speed. The attraction for this circuit is that no clock oscillator is used. The pulse width can be adjusted by altering the value of the capacitor of the 74121 one-shot IC. As the values get smaller, the pulse width gets narrower. For instance, placing a 39pF capacitor would enable data to be transmitted at 115200 bps.

## 2.4 LED AND PHOTODIODES

For the convenience of our experiment and calculations, only one LED is used as the transmitter in the tests of the five prototypes. The LED used is the CREE 5mm cool-white through-hole, with luminous intensity 32900 mcd, viewing angle  $15^\circ$ ,  $I_F=25\text{mA}$ , and  $V_F=3.2\text{V}$ . Eye-response and PIN photodiodes can be used in all the circuits. We tried with a PIN photodiode (Vishay's BPV10) and two eye-response photodiodes (Sharp's BS520 and Centronic's OSD50-E) and all of them performed very well. The function of eye-response photodiodes is to isolate any other frequencies outside the visible range. Their spectral sensitivity peaks at around 520nm. Since the receiver should only detect white light, eye-response photodiodes are found to be more suitable than the PIN photodiode BPV10 (whose spectral sensitivity peaks at 900nm). One should keep in mind that the common white LED is a single-chip device. It actually gives off blue light which reacts with the phosphor to give out the white glow. Hence, for these prototypes, any photodiode peaking around the blue region (520nm) will be suitable. The drawbacks of using eye-response photodiodes are that you would not be able to achieve high frequency, and also, signals will be more prone to ambient-light interference (or noise). The BPV10 is found to be the best choice for high data-rate transmission, although it is not as sensitive to white light as the OSD50-E and BS520. It also has a small active area which requires a bit of time to focus with a concentrator. Their specifications are listed in Table 2.1.

**Table 2.1**  
Comparison of Eye-Response Photodiodes

Type	Active Area ( $\text{mm}^2$ )	Responsivity	Cost (USD)
BS520	18	$10 \text{ nA/Lux}$	5.47
OSD50-E	50	$28 \text{ nA/Lux}$	96
BPV10	0.78	$0.55 \text{ A/W}$	0.57

All the photodiodes can be used in all the prototypes. OSD50-E is more sensitive due to its larger active area, thus it can be used when the transmitter has to be further away from the receiver. The drawback of this photodiode is that it is quite expensive (US\$96) compared to the BS520 (US\$5.47). BS520 has a smaller active area and is less sensitive. The BPV10 costs US\$0.57.

## 2.5 CONCENTRATORS

For the distance of 2m, the LED and the photodiode requires a concentrator (or magnifying glass). At the transmitter, a magnifying factor (MF)  $\times 10$  concentrator is used to magnify the LED light for propagation over air; concentrators with an MF between  $\times 4.5$  to  $\times 6$  can be used at the receiver to focus light onto the photodiode. The concentrators can be found easily at marketplaces. They are basically magnifying lenses old folks use for reading newspapers.

## 2.6 EXPERIMENTAL SETUP FOR PERFORMANCE TEST

The setup of the experiment is described in Fig. 2.12. A pair of LED transmitter stands are cross-linked and connected to their respective transceivers. Each desktop is connected to a transceiver by a USB cable. The height between the transmitter and the receiver is standardized at 2m for all the five prototypes. Windows XP's built-in HyperTerminal is used to transfer a 100 KB picture file from one PC to another. A freeware serial data tracer is used to trace the bytes transmitted and received. Working data rates are determined by text transmission to ensure that the characters received using each baud rate are 100% correct over a sample of 960 letter 'e's. After that, file transfer is tested at these best baud rates. When the HyperTerminal shows no bad packets, no halts, and instant handshake, the best baud rate for file transfer is determined.

## 2.7 PERFORMANCE

In our serial communication test, Prototype 1 and 2 achieved a working baud rate of 9600 bps. Both Prototype 1 and 2 use PPM modulation and demodulation scheme. They cannot go beyond 9600 bps due to the limitation of their IR receivers. Prototype 3 is able to operate up to 230400 bps for text transfer and 115200 bps for file transfer because of two reasons: firstly, it has a bit of delay due to the D

flip-flop; secondly, it uses the operational amplifier CA3140 which is able to handle frequencies up to 4.5 MHz. For text transfer, Prototype 3 performs well at 115200 and 230400 bps. For Prototype 4, the working baud rates are 2400 to 57600 bps. We found that it is easier to synchronize with the transmitter than Prototype 3. On the other hand, the advantage of Prototype 3 is that it is more stable and is less affected by external fluctuations. The intensity of the LED at the transmitter of Prototype 5 is slightly weaker. Table 2.2 shows a list of the prototypes with their corresponding operating data rates. From overall observation, Prototype 3 and 4 are the best circuits.

**Table 2.2**  
Performance Evaluation of the Prototypes

Prototype	Operational Baud Rate (Text)	Best Baud Rate (File Transfer)
1	1200-9600 bps	9600 bps
2	1200-9600 bps	9600 bps
3	115200-230400 bps	115200 bps
4	2400-57600 bps	57600 bps

Table 2.3 to Table 2.6 compare error rates across different baud rates in detail.

## 2.8 CONCLUSION

In this paper, we have seen that efficient optical transceivers do not have to be expensive. For these prototypes, we go for moderate speeds, since high-speed development comes with a cost. The ease of synchronization and the robustness of light propagation and reception are critical areas to take note. The availability of components, cost, and the ease to build a usable device are also just as important. Prototype 1 is the cheapest to build, followed by Prototype 3 and 4, and then Prototype 2. In terms of complexity, Prototype 2 is the most complex to build. Prototype 1 is a hybrid construction between IR and white LED. It performs better than Prototype 2. Prototype 3 shows the best performance without any form of modulation. It also shows that simplicity is the key to circuit development for free-space optical transceivers. The next best circuit is Prototype 4. Prototype 1 and 4 do not need a very specific line-of-sight to synchronize with the transmitting LED. This is due to the multiplexing of their clocks and data. Prototype 5 leaves

**Table 2.3**

Prototype 3: Baud Rates vs. Error Rates (A)

Baud Rate (bps)	9600	19200	38400	57600
No. of Samples	960	960	960	960
No. of Errors	960	960	947	73
Error Rate (%)	100	100	98.6	7.60

**Table 2.4**

Prototype 3: Baud Rates vs. Error Rates (B)

Baud Rate (bps)	115200	230400	460800	921600
No. of Samples	960	960	960	960
No. of Errors	0	0	159	960
Error Rate (%)	0	0	16.60	100

**Table 2.5**

Prototype 4: Baud Rates vs. Error Rates (A)

Baud Rate (bps)	9600	19200	38400	57600
No. of Samples	960	960	960	960
No. of Errors	2	0	0	0
Error Rate (%)	0.2	0	0	0

**Table 2.6**

Prototype 4: Baud Rates vs. Error Rates (B)

Baud Rate (bps)	115200	230400	460800	921600
No. of Samples	960	960	960	960
No. of Errors	11	163	960	960
Error Rate (%)	1.15	17	100	100

plenty of room for high-speed development if an interface other than RS232 is used.

Further improvements could be made to these 5 prototypes by replacing the slower components by faster ones; however, they come at a higher cost.

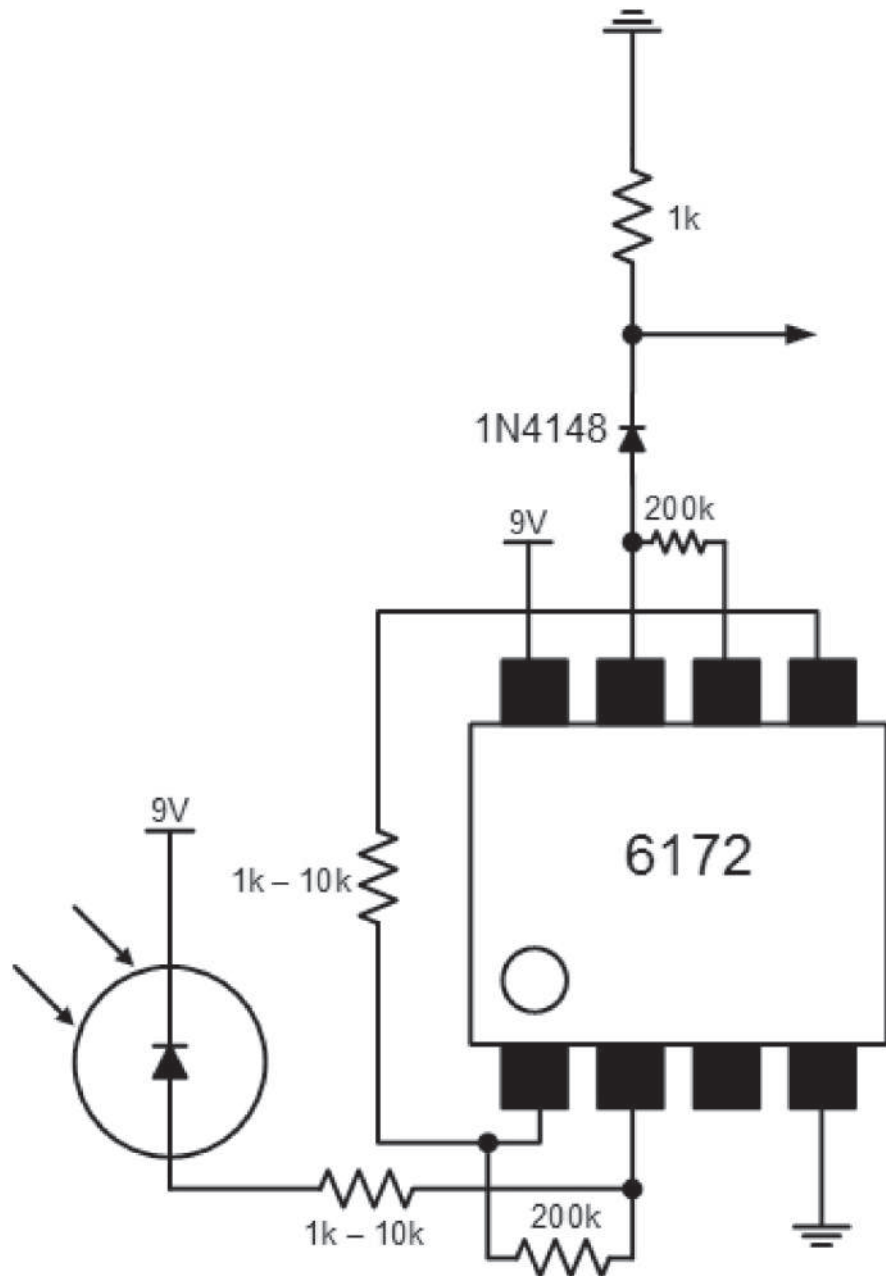


**Figure 2.2** You can also use the LM6172 dual amplifier IC to reduce board size.

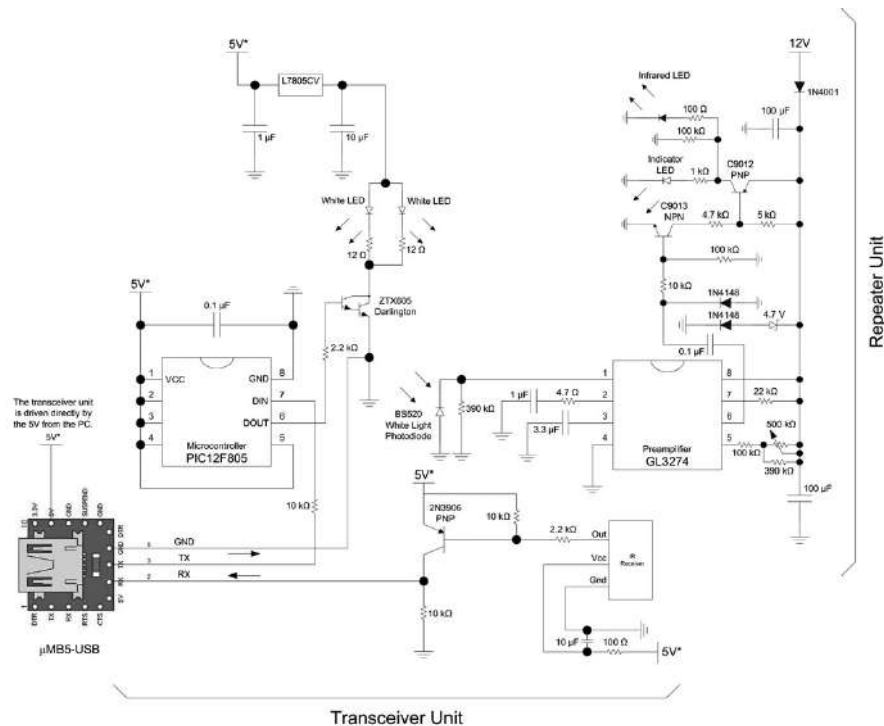


**Figure 2.3** Prototype 1 circuit.

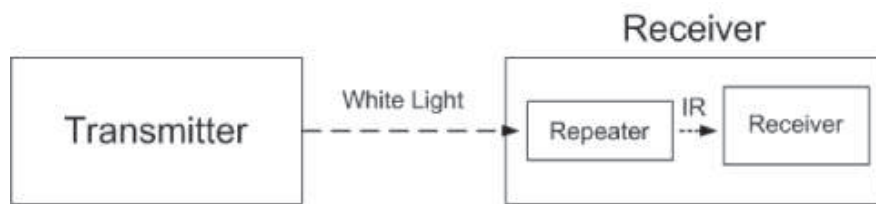


**Figure 2.4** Functional diagram for Prototype 1.

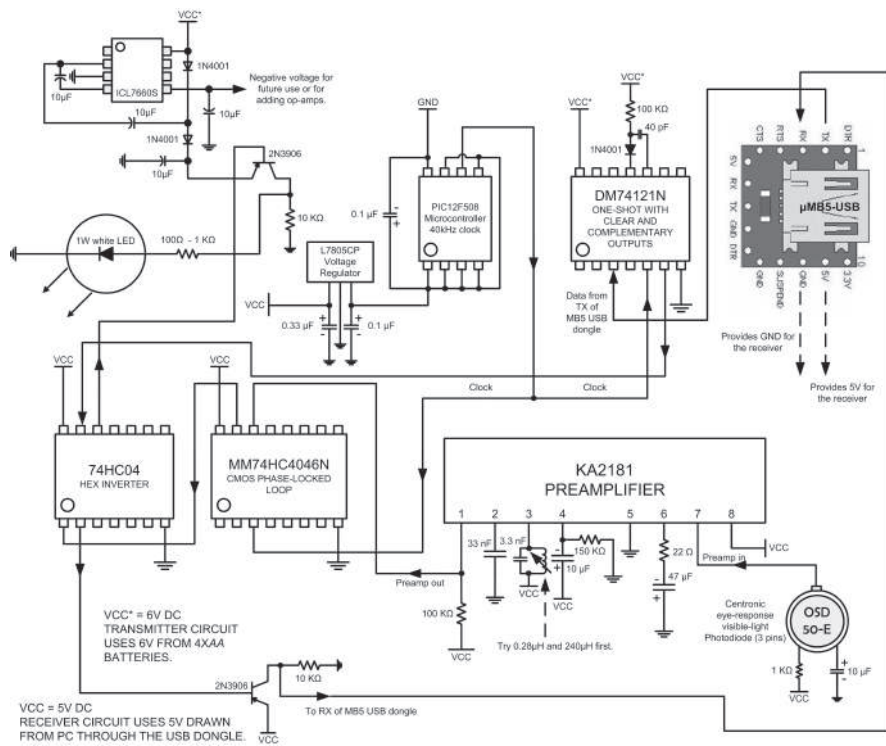


Figure 2.5 Prototype 2 circuit.

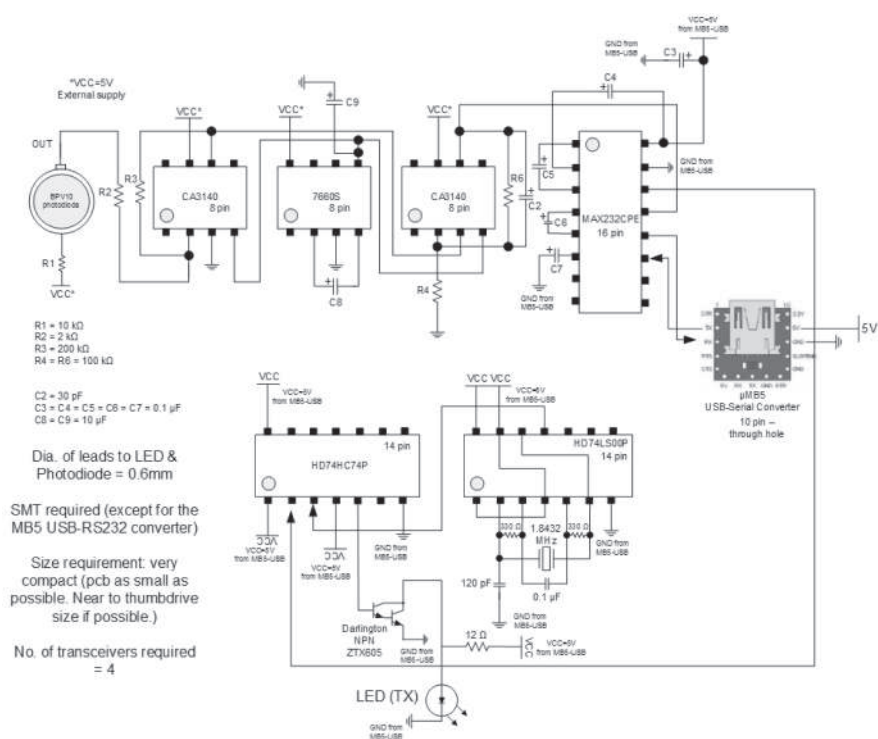
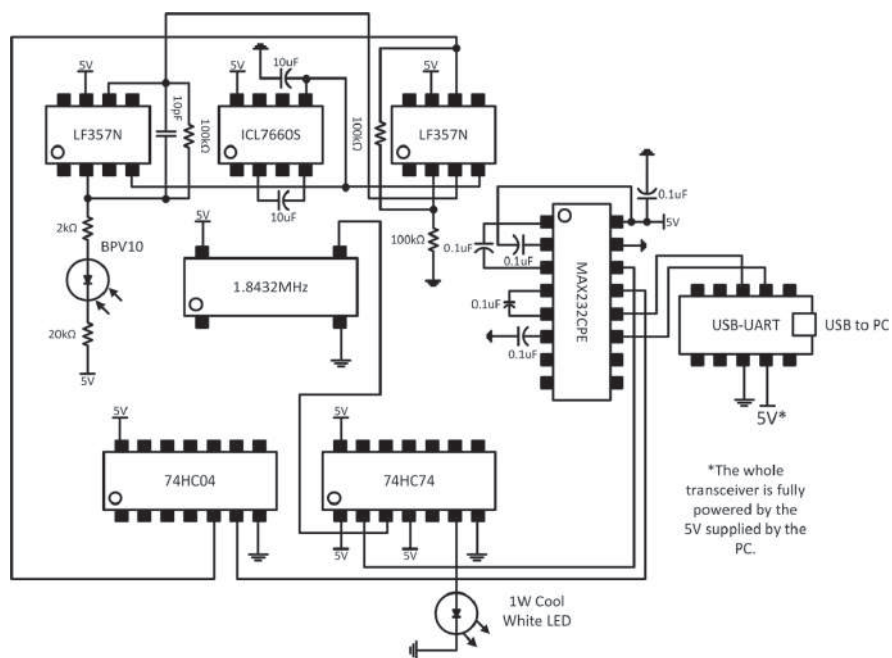


Figure 2.6 Prototype 3 circuit.



**Figure 2.7** Low-power Prototype 3 circuit. You can just use the 5V from the MB5 dongle to power the whole transceiver.

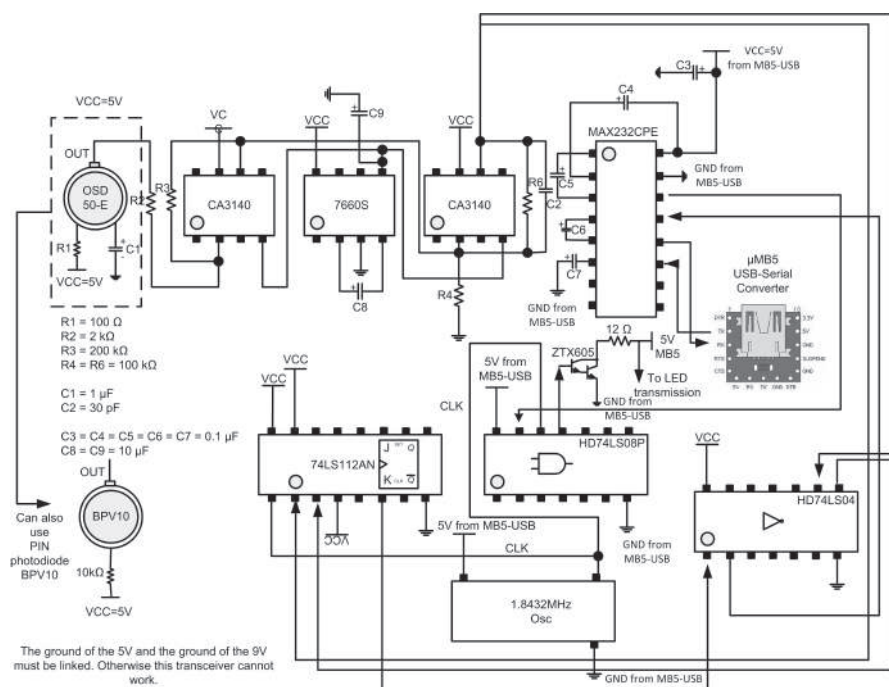
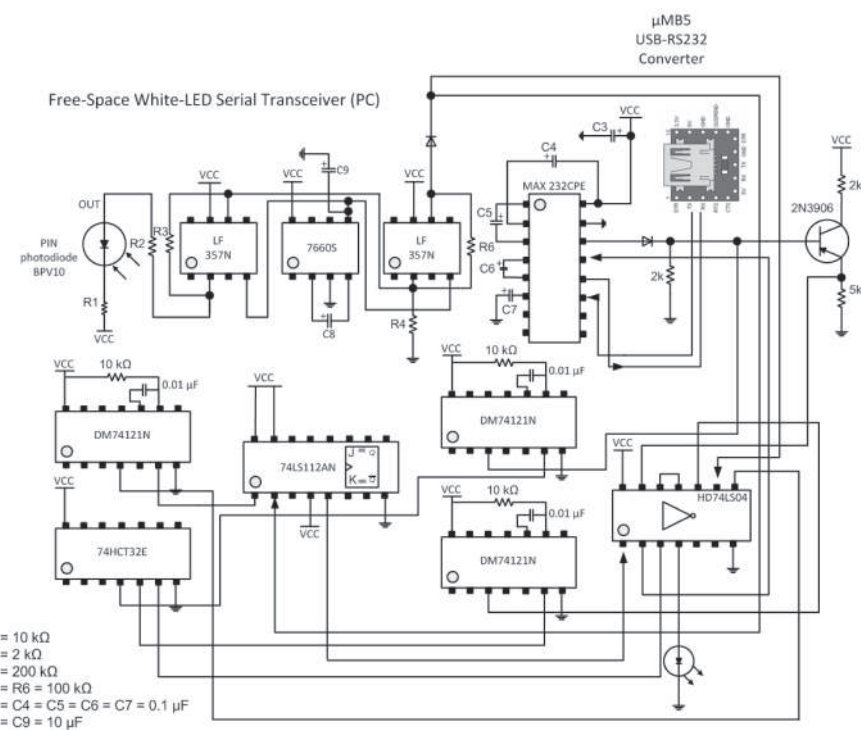
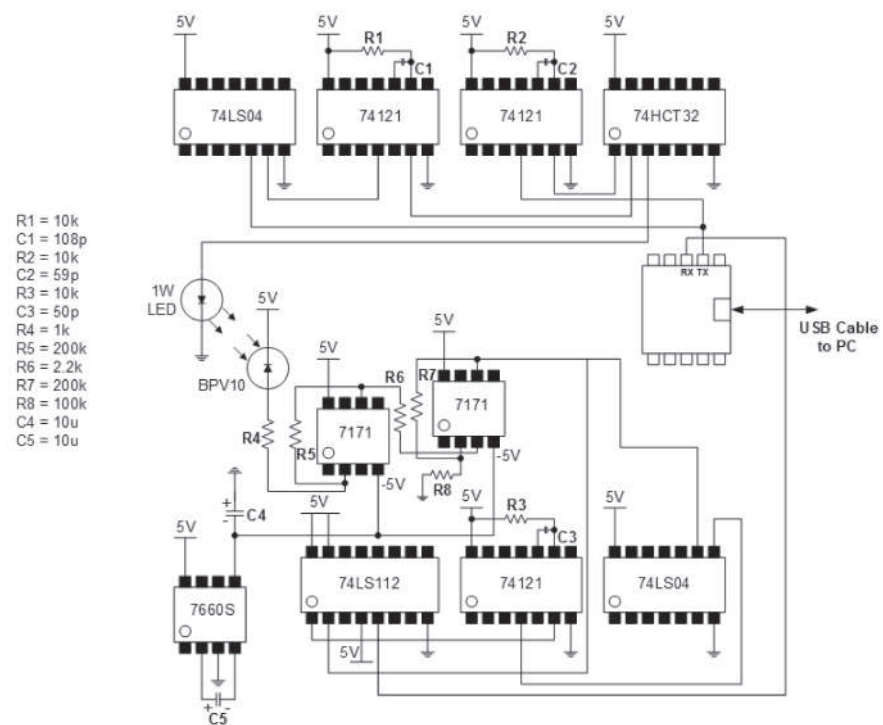


Figure 2.8 Prototype 4 circuit.



**Figure 2.9** Prototype 5 circuit.



**Figure 2.10** Prototype 5 circuit using LM7171 (high speed, high current).



**Figure 2.11** Photos of some of the circuits.

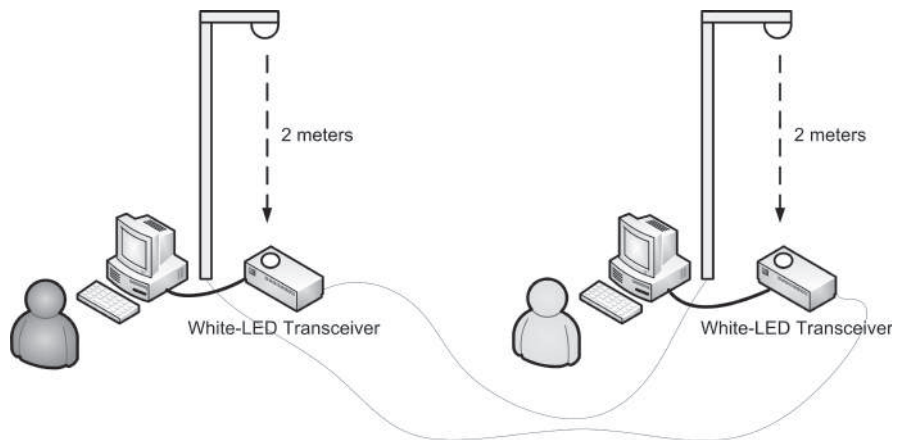


**Figure 2.12** Test setup.

# **Chapter 3**

## **Designs of Audio VLC Transceiver Circuits on Commercial Airliners**

### **3.1 ABSTRACT**

Based on visible light communication (VLC) technology, three designs of audio transmitters and receivers have been built and tested successfully. The simplicity of these circuits and the very few components that are used enable them to be mass manufactured for use on passenger aircrafts. The receiver circuits can be implemented on headphones. The transmitter circuits can be integrated with LED reading lights above passengers' seats. The circuits presented here have different performance characteristics and sound quality, depending on the type of audio ICs that are used.

### **3.2 INTRODUCTION**

In [11][12], the authors conducted experiments and investigated the LED transmission of visible light for data communication on a passenger plane. However, there is lack of literature reviews on actual VLC audio circuits for headphone applications and audio IC tests. For example, we found no study of such audio transmitter and receiver circuits that can be implemented readily on an aircraft or space shuttle.

Therefore, we started this project by reviewing the cross-section of the *Airbus A380* passenger plane cabin [13] to find out the distance between the reading lights and the passenger's head (Fig. 3.1). We are able to estimate that this distance

is between 570mm and 740mm. The reading lights are high-brightness, bulbless, warm-white LEDs that have about 150 degrees of movement in the X and Y axes.

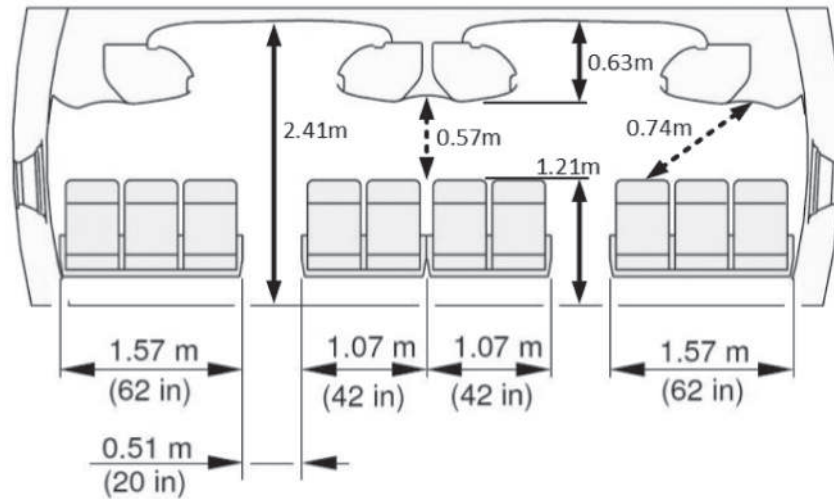


**Figure 3.1** Cross-sectional dimensions of the economy passenger cabin of an *Airbus 380* [13].

In the sections below, three sets of circuits are presented. Shown in Fig. 3.2, each transmitter is built to work with a 25mA LED with a concentrator. Each receiver can be integrated with a headphone like the prototype shown in Fig. 3.2. For the convenience of readers, we present all the circuits in the simplest form. For stereo designs, these circuits can be duplicated to send the L channel and R channel at the same time. All the ICs are high performance audio chips. All the circuits are powered using 5V DC.

### 3.3 OPA2134

Having a slew rate of  $(20V/\mu s)$ , OPA2134 is used for its wide output swing to within 1V of the rails. This circuit (Fig. 3.3) produces clear and distinctive sounds. It has the loudest volume compared to the other two circuits. TL072 is used as a preamplifier because it has a suitable slew rate ( $13V/\mu s$ ) for amplifying audio

signals in the form of light. TL062 has a lower slew rate of only  $3.5V/\mu s$ . This is suitable for use as a transmitter since we want to avoid amplifying noises.

### **3.4 LM833**

This circuit (Fig. 3.4 left) produces a good rich bass. LM833 shows no deadband crossover distortion and has a slew rate of  $7V/\mu s$ . However, it needs more power and gain to achieve the same volume as that of the OPA2134 circuit.

### **3.5 LME49860**

The LME49860 circuit (Fig. 3.4 right) gives the best sound quality amongst all. It has the same slew rate as OPA2134; however, it has a gain bandwidth product of 55MHz, which is much higher than OPA2134's 8MHz. The circuit generates a bass effect that is not as heavy as that of the LM833 circuit but is not as weak as that of the OPA2134 circuit.

### **3.6 TONE CONTROL**

Tone characteristics for all the three circuits can be adjusted using the configuration in Fig. 3.5. The reader should take note that there are different manufacturers for the negative voltage converter 7660S. More than half of these 7660S on the market would produce an audible high frequency whining sound even if you tie Pin 1 to HIGH. The trick is to try out different types and different brands. In this work, we use 7660S-CPA and MAX1044 since they are available in our labs and we found that they do not 'whine'.

### **3.7 PHOTODIODES**

For simple audio prototypes like this, you can find a lot of photodiodes on the market that can be used. Low frequency photodiodes are usually very cheap. I have provided a list of photodiodes here. The specs to look for in a photodiode is its wavelength range. The ideal one for visible light communication should have a spectral responsivity of 0.55 A/W or more between 450 nm and 650 nm. These are called the short-wavelength type. You should also take note of the gain and the size

of the active area, but they are not that important. Try to choose a photodiode that best fits your application and is within your consumer's affordability.

1. Vishay  
BPV10 (250MHz)

Spectral response range: 450 nm to 1050 nm. Peak sensitivity: 920 nm.

2. Sharp  
BS520 (below 500KHz)

Spectral response range: 400 nm to 700 nm. Peak sensitivity: 560 nm.

Normally, I prefer to use the BPV10 in all my circuits. The reason is that its peak sensitivity is 920 nm, which is well away from the middle of the visible spectrum (i.e. blue-to-green 490 nm-550 nm). This will cut down on the sensitivity of the reception. Noise will increase with increased sensitivity. Of course, if you want your prototype to be very sensitive to white-light signals, photodiodes with peak sensitivity close to the blue spectrum wavelength are the best choices. You may construct active or passive filters to control the noise later. In addition, you may like to use a blue filter over the photodiode to improve the received signal. White LEDs are primarily blue LEDs, except that they have been coated with a layer of phosphor. I believe many of you must have wondered what the yellow substance on the inside of the LED is. That is phosphor. I shall introduce more advanced photodiodes later.

### 3.8 CONCLUSION

Audio circuits should be the first step into the development of wireless airline entertainment systems. Wireless optical communication using visible light has the largest potential because they can be integrated easily into existing devices on the plane and do not interfere with the aircraft's control systems. The 3 sets of basic VLC audio circuits demonstrate the maturity of modern day audio technology that can revolutionize our travels in the skies.

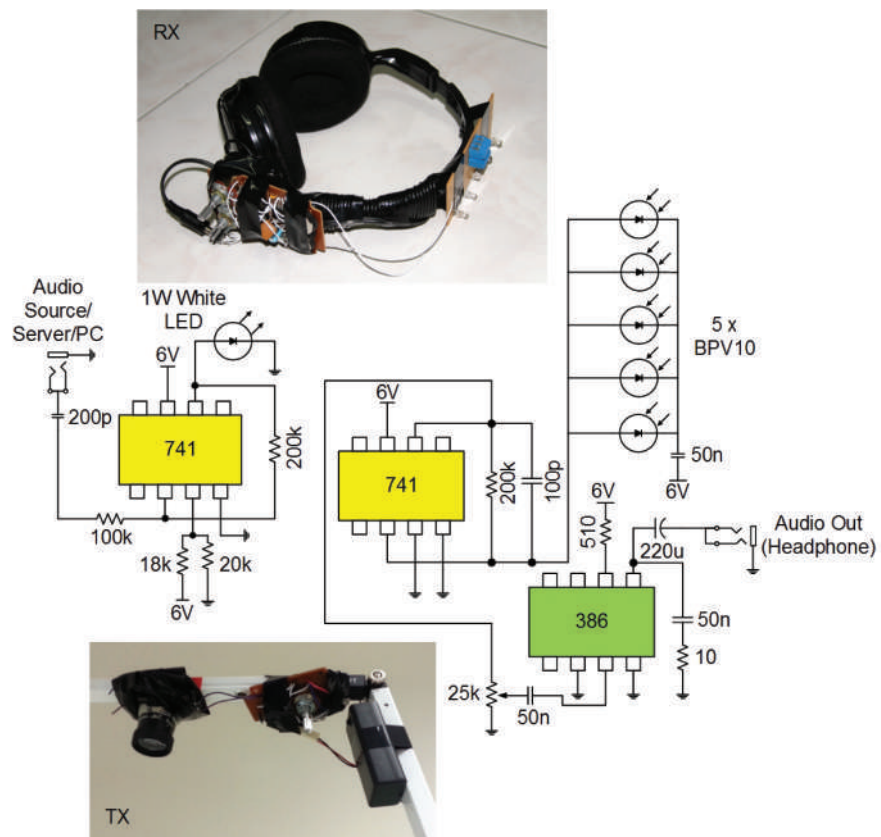


**Figure 3.2** Basic circuit and constructed prototype for airline entertainment VLC audio transmission system.

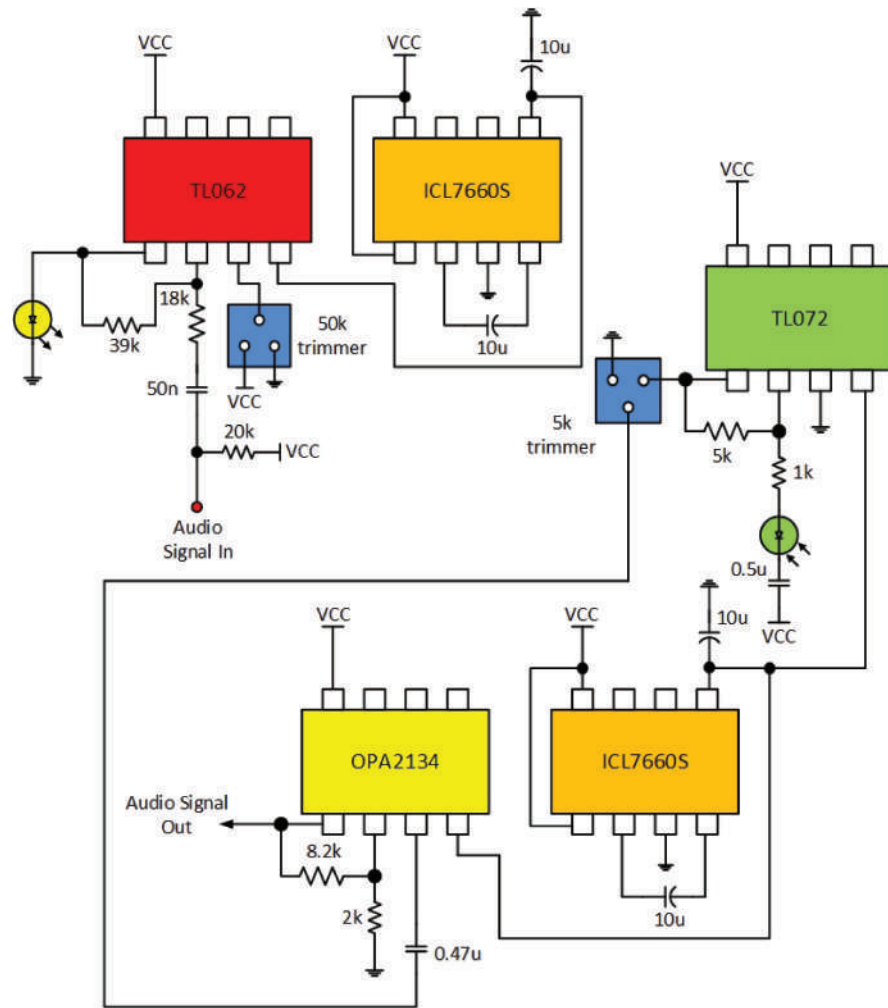


**Figure 3.3** OPA2134 VLC audio transmitter and receiver circuit.

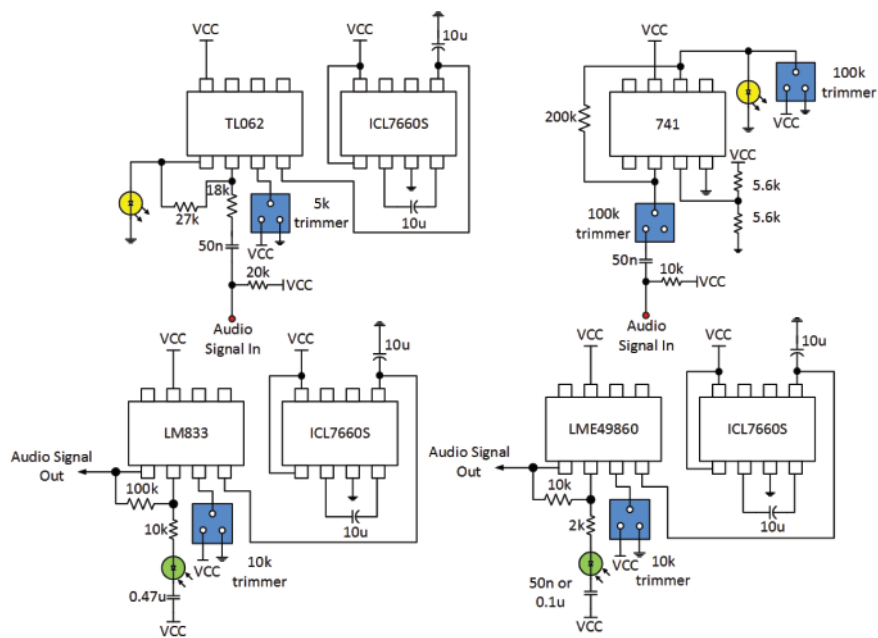


**Figure 3.4** Left: LM833 VLC audio transmitter and receiver circuit. Right: LME49860 VLC audio transmitter and receiver circuit.

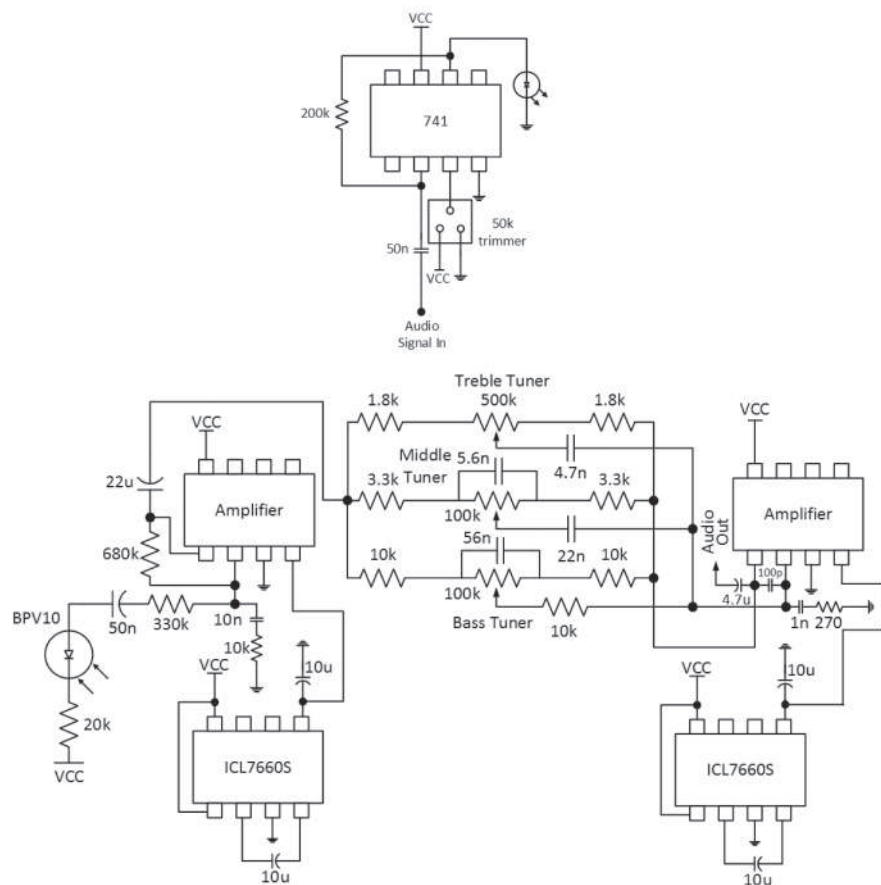


**Figure 3.5** Receiver with tone controls for tuning bass, middle, and treble frequencies.

# **Chapter 4**

## **Designs of VLC Mass-Storage Transceiver for SD-Card File Transfer**

### **4.1 ABSTRACT**

Two visible-light mass-storage prototypes have been constructed. They enable file transfers between the SD (Secure Digital) memory card and the PC via white-LED light. The entire system consists of a pair of identical white-LED transceivers: one is connected to the PC, whereas the other is connected to the SD-card subcircuit. File transfer operation is able to execute at 19200 bps. Prototype 1 is based on pulse-position modulation (PPM), while Prototype 2 is based on pulse-width modulation (PWM). It was found that the PPM design consumes less power and is more stable. Full-speed (12 Mbps) USB 2.0 VLC transceiver designs for slave and host devices are also included.

### **4.2 INTRODUCTION**

The concept of the VLC mass-storage transceiver has potential in applications such as optical thumbdrives, cameras, smart phones, and even tablets. One can argue that IRDA is also able to do the same thing. However, VLC technology has two main advantages over infrared: it is able to integrate with LED lighting and is less hazardous to health and eyes. We should expect a sudden burst of popularity in white-LED file access in the next generation of personal computers after IBM [14] and Intel [15] have successfully fabricated and tested their new optical core

processors. Future PCs would probably have optical I/O ports which could connect to LED ceiling lights, wall lights, or desk lamps.

Visible-light communication (VLC) enables convenient wireless access of information by the use of light in the visible spectrum. In the future, VLC technology will be used not just for Ethernet access [16][17], but also for ad-hoc file transfers. Currently, there is no literature involving the investigation of VLC devices for SD-card file transfers. Therefore, the authors of this paper made an attempt to construct a simple pulse-position modulation (PPM) transceiver prototype whose design can be applied to mass-storage access. Along the way during experiments, a PWM version was constructed for cross verification. The PPM technique does not require varying the amplitude and pulse width, thus the transmitter power can be kept constant.

A VLC SD-card file access system based on FAT32 (*File Allocation Table 32 bits*) [18] has been built and successfully tested. The authors also investigated and designed a 12 MHz version based on the USB 2.0 mass storage class specifications.

### 4.3 PROTOTYPE 1: CIRCUIT DESCRIPTION

#### 4.3.1 Transmitter Operation: SD-Card Side

With reference to Fig. 4.1, the top portion is the SD-card circuit. The ATMEGA32 microcontroller is responsible for the conversion between SPI (SD card) and RS232 (LED) signals. SPI (or *Serial Peripheral Interface*) operates by 3 wires (TX, CLK, RX) using a master-slave protocol. Since SPI has an extra CLK line, a microcontroller is needed to convert it to the EIA-232 standard (i.e. two lines). From PIN 15 of the microcontroller, the signal from the SD card enters the MAX232N (PIN 11) to be level shifted and outputs from PIN 14. From PIN 14, the signal splits into two - one going directly to a one-shot IC (DM74121N) while the other going through an NPN BJT (2N3906) to be inverted first before entering a one-shot IC. In this way, we are able to obtain a positive-edge triggered signal and a negative-edge triggered signal. Finally both signals enter the OR gate IC (74HC32) to be logically ORed (Fig. 4.2). This process is PPM modulation. The ORed signal is then emitted by the white LED. The user may insert a  $500\ \Omega$  -  $1\ k\Omega$  variable resistor to control the current supplied to the LED.

#### 4.3.2 Receiver Operation: PC Side

With reference to Fig. 4.3, the PIN photodiode receives light signals from the air and converts it to current. The first op-amp LF357N acts as a preamplifier that converts this current to voltage. As the signal is converted to voltage, the op-amp also amplifies it. The second op-amp is a comparator whose responsibility is to trim or level-shift the signal voltage. The output from the second op-amp splits into two paths: one goes directly to a 74LS112A JK flip-flop (K pin) while the other goes to a one-shot IC after getting inverted in the inverter 74LS04. The output from the one-shot is passed to the CLK pin of the JK flip-flop. The output from PIN 5 of the JK flip-flop is the PPM demodulated signal. The original data signal is recovered after the demodulated signal passes through an inverter. This signal then goes into the MAX232 IC to be level shifted and enters the MB5-USB converter to be converted back into USB signals. The USB signals are finally passed to the PC.

### 4.4 PROTOTYPE 2: CIRCUIT DESCRIPTION

In Prototype 2, the design of the transceiver was changed to a PWM design. The transceiver circuit at the PC side consists of a simple transmitter and receiver that work on a 1.8432 MHz clock carrier. In the transmitter, USB signals from the PC flow to the  $\mu$ MB5 USB-Serial Converter to be converted to an RS232 signal. The signal is then multiplexed in the AND gate 74LS08 with the clock carrier before sending to the LED for transmission. The output waveform of the 74LS08 can be found in Fig. 4.4. In the receiver, the signal received by the PIN photodiode BPV10 is amplified by the first CA3140 op-amp and subsequently trimmed by the second CA3140 which acts as a comparator. Next, the signal is passed to the 74S112AN J-K flip-flop to separate the data from the multiplexed signal. The demultiplexed signal is then inverted in the 74LS04 inverter. Finally, the inverted signal enters the MAX232 to be converted to a TTL signal which is sent to the PC by the  $\mu$ MB5. Fig. 4.5 and 4.6 show the schematics of the PWM transceivers.

### 4.5 SOFTWARE DESCRIPTION

AVR Studio 4 was used to develop the program for the microcontroller. After compiling, the *hex* file was programmed into the ATMEGA32 using the *PonyProg* (a serial device programmer software).

#### 4.6 PERFORMANCE

The test for Prototype 1 was set up as in Fig. 4.7. A supply voltage of between 6.4V and 6.6V can be used for the whole SD-card circuit (including the transceiver). The PC-side transceiver is powered by the  $\mu$ MB5 USB-RS232 converter. A distance of about 1 cm between the LED and the photodiode is suitable for good transmission. For distances farther than 3 cm, concentrators need to be used.

In Prototype 2, the SD-card side uses a supply voltage of between 6.9V and 7.0V. The PC-side transceiver uses separate power supplies for the transmitter and the receiver: 5V from the  $\mu$ MB5 USB-RS232 converter for the transmitter and 5V from an external DC supply for the receiver. This is due the use of the CA3140 op-amp which is better but needs a higher current than the LF357.

Microsoft XP's *HyperTerminal* was used as the interface platform to display and execute the command menu. For both prototypes, files with sizes less than 1 GB were successfully 'read' and 'written' at the speed of 19200 bps. The transceiver system is unable to perform beyond this speed due to the conflict between the RS232 baud rate and the microcontroller clock rate. Internally, it defaults itself back to 19200 bps.

#### 4.7 REDUCING THE NUMBER OF COMPONENTS

The authors minimize the size of the transceiver circuit by cutting down the number of components. This simplification removes modulation and demodulation, but still synchronizes the data with the clock using a D flip-flop 74HC74. The schematic design in Fig. 4.8 provides stable transmission and reception of signals; however, its shortcoming is that it is more sensitive towards alignment than the two aforementioned prototypes.

#### 4.8 12 MHZ DESIGN: WHITE-LED MASS STORAGE TRANSCEIVERS

For higher data rates, SPI technology is usually used because the RS232 level shifter has its limits. Normally, a USB transceiver and a USB controller are needed. Gone were the days when one would find them in separate units. They are now integrated in a single chip. Fig. 4.9 shows the architectures of two full-speed VLC transceivers suitable for host and slave implementations. RS232 interface has been changed to USB 2.0 protocol hardware. The PPM design in Prototype 1 uses only a resistor and

a capacitor to trigger a ‘shot’ (74121). No clock is required. In this design, the SPI clock is used to trigger a ‘shot’. Hence, a product developer may use a phase-locked loop (e.g., TLC2932) to detect the clock at the receiver (*see shaded block*).

The MAX3420E is a USB 2.0 peripheral controller that comes with a built-in full-speed USB transceiver. It can be used for storage access on cameras, mobile phones, tablets, and other customized USB devices. The MAX3421E can be used as a peripheral or a host controller. It gives the front end VLC system the freedom to access any microprocessor, ASIC (application-specific integrated circuit), or DSP (digital signal processing) when it operates as a USB host.

The FT232H is a single-channel USB 2.0 to UART/SPI/FIFO IC. In this work, it converts USB signals conveniently to SPI signals. The ST72681 provides NAND flash interface for mass-storage implementation.

Many types of preamplifiers can be used to amplify the optical signals received by the photodiode. The authors recommend the LM7171 (200 Mhz, 4100  $V/\mu s$ ), LMH6672 (90 Mhz, 135  $V/\mu s$ ), LM6172 (100 Mhz, 3000  $V/\mu s$ ), LM6181 (100 Mhz, 2000  $V/\mu s$ ), and LMH6723 (370 Mhz, 600  $V/\mu s$ ), depending on user requirements.

This design caters only to USB 2.0 full-speed (12 MHz) communication. The authors will not elaborate on this section as it is not the main focus of this paper.

#### 4.9 CONCLUSION

Both PPM and PWM prototypes of the VLC SD-card transceiver have been successfully built and tested. They can operate at the baud rate of 19200 bps and below. The transceiver design for Prototype 1 is based on one-shot triggers to generate PPM signals of equal pulse width on positive and negative edges. Prototype 2 is based on the ANDing of the clock and the data signals, thereby producing PWM modulation. Compared to Prototype 2, Prototype 1 consumes less power and is more stable. Further improvement can be made on better microcontrollers or FPGAs. The applications of these two designs will be dependent on the power source and the target devices. A PWM transceiver may take up more power, but such a design can be integrated more easily in present light control systems as most current control drivers for LED lights are PWM based. On the other hand, a PPM transceiver is ideal for use in low-power communication devices. Two designs for the USB 2.0 standard that are operable at full speed (for slave and host devices) have also been proposed.

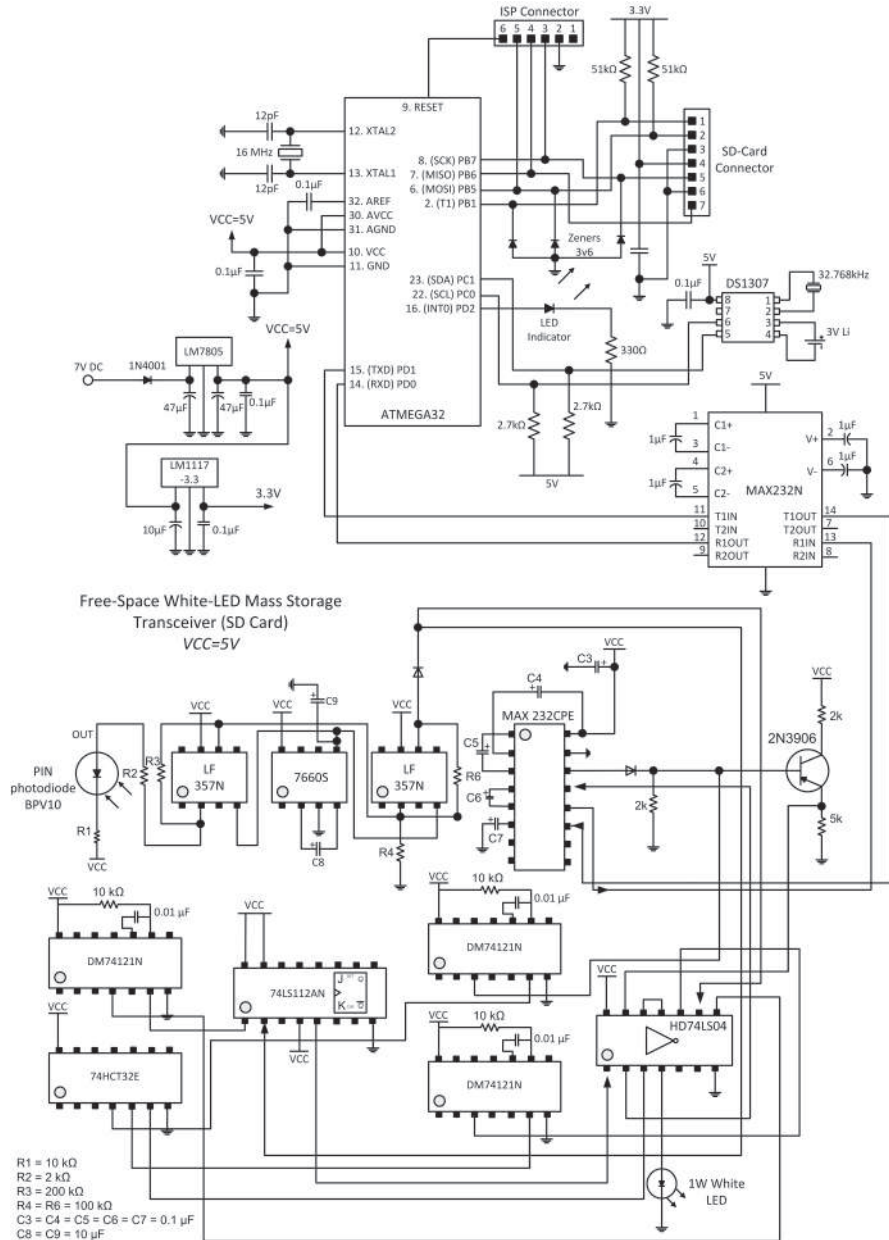


**Figure 4.1** Prototype 1 (PPM): full circuitry of the SD-card-side transceiver.

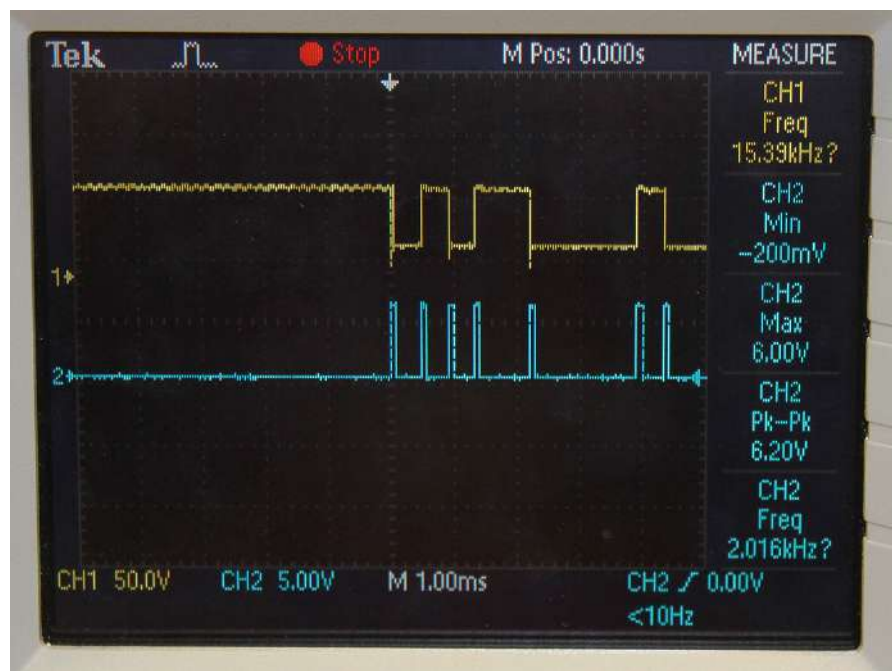


**Figure 4.2** A view of the PPM waveform on the oscilloscope. Here shows the waveform during initialization. The probe is placed at the OR gate output.

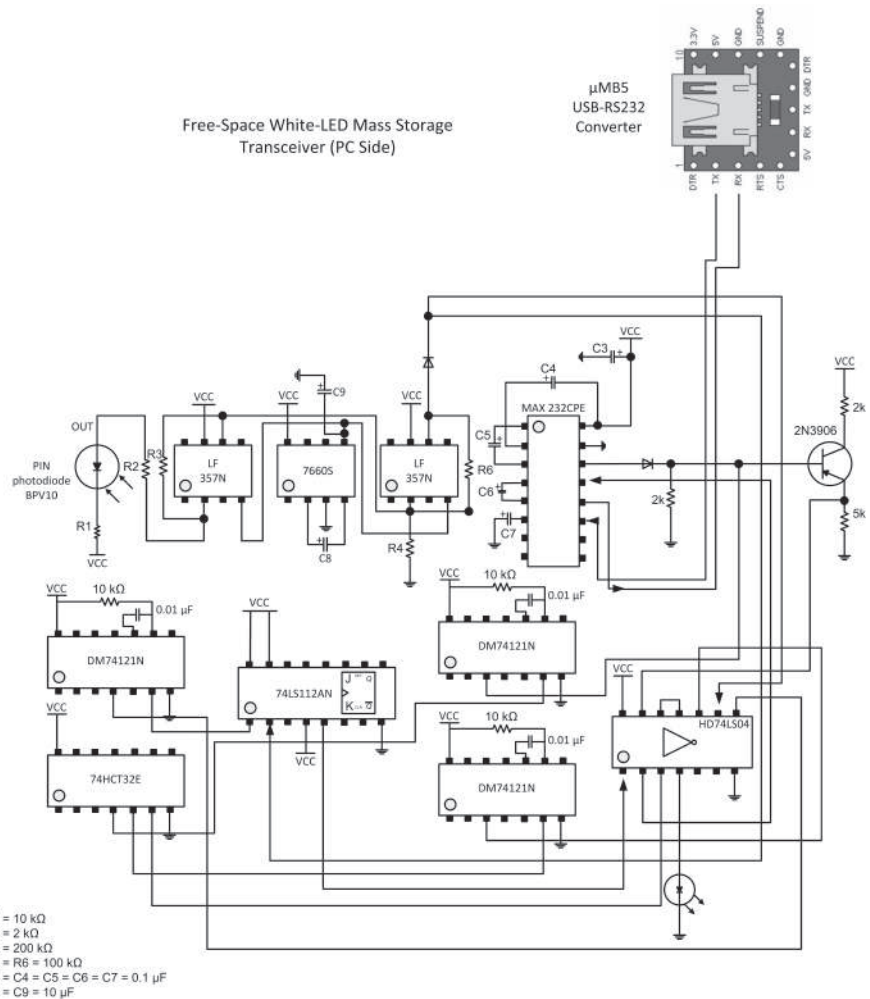


**Figure 4.3** Prototype 1 (PPM): full circuitry of the PC-side transceiver.

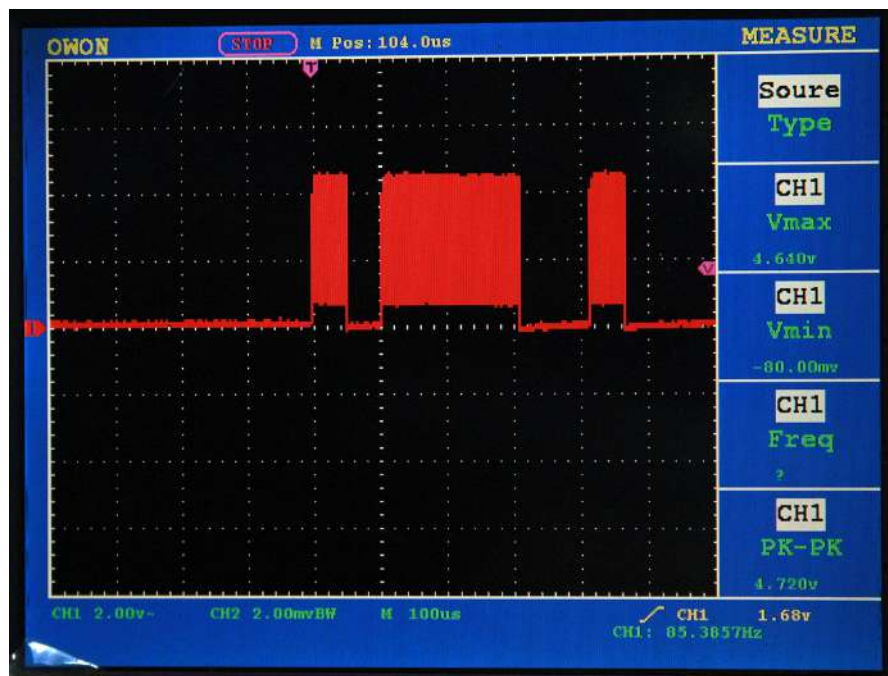


Figure 4.4 Multiplexed waveform of data and clock.

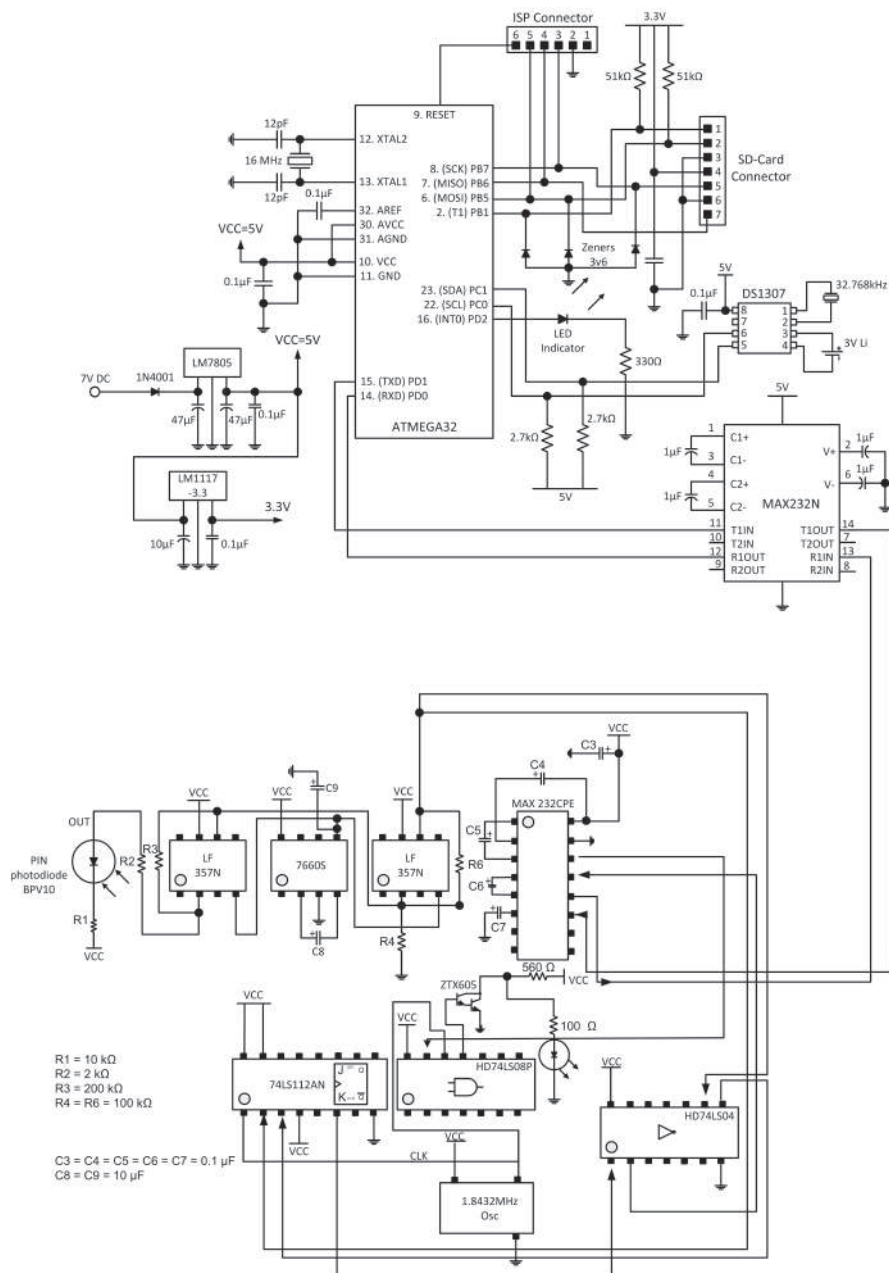
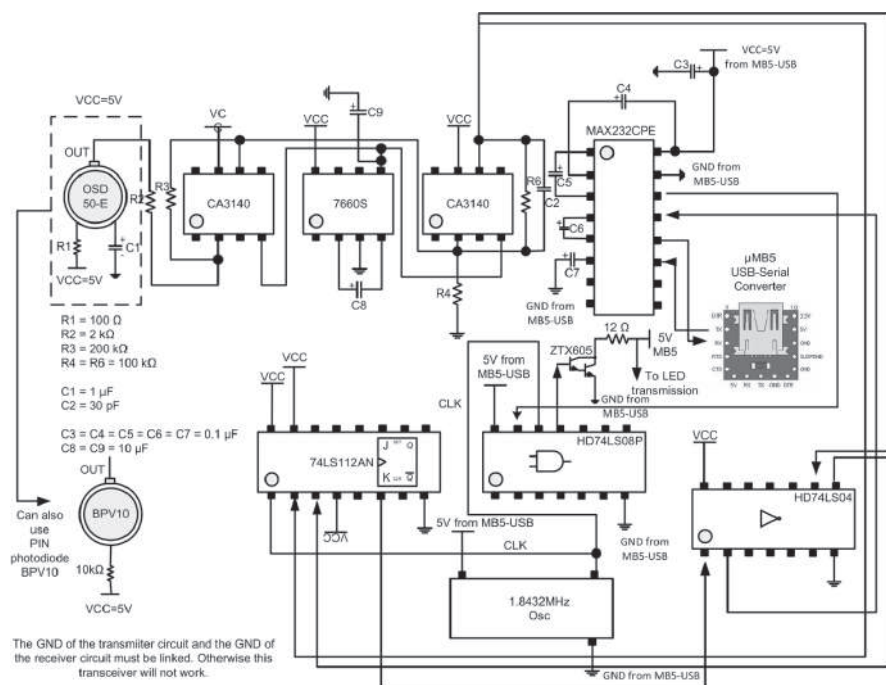
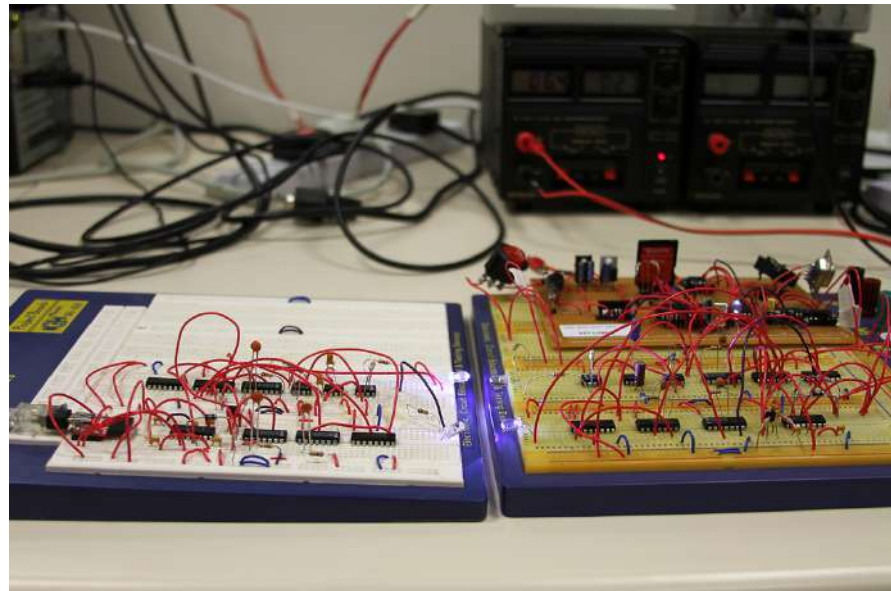


Figure 4.5 Prototype 2 (PWM): full circuitry of the SD-card side.



**Figure 4.6** Prototype 2 (PWM): full circuitry of the PC side.



**Figure 4.7** The full test setup of the VLC SD-card system.

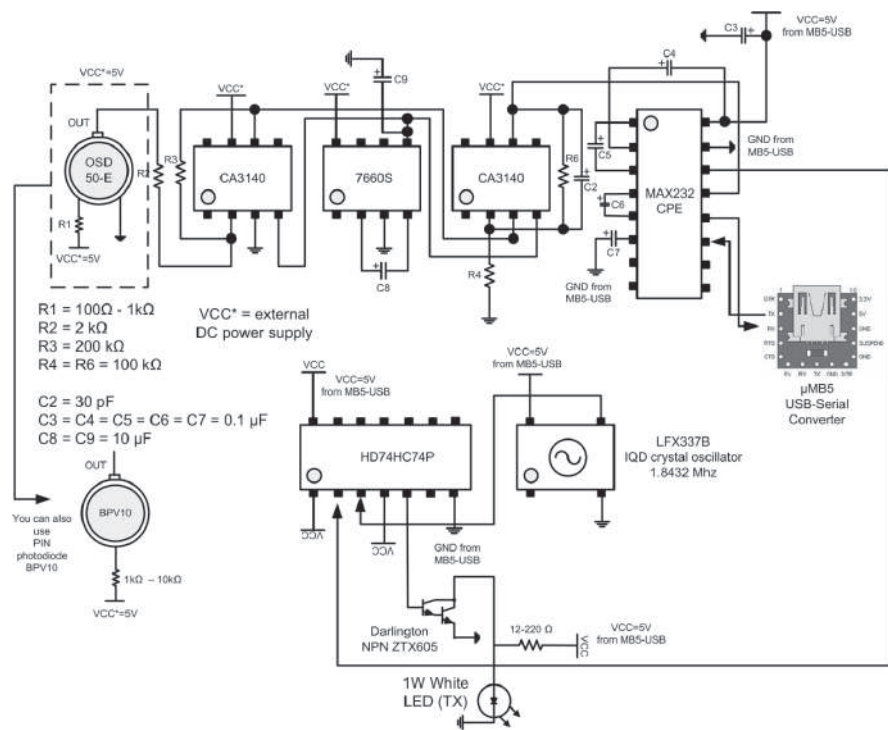


**Figure 4.8** The “Nomod” (no-modulation) design is surprisingly robust, but it is unsuitable for high-speed clocked devices.

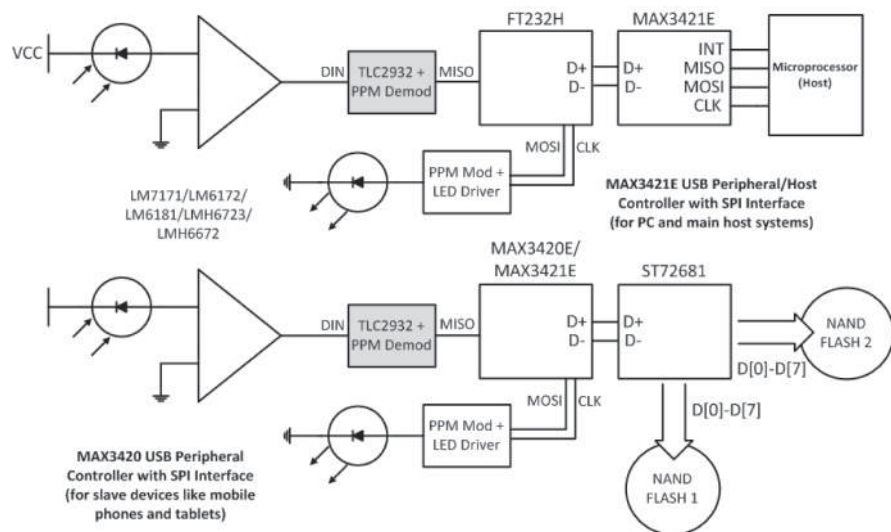


**Figure 4.9** USB 2.0 white-LED transceivers for host systems (top) and slave devices (bottom).

# **Chapter 5**

## **Audio, Video, and Data VLC Transceiver Design for Smartphones and Tablets**

### **5.1 ABSTRACT**

Today, the Bluetooth transceiver is integrated into almost all modern mobile devices. Although it can transmit audio signals, it is unable to transmit video signals. This is its biggest flaw. With advances in visible light communication (VLC) research, it is highly possible that one day mobile equipments would include the visible-light transceiver for wireless optical access to the Internet and multimedia entertainment. In this paper, visible-light audio, video, and data transceivers are presented. Real-time video and pulse-position modulated audio signals are transmitted by a white LED and received by a PIN photodiode over free space. The success of the prototypes opens up a new level of multimedia experience for consumers other than Bluetooth. VLC can also be implemented as an external accessory to smart phones and tablets operating on Android platforms above Version 2.3.4. During operation, a VLC data dongle can be connected to the device's USB Micro-B port which is available on all portable communication devices. The dongle uses a USB Android host IC to bridge smartphones to external VLC peripheral hardware. This work presents the VLC architecture, circuit design, and the components used for digital data transmission alongside the video and audio system for next-generation smart mobile applications.

## 5.2 INTRODUCTION

Although communication using light is not a new technology, it was only in the 1990s that optical communication began to attract more attention. In the last thirty years, great strides have been made in electro-optics. Light-beam communication devices are finding their way into some appliances and equipments. The increase in the research on wireless optical communication is due to the limited frequencies available on the radio frequency spectrum. By using modulated light as a carrier, an almost limitless and so-far unregulated electromagnetic spectrum becomes available. Although visible light communication generally requires a clear line-of-sight between the transmitter and the receiver to form an information link, optical-through-air systems have an added advantage of being ‘cableless’ and fast. Over the last decades, researches have been conducted on the transfer of audio [19] and video [71][21] signals via white light. The integration of VLC video and audio devices into our communication gadgets would see easier and faster interaction between people, and probably more fusion between people and machines.

Stereo [22], also called stereophonic sound, is created by two independent audio channels that provides a sense of directionality, since sounds can be heard from different directions. Stereo sound is a common form of sound reproduction. The signals that are reproduced have a specific level and phase relationship to each other [23]. Our audio prototype uses a stereo encoder to multiplex the L and R lines at the transmitter. At the receiver, a stereo decoder is used for demultiplexing to recover the L and R channels.

PAL (phase alternating line) [24] is the video standard (or video signal) that is used in most countries in the world. 25 frames are transmitted each second. Each frame is made up of 625 individual scan lines. PAL is a widely-used color encoding system for analogue television used in broadcast TV systems and securities CCTVs. Our video prototype uses a direct but effective method to transmit and amplify PAL signals at the transmitter and receiver, respectively.

The Android operating system is the current open standard for mobile devices [27] propelled by the *Open Handset Alliance*, a consortium of technology companies including Google, HTC, Samsung, Sprint Nextel, T-Mobile, Qualcomm, and Texas Instrument. Handset applications are developed in Java language using the Android SDK. Serial communication apps that are suitable for UART RS232 connections (e.g., Slick USB, AL Mass Storage) have been developed and available for download. What the market lacks is a UART VLC transceiver. It will offer a choice to consumers along with Bluetooth.

### 5.3 VLC AUDIO CIRCUIT

In our stereo audio prototype (Fig. 5.1), the transmitter mainly consists of a stereo encoder, a band-pass filter (BPF), and a PPM modulator. The receiver consists of a preamplifier, a PPM demodulator, a low-pass filter (LPF), and a stereo decoder.

Figure 5.2 is a block diagram of the audio transmitter and receiver circuit. Audio signals from a Samsung S3 first passes through a stereo audio encoder to combine the left and right audio channels. Then it goes into the 19 kHz BPF to remove high frequency components. After filtering, the signal is passed into the pulse-position modulator and the PPM signal exits through the LED. At the receiver end, the photodiode first captures light signals in the form of current and passes it to the pre-amplifier. The pre-amplifier converts the current to voltage and amplifies the signals with a suitable gain. The signal is then PPM demodulated in the 555 timer. Next, the signal enters an 8th-order LPF to remove unwanted high frequency components. After filtering, the signal goes into the stereo audio decoder for left and right channel decoding. The *L* and *R* signals are eventually delivered to the speaker via audio cables.

#### 5.3.1 VLC Audio Transmitter: Hardware Description

This circuit needs a DC source of 4.6V to function since a 1W LED is used for the emitter. There would be a voltage drop of 3.6V to drive the LED. If a 9V source is used, there would be wastage of 2W. Thus, a 4.6V supply was selected.

The audio signal from the Samsung S3 enters the stereo encoder for multiplexing. This encoder circuit uses a NJM2035 stereo modulator IC. It is used to generate a stereo composite signal of the *L* and *R* channels and operates within 1.2V to 3.6V. Two diodes are used to drop the voltage to 3.2V. The NJM2035 uses a 38-kHz quartz crystal to control the 19-kHz pilot signal so there is no need to do any calibration or re-adjustment to the circuit. The 19-kHz BPF (first 1458) and the 60-kHz LPF (second 1458) are introduced to remove high frequency components from the pilot signal and the multiplexed signal.

The pulse-position modulator circuit consists of a 555 timer configured in an astable mode. The output is connected to the cathode of the LED. The output PPM frequency is determined by Eqn. 5.1. By varying the respective resistors and capacitor value of  $R_A$ ,  $R_B$ , and  $C$ , the frequency can be varied. The width of the pulse is determined by the resistor  $R_A$ .

$$f = \frac{1.44}{(R_A + 2R_B)C} \quad (5.1)$$

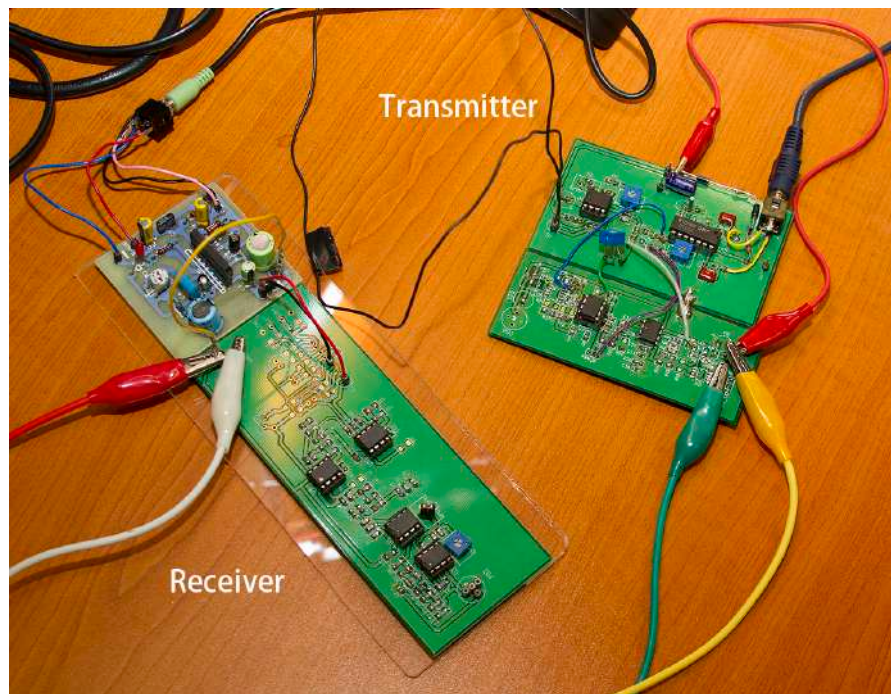


**Figure 5.1** Photo of the VLC audio transmitter and receiver.

Modulation frequencies below 50 kHz should not be used since that would cause the LED light to flicker. Frequencies that are too low also result in intermittent beats from the speaker. Hence, a 240 kHz frequency was chosen. Decoupling capacitors are incorporated into the circuit to remove noise from the power supply.

### 5.3.2 VLC Audio Receiver: Hardware Description

The pre-amplifier section is the most important part of the receiver circuit. It has to effectively amplify the received current signal from the photodiode since the lightwave signal captured by the photodiode is very weak. In order to achieve good amplification, the op-amp for the pre-amplifier needs to have a wide-gain bandwidth. A unity-gain 8th-order LPF is implemented using a Sallen-key topology with a cutoff frequency of 60 kHz. The Sallen-key topology uses passive components like

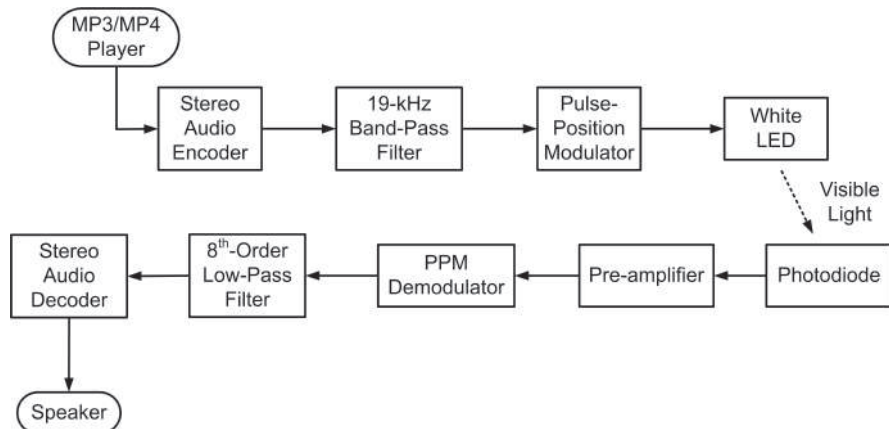


**Figure 5.2** Block diagram of the free-space white-LED audio transmitter and receiver.

resistors and capacitors to implement the filter. The stereo decoder circuit requires at least 4.5V to function. Thus, 6V was chosen as the supply voltage for the receiver after some trial and error. We find that 6V gives the best performance. The choice of the photodiode used for this project is determined by the sensitivity. Quality operation of the receiver requires a photodiode sensitivity between 0.55 A/W and 0.91 A/W. Two types of photodiodes - the S3071 *Si* PIN photodiode from *Hamamatsu* and the BPV10 *Si* PIN photodiode from *Vishay* - can be used in the prototype. The S3071 PIN photodiode was chosen due to its low dark current and high-speed pulsed light detection. The BPV10 PIN photodiode was chosen due to its sensitivity to visible radiation and low cost. The cost of the BPV10 is about a hundred times cheaper than the S3071.

The LM6172 dual op-amp is selected for the pre-amplifier due to its wide unity-gain bandwidth and high slew rate. The first op-amp acts as a pre-amplifier to convert current into voltage. The second op-amp acts as a threshold detector or comparator. The reference voltage is dependent on the potentiometer connected to Pin 6 of the LM6172. The signal output is fed into Pin 2 of the LM555 for demodulation. The PPM demodulator circuit consists of a 555 timer and some associated components to form a frequency-to-voltage converter. It is similar to a monostable configuration. The output frequency is determined by Eqn. 5.2. By varying the resistor and capacitor value of  $R_A$  and  $C$  respectively, the frequency can be varied.

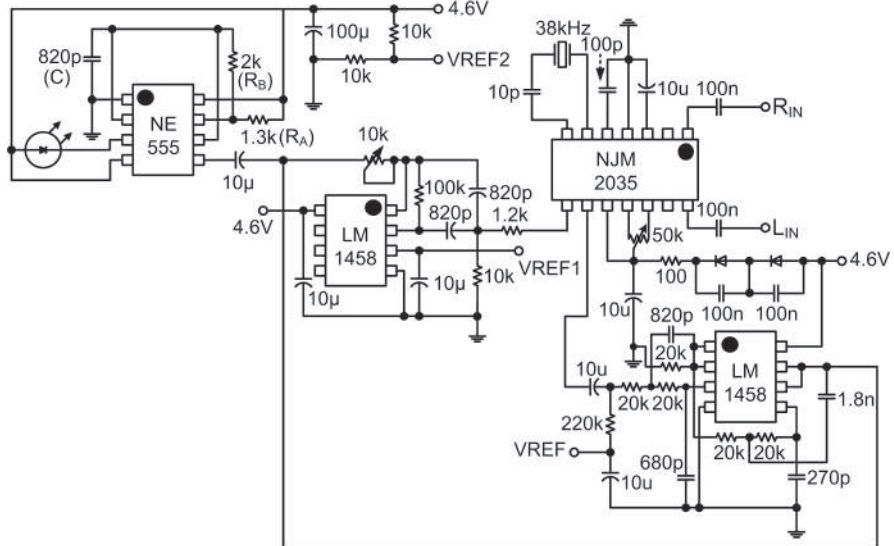


**Figure 5.3** Full circuitry of the transmitter.

$$f = \frac{1}{1.1R_A C} \quad (5.2)$$

To achieve optimum demodulation, the frequency used must be at least double the frequency used for PPM modulation. Therefore we used 454 kHz. After demodulation, the signal is fed to an 8th-order LPF to remove high frequency components.

The 8th-order LPF uses the LM1458 IC which contains dual op-amps. The LPF circuit consists of two stages and has a cutoff frequency of 60 kHz and unity gain. A Sallen-key LPF calculator [25] was used to fine-tune the filter design to achieve better sound quality. The output from the LPF is then passed to the stereo decoder circuit.

The stereo decoder circuit implements a TFK U2343 stereo decoder IC with an operating voltage between 4.5V and 12V. Adjustment of its internal voltage-controlled oscillator (VCO) is made by a potentiometer. When the stereo decoder receives signals from the LPF circuit, the U2343 demultiplexes them into left and right channels which finally output to the stereo speakers. The setup for experiment is shown in Fig. 5.5.

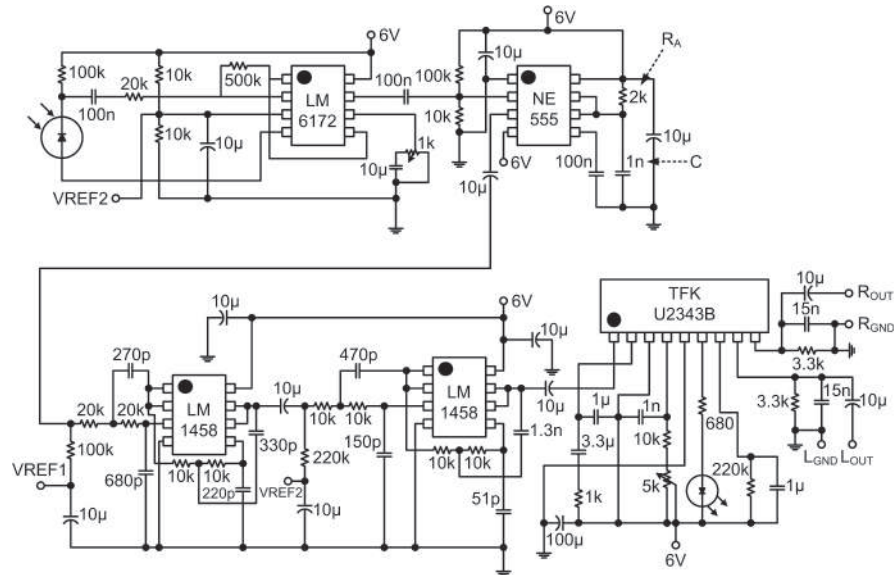


**Figure 5.4** Full circuitry of the receiver.

#### 5.4 VLC VIDEO CIRCUIT

This video transceiver prototype (Fig. 5.6) is able to transmit TV and CCTV video signals. It is a simple circuit using only a pair of LM7171 amplifiers and negative voltage converters 7660S. The LM7171 is just the right IC for our video circuit. As its datasheet mentions, this IC can be used in video amplifiers, professional video cameras, HDTV amplifiers, CATV, fiber optics signal processing, and pulse amplifiers. The biggest attraction comes from its 4100 V/ $\mu$ s slew rate and wide unity-gain bandwidth of 200 MHz. The configuration of resistors around Pin 2, 3, and 4 serves the purpose of level shifting. Technically, they are called voltage dividers. They help to shift signals along the amplitude plane in order to agree with the standard video and audio voltage boundaries.

Fig. 5.7 shows the soldered transmitter and receiver. The transmitter board is connected to the camera board (which is dismantled from a used CCTV camera). The receiver board is connected to a BNC-VGA video converter which then connects to a VGA monitor.

To power the transmitter and the camera, eight AA-sized batteries (12V) are fixed at the base of the lamp. The receiver is powered by four AA-sized batteries (6V).

### **5.5 A MULTIMEDIA SYSTEM: INTEGRATING VIDEO AND AUDIO SIGNALS**

Now that we have the video and audio transceivers working properly, the fusion of the two becomes much easier (Fig. 5.9, left). We require an 8 MHz clock signal because the frequency required by the PAL signal is 5.5 MHz. Audio signals are low in frequency, thus they are not much of a problem. The only problem with audio signals is noise, which can be made worse when we use light to transmit. The right hand side of Fig. 5.9 shows the pins that are required for multiplexing and demultiplexing. The 4053 is a 2-channel analogue multiplexer and demultiplexer which has a good switching response of 190 MHz.

Today, three wireless communication systems are present in our smartphones: 4G, Wi-Fi, and Bluetooth. All the three require licensing. In ad-hoc applications like face-to-face sharing and transfer of files, we usually use Bluetooth because the other two are costly. Bluetooth is able to transfer data as well as sound, but due to its limited data rate and architecture, it is unable to transmit and receive real-time video signals. Therefore, the authors of this work are looking into visible light communication (VLC), since it is able to efficiently perform data, audio, and video transmissions at the same time. At the moment, this work focuses on the transmission of UART and SPI data signals.

The fusion of a VLC data transceiver peripheral with our portable devices will renew the way we communicate in the future, although communication using white light may not be popular during this generation. We should not underestimate the potential of VLC, because by the time all lights are replaced by LED lamps, a myriad of innovations regarding light transmission will render our proposed device as a necessity. The LED was initially not made to do switching, but solid-state scientists are making great progress in fabricating LEDs that can switch at high speeds.

### **5.6 USB-ANDROID BRIDGE TO UART INTERFACE**

The FT311D chip bridges the USB port of Android devices to six selectable interfaces. Only UART and SPI will be covered here. The chip serves an obvious

purpose, that is it provides access to peripheral hardware from an Android platform via the USB 2.0 port. The VLC transceiver interfaces with the smartphone or tablet using this chip. If two smartphones have the VLC dongles attached, they will be able to transmit text and files between each other.

### **5.7 THE VLC TRANSCEIVER**

The transceiver (Fig. 5.10) circuit consists of two operational amplifiers LF357N. The first functions as a preamplifier and buffer, while the second functions as a comparator as well as a low-pass filter. LF357N is a JFET input operational amplifier. It is picked for its low voltage and current noise and low  $1/f$  noise corner. It has a wide gain bandwidth of 20 MHz.

The D flip-flop 74HC74 accepts data and clock signals (from the crystal oscillator) to generate state-triggered signals for transmission. Without the clock oscillator, there will be no continuous light. The MAX232CPE IC is used to convert signal levels between RS232 and TTL. This work is an extension of our previous research on VLC USB modulation systems [26]. This system can be integrated into motherboards of smartphones and tablets that use Android Version 2.3.4 and above, powered by the USB voltage from the host device.

### **5.8 CONCLUSION**

VLC video, audio, and data prototypes have been presented. This work opens up greater possibilities of integrating VLC with portable communication devices. The authors are optimistic that one day such a system would appear in tiny PCB or IC form, one that can be easily integrated into mobile phones, tablets, computer units, robots, and even our watches. The advantages of such systems include real-time interaction and simultaneous availability of sight and sound. VLC will change the way we enjoy entertainment. The technology can be used in desktop webcams, street surveillance, patient monitoring in hospital wards, and direct broadcast of concerts, lectures, and seminars where attendees need to be away from the venue. Besides the audio and video transceivers, the VLC data dongle will be an essential part of data communication in our everyday lives when the revolution of indoor lighting spurs in a decade - that is, the replacement of fluorescent lamps by LED lamps is going to happen.

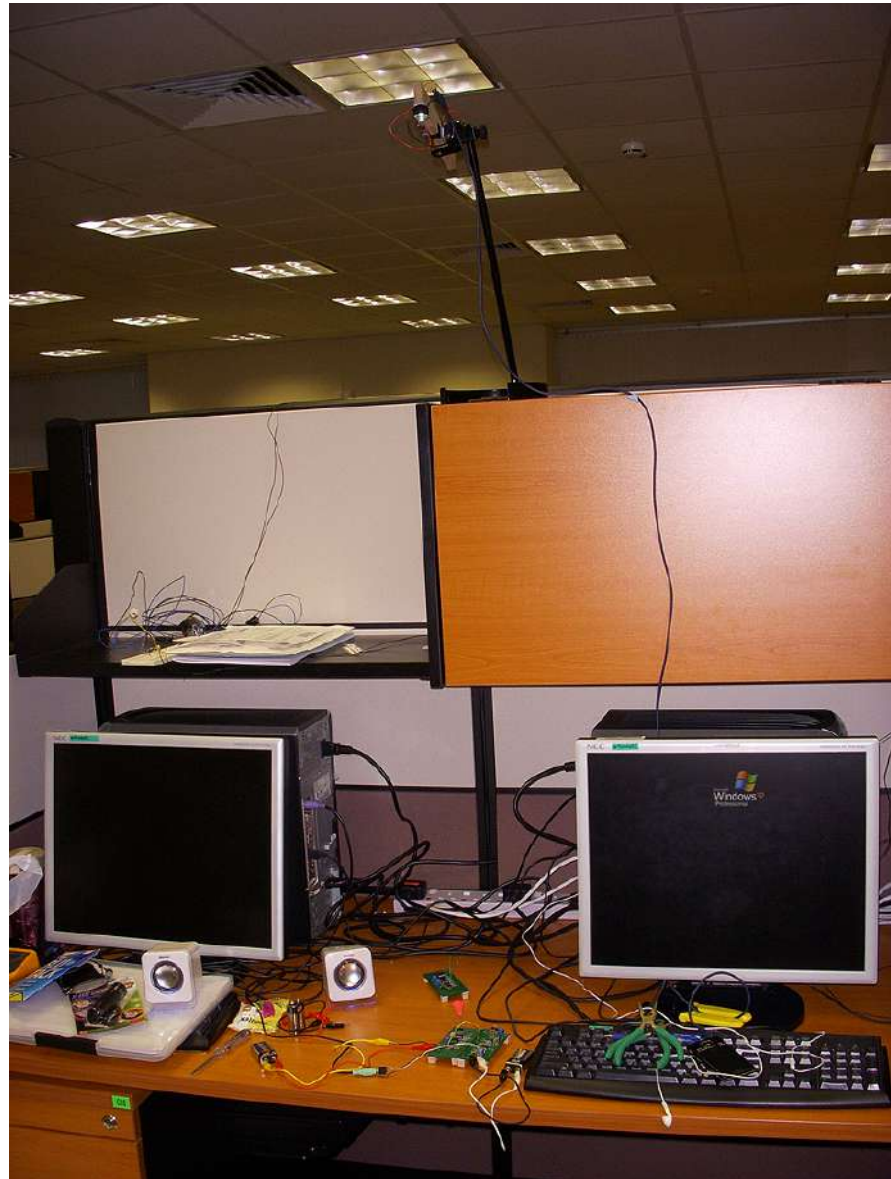


**Figure 5.5** VLC stereo audio transceiver setup and testing.

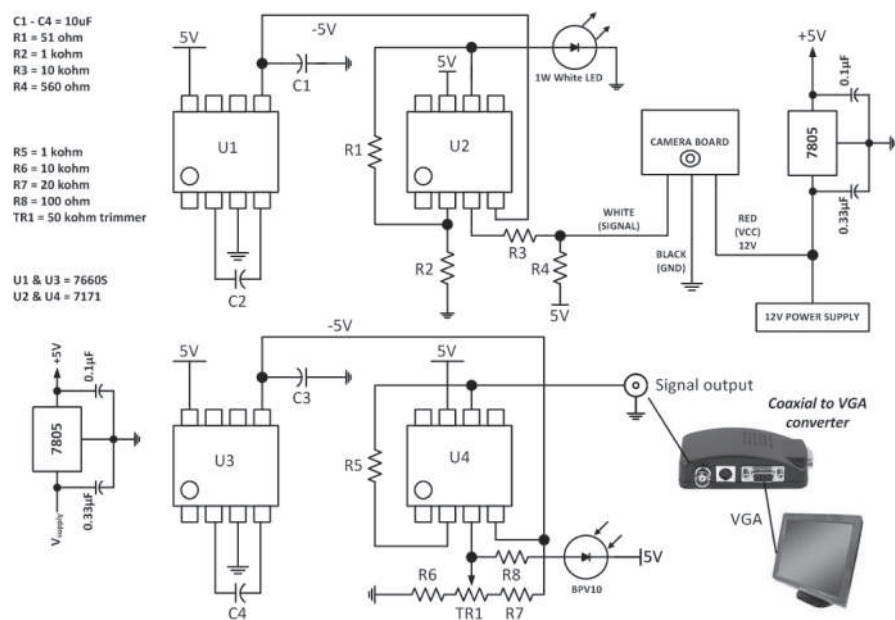


**Figure 5.6** Schematic diagram of the VLC video transmitter and receiver.

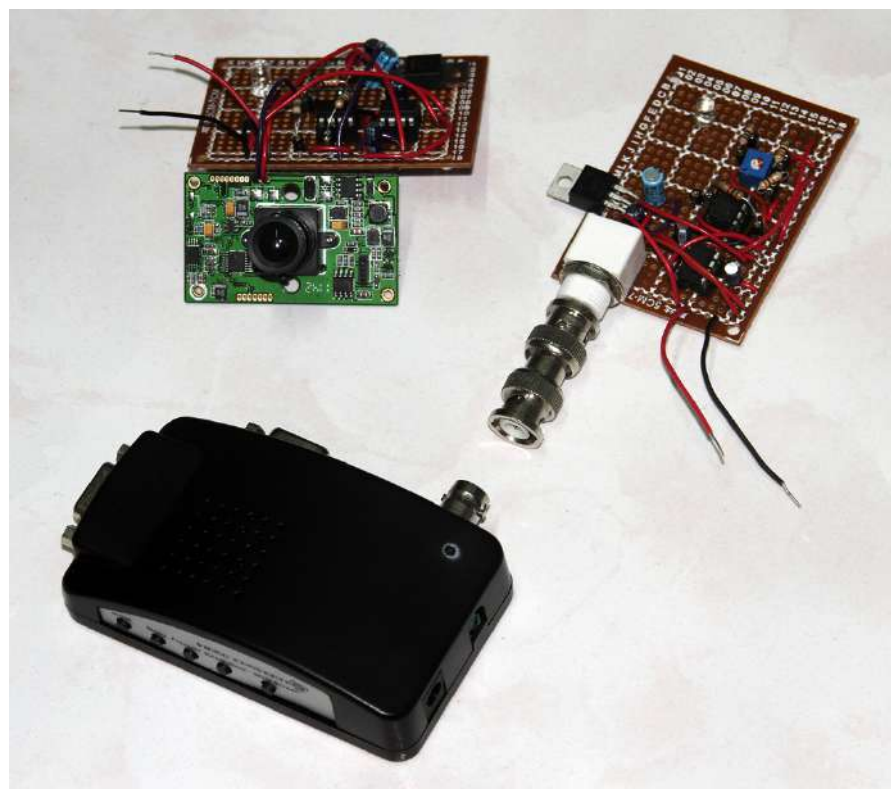


**Figure 5.7** VLC circuits and components soldered on perfboards.

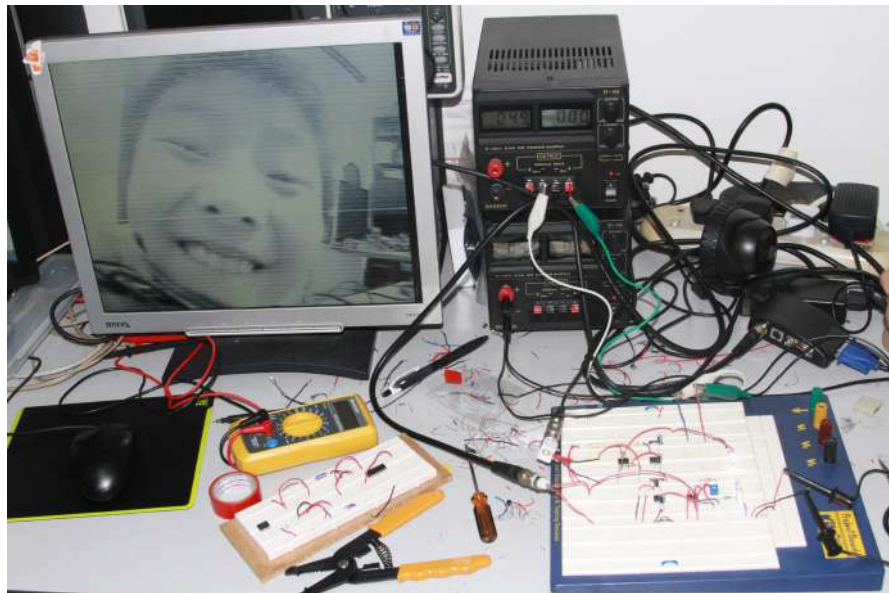


**Figure 5.8** Test setup of VLC video communication.

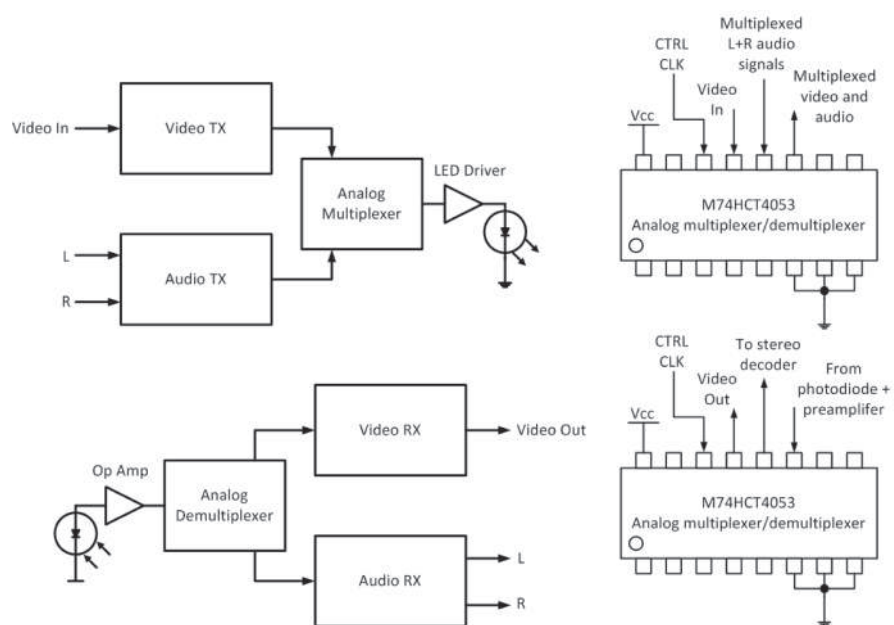


**Figure 5.9** (Left) Block diagram of integration between the video and audio modules. (Right) The use of the multiplexer(top)/demultiplexer(bottom) IC 4053 for combining and splitting video and audio signals, respectively.

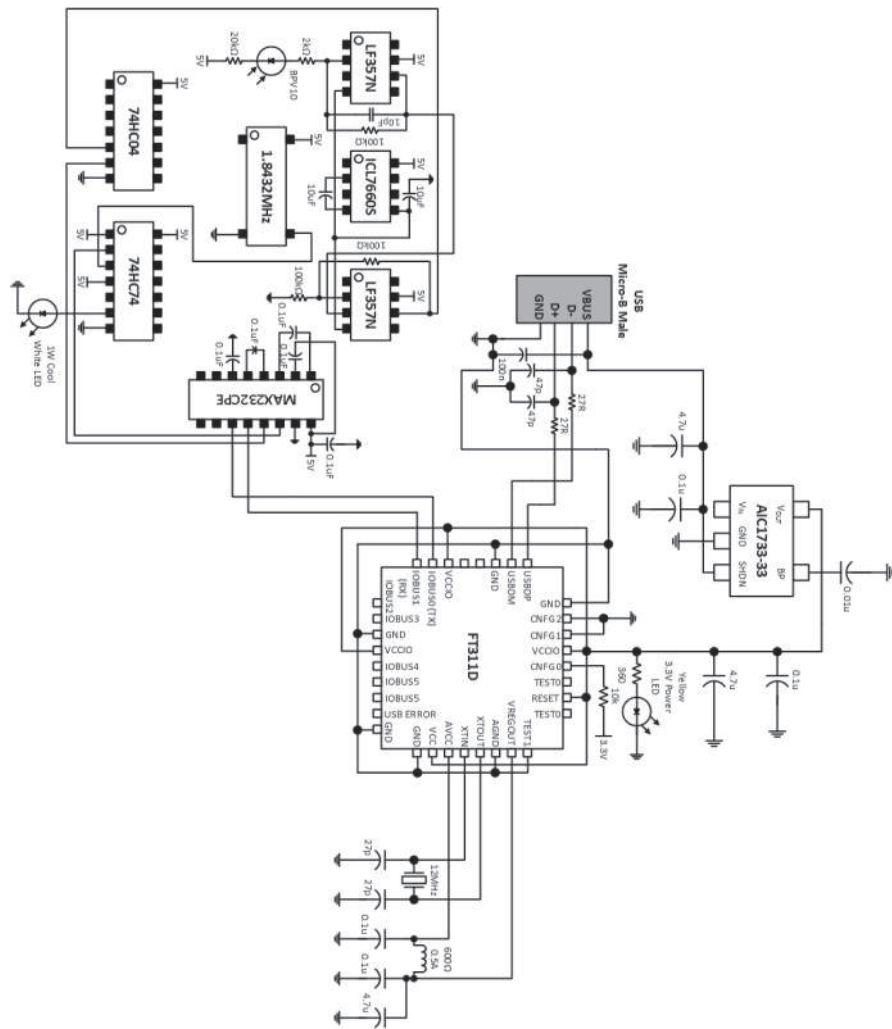


**Figure 5.10** Full schematic for VLC data dongle for Android smartphones based on the latest FT311D bridge.

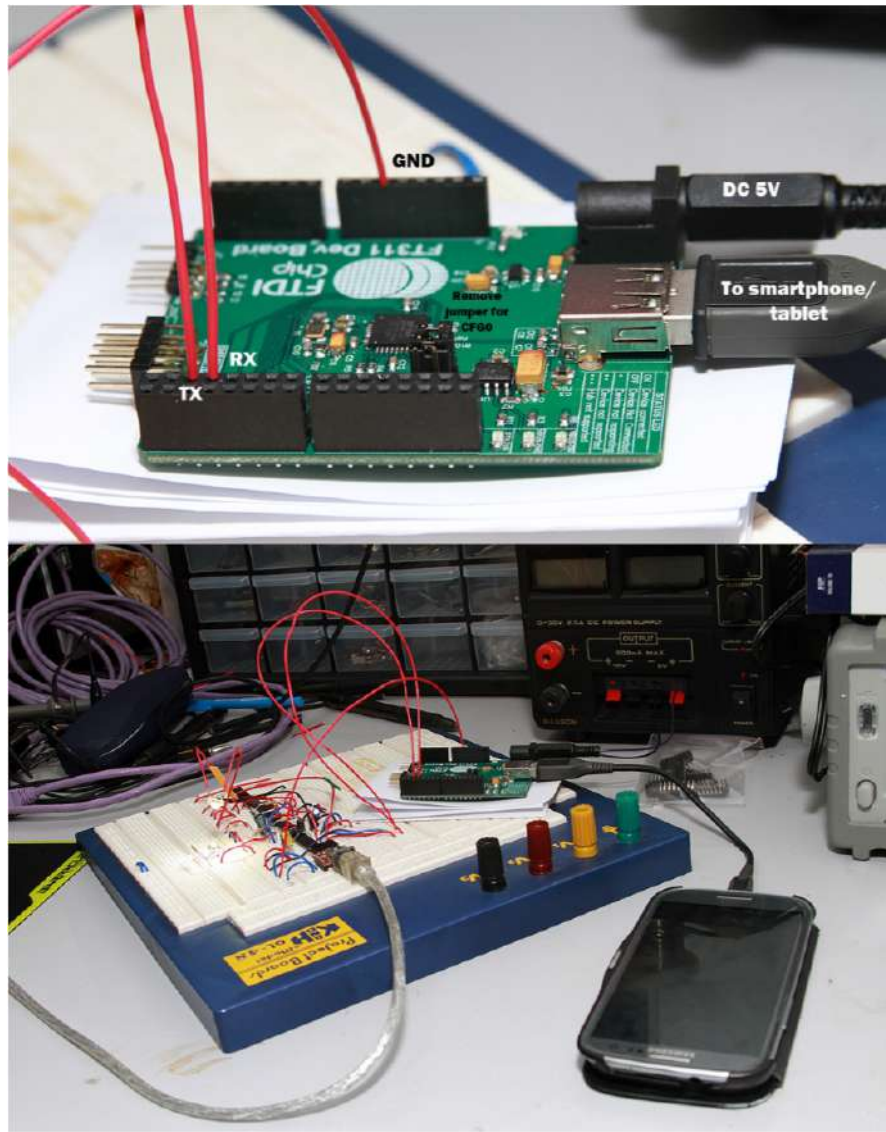


**Figure 5.11** Pictures of the setup and connection between a smartphone and the FT311D bridge.

# **Chapter 6**

## **Early Tsunami Forecasting Using Deep-Sea Visible-Light LEDs**

### **6.1 ABSTRACT**

A sea-level measuring and detection system is proposed for application in the detection of seabed movements to forecast tsunamis. Target implementation objectives include flood control systems and ocean meteorology where LEDs will be installed on sea floors and river beds. Light intensity received is converted to the length of vertical displacement to reflect any rise or fall of the sea floor. Sea level and the amplitude of wave movements can also be measured using this method. The design of such a prototype is discussed.

### **6.2 INTRODUCTION**

During the undersea megathrust earthquake in 2004 that hit landmasses bordering the Indian Ocean on Boxing Day, the sea floor is estimated to have risen by several metres, thus displacing 30 cubic kilometres of water and triggering devastating tsunami waves that took 230000 lives. Currently, the DART (Deep-ocean Assessment and Reporting of Tsunamis) system is used to predict tsunamis around the world [28]. The system consists of a bottom pressure recorder (BPR) and a tagged detection buoy on the surface of the ocean. Sea pressure is converted to surface height between the ocean surface and ocean floor. The BPR and the buoy are linked by acoustic communication. There are 39 such stations globally. These

DART systems and the Tsunami Warning Centers (TWCs) are connected by the iridium commercial satellite which enables a two-way communication.

Acoustic communication [29] is used because RF communication works badly in thick electrical conductors like sea (or salt) water. Another way to detect sea level with respect to vertical shifts of the ocean floor is to install a high-brightness LED array farm on the seabed. Any passing vessel or docking harbour with a relative optical detector will be able to determine the sea level based on the *Beer-Lambert-Bouguer Law* (BLB) [30]. Besides that, these LEDs also act as an underwater lighthouse for passing ships. Position information can be sent by the LEDs to these ships and even low-flying aircrafts.

The advantage of using LEDs is that it has a long lifetime. This makes them suitable for installation in places that are difficult to reach and where maintenance are not so regular. The deepest trench in the world, located along the Mariana Trench, is about 11 km deep. The average depth of the Pacific Ocean is around 4.28 km. Thus it is not impossible to have an LED farm planted at the base of ocean floors and the light detected above sea level. The LED farm can just draw its power from any coastal wind farm. Since LEDs are energy saving and specially-designed lenses can be used, they do not require high electrical power.

### 6.3 OPERATIONAL THEORY: BEER'S LAW

Basically, the intensity of light decreases as it passes through water. The sea level can be computed by the *BLB Law*:

$$\ln(I_0/I) = 0.015d \quad (6.1)$$

where  $I$  is the intensity of light at the depth of  $d$ ;  $I_0$  is the intensity of light in the atmosphere; and 0.015 is the exponential slopes of the UV and/or visible light absorption spectra of the Indian Ocean [31].

Tsunamis are also called *shallow water waves* since their wavelengths  $L$  are greater than the water depth  $D$ . We use this principle of nature to acquire the velocity  $v$  of a tsunami and eventually determine the time it takes to reach a certain place [28]. First, by installing the LED farm on the seabed near the fault line (Fig. 6.1), the detector on the buoy is able to mark the change in the height of the seabed  $\delta d$  during an underwater earthquake. The equations are given in (2)-(5).

$$\delta d = d_2 - d_1 \quad (6.2)$$

$$L = d_1 * 2 \quad (6.3)$$

$$D = L/20 \quad (6.4)$$

$$v = \sqrt{g * D} \quad (6.5)$$

$g$  is the acceleration of gravity and  $D$  is the real depth.

## 6.4 PROPOSED DESIGN OF THE PROTOTYPE

A cluster of white LEDs is installed at the base of an aquarium tank connected to a transmitter driver circuit. The LED board is vertically adjustable. A mobile water-proof receiver with high-sensitivity photodiodes is connected to an *Infineon* microcontroller which is linked to the PC. The microcontroller is programmed and configured according to the pathlength versus light intensity received. The tank is filled with seawater. Fig. 6.2 shows the diagram of the prototype.

### 6.4.1 Receiver Circuit

The receiver (Fig. 6.3) consists of a luminosity sensor which is connected to *Infineon's* XMC4500 microcontroller. Programming is done on the XMC4500 to convert illuminance (lux) to depth (cm). The real-time depth readings will be reflected on the PC which is connected to the XMC4500. The receiver can be fixed or floating. A fixed receiver measures the change of height vertically, while a floating receiver imitates the DART detection buoy which is effective in measuring height as well as wave amplitude.

## 6.5 CONCLUSION

The prototype is a viable and economical demonstration of the possibility of measuring sea depth by installing LEDs at the base of river beds, seabeds, or ocean floors. All measurements will be relative to the seabed such that a global tsunami alert may be sent if there is an abrupt plate shift along the trenches.

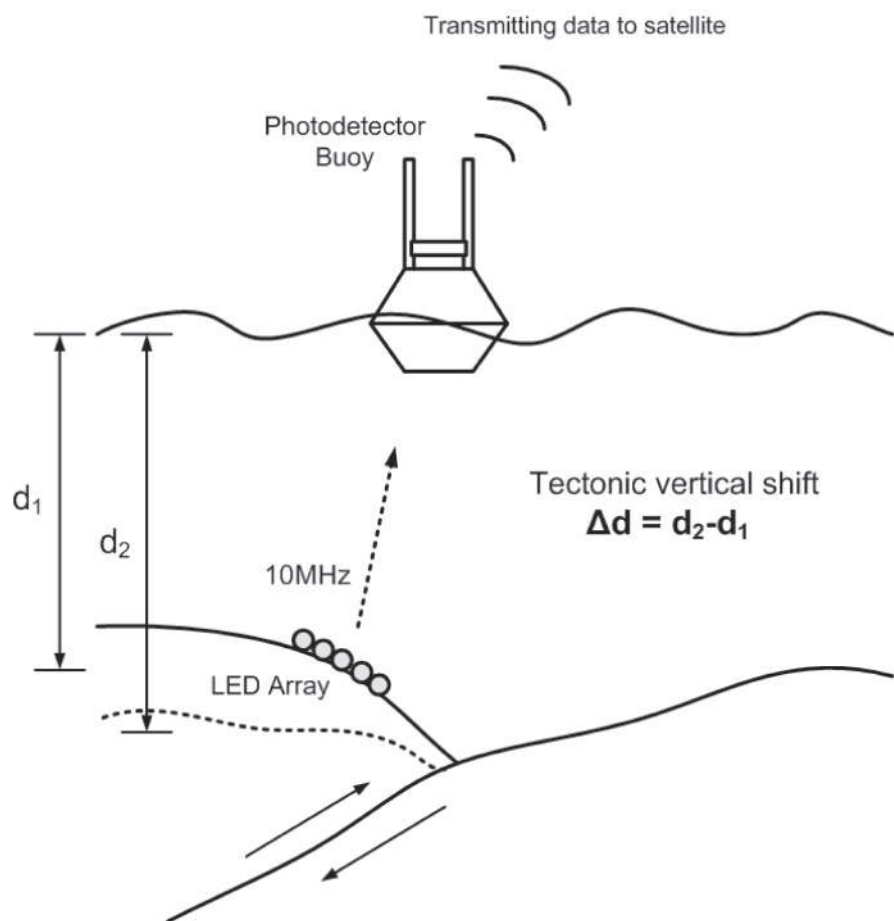


**Figure 6.1** Application of high-brightness visible-light LEDs in early tsunami prediction.

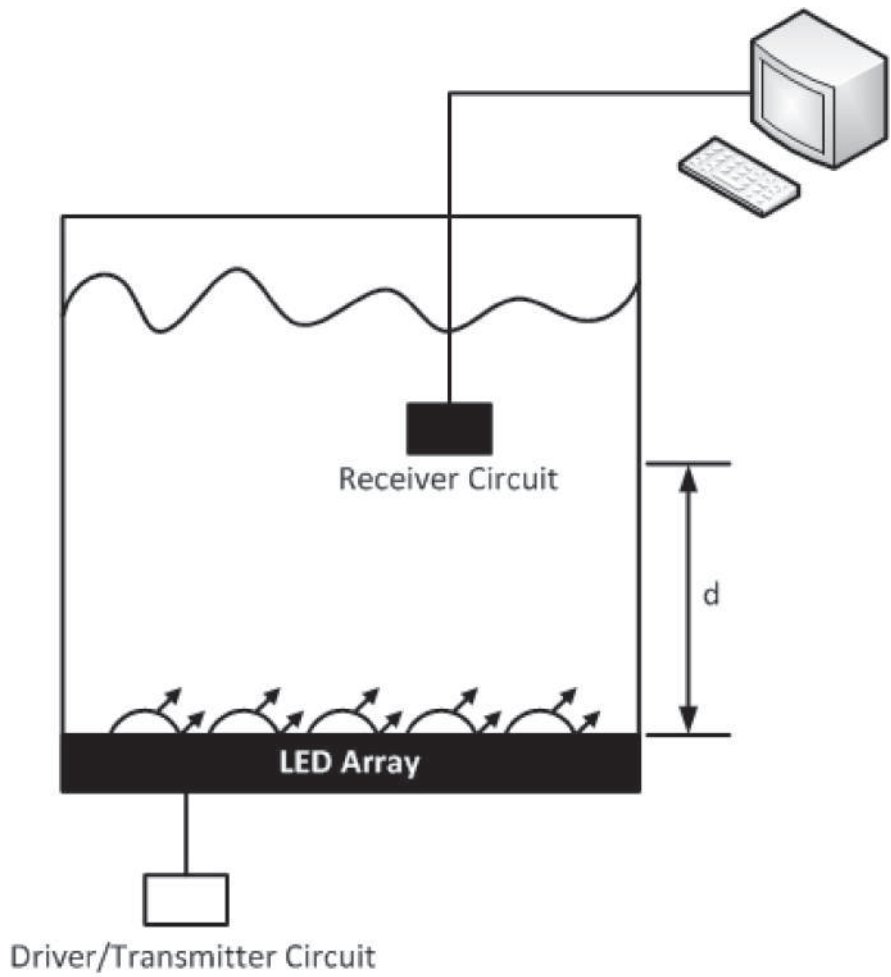


**Figure 6.2** An overview of the proposed prototype.

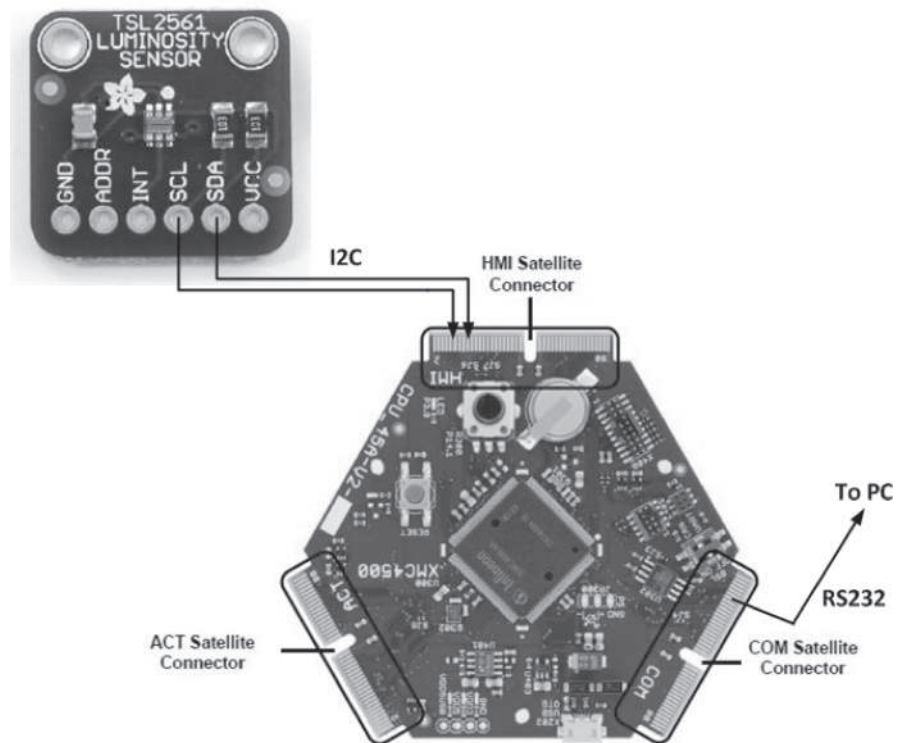


**Figure 6.3** The receiver circuit using TAOS' luminosity sensor and Infineon's XMC4500 microcontroller.

# **Chapter 7**

## **MIMO-Diversity Switching Techniques in Visible Light Communication**

### **7.1 ABSTRACT**

In this work, we propose two decision techniques that interchange between MIMO and diversity schemes for improving shadowing and alignment problems. In a visible-light communication (VLC) system, the transmission nature can be of two types: (1) all LEDs transmit the same signal stream simultaneously; or (2) each LED transmits different parts of a signal stream independently. The MIMO-diversity technique detects and computes the transmitted signal power during reception and conditionally informs the transmitter to switch between Type (1) and Type (2) transmission. Two experimental models have been tested to show the feasibility of such a technique. In the first model, we constructed a full transceiver and uses a switch IC to switch between MIMO and diversity. The second model uses a microcontroller and software decision to switch between two COM ports, each of them dedicated to MIMO and diversity output respectively. Results suggest that shadowing and alignment problems commonly encountered in visible-light communication systems can be readily solved using these methods. A focusing equation has also been formulated to predict signal intensity more accurately. The focusing gap between the concentrator and the photodiode is taken into consideration during channel computation.

## 7.2 INTRODUCTION

MIMO (multiple input, multiple output) refers to the use of multiple, simultaneous signals (two or more radio or optical waveforms) in a single frequency channel to exploit multipath propagation and thereby multiply spectral efficiency [32]. MIMO technology has been widely used in our *Wi-Fi* (or 802.11n) systems to increase bandwidth efficiency and speed. However, in recent years, researchers of visible light communication (VLC) systems start to include MIMO into the LED-photodiode link configuration [33][34][35].

Komine [74] proposed a distributed (or emitter diversity) model to alleviate shadowing problems. Each LED emits the same stream of data. In this method, multiple light sources that are properly distributed on the ceiling are able to reduce dark areas or shadows. However, it is prone to intersymbol interference (ISI). Zeng [33] proposed a MIMO technique whereby a data packet is broken into blocks. After that, each block is sent independently through different individual emitters. This method has been proven to yield high data rates, but the disadvantage is that all the LEDs are critical since each of them carries a different portion of information.

To resolve the problems of shadowing or blocking, signals must be available from more than one emitting source. The diversity model looks like a promising solution as it has high SNR, but that does not improve the data rate and ISI problems. MIMO holds the key to remedy these problems. Nevertheless, it requires a full-rank channel matrix; that is, if any one LED is blocked or damaged, the communication link is broken. Technically, this problem can be overcome by the diversity model.

In this work, the authors propose a switchable MIMO-diversity system which can be achieved using either hardware in-circuit switching or COM port switching (Fig. 7.1). By default, the model operates in MIMO mode. Once any receiver encounters a marked decrease in optical power, the system will switch the transmitter to parallel diversity mode so that all the LEDs contribute to the deficient signal strength.

The proposed switching scheme is a negotiation technique (Fig. 7.2) that combines Komine's diversity scheme [37] and Zeng's MIMO scheme [33] to incorporate their strengths. In the open-loop method, the receiver performs a channel estimation. In the closed-loop method, the receiver reports the channel status to the transmitter via a feedback channel. This makes it possible for the system to respond to changing circumstances [38]. If transmission matrix  $H$  is known, the cross-components can be calculated by the receiver.

The first half of the paper will present two practical methods to switch between MIMO and diversity channels. In the next half, a set of equations that

deals with the concentrator's focusing gap is formulated. The focusing gap is critical because the standard channel model that deals with spatial transmission of light does not take the focusing length into consideration when a concentrator is used.

### 7.3 CONCEPT FORMULATION

The MIMO-diversity switching technique is determined by the detected received power of one or more photodiodes. The received signal matrix  $R$  is multiplied by the inverted channel gain  $H^{-1}$  to compute the signal strength matrix of the emitter  $T_{est}$  [33]:

$$T_{est} = H^{-1}R \quad (7.1)$$

The computed value of  $T_{est}$  is an estimate of the transmitted power of an LED or a group of LEDs received by a photodiode or photodiode array. In the MIMO-diversity decision algorithm in (7.2) and (7.3), the value  $T_{est}$  is first subtracted by the standard illuminance power  $I$ . If the difference is larger than a certain threshold  $Q$ , the nearest neighbor algorithm will identify any transmitter that is in close proximity to any problematic LED and switches them to diversity mode.

$$\text{MIMO: } \begin{bmatrix} D_{11}(b_1) & D_{1j}(b_2) \\ D_{i1}(b_3) & D_{ij}(b_n) \end{bmatrix} \text{ if } T_{est} - I < Q \quad (7.2)$$

$$\text{Diversity: } \begin{bmatrix} D_{11}(b_n) & D_{1j}(b_n) \\ D_{i1}(b_n) & D_{ij}(b_n) \end{bmatrix} \text{ if } T_{est} - I > Q \quad (7.3)$$

where  $b$  is the frame or packet;  $n$  is the frame or packet number; and  $D$  is the datastream to be transmitted through the LED at position  $i, j$  (i.e. the  $x$  and  $y$  axes). In the following sections, two prototypes that are able to realize the MIMO-diversity model are discussed.

### 7.4 METHOD 1: A 4 BY 4 MIMO-DIVERSITY AUTO-SWITCHABLE TRANSCEIVER

We built a 4-by-4 (4 LEDs and 4 photodiodes) configuration transceiver that auto-switches between the MIMO circuit and the diversity circuit. The prototype transceiver circuit is shown in Fig. 7.3 and Fig. 7.4.

#### 7.4.1 Transmitter Description: MIMO Scheme Circuitry

We made use of a four-phase clock generator to split RS232 data into 4 sequential bits that exits through 4 corresponding LEDs (Fig. 7.3). Generating multiple clock sources is a common requirement for digital circuit design. Here, we feed in a data signal instead of a clock in order to divide the data into 4 separate bit-streams. This MIMO circuit is a 4-bit data splitter producing non-overlapping data pulses. The ENABLE input of the 74LS139 (dual 2-to-4 line decoder/multiplexer) receives data input from the USB-RS232 converter. This circuit can be easily expanded to an 8 or 16-phase clock generator by adding flip-flops and using a 74LS138 decoder.

#### 7.4.2 Transmitter Description: Diversity Scheme Circuitry

The diversity scheme outputs the same datastream simultaneously through all the LEDs. The simplest way is to use a multi-LED torchlight. However, we devised a simple circuit using a serial-in parallel-out shift register 74HC164 (Fig. 7.3). The 74HC164 is an edge-triggered 8-bit shift register with serial data entry and an output from each of the eight stages. Data was entered serially through one of two inputs (A or B). Either of these inputs can be used as an active High Enable for data entry. Each LOW-to-HIGH transition on the clock (CP) input shifts data one place to the right and enters into outputs  $Q_0$  and so on. Any four of the eight output pins can be used to connect to the respective LEDs.

#### 7.4.3 Receiver Description

The receiver circuit (Fig. 7.4) consists of 4 op-amps (CA3140) together with their individual photodiodes. ICL7660S provides negative voltages to the op-amps. Either SFH213, BS520, OSD50-E, or BPV10 can be used as photodetectors. When the light channel to any photodiode is blocked, the default MIMO scheme is automatically switched to the diversity scheme by the MAX325 switch (Fig. 7.3). The MAX325 is a precision, dual, SPST analog switch. It has one normally-open (NO) switch and one normally-closed (NC) switch. The op-amp CA3140 has a bandwidth of 4.5 MHz, which is sufficient for RS232 use. If you need an op-amp that is more sensitive and has a higher (i.e. hundreds of megahertz) bandwidth, LM6172 and LM7171 are good choices.

A simple microcontroller (e.g. PIC12F508, PIC16F690, PIC16F684, etc.) or a 4-input AND gate (HEF4082B/74HC21) can be used together with the MAX325,

such that once any drop in voltage is detected, all the four LEDs will be switched to diversity scheme to send data in parallel mode.

#### 7.4.4 Test Setup and Experiment

Two people are needed to conduct this experiment: one standing at the transmitting PC and one standing at the receiving PC. Both will start the transmitting and receiving process at the same time by pressing F5 (the RUN command in MATLAB) together. The transfer time is the time recorded at the receiver. The test data is a text string of ‘1’s in numbers of 40, 80, 120, and 160.

The transmitter and receiver were placed 4 cm apart, each connected to a PC. First, the time taken for all the data to be transferred successfully without any blocking was recorded. After that, the transfer time with blocking was recorded. The final switching results obtained were the values from the latter minus the values from the first. Blocking was done by putting a finger between one of the light paths in the middle of a transfer. When one of the LEDs was blocked, the low voltage was alerted by the microcontroller (or AND gate), causing MAX325 to switch on the transmitter’s diversity circuit components. At the same time, an optional OR logic was activated in the microcontroller, thus ignoring any defective channel. When the finger was removed, the channel that was blocked resumed a HIGH state at the photoreceiver. This triggered MAX325 to switch back to MIMO and subsequently the microcontroller reverted to AND detection logic again. An oscilloscope was used to check if the LEDs had switched between the desired channel modes. The ways data were sent from the transmitting PC and received by the target PC are described in the next section (Fig. 7.8 and Fig. 7.9). In the second experiment, we misaligned one of the LEDs by 1 cm. The response of the system is similar to that due to blocking. A simpler test method would be to use only one computer (MATLAB) to send data to itself and mark the transfer time using ‘tic’ and ‘toc’.

### 7.5 METHOD 2: MIMO-DIVERSITY SOFTWARE-CONTROLLED COM PORT SWITCHING

A simple UART white-LED transceiver (Fig. 7.5) has been designed and constructed for the COM port experiment as well as for the focusing gap experiment later. Fig. 7.6 shows the circuit of our transceiver.

To ensure accurate data from the experiment, channel transmission must be in its most basic form. The proposed transceiver has to be modulation free. That means

we send and receive data as they are, without altering the PC's EIA232 standard packet. The circuit consists of two operational amplifiers CA3140E. The first functions as a preamplifier and buffer, while the second functions as a comparator as well as a low-pass filter. CA3140E is a BiMOS operational amplifier with MOSFET input and bipolar output. It has a good speed performance up to 4.5 MHz. Alternatively, you may also use the low power op-amp LF357. The clock oscillator is only used to provide continuous light when there is no data transmission. Clock signals are sequenced with data signals in the D flip-flop. The MAX232CPE IC is used to convert signal levels between RS232 and TTL.

### 7.5.1 Test Setup and Experiment

Three people are needed during the experiment: one standing at each transmitting PC and one standing at the receiving PC. All will start the transmitting and receiving process at the same time by pressing the RUN button together. The transfer time is the time recorded at the receiver.

We set up the experimental circuit (Fig. 10.2) based on a simpler 2-by-2 matrix, i.e. using only a pair of white LEDs and a pair of PIN photodiodes. Three PCs were used: two PCs (each connected to a transmitter circuit) were used for sending streams of text data through their corresponding LEDs. The remaining PC (connected to a receiver circuit) was used only for receiving. Text were sent through the serial port by a MATLAB script on the respective transmitting PCs. The receiving PC used Microsoft's *HyperTerminal* (ZModem protocol) to receive text. All the terminals operated at the baud rate of 115200 bps.

First, we wanted to test both transmission schemes regarding their speeds to send  $M$  characters. For the MIMO scheme, we broke the string into two parts and used PC1 and PC2 to send  $M/2$  number of characters each. For the diversity scheme,  $M$  number of characters were simultaneously sent out through both emitters. Fig. 7.8 contains the codes for transmitting a stream of '1's through the serial port of the transmitting terminal. The receiving script of the receiving terminal is shown in Fig. 7.9.

Next, we tested the MIMO-diversity channel switching. A PIC microcontroller 18F4550 was connected to a third COM port. It detects voltages at the output of each op-amp and calculates the estimated transmitted power  $T_{est}$ . The calculated values are then sent back to the two transmitting PCs, where the MIMO-diversity negotiation program will decide between MIMO and diversity schemes (Fig. 7.10). The MIMO-diversity switching tests are similar to the hardware switching experiments. First, a finger was used to block the lightpath of one of the LEDs. Next,

a misalignment test was done by shifting an LED 1 cm out of LOS with the corresponding photodiode. For both the shadowing and alignment experiments, the switching speed of the MIMO and diversity COM ports is the same, i.e. 0.34s on the average (three readings were taken). The MIMO channel resumed when the finger was removed. A HIGH state at the photodiode triggers the microcontroller to turn on the MIMO scheme.

## 7.6 ANALYSES

We discovered that software-controlled COM port switching (Method 2) took a longer time to switch between MIMO and diversity than hardware circuit switching (Method 1).

Hardware switching is done by the SPST switch MAX325. This IC has a switching time of roughly 150ns, which means the MIMO circuit takes a shorter time to switch to the diversity scheme. Although hardware switching is faster, software switching is easier to customize based on changing environments. Finger blocking revealed that port switching needed about 0.34s while circuit switching was immediate. If we include the response time of the microcontroller, it would be about 170ns. However, 20ns is negligible, according to the Microchip datasheet.

Measured results in Table 7.1 indicate that the baud rates for pure MIMO transmission (Column 2) improve by twice that of pure diversity scheme (Column 3). In the MIMO-diversity technique, we sent  $N/2$  characters using the MIMO scheme, after which MIMO was made to switch to diversity by blocking and misalignment. Thereafter, the remaining  $N/2$  characters were sent using the diversity scheme. Timing was taken after the last character was received. If we include the time for port switching, the results are added by 0.34s (Column 4). In Column 5, the results are added by 150ns, which is the time taken for the hardware circuit to switch. This fast switching time is usually negligible in low-speed systems. The total time taken to transmit and receive  $N$  characters is calculated by Eqn. (7.4):

$$\tau_N = \tau_{N/2} + \tau_{switch} + \tau_{N/2} \quad (7.4)$$

The reader should note that it is only during these circumstances where switching will occur: (1) damaged LEDs, (2) blocked receivers (by shadows or objects), and (3) positional problems (symmetry) between the LEDs and photodetectors. In both the hardware and software switching methods, we intentionally misaligned the line of sight by shifting all the LEDs 1 cm out of symmetry with the photodiodes. Since the received optical power from all the photodiodes were

weak, the microcontroller did not activate the switch to change to diversity mode. This led us to add a NOR function to the microcontroller program, which will ensure that there will be a switch from MIMO to diversity when all the signals received are low.

**Table 7.1**  
Time taken to send  $N$  no. of characters

Number of Char.	MIMO	Diversity	Port Switching	Circuit Switching
40	0.0399s	0.0799s	0.3999s	0.0601s
80	0.0809s	0.1609s	0.4609s	0.1211s
120	0.1238s	0.2429s	0.5234s	0.1835s
160	0.1629s	0.3238s	0.5834s	0.2435s

The port switching prototype is a 2x2 configuration, whereas the circuit switching prototype is a 4x4 configuration. In principle, a 4x4 configuration should be twice as fast as the 2x2 version for MIMO transfers. However, both prototypes give almost identical values for pure MIMO (Column 2) and pure diversity (Column 3) transfers. There can be several reasons: (a) the limits of the RS232 protocol, (b) the spacing and brightness of the LEDs, and (c) the sequencing of the channel caused by the nature of the circuit.

## 7.7 OPTICS: FOCUSING GAP

During our experiments for text and file transfer, we discovered an issue that has to do with the distance between the photodiode and the concentrator. If we place the photodiode at the focal point of the concentrator lens, the concentrated intensity will render the photodiode unfunctional. No data will be transmitted. If we shift the concentrator slightly further away from the photodiode, data transfer resumes, but the shift distance cannot exceed a certain length. This raised our curiosity to investigate the focusing gap. It is necessary to find a way to determine the range of the optimum focusing gap.

To calculate the focusing length between the concentrator and the photodiode, we need to make use of the popular lensmaker's equation:

$$\frac{1}{f} = (n - 1) \left[ \frac{1}{R_1} - \frac{1}{R_2} + \frac{(n - 1)d}{nR_1R_2} \right] \quad (7.5)$$

where  $f$  is the focal length of the lens;  $R_1$  is the radius of curvature of the lens surface closest to the light source;  $R_2$  is the radius of the curvature of the lens surface farthest from the light source;  $d$  is the thickness of the lens;  $n$  is the refractive index of the lens material.

With the focal length obtained in (7.5), we propose *Png's focusing gap*, which is expressed as

$$P_{gap} = f \times s_r \times V_F \quad (7.6)$$

where  $s_r$  is the absolute spectral responsivity [A/W] and  $V_F$  is the maximum recommended forward voltage for the photodiode. The two parameters are usually specified in most datasheets. The diagram in Fig. 7.11 illustrates the focusing gap.

## 7.8 TEST SETUP AND EXPERIMENT

The circuit is shown in Fig. 7.6. At the front end of the receiver, we used a *Vishay BPV10* photodiode. It has an active area of  $0.78 \text{ mm}^2$ , bandwidth 250 MHz at  $V_R=12\text{V}$ ,  $I_{ra}=70 \text{ mA}$ ,  $\lambda_{0.1}=380$  to  $1100 \text{ nm}$ , and an angle of half sensitivity  $20^\circ$ . The *BPV10* has an absolute spectral sensitivity of  $0.55 \text{ A/W}$  and a typical  $V_F$  of  $1.0\text{V}$  (max.  $1.3\text{V}$ ) at  $I_F=50 \text{ mA}$ .

The LED used for the signal emitter is a normal 5mm cool-white LED. Its luminous intensity is 32900 mcd, viewing angle  $15^\circ$ ,  $I_F=20 \text{ mA}$ , and  $V_F=3.2\text{V}$ .

We experimented with 4 different types of concentrators at the receiver (Fig. 7.12). These are basically magnifying lenses old folks use for reading and can be purchased cheaply at any one-pound shops.

The setup of our experiment is illustrated in the diagram in Fig. 7.13. The transmitters were cross-connected with the transceivers, and each transceiver was connected to a desktop. A DC voltage of  $5\text{V}$  was supplied to each transceiver. Microsoft XP's *HyperTerminal* was used for text and file transfer.

### 7.8.1 Range of the Focusing Gap

We varied the  $P_{gap}$  as we keyed in the letter 'a' for each concentrator (Fig. 7.12). The range of the gap was recorded when the received letter appeared correctly for three consecutive lines (Table 7.2).

**Table 7.2**  
Focusing Gap of Concentrators (Calculated\* and Measured†)

Magnification Factor	Focal Length (cm)	$P_{gap}^*$ (cm)	$P_{gap}^\dagger$ (cm)
× 4.5	2.3	1.6445	1.7
× 6	3.2	2.2880	2.4
× 10	2.6	1.8590	2.0
× 15	1.2	0.8580	0.95

We used  $s_r=0.55$  and  $V_F=1.3V$  to calculate  $P_{gap}$ . Both parameters can be found in the datasheet for the PIN photodiode *BPV10*. The calculated and measured data are very close, suggesting the viability of Eqn. (7.6). In addition, it was noticed that the photodiode should not be placed directly at the focal point, as the light would be too intense to deliver any signal. We recommend a small offset of about 2mm. Another thing to note is that the glass/plastic covering the photodiode may also have some magnifying, filtering, and refractive characteristics.

### 7.8.2 Received Power Measurement

The received power of the photodiode was obtained by measuring the current at the photodiode output and then dividing it by the responsivity 0.55. The transmitter lightstand is 1.48m tall. Since the LED used has a viewing angle of  $15^\circ$  (which means its half angle  $\phi=7.5^\circ$ ), the cone radius on the surface of the table was calculated and measured to be approximately 20 cm. We took current and intensity readings at (a) the center of the cone, (b) 1/3 of the cone radius, (c) 2/3 of the cone radius, and (d) the rim of the cone. Interpolation was done to find the power along the cone slope. By doing so, we are able to compare the experimental and simulated versions of the cone. The readings in Table 7.3 were recorded without taking ambient light into account.

The third and fourth columns in Table 7.3 indicate that the channel gain  $H(0)$  is about 10.

**Table 7.3**Luminous Intensity (cd) and Current Readings ( $\mu A$ ) With Concentrator \* and Without Concentrator †

Photodiode Position	Luminous Intensity	Current*	Current†
Center of Cone	21.9	24.33	2.38
1/3 of Cone Radius	20.9	16.23	1.9
2/3 of Cone Radius	14.9	9.83	0.95
3/3 of cone Radius	6.6	4.88	0.46

## 7.9 MODIFICATION OF THE CHANNEL GAIN EQUATION

If implementation of the transceiver requires the concentrator to be moved, the channel DC gain [37] for visible-light communication can be expressed as

$$H(0) = \begin{cases} \frac{(m+1)A}{2\pi(d \pm P_{gap})^2} \cos^m(\phi) T_s(\psi) g(\psi) \cos(\psi) & 0 \leq \psi \leq \Psi_c \\ 0 & \psi > \Psi_c \end{cases} \quad (7.7)$$

If the implementation also requires the light source to be moved  $y$  distance, the channel DC gain [37] can be expressed as

$$H(0) = \begin{cases} \frac{(m+1)A}{2\pi(d \pm P_{gap})^2} \cos^m(\phi) T_s(\psi) g(\psi) \cos(\psi) \frac{d-y}{d} & 0 \leq \psi \leq \Psi_c \\ 0 & \psi > \Psi_c \end{cases} \quad (7.8)$$

$T_s(\psi)$  is the signal transmission coefficient of the filter (usually the value is 1.0);  $g(\psi)$  is the concentrator gain;  $\Psi_c$  is the receiver's half field of vision;  $\phi$  is the angle of irradiance;  $\psi$  is the angle of incidence;  $m$  is the order related to the transmitter's semi-angle at half power.  $A$  is the photodiode's active area; and  $d$  is the distance between the transmitter and the receiver.

$(d - y)/d$  is *Png's focusing ratio*, where  $y$  is the distance moved by the LED (emitter). Eqn. (7.8) may be used to determine the minimum channel gain to ensure good optical signal strength. Assuming that  $d$  is the distance from the emitter to the surface of the photodiode,  $P_{gap}$  is the longest distance the receiver (or the concentrator) can move without encountering errors. If the receiver must remain stationary, the concentrator can move  $\pm P_{gap}$ , but not exceeding it. The received power  $P_r$  is obtained by  $P_r = H(0) \cdot P_t$ . The concentrator gain  $g(\psi)$  is computed by [39]

$$g(\psi) = \begin{cases} \frac{n^2}{\sin^2 \Psi_c} & 0 \leq \psi \leq \Psi_c \\ 0 & \psi > \Psi_c \end{cases} \quad (7.9)$$

where  $n$  is the refractive index of the lens.

In short, there is a problem with the current white-LED communication channel model: that is, gain  $H(0)$  is influenced only by the distance  $d$  between the transmitter and receiver. When  $d$  decreases, gain increases. It assumes that the concentrator always gives an ideal focal point at the photoreceiver. The focal length and focal range of the concentrator, together with its relationship with the photodiode, are somehow forgotten in the full picture. If we take these optical issues into account, ‘gain is inversely proportional to  $d$ ’ will no longer be true. Eqn. (7.8) is therefore a more accurate formula.

## 7.10 CONCLUSION

The authors have proposed two practical techniques for solving alignment and shadowing problems in visible-light communication systems by the use of self-deciding channel-switching techniques. The first method is an auto-switching circuit that switches between MIMO and diversity. This is a straightforward and faster circuit. The second method is a more tightly-controlled but slower technique. The receiver decides the scheme to use by comparing the estimated transmitted signal power with the ideal threshold power. The estimated transmitted power is computed by the receiver by multiplying the received power with the inverse of an existing transfer function matrix. In the future, smart MIMO systems like these will be even more efficient as it can be further customized to control the modulation techniques in LED clusters for ill-conditioned light matrix. The channel gain equation has also been improved by considering the focusing gap of the concentrator. This is important because VLC mobile devices require consumers to have knowledge of the optimal focusing distance to perform an efficient information or file transfer.

The authors have proposed two practical techniques for solving alignment and shadowing problems in visible-light communication systems by the use of self-deciding channel-switching techniques. The first method is an auto-switching circuit that switches between MIMO and diversity. This is a straightforward and faster circuit. The second method is a more tightly-controlled but slower technique. The receiver decides the scheme to use by comparing the estimated transmitted signal power with the ideal threshold power. The estimated transmitted power is computed by the receiver by multiplying the received power with the inverse

of an existing transfer function matrix. In the future, smart MIMO systems like these will be even more efficient as it can be further customized to control the modulation techniques in LED clusters for ill-conditioned light matrix. The channel gain equation has also been improved by considering the focusing gap of the concentrator. This is important because VLC mobile devices require consumers to have knowledge of the optimal focusing distance to perform an efficient information or file transfer.

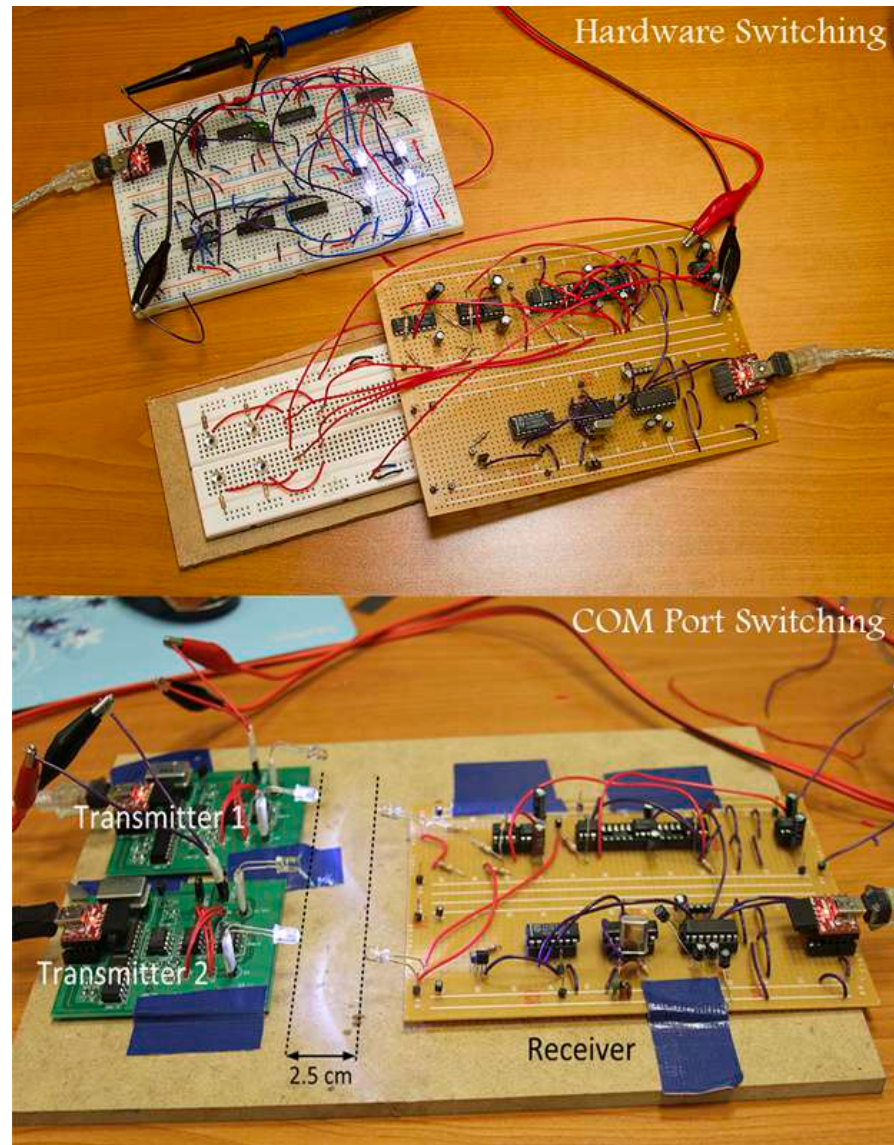


**Figure 7.1** Initial constructions of the two systems for MIMO-diversity channel switching: (top) circuit switching; (bottom) COM port switching.

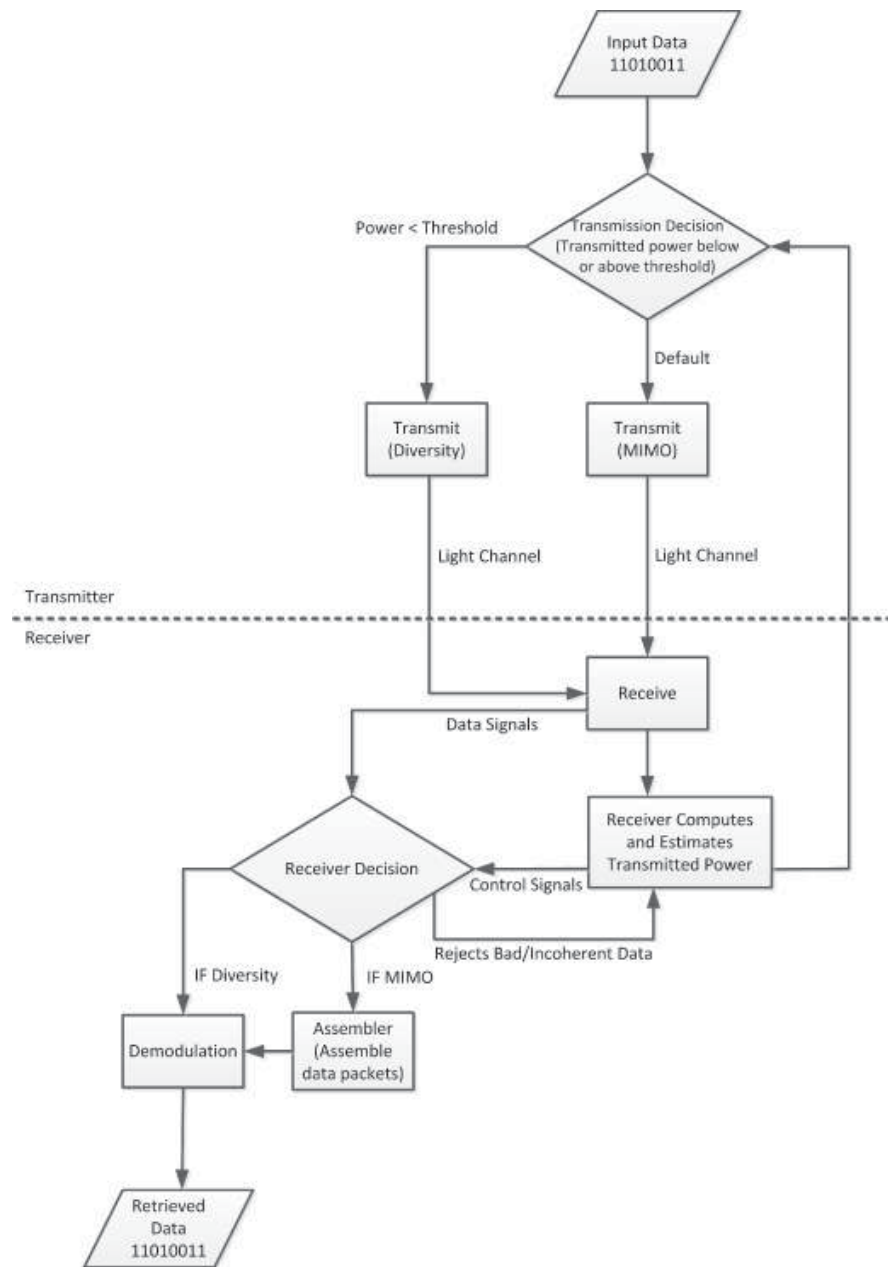
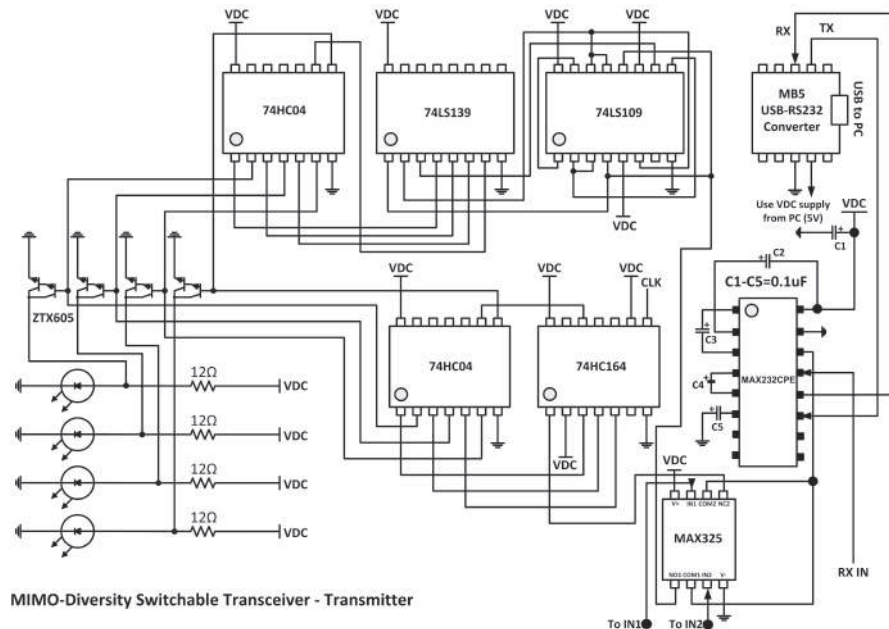


Figure 7.2 A flow chart of the diversity-MIMO switching technique.



**Figure 7.3** MIMO-diversity circuit-switching transceiver: transmitter circuit.

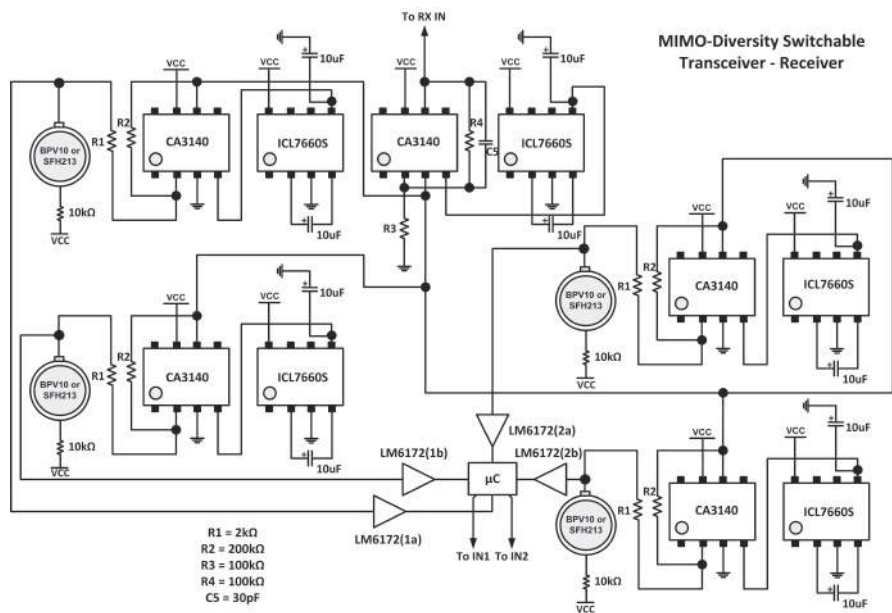


Figure 7.4 MIMO-diversity circuit-switching transceiver: receiver circuit.



**Figure 7.5** Photo of the serial transceiver.

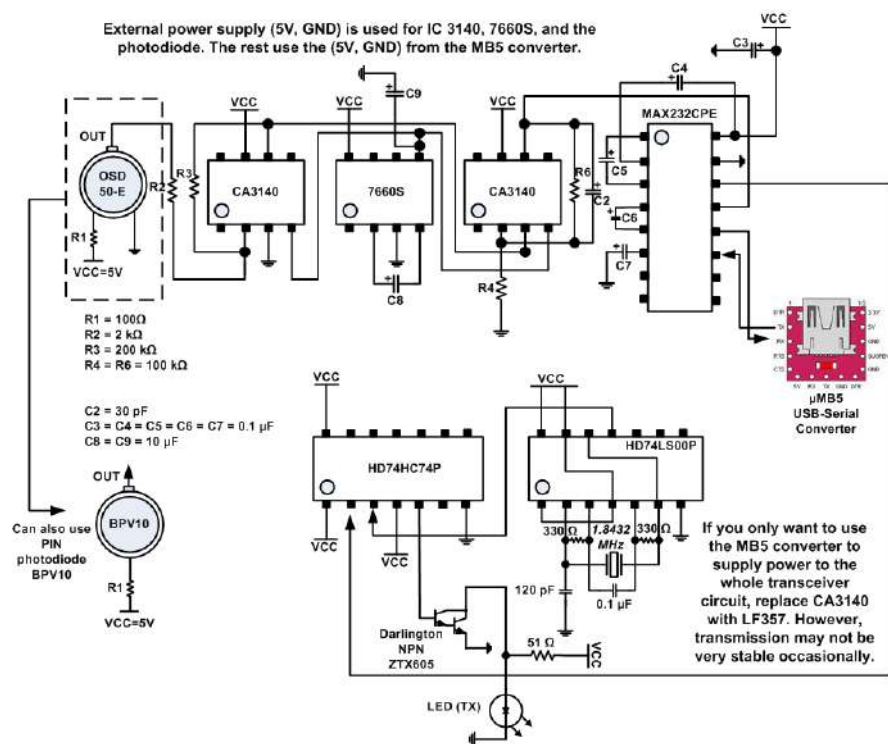
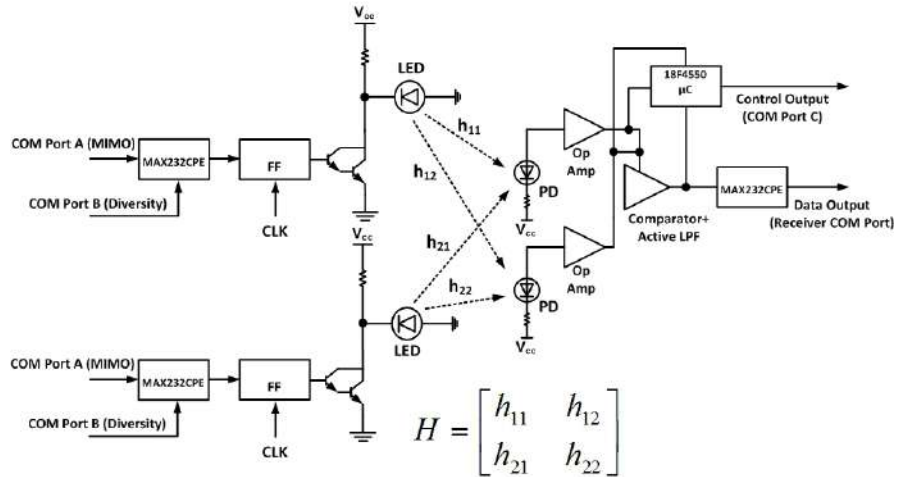


Figure 7.6 Schematic diagram of the transceiver.



**Figure 7.7** MIMO-diversity COM port-switching technique: a 2-by-2 configuration. Blocking and misalignment cause the pair of transmitting PCs to switch to diversity COM ports simultaneously.

```

serialport = serial('COM3');
set(serialport,'BaudRate',115200,'DataBits',8,
'Parity','none','StopBits',1,'FlowControl',
'none')
fopen(serialport);
tic
%For MIMO, x is iterated 20 times by each PC,
%so that both PCs transmit 40 '1's together.
%For diversity, x is iterated 40 times so that
%40 '1's are sent to the
%transmitters at the same time.
for x = 1:20
fprintf(serialport,'%s','1');
end;
toc
fclose(serialport);
delete(serialport)
clear serialport

```

**Figure 7.8** MATLAB codes for serial port transmission.

```

serialport = serial('COM3');
set(serialport,'BaudRate',115200,'DataBits',8,
'Parity','none','StopBits',1,'FlowControl',
'none')
fopen(serialport);
tic
%out is the received signal.
out=fscanf(serialport);
toc
fclose(serialport);
delete(serialport)
clear serialport

```

**Figure 7.9** MATLAB codes for serial port reception.

```

.....
if (detectedPD<ThresholdVolt)
%Port 1 is diversity scheme, which is direct parallel
%transmission through all the LEDs using a 74HC164.
ZModem.ZModem zm1 = new ZModem.ZModem(port1);
zm1.ZmodemTransmit(buffer, length);
else
%Port 2 is MIMO scheme. (Data goes through
%a 4-phase generating circuit using a 74HC109 and a 74HC139 before
%going out through their respective LEDs.)
ZModem.ZModem zm2 = new ZModem.ZModem(port2);
zm2.ZmodemTransmit(buffer, length);
end;
.....

```

**Figure 7.10** C# codes for MIMO-diversity port switching.

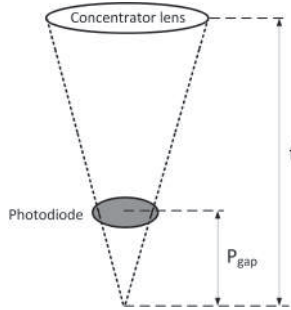


**Figure 7.11** Diagram illustrating the focal length  $f$  and the focusing gap  $P_{gap}$ .



**Figure 7.12** The variety of concentrators tested in our experiment.

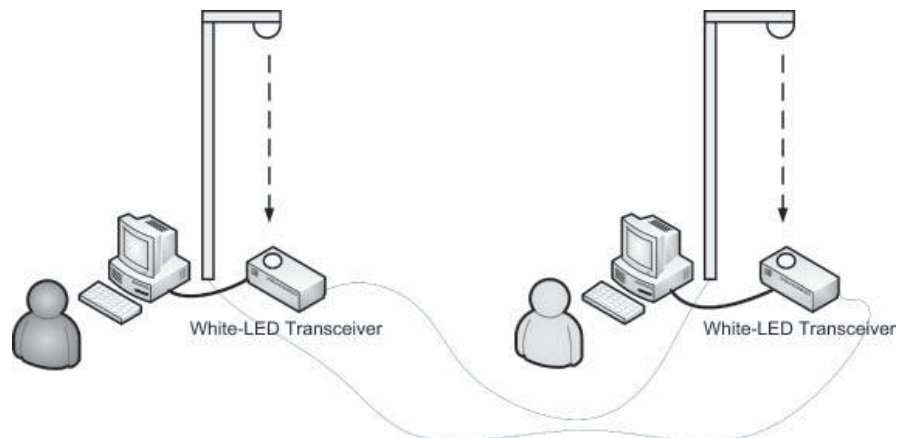


**Figure 7.13** Test setup for SISO communication.

# **Chapter 8**

## **Optical Infrastructure for VLC for Public Housing and Commercial Buildings**

### **8.1 ABSTRACT**

We propose a free-space optical system to replace wireless LAN in commercial and residential premises. Closing the last mile using wireless optical (WOP) communication provides the advantages of a cableless environment, mobility freedom, and faster data transfer rate. Trunk optical signals from the metropolitan core terminate at the optical control panel (OCP) in premises, after which signals are filtered, recoded, and emitted via LEDs to the different areas of the house or office. Photoreceivers, on the other hand, absorb light signals and convert them back to electrical signals for the devices. Since light has become the medium of communication, a few devices have been proposed so that transmission and reception of optical signals are optimized.

### **8.2 INTRODUCTION**

Famous historical applications of free space optical transmission [1] include the Chappe telegraph, Mangin's optical telegraph, the heliograph, and Alexander Graham Bell's photophone. Although gaining popularity, free-space optics, unlike wired optics, is a telecommunication technique that has not been fully developed and utilized. Wired optics has already been widely used in present-day communications. In the next ten years, wireless optics is likely to become an integral part of the

wireless family, especially in indoor environment like homes, offices, classrooms, and industrial premises [2-6].

WOPCOM is an extension technology that is designed to solve FTTD's (Fiber-to-the-Device) problems. In the FTTH (Fiber-to-the-Home) delivery network [7,8], optical signals from service providers reach homes or office premises via the optical network terminal (ONT). However, the "last mile" to devices is usually connected by Ethernet coaxial cables from the ONTs. Inefficiencies in transmission therefore arise due to the differences between optical and Ethernet characteristics. In other words, the speed of light is not effectively exploited up to device level. One of the objectives of WOPCOM is to eliminate the use of cables and wires between as many communication devices as possible. WOPCOM aims to transmit information wirelessly not only between devices, but also between devices and multiple services that are provided to homes and offices. For example, a speaker and a TV screen do not have to be connected to a DVD player by audio and video cables; a PC CPU can go online without connecting to the Internet modem and operate without connecting to the mouse, keyboard, LCD monitor, and printer via Ethernet, USB, or video cables; pictures in a digital camera can be downloaded onto a PC CPU without a USB cable or can be displayed directly on a projection screen or TV without the need for a video cable. Block diagrams have been provided in Fig. 1 to visualize this implementation.

The proposed wireless optical communication (WOPCOM) system is a high-speed, high-capacity technology that transmits information by the use of optical light over free space. WOPCOM technology operates a little differently from the existing optical networks [9-14]. By converting data into optical signals in Pulse Position Modulated format (PPM) and transmitting via light from white LEDs or exposed optical tubes, WOPCOM allows light to provide illumination and even light-converted energy while enabling information to be exchanged freely among devices and services.

The paper is divided into hierarchical sections, starting from the broader metropolitan network, building layout, right down to the WOPLAN operations and devices.

### **8.3 SPIDER-WEB METROPOLITAN AREA NETWORK**

Current MANs use mesh topology. For a more organized MAN network, a spider-web topology (Fig. 2) has been proposed to introduce scalable optical paths. The spider-web architecture is a variant of the star network. Both have a centralized

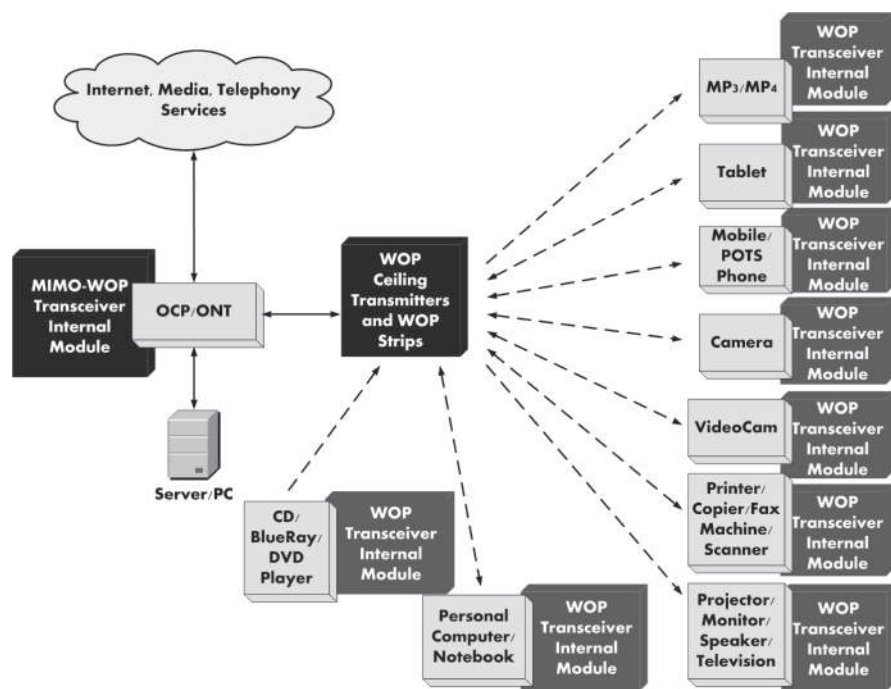


**Figure 8.1** Multi-device WOPCOM transmission.

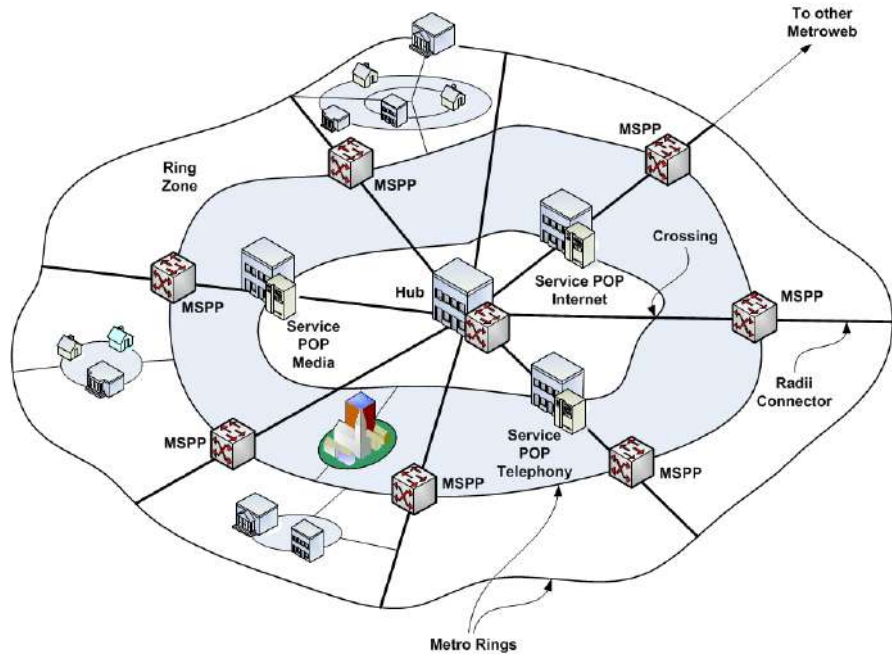


**Figure 8.2** Metropolitan spider-web architecture for SONET.

optical hub. The difference is that a spider-web MAN introduces concentric rings expanding from the city to the suburbs on top of a star architecture.

A spider-web topology can be integrated with the SONET metropolitan area network. This hybrid combination is called a WOP Metropolitan Area Network (WOPMAN). A WOPMAN is MSPP (Multiservice Provisioning Platform) based [11,12] and may run on the traditional ring or the spider-web metro network. The center of the web is the WOPCOM hub belonging to the metropolis. The hub network architecture accommodates unexpected growth and change more easily than other networks. A hub concentrates traffic at a central site and allows easy reprovisioning of subnetworks. The spider-web MAN architecture is hub-based for this reason, and by combining with the concentric ring architecture, it enjoys the strengths of both ring and hub network topologies, thus allowing cross-connection of tributary services at tributary level.

Radius connectors (RC) transport bulk information to and from the rings. WOPMAN rings follow a concentric model which span from the city center to the outer rings of suburbs. The RCs are critical optical canals that pump optical signals to each ring. Any building can be directly connected to more than one ring, but only government buildings can be directly connected to an RC. For security purposes, a major government building can connect to more than one RC, so that the building can still access another RC if the connection to one RC is broken. In brief, the main advantages of a spider-web architecture are: (1) any segment of a ring or RC can be shut down for maintenance; (2) any node can be switched to another ring or radius connector flexibly; (3) scalability: rings can be expanded and RCs can be extended. A regenerator [11] is needed to recondition weak optical signals at the crossing between a ring and an RC, depending on the distance and strength of the optical signals between each crossing. The role of a regenerator is to remove noise, jitter, and distortions, and amplify signals. A smaller spider-web or a ring network is allowed inside a ring zone. A ring zone is defined as an area on a spider-web network that lies between two adjacent rings and two RCs.

#### **8.4 INTER-BUILDING AND INTRA-BUILDING WIRING**

Distribution of backbone capacity to the tributaries can be quite challenging, especially when we define the internal layout of a building premise. Fig. 3 illustrates the levels of architecture from the MAN to the WOPLAN (Wireless Optical Local Area Network) and to the WOPPAN (Wireless Optical Personal Area Network). At the top level, there is the SONET MSPP MAN working as the backbone of WOPLAN. The MSPP combines the different levels of technologies and transmission techniques to provide a converged set of services to the public [10-14]. The said services - PSTN, Internet, cable media - are delivered to WOPLANs through the OCP.

Inter-building cabling [7,15,16] can be in the form of a simple ring, star, or of a more complex spider-web topology. A spider-web inter-building wiring topology is characterized by a centralized hub (i.e., the district switch) which connects a particular group of buildings or residences to the MAN SONET.

The end-user building wiring topology [7-9] for WOPCOM can be a lateral connection from one of the breakout points of the WOPMAN. The internal wiring of a building is basically a star approach (Fig. 4). Optical signals from the district switch are passed to the building's centralized switch. From the centralized switch, optical signals are distributed to the OCPs belonging to different storeys and offices.

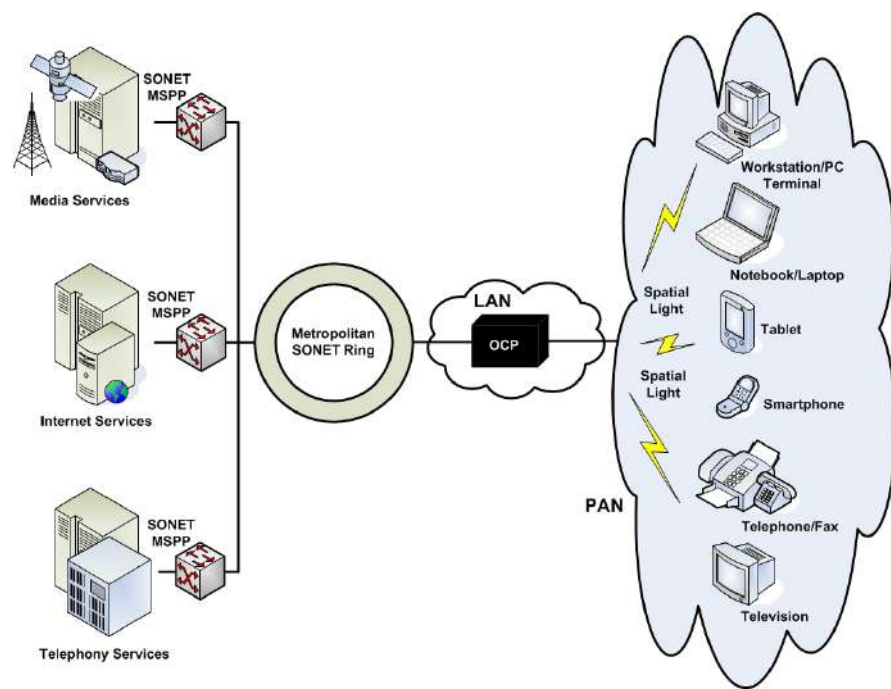


**Figure 8.3** Service-to-device WOPCOM network via SONET (from LAN to PAN).

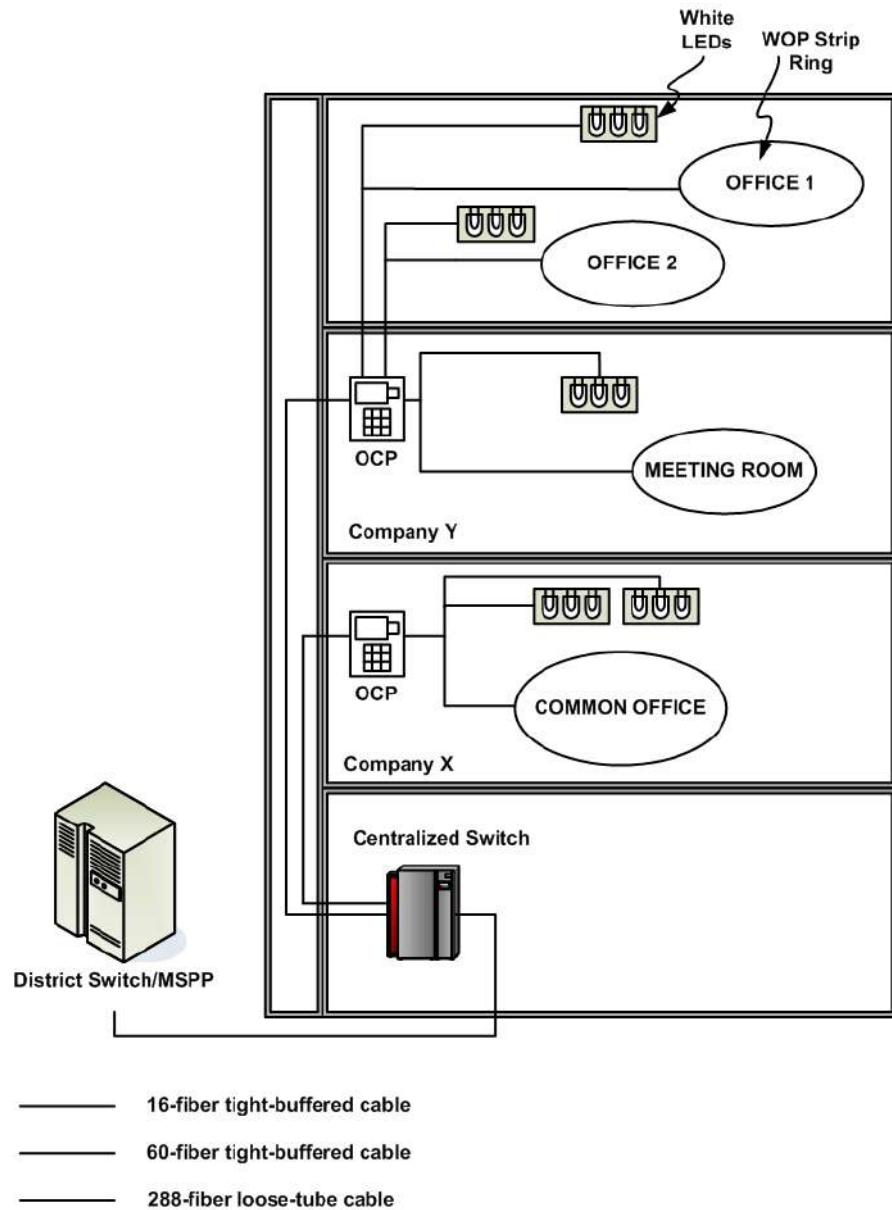


**Figure 8.4** Star-ring intra-building wiring for WOPNET.

A district switch is in fact a SONET edge optical switch between a MAN and a building [7-9]. SONET trunk cables terminate at each building's local switch where a star topology is used to supply bulk signals to the rest of the floors or offices. In the next stage, each floor or office has an OCP to form an individual WOPLAN. The OCP is the entry point for subscribed services or information to enter a LAN. For instance, in Fig. 4, Company X and Y have separate OCPs, each serving their own companies. Company X has only a common office. Therefore, it only needs a WOP strip around the premise and two WOP ceiling transmitters to cover the large area. Company Y has two offices and a meeting room; hence ceiling transmitters and WOP strips have to be individually installed within the respective rooms.

## 8.5 WOPCOM IN OPERATION

WOPCOM technology is implemented in two types of connections (Fig. 5): (1) service providers to devices. With WOPCOM, PSTN, Internet, and media service providers are able to provide voice, data, and video services directly to devices (e.g. PC, POTS (Plain Old Telephone Service) phone, television) in homes and offices via white LED light or direct optical light from WOP strips. The use of Ethernet, video, or phone cables are not required. (2) devices to devices. Devices in homes or office can communicate with each other via white LED light or direct optical light from WOP strips. The use of USB, serial, and parallel cables is not required.

WOPCOM is an indoor wireless system that enables simultaneous communication for data, voice, and video signals between a wide variety of devices. Shown in Fig. 6, optical signals can be transmitted to devices (CPU, notebook, printer, fax and POTS phone, smartphone, tablet, MP3) by the ceiling transmitter or the WOP strip transmitter. The WOP strip receiver receives optical signals from these devices and delivers them to their specific destinations via the OCP. For bulky devices (such as a photocopier machine) that are difficult to be moved around, a WOP strip can be installed individually near to such devices. Mouse, keyboard, LCD/LED monitor, and speakers communicate with the CPU directly via their own transceivers by pointing. If the printer is near the CPU, communication between them does not have to go through the OCP. In the living room, subscribed TV programs, Internet, and PSTN services are delivered via the OCP. The TV receives cable/optical television programs from the ceiling transmitter. Since speakers, CD/BlueRay/DVD player, video game console, and TV screen are generally near one another, they are able to communicate by direct line of sight.

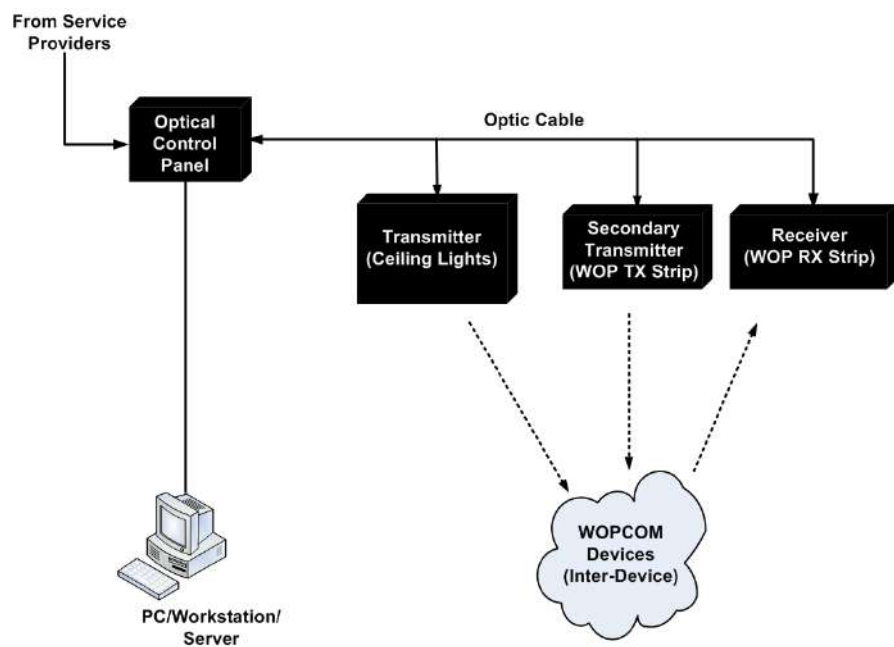


**Figure 8.5** WOPCOM methods of access.

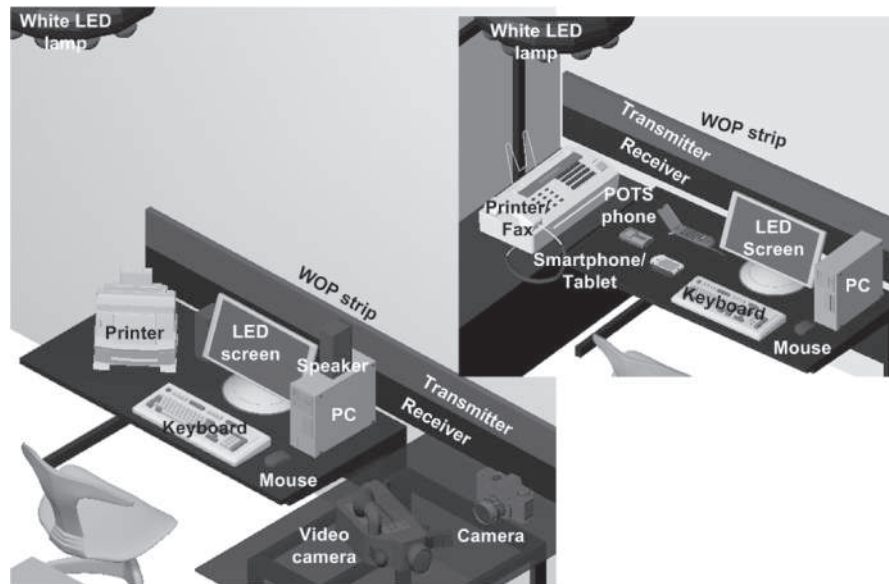


**Figure 8.6** WOPLAN operation indoors.

## 8.6 WOPCOM DEVICES

Besides the proposal for a spider-web network as the backbone for WOPCOM applications, a few communication devices have been proposed to generate light of human-suitable wavelengths and optimize lightpaths for optical communication. The optical devices presented below are the optical control panel, the WOP ceiling transmitter, and the WOP strip.

### 8.6.1 Optical Control Panel (OCP)

The proposed OCP (Fig. 7) comprises of three units: the WOPLAN configuration unit, the optical converter, and the optical router. The ROADM (Reconfigurable Optical Add-drop Multiplexer) [10,11] is built within the optical router. The configuration unit is used for the allocation of channels and slots for the WOPCOM devices and users on the WOPLAN respectively. It consists of a small LCD display, a small keyboard, and a programmable controller. The optical converter comprises of a light mixer and a TDM-PPM/PPM-TDM converter. The light mixer contains a wavelength converter and a white light laser. Incoming signals from the SONET MAN are in DWDM format and transmitted by TDM. DWDM signals normally have longer wavelengths that are over 1000 nm. Indoor illumination requires visible white light; therefore, DWDM wavelengths must be converted to wavelengths of the visible spectrum at the wavelength converter and then to white light by the white spectrum laser. After conversion from TDM to PPM format at the TDM-PPM converter, white light optical signals are passed to the optical router to be sorted into their respective destinations and finally sent out. Returning PPM signals from the devices need not be white optical signals. Wavelengths in the green spectrum are used to identify WOPCOM devices because (1) green is more friendly to the eyes compared to other colors; (2) the green wavelength is suitable for propagating optical signals over short distances such as a WOPLAN. Returning PPM signals are first converted back to TDM signals at the PPM-TDM converter and then upgraded back to long-wavelength signals at the wavelength converter. The white light laser provides signal regeneration which gives boost to outgoing TDM signals by amplifying itself to the associated wavelengths. The said signals are eventually sent out to the SONET MAN via these lasers in the OCP. For every WOPLAN, there is an OCP that supplies incoming data to devices. Being the terminal between a MAN and a LAN, the main job of the OCP is to manage all incoming and outgoing optical signals inside a WOPLAN. A home or a small office normally needs only one OCP. Users and devices for a personal area network can be configured by the subscriber

directly via the configuration unit installed on the OCP or by connecting the OCP to a PC whereby the subscriber configures via software.

### 8.6.2 WOP Ceiling Transmitter

The proposed WOP ceiling transmitter (Fig. 8) comprises of a group of white LEDs and a converter to convert PPM optical light to PPM current. The current is then used to drive the group of LEDs to provide illumination and transmit optical signals.

The ceiling transmitter is the main transmitter of optical signals from the OCP. When the ceiling transmitter is not required and needs to be switched off during the night, the WOP transmitter strip will act as a secondary transmitter (Fig. 9).

### 8.6.3 WOP Strip

The proposed WOP transmitter strip (Fig. 10) comprises of a transparent optical tube, a diffuser, a magnifying filter, and a cover. At each end of the WOP transmitter strip, there is a WOP-strip-to-fiber-interface. A WOP receiver strip comprises of a series of organic photovoltaic cells and a contrast filter. At each end of the WOP receiver strip, there is a PPM demodulator and a WOP-strip-to-fiber-interface. The transparent optical tube is a waveguide as well as an emitter for optical light from the OCP. The magnifying filter is used to magnify optical signals emitting from the transparent optical tube. On top of the magnifying filter, the diffuser (a specially-made lens similar to a camera's diffuse filter) is used for diffusing (or scattering) the magnified optical signals in order to soften their intensity for a more soothing indoor environment. The cover can be used to prevent glare when the transmitter strip is not in use, and can also be used as a waveguide because it can prevent optical signals to propagate in another direction by partially covering a certain transmission angle. Organic photovoltaic (or solar) cells are used for the receiver strip due to their bendable and ultra-thin characteristics. In WOPCOM, information is encoded in PPM format; therefore a contrast filter is used to generate more distinctive pulses in the optical signals before they enter the photovoltaic cells.

The application of WOPCOM also triggers a wide range of modifications to communication devices. If the back surface of the LCD/LED monitor, the top and side surfaces of the CPU, and the top surface of the notebook are installed with photoreceivers (as well as LED emitters), optical signals and light energy will be able to reach and serve these devices effectively (Fig. 11). A proposed architectural system design of such a device is shown in Fig. 12. If a WOPCOM device is fixed and not mobile, the area with the most direct incidental contact with

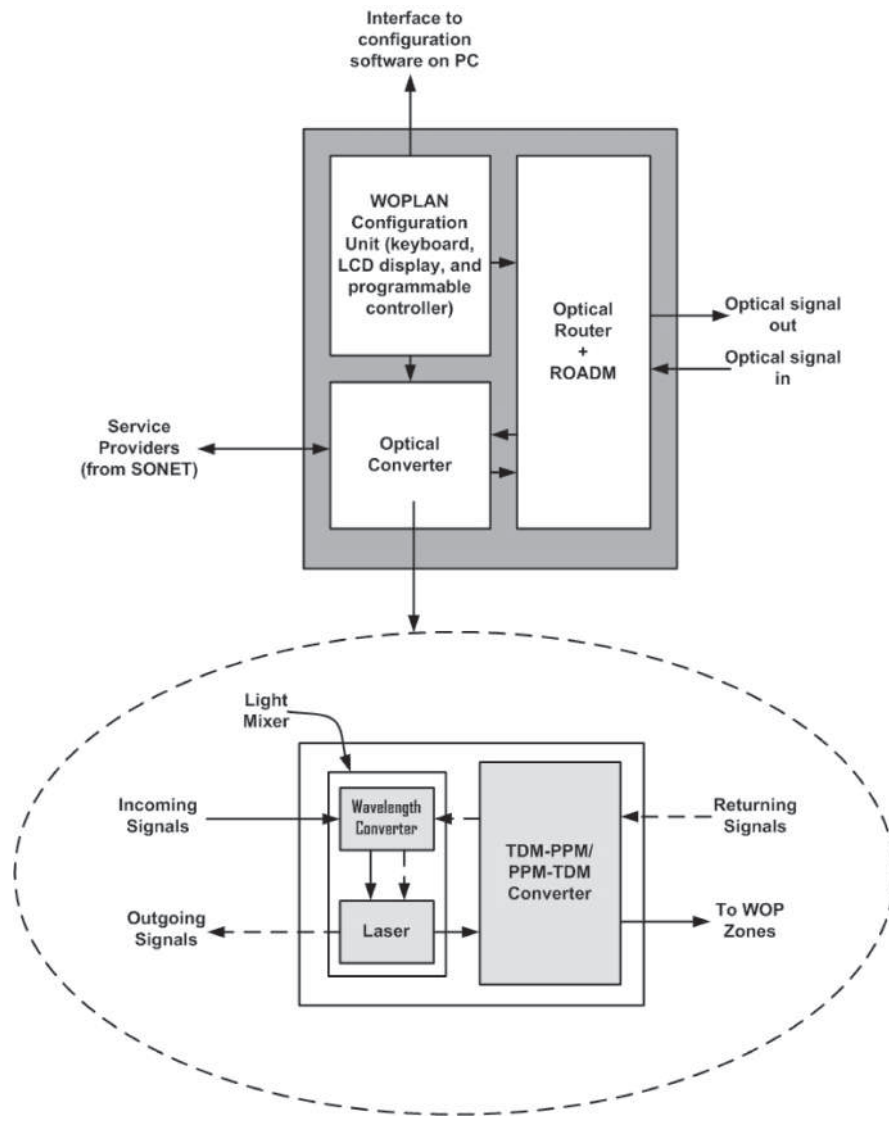


**Figure 8.7** Optical control panel (OCP).

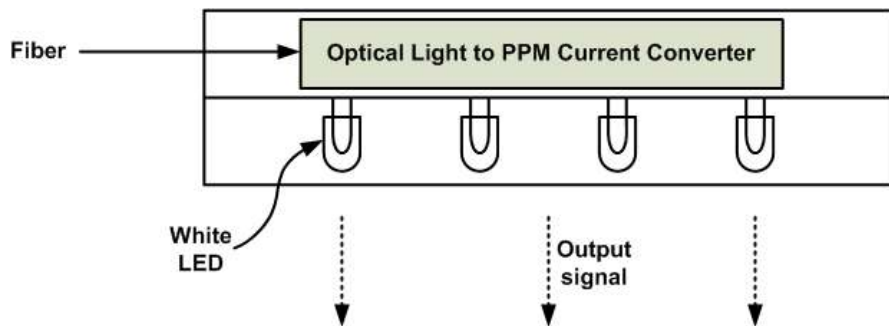


**Figure 8.8** WOPCOM ceiling transmitter.

the light transmission should be chosen as the receiver surface. In some cases, extra photovoltaic cells or plates might be necessary.

In a WOPLAN, WOP ceiling transmitters and WOP strips are installed on ceilings and walls respectively. Devices receive optical information from the ceiling transmitters and transmitter strips, while optical signals from devices are sent out through the WOP receiver strip. WOPCOM devices receive PPM signals from WOP ceiling transmitters, WOP transmitter strips, or directly from the light emitted by transmitters of other WOPCOM devices. White optical light is generated by lasers in the OCP. It passes through the optical cables and is delivered through the transparent optical tubes in the transmitter strip. The fiber-to-WOP-strip interfaces connect optical cables to WOP strips.

In a WOPCOM connection for an apartment or office (Fig. 13), a WOP strip is connected in a loop or ring, whereas a WOP ceiling transmitter is installed at the end of a bus branch. A bus branch is an extension from a bus. There can be many buses extending from the OCP, thus forming a star-bus-ring hybrid network. A set of rings connected to a bus forms a bus-ring cluster.

## 8.7 CONCLUSION

The authors have presented a set of infrastructure for the wireless optical age. Due to the large demand for convergence in digital consumer electronics, WOPCOM technology could manifest itself as the next-generation access medium since RF

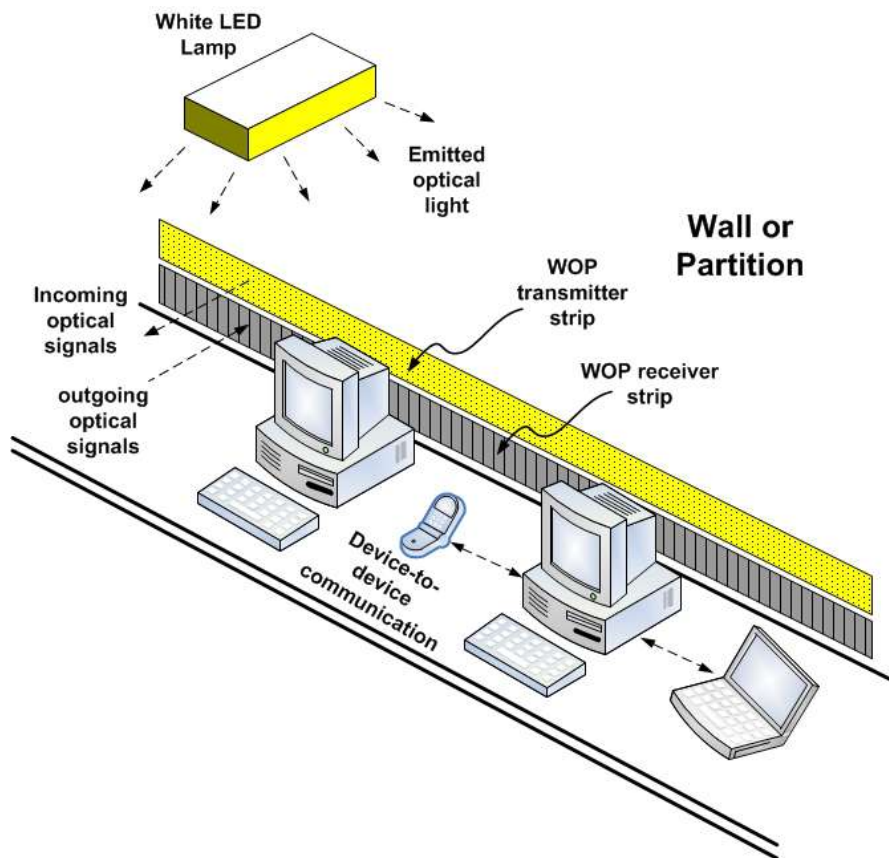


**Figure 8.9** Installation of WOP strip and ceiling transmitter.

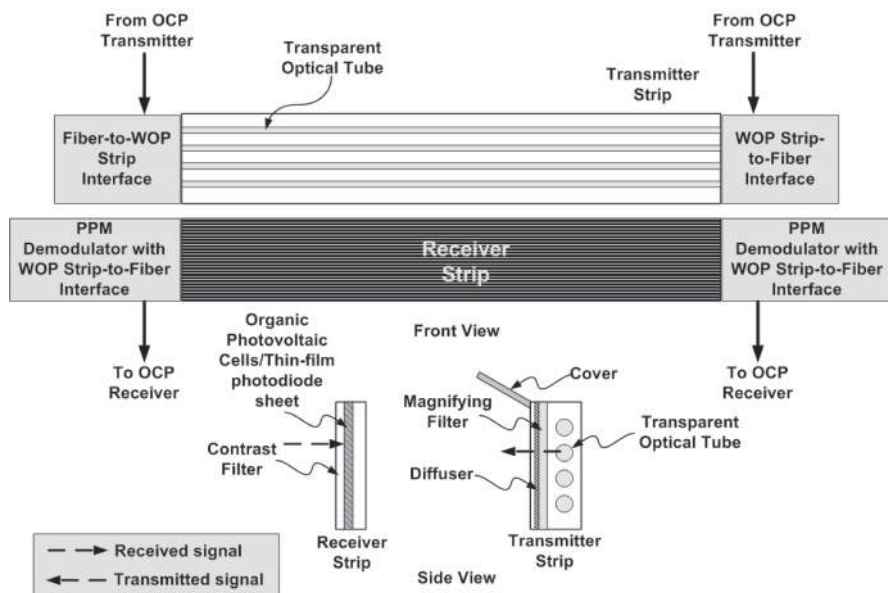
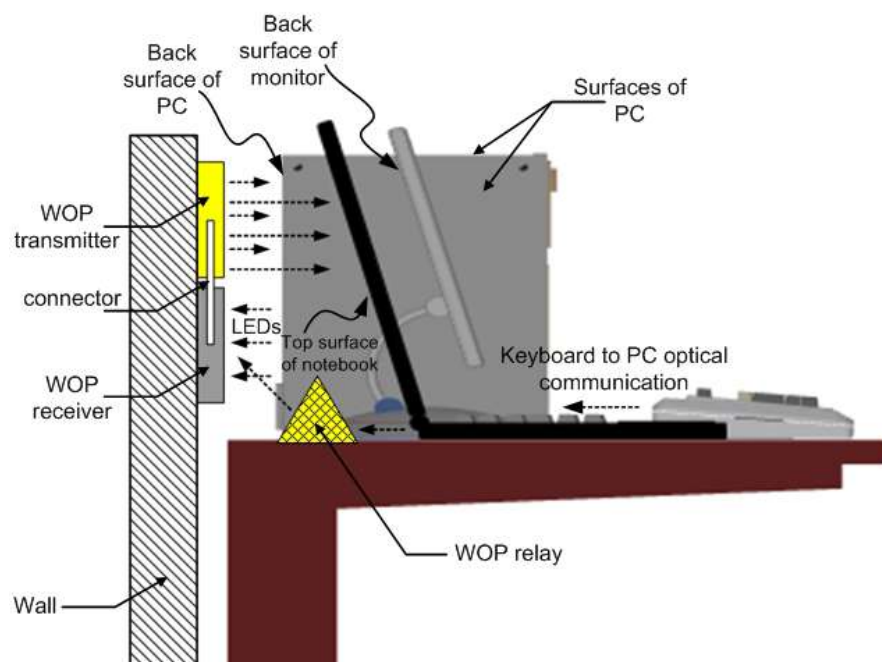
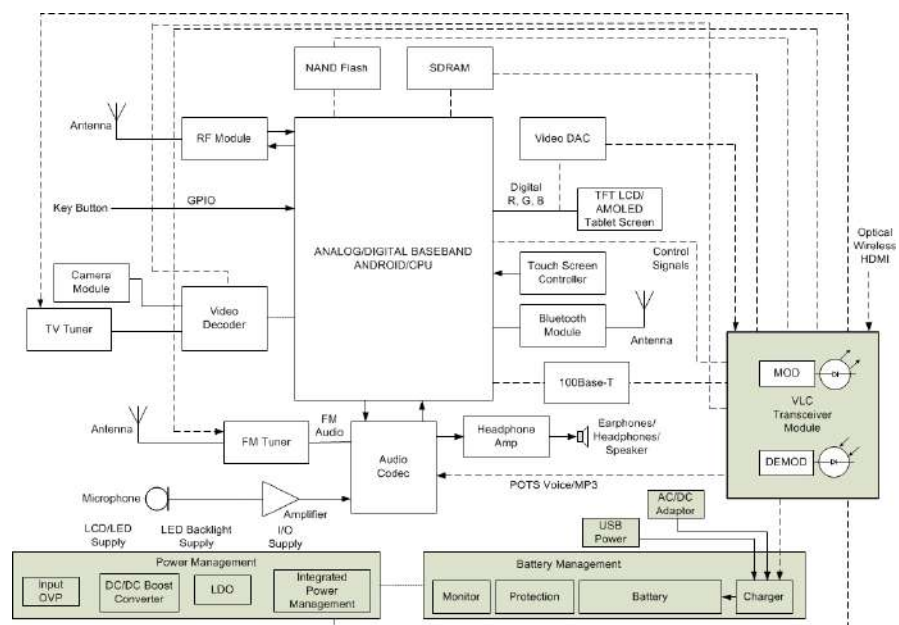


Figure 8.10 WOP strip components and design.



**Figure 8.11** WOPCOM implementation for desktop devices.



**Figure 8.12** Architecture implementation of WOPCOM system on a smartphone/tablet/computer motherboard.

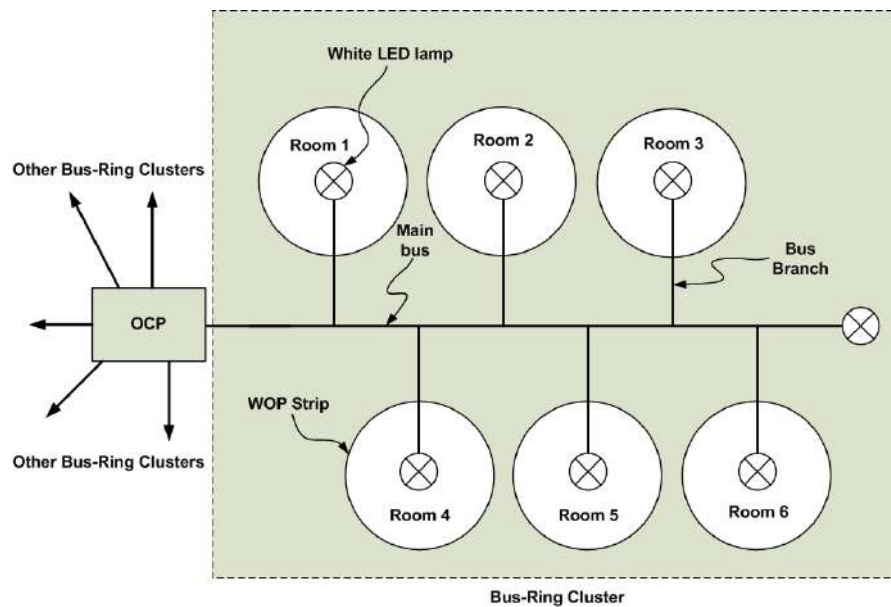


**Figure 8.13** Star-bus-ring topology LAN wiring for WOP ceiling transmitters and WOP strips.

microwave have not been keeping up with the bandwidth capacity of optical systems.

WOPCOM is targeted to improve network behavior in relation to transparency, wavelength capacity, service aggregation, and density. The strengths of WOPCOM are: (1) mobile, high-speed, and free-space access without cables; (2) multiple types of data and services on one fiber; (3) scalable and contention free: one-to-one channel to device dedication; (4) security: users are allocated by slots on a transmission channel.

It is conceived that it would be feasible to close the “last mile” with a wireless optical connection. Demands for faster data transfers and Internet accessibility would grow in the future. Therefore, providing free-space optical light as another medium of transmission in a LAN environment could ensure constant future needs because light is the ultimate speed. “Cableless” transmission of voice, files, cable television, and Internet services would enjoy greater flexibility and convenience.

# Chapter 9

## Designs of VLC LAN Transceivers

LAN VLC systems are the most difficult to make because there will be lots of tuning and changes. Most cannot get past the 10base-T (10 Mbps) mark. It should be noted that LAN is an analog system. It should be approached from the perspective of analog system design. If you are good in analog-digital conversion, you should remake the whole system to become fully digital. However the challenge is still there, since the IEEE standard has been there for decades and the protocol is widely used. It is not going to be easy.

In this work, the authors investigate the designs of high-speed VLC LAN transceivers. 10base-T (10 MHz) VLC systems have been widely discussed and demonstrated. However, 100base-T (100 MHz) systems are not often talked about and demonstrated at conferences.

### 9.1 CHOOSING THE LAN CONNECTOR

The choice of the types of RJ45 connector is very important. Do you know of the famous Raspberry Pi? Why was there a delay in its first batch of release? The delay was actually caused by that. The manufacturer used an RJ45 that has no magnetics (or transformer). It looks like a very small problem, but that is the fun of it, the whole device was unable to work.

A good lesson learnt. If you want to learn more of this hiccup, you may go to this website to have a good read. It is very interesting! <http://www.raspberrypi.org/archives/781>.

Well, let us be clear about how RJ45 with and without magnetics look like.

RJ45s without built-in magnetics have 8 pins where 4 are redundant [56]. Two twisted pairs - 1 differential pair for TX and 1 differential pair for RX - are the standard Ethernet interface.

I leave it to you guys to google why they have to be differential. Now the next big question: why do we need the transformer circuitry for the RJ45?

The fundamental reason is actually to isolate the power supply between the PC and the external circuit and to prevent blowing up the network interface card (or NIC) in your PC. Imagine if you have a short circuit accidentally in the external circuit which you are building, the current surge will burn the NIC. Of course things may not be as simple as it looks. Here is a more technical explanation ripped from the Internet.

*"The correct answer is because the ethernet specification requires it. Although you didn't ask, others may wonder why this method of connection was chosen for that type of ethernet. Keep in mind that this applies only to the point-to-point ethernet varieties, like 10base-T and 100base-T, not to the original ethernet or to ThinLan ethernet. The problem is that ethernet can support fairly long runs such that equipment on different ends can be powered from distant branches of the power distribution network within a building or even different buildings. This means there can be significant ground offset between ethernet nodes. This is a problem with ground-referenced communication schemes, like RS-232. There are several ways of dealing with ground offsets in communications lines, with the two most common being opto-isolation and transformer coupling. Transformer coupling was the right choice for ethernet given the tradeoffs between the methods and what ethernet was trying to accomplish." [57]*

## 9.2 TRANSFORMER CIRCUIT

Now, let us have a look at what really are inside an RJ45 breakout board with magnetics. Fig. 9.2 is the internal transformer coupling circuit for the RJ45 connector HANRUN HY911103A [58].

For P3 and P6, you have to feed in a power supply of 3.3V. For example, if your transceiver circuit uses 5V, you need to use a voltage converter (LM1117-3.3) to supply these two pins with a 3.3V. P4, P5, P10 and P11 are all grounded.

The left side connects to your VLC circuit board. The right side (UTP) is of course where you plug in your CAT 5 cable connecting to your computer. Fig. 10.4 shows a simple VLC circuit for 10Base-T LAN. The TX and RX pairs of I/O on the left connect to the respective pins of the HY911103A breakout board in Fig. 9.2.

The LM7171 is a very high speed, voltage feedback amplifier. It consumes only 6.5 mA supply current while providing a unity-gain bandwidth of 200 MHz and a slew rate of 4100V/s. It also has other great features such as low differential gain and phase and high output current.

If you need to combine the TX+ and TX- signals to get a single output, you need three 7171 ICs to do a proper combination of the differential video signals. This circuit is available in the 7171 datasheet.

Alternatively, you may use the AD8130 IC (or other ICs that are similar). It already has three ICs built in which can also convert a differential line to a single-ended line. This single-line signal is then be transmitted out via a white LED.

At the receiver you need one more IC, the LM7171, to amplify light signals received by the photodiode. After that, the AD8131 is used to convert this signal back to differential outputs. This pair RX+ and RX- go to the receiving device. For the whole duplex operation, you need a pair of transceivers to work (Fig. 10.5).

You can also try to build a 100base-T (100Mbps) system using optical fiber ICs like the MAX3967A in Fig. 9.5. Take note of component placement and pcb design issues when designing such high-speed circuits. If possible, you need to work with people who are experienced in photonics and high-speed optical systems.

The next chapter will discuss the LAN VLC system in Fig. 9.6, 9.7, and 9.8.

### 9.3 CONCLUSION

The trick to build a robust system is to convert the Ethernet signals (analog) to digital signals before feeding them into the LED. If you want to break the mould, try to convert MLT-3 to binary before transmitting. At the receiver, you can convert binary back to MLT-3. This will take up plenty of research time, but it is worth the try.

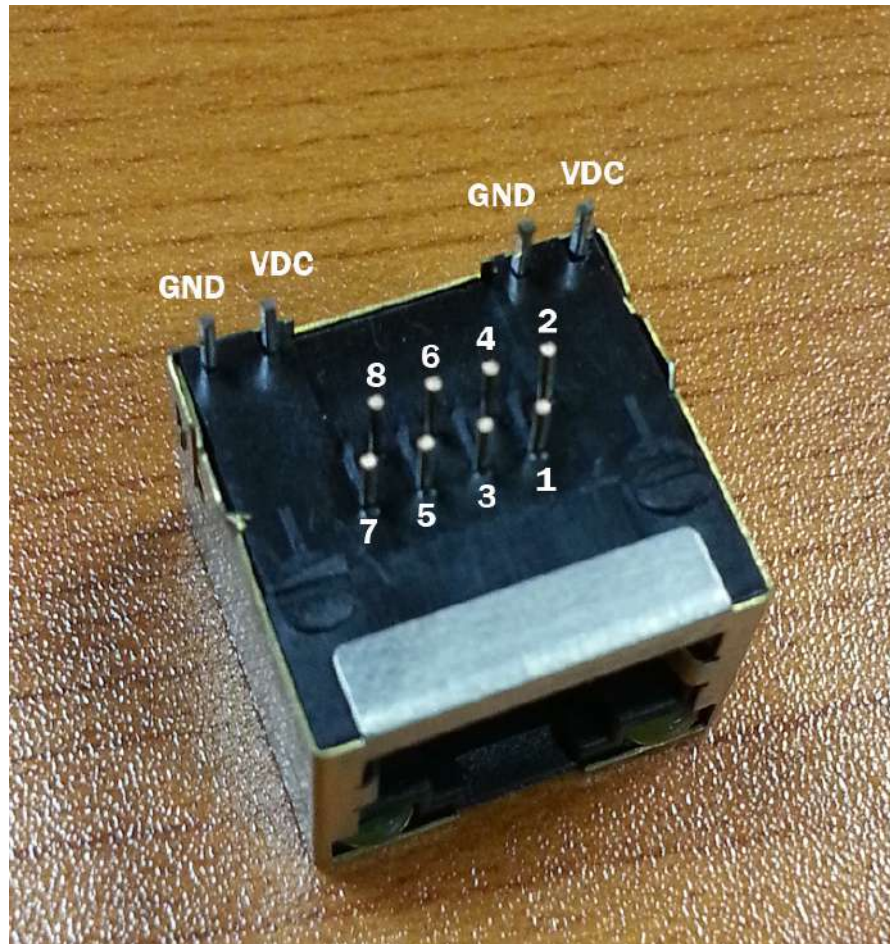


**Figure 9.1** Ethernet RJ45 connector without transformer magnetics. TX+ (PIN 1), TX- (PIN 2), RX+ (PIN 3), and RX- (PIN 6). The pair of VDC and GND pins at the rear connect to the two indicator LEDs in front, respectively.

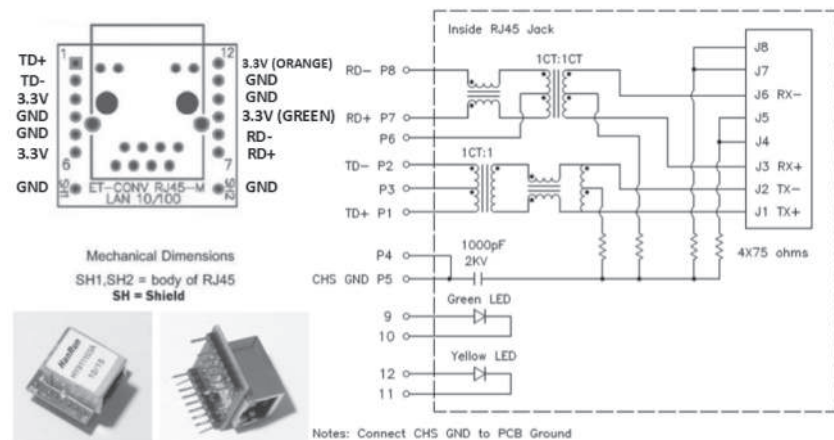


**Figure 9.2** Breakout board schematic for HANRUN HY911103A.

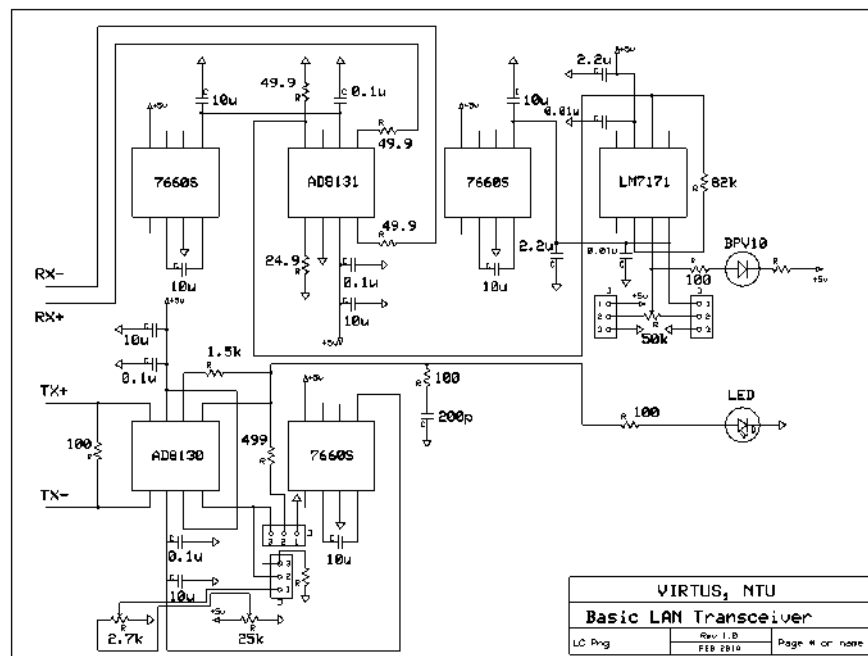


**Figure 9.3** Schematic of Ethernet LAN 10Base-T transceiver for visible light communication.



**Figure 9.4** Ethernet LAN 10Base-T VLC transceiver prototype.

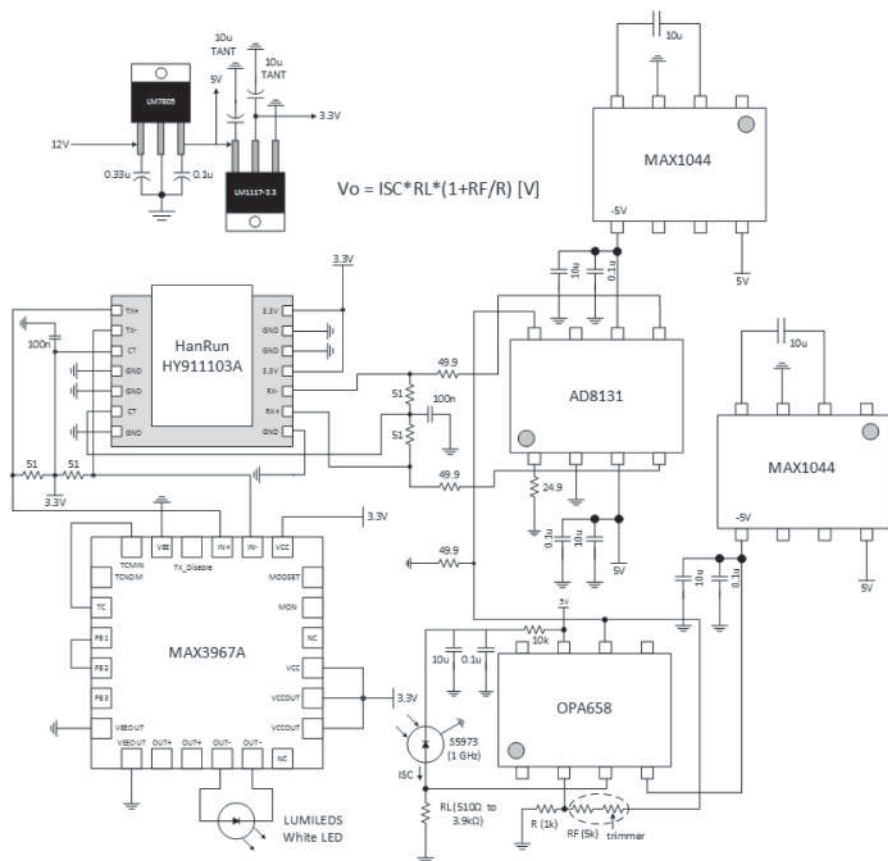
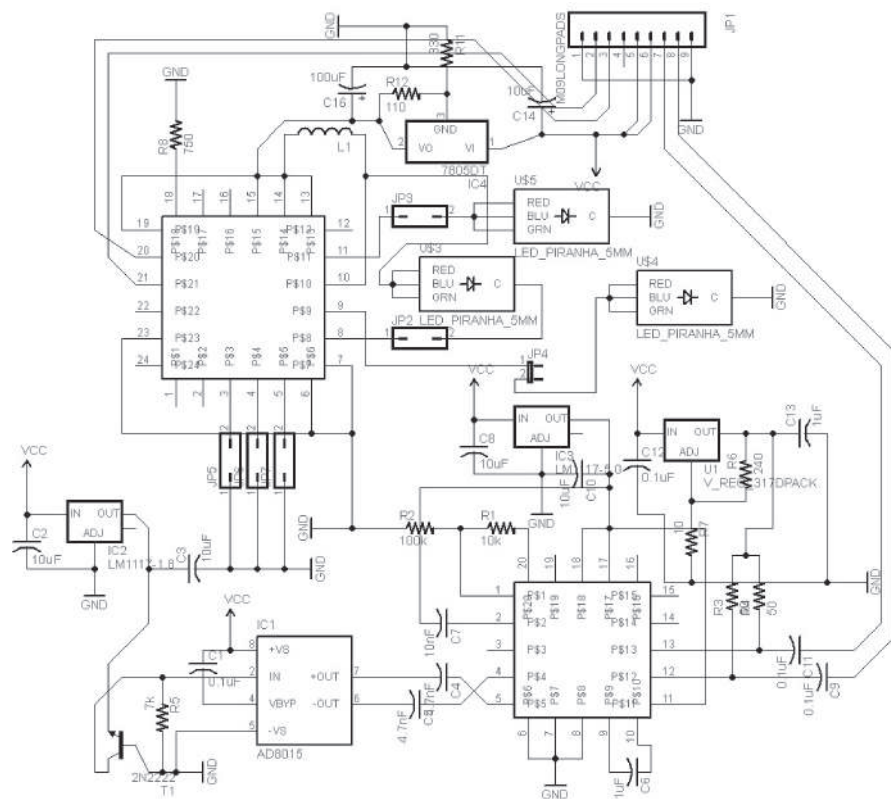


Figure 9.5 Ethernet LAN 100Base-T VLC transceiver prototype.



**Figure 9.6** Convenient plug-in to the TX-FX (LAN to optic fiber) media converter.



**Figure 9.7** Detailed schematic of the VLC transceiver for the TX-FX (LAN to optic fiber) media converter.

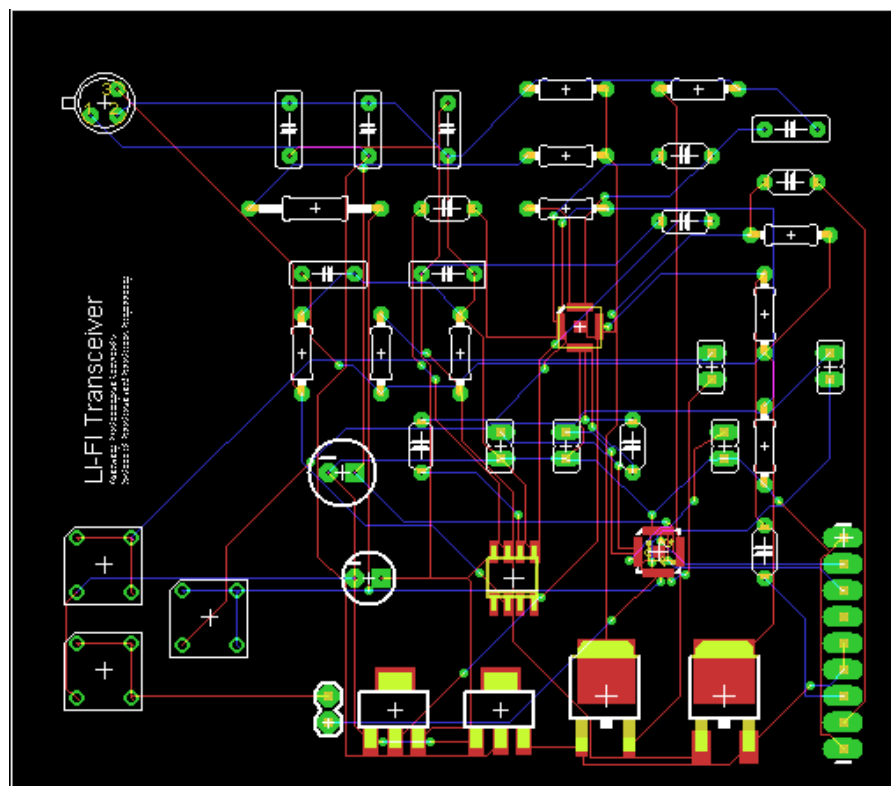


**Figure 9.8** Detailed layout of the VLC transceiver for the TX-FX (LAN to optic fiber) media converter.



# **Chapter 10**

## **VLC Designs for Audio-Video Streaming, Ethernet Connectivity and Indoor Positioning**

### **10.1 ABSTRACT**

Visible light communication (VLC) is projected to become an alternative means of wireless connection due to its efficiency and high bandwidth. An audio/video (AV) VLC transceiver and two Ethernet VLC transceivers (10Mbps and 100Mbps) are constructed. A 16-channel MIMO transceiver is designed to transmit signals at GHz speed. Workable integration designs of the AV and Ethernet VLC transceivers are presented. This work demonstrates the feasibility of creating affordable add-ons to existing computers and smartphones for entertainment as well as general position detection or homeland security monitoring. An LED indoor positioning system is also presented.

### **10.2 INTRODUCTION**

VLC might not replace radio frequency (RF) for the time being, but it has the flexibility to form hybrids with 60 GHz, 5G, and Wi-Fi technologies to increase capacity and speed [59][60]. Even if it is alone, VLC can have many applications in an indoor environment (Fig. 10.1). Firstly, we need it for entertainment. We want to enjoy good quality audio and video while watching broadband TV. Secondly, we want to access massive information on the *WorldWideWeb*. Thirdly, we want

to know the position of a person or object based on the position of the LED lamp above it. We will soon be able to control cars, robots, or air vehicles indoors using VLC. VLC's biggest advantages are being 'cableless' and having illumination and data at the same time.

In recent years, establishing indoor locations of personnel and individuals have become more and more important during cases of emergencies in public places. Government agencies are concerned with issues like terrorism, airport security, and patient tracking in overcrowded hospitals. Therefore, visible-light indoor positioning systems (VLIPS) are fast becoming a field of popular research [61][62][63]. We need a fully integrated surveillance system with not just the IPS, but also the transmission of video and sound to security officers on duty over LED lighting. Nowadays, video and audio information from surveillance devices are transmitted through Ethernet cables. Every CCTV has an IP address. Hence, it would also be practical to develop a VLC system that works on the Ethernet protocol.

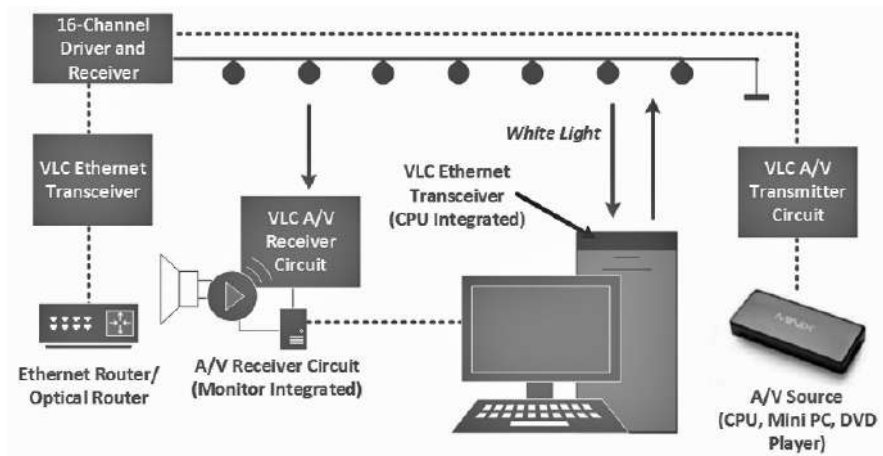


**Figure 10.1** Overview of a visible-light wireless optical system for audio, video, and Ethernet.

Researches in VLC audio and video transmission and reception are already quite established [64][65]. Except for 100base-T (i.e. 100 Mbps) VLC transceivers, 10base-T (i.e. 10 Mbps) VLC transceivers for Ethernet connection have also been widely demonstrated [66][67]. In this work, the authors present a fundamental

approach to build these VLC transceivers that are able to transmit and receive analog signals at moderate and fast data rates.

### 10.3 STEREO AUDIO AND COMPOSITE VIDEO VLC TRANSMISSION CIRCUITS

For this part of the project (Fig. 10.2), a MINIX Android Pocket PC is used as the video source. In fact any device that has an HDMI output can be used (e.g. Raspberry Pi). We also need an HDMI-to-AV converter for the transmitter circuit and an AV-to-HDMI converter for the receiver. These conversions are required since HDMI signals are too fast to be transmitted by conventional white LEDs.

The LM7171 voltage feedback amplifier is used throughout the entire circuit (Fig. 10.3) for all the RCA signals - yellow (video), white (audio L), and red (audio R). The LM7171 is a high-speed video amplifier. It consumes only 6.5 mA supply current but has a high output current (100mA) which can easily light up a 3W LED. It has a unity-gain bandwidth of 200 MHz and a slew rate of 4100V/s. Using ICL7660 (a negative  $V_{CC}$  generator IC) for the audio circuit may give you a whining sound. MAX1044 should be used instead and Pin 1 must be tied to  $V_{CC}$ . There are many types and brands of video amplifiers in the market. The authors encourage readers to experiment with other video ICs and relevant circuits.

### 10.4 10MBPS ETHERNET VLC CIRCUIT

10base-T Ethernet uses Manchester encoded signals (BPSK) while 100base-T uses MLT-3 (*Multi-Level Transmission 3*) encoded signals. Manchester encoded signals are easier to process and transmit since they have only two states (+2.5V, -2.5V), i.e. ON and OFF. MLT-3 signals are more difficult to transmit over an LED because it is not two states, but three states (+1V, 0V, -1V). We will touch on the solution a bit later.

Starting off at the transmitter, you need to combine the TX+ and TX- signals to get a single output. Usually three 7171 ICs are required to do a proper combination of the differential signals. This circuit is available in the 7171 datasheet. Alternatively, you may use the AD8130 or other ICs that are similar. AD8130 already has three amplifiers internally which take care of the impedance. A normal or Darlington BJT may be used at the output to boost the signal current to drive the LED.

At the receiver, you need the LM7171 to amplify light signals received by the photodiode. After that, the AD8131 or AD8132 is used to convert this signal back to differential outputs where RX+ and RX- go into the receiving device. For full duplex operation, you need a pair of transceivers to work. AD8015 can also be used as a single receiver or a preamplifier. It is a wideband transimpedance amplifier that is able to amplify photodiode signals and give out differential outputs directly.

Fig. 10.4 shows a simple VLC circuit for 10Base-T LAN. The TX and RX pairs of I/Os on the left connect to the respective pins on a HY911103A RJ45 connector. Remember to use RJ45 connectors that have transformers built in. Transformer coupling is required to compensate for ground offsets. Fig. 10.5 is a picture of the prototype.

### 10.5 16-CHANNEL MIMO: VLC TRANSMITTER DESIGN

The 16-channel MIMO transceiver can be used for digitized audio, video, and Ethernet signals. In the transmitter design, 74HC393, a binary ripple counter, and 74HC4514, a 4-16 line decoder are used to split serial data into 16 channels. This type of circuit is also called a phase generator. A sequential delay is created in the decoder to split a single continuous stream of data into discrete blocks, so that each block is transmitted by each LED independently. In the ideal case, the capacity will be increased by 16 times. A total of 16 2N4401 bipolar junction transistors (BJTs) are used to drive all the 16 LEDs. Fig. 10.6 shows the transmitter schematic.

### 10.6 16-CHANNEL MIMO: VLC RECEIVER DESIGN

On the receiver, there are a total of 16 identical receiver units. The OPA847 amplifier IC has a very high gain bandwidth (3.9 GHz) while using only 18mA of the supply current. It is an ideal wideband transimpedance amplifier for fiber optic application in OC-3 (155Mbps). The board works well when we used photodiodes like S5973-02 and BPV10. The circuit of one unit of the receiver is shown in Fig. 10.7. The full transceiver prototype is shown in Fig. 10.8.

We connected the transmitter board to a 100 MHz sinusoidal signal. The output from the MIMO receiver board is about 1.2 GHz, which is slightly less than half of what we expected (3.9 GHz divided by 2). This is probably due to (1) the loss of data during transmission, (2) malfunctioning of certain chips, or (3) bad trace connections on the transceiver board. It is also important to use concentrators to focus light onto the photodiodes. Some other factors influencing

the performance include ambient lighting conditions and sometimes sunlight. To achieve better signals, it would be good to use multi-chip RGB LEDs instead of conventional white LEDs. However it would take some effort to generate white light by tuning the current of the red, green, and blue components. A prism or a specially-designed mirror formation is recommended for this purpose.

## 10.7 RECEIVER INTEGRATION WITH NOTEBOOKS AND PCS

Normally in PCs, mini PCs, tablets, and notebooks, there are interface ICs between the microprocessor and the I/O ports which enable us to connect external devices. In Asia, there is widespread use of Wolfson's WM9713L IC for AC97 audio and touchpanel codec interface. For composite video output, JRC's low voltage video amplifier NJM2561 is used. Both chips are often seen interfacing with Samsung's RISC microprocessor S5PV210 or Allwinner's ARM Cortex-A10 SoC. We decided to use a more modern chip to present our interface circuit. Nowadays, these SoCs have built-in peripheral I/Os (including drivers and codecs). This enables direct connection to our VLC transceivers. Broadcom's BCM2835 (ARM11) is used in the Raspberry Pi. Fig. 10.9 is an integration schematic of BCM2835 with VLC transmitters for audio and video applications.

Audio and video signals are multiplexed by using a common 74HC4053 multiplexer/demultiplexer. It should be noted that audio signals are usually very weak. They need to go through an operational amplifier (e.g. TL062/TL072, JFET input) to increase the peak-to-peak voltage in order to be multiplexed. Video signals have a peak-to-peak voltage ( $V_{pp}$ ) of 1V already, thus they do not have to be amplified before multiplexing. Only audio signals coming out of a desktop PC have a  $V_{pp}$  of 1V which needs no further amplification. After multiplexing, the combined signals are made to pass through a driver (in this case a 7171) to increase their current to drive the white LED. The reader should adjust the power supply and use a screw driver to tweak the trimmer potentiometers for optimum and balanced performance. The receiving device is the LCD/LED monitor. Modern displays normally have integrated speakers and include many types of AV I/O ports due to the improvement of video chip technology. In the Asian electronics market, it is common to see the T.VST29.O3B (03\_A3) chipset board. It uses MStar's TSUMV59XU chip which handles analog TV and video systems while supporting multimedia decoding and home theater sound. The schematics of the chip's application are not available. Therefore, the best we can do is to present a picture of the board (Fig. 10.10). Readers have to imagine that the red, yellow,

and white RCA connectors have been removed. You may also use the HDMI port as the receive port, but you will need an AV-to-HDMI converter (or its IC) between the HDMI connector (or pins) and the output of the VLC receiver which is illustrated in Fig. 10.2. OPA2134 or LME49860 can be used as audio amplifiers. They are high-fidelity audio op amp chips and their circuits can be expanded to produce high-quality stereo output. For Ethernet integration, we choose LAN9512 to integrate with our VLC Ethernet transceiver. Commercially, this chip is used on the Raspberry Pi to provide USB as well as 10/100base-TX networking. It has USB 2.0 to 10/100 Ethernet controllers with a 2-port USB 2.0 hub. There are MAC and PHY units in it; therefore, it is a fully-integrated chip that is suitable not only inside a PC, but also on a smartphone if you want to develop and integrate other communication technologies.

The microprocessor talks to the outside world via the LAN9512. The PHY interfaces between line modulation and link-layer packet signaling which involve the fields of analog and digital circuit design, respectively. MLT-3 encoded signals are not suitable for transmission over an LED, especially if you want it at the speed of 100base-T. Hence, we need to look at the optical fiber system. In this kind of transceiver, the 100base-T(X) signal has to be converted to a 100base-FX signal. The FX signal is NRZI digital (only 1 and 0) and thus can be transmitted over light as pulses. In an Ethernet controller, data are 4B/5B encoded which outputs as NRZI data. This signal then goes through a scrambler and an MLT-3 encoder to generate the signal for the twisted pair. In other words, the fiber Ethernet system bypasses the last two processes to output NRZI signals for optical communication. In some Ethernet controller ICs, the user has freedom to configure the chip for copper wire (MLT-3) or fiber (NRZI) communication. NRZI signals can also be termed as PECL (positive emitter-coupled logic) signals because they need the ECL logic to do transmission. There is always a PECL driver and a PECL receiving amplifier in a fiber optic transceiver.

We borrowed and modified the fiber optic system to cater to our application on the LED. Realtek's RTL8306, Micro Linear's ML6652, and Davocom's DM9301 are all TX-FX converters. Either one can be used to convert the copper differential pairs to PECL for transmission and convert back from PECL to copper MLT-3 during reception. During designing, the VLC transmitter and receiver circuits must not share the same supply voltage even though they are on the same PCB. They must have separate  $V_{cc}$  and GND. In Fig. 10.11, a fiber optic LED driver MAX3967A accepts TX signals from the 9512 chip and converts them to FX signals. The FX signals are transmitted out by an RGB multi-chip LED. At the receiver, the transimpedance amplifier AD8015 (TIA, 240MHz bandwidth) is used to amplify

light signals from Hamamatsu's S5973-02 1 GHz photodiode. After that, the TIA passes its signals to Maxim's MAX3969 limiting amplifier (LA). The LA then returns its output PECL signals to the 9512 chip. The 9512 converts them back to 100base-T(X) signals for the PC (Figs. 10.12, 10.13, 9.6, 9.7).

## 10.8 VLC UART TRANSCEIVER SHIELD

Both the USBDroid and the UMFT311EV modules are Arduino-compatible. They can be programmed to become TX, RX or both, depending on the pins available. The transceiver shield (Fig. 14.11) sits on top of the USBDroid or UMFT311EV and only performs the sending and receiving of optical signals. Optical signals are sent out directly to the white LED from any of the digital pins that is customized to become a TX pin. The output signal voltage is 5V. The signal stream is on-off keying (OOK), and the transmitter baud rate is set at 38400bps to prevent the LED from flashing.

In the receiver portion, the BPV10 PIN photodiode receives light signals from the transmitter and converts them to current signals. The current signals are then converted to voltage signals and amplified by the first LF357 amplifier. The second LF357 serves as a comparator which trims or level-shifts the signal voltage. The output signal is then fed to the USBDroid/UMFT311EV UART input pin. USBDroid and UMFT311EV are in fact microcontrollers boards, but they have a smart interface which allows them to act as a host to interact with smartphones automatically. They are technically termed as *Android bridge*. The Arduino program in the USBDroid/UMFT311EV helps to pass whatever data it receives to the Android application by the use of the Android Accessory Library.

The transmitter can be any 1W LED (Fig. 10.16) which is directly connected to the TX pin to which the bridge module (or any Arduino board) gives out signals.

Another application of the VLC transceiver is the mobile car or robot (Fig. 10.17). In the future, we will be able to control a robot or a vehicle operating indoors by just using LED lamps on the ceiling to transmit instructions to these machines. It can be implemented in warehouses, factories, hospitals, and many more indoor environments.

## 10.9 VLC IPS ANDROID APP

Philips recently did a ground-breaking collaboration with Carrefour to implement the world's first application of VLC indoor positioning technology in a supermarket

in Lille, France [68]. The lights in the supermarket are replaced by LED lamps which are able to transmit simple position indicators to consumers' smartphones. Any phone installed with the application program is able to map and zoom in on the location of the shopper. The phone receives light signals through its built-in camera.

Our initial app was constructed using Android Studio 1.2.2. Signal is received by the transceiver shield and passed to the Android bridge module. The module then transfers the data to the smartphone using UART. In Fig. 10.18, the screen on the phone shows information of the position sent by the transmitting LED. The reader should be alerted that from our tests, USBDroid works perfectly with HTC phones and tablets, while UMFT311EV works perfectly with the popular Samsung series of phones and tablets.

In the improved app, the Android development consists of three parts: a database, a USB accessory manager and a Google map fragment. The database uses the SQLite database engine. A table is created whereby the primary key is a 16-digit search key and the attributes of the table are *latitude* and *longitude*. Other attributes may be added to the table for other location-based services. The USB accessory manager handles connection with the receiver device over USB. It detects whether connection to the receiver has been set up. The key string received by the USB manager is a single character file in a buffer. A string builder assembles the 16 characters and forms a string. With the search key, the application searches the database and retrieves the corresponding latitude and longitude.

The indoor Google map is shown in Fig. 10.19. A toggle button is placed at the bottom center of the screen to toggle between indoor (VLIPS) and outdoor positioning (GPS). The figure shows the floor plan of the first author's workplace. It is placed as an overlay on Google Maps. When the transceiver receives light, Google Play Services will zoom to the exact position that is transmitted by the LED light.

The Version 3 transceiver (Fig. 14.11) was developed due to the need to switch between the two types of bridge modules for wider compatibility. Users can have a choice to use the shield for either UMFT311EV or USBDroid. The user only has to change the jumper pins.

## 10.10 CONCLUSION

A full integration with the personal computer or smartphone will probably take some time, but the authors are optimistic about the future of such a system for homes and offices. Everything would be 'cableless'. They can fuse easily with our

cloud infrastructure on mobile devices, especially when optical broadband access are being introduced to homes in recent years. For the multimedia age, the design of VLC devices for desktop applications should have high sound quality, high resolution images, high-speed Internet, and fast storage access. This is different from VLC systems for mobile devices where compactness and simplicity are required to save space. Some of the circuits here can be implemented in mobile devices. If we (or manufacturers) can shrink the size of these circuits by at least a quarter or make them into a chip, their implementations will be endless. There will be instant entertainment and instant information as long as we are under an LED lamp. In the future, no signal will be cut off even if a train enters a tunnel in the mountains, because the Internet will be available from the LED lamps on the train.

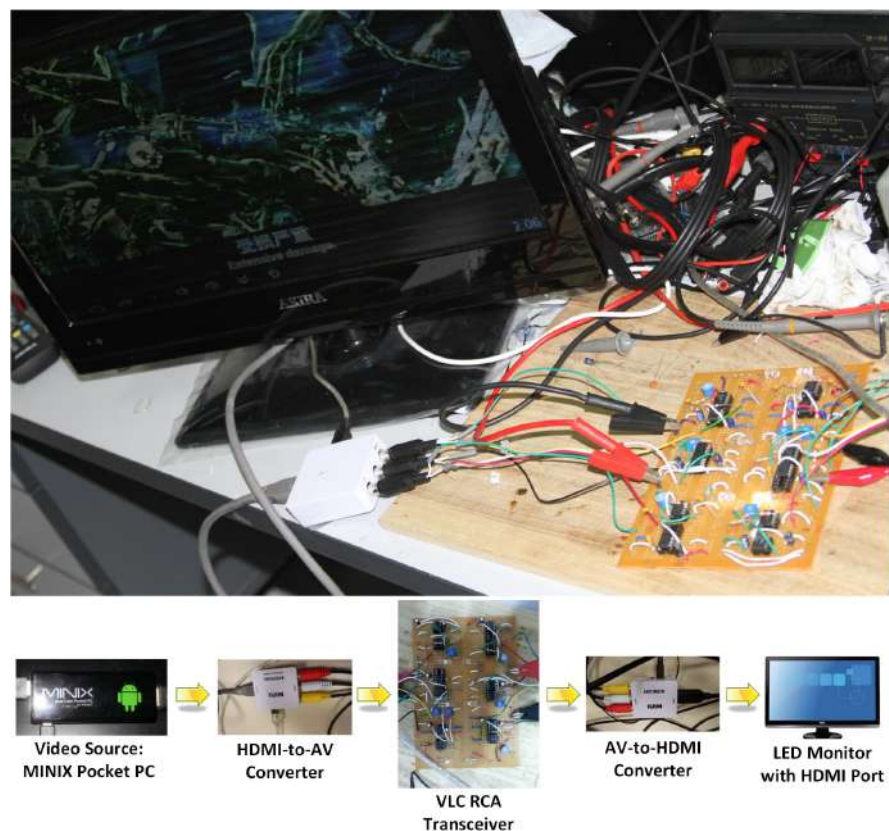


**Figure 10.2** Test setup of the VLC audio and video transceiver.

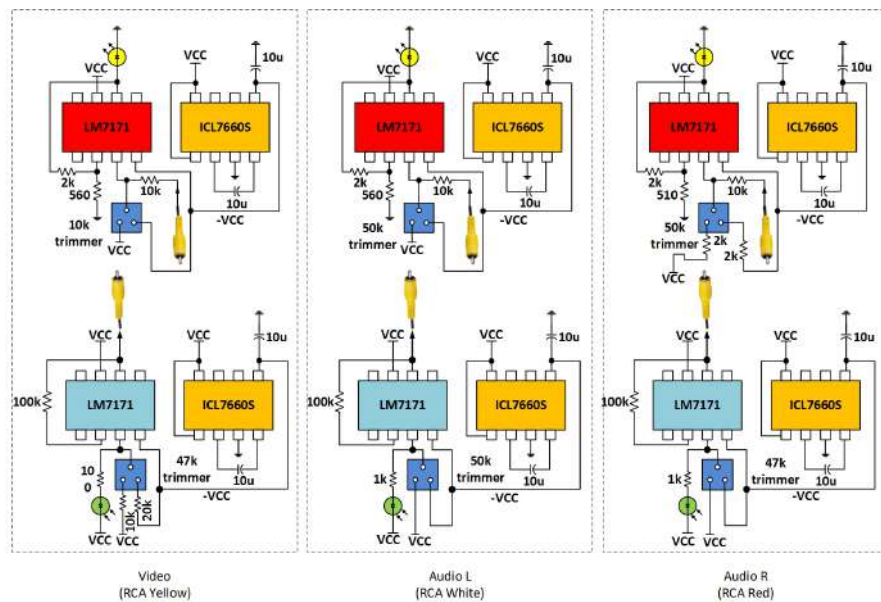


**Figure 10.3** Schematic diagram of the VLC audio and video transmitters and receivers.

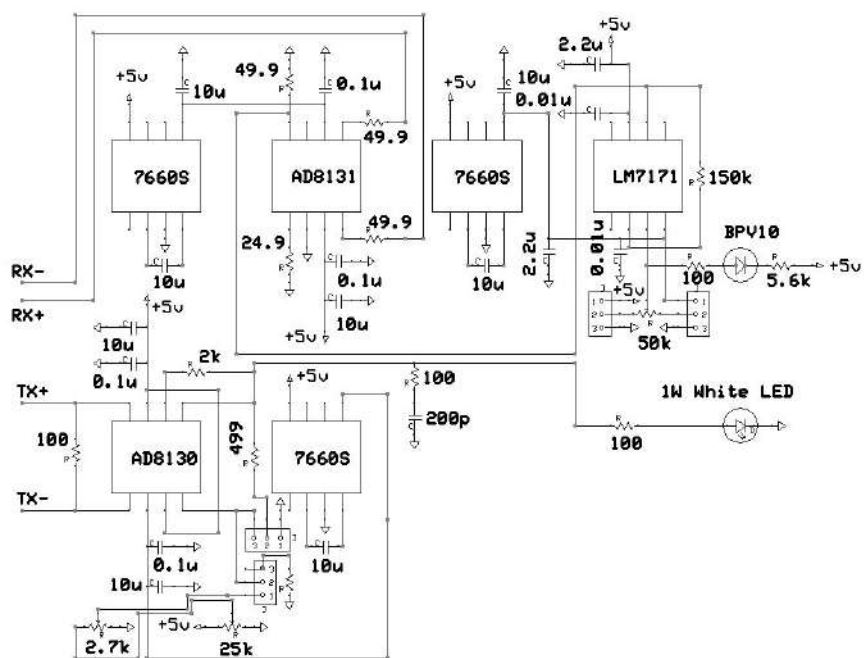
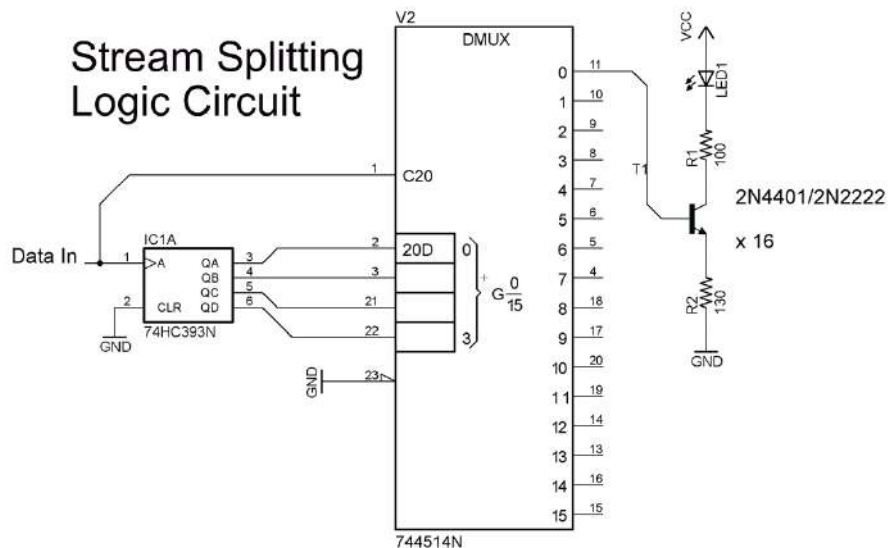


Figure 10.4 Schematic diagram of the VLC Ethernet LAN 10Base-T transceiver.



**Figure 10.5** Picture of the VLC Ethernet LAN 10Base-T transceiver for full duplex communication.



**Figure 10.6** Schematic diagram of the 16-channel VLC transmitter.

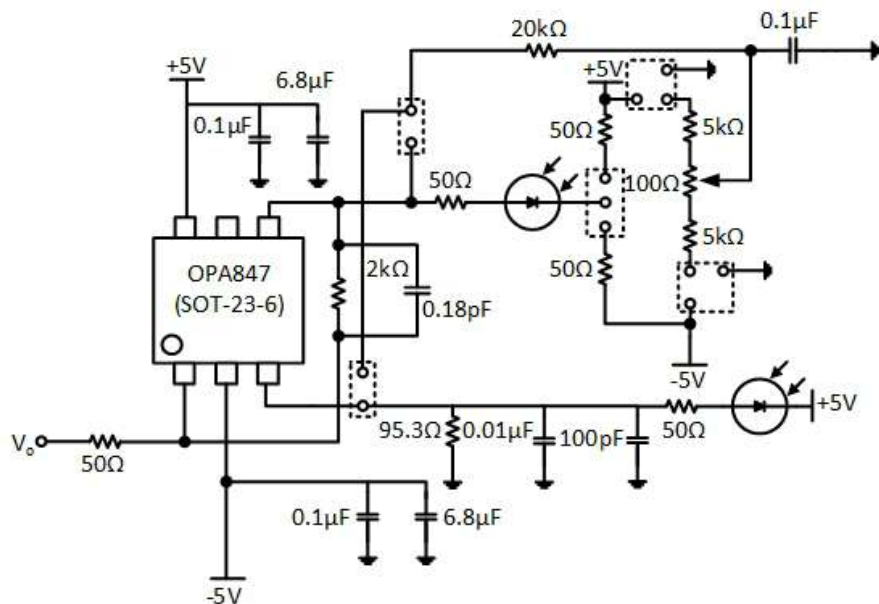


**Figure 10.7** Schematic diagram of one unit of the receiver. N. B. There are 16 sets of this circuit.

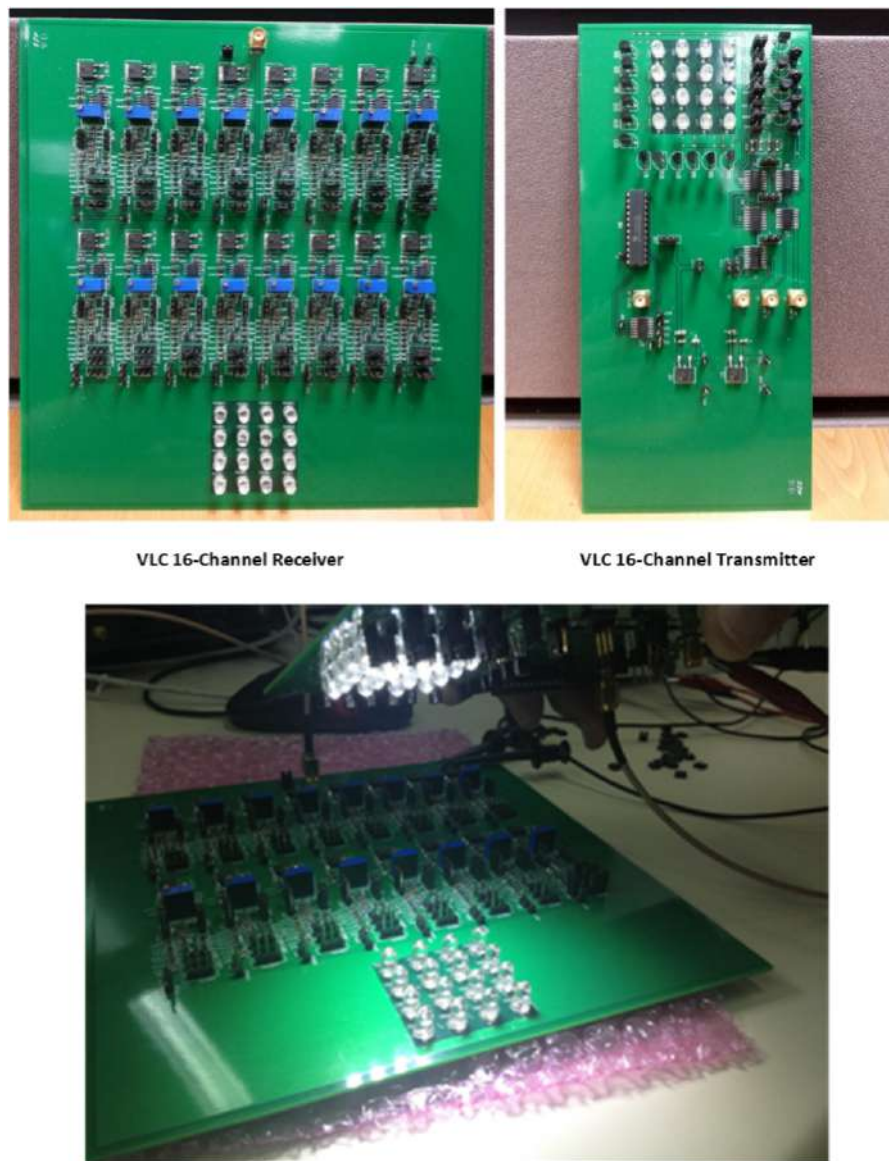


**Figure 10.8** Photo of the 16-channel VLC receiver (top left) and transmitter (top right).

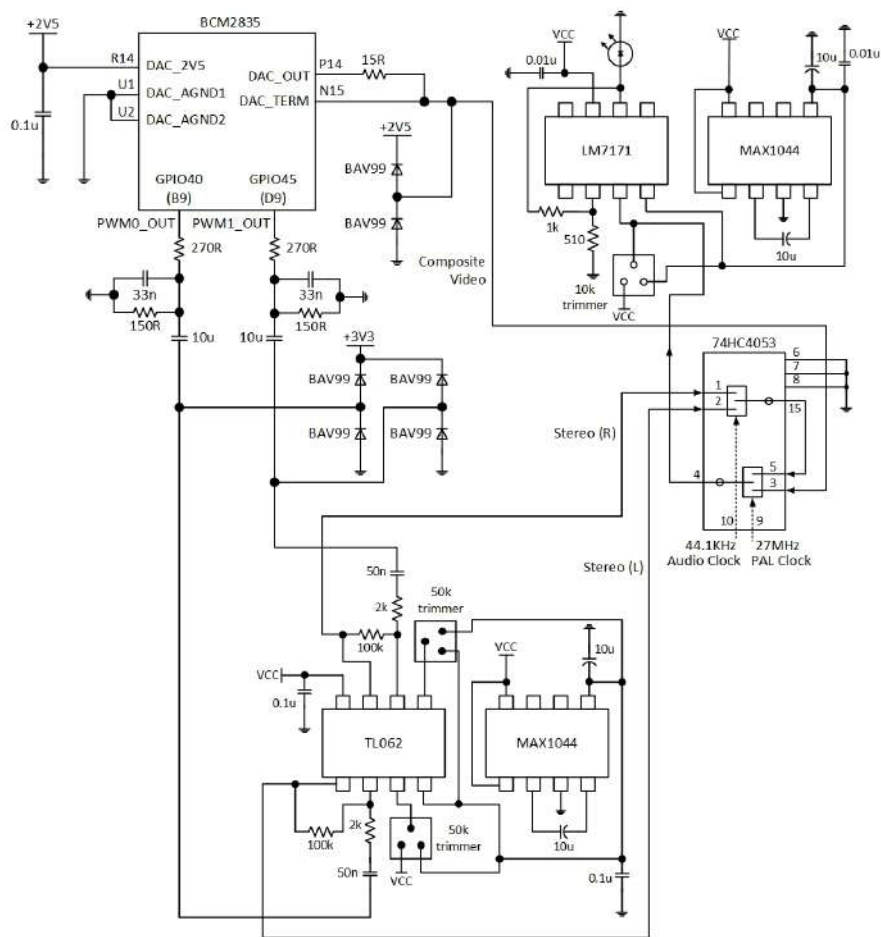


Figure 10.9 VLC audio/video transmitter integration circuit with Broadcom's BCM2835.

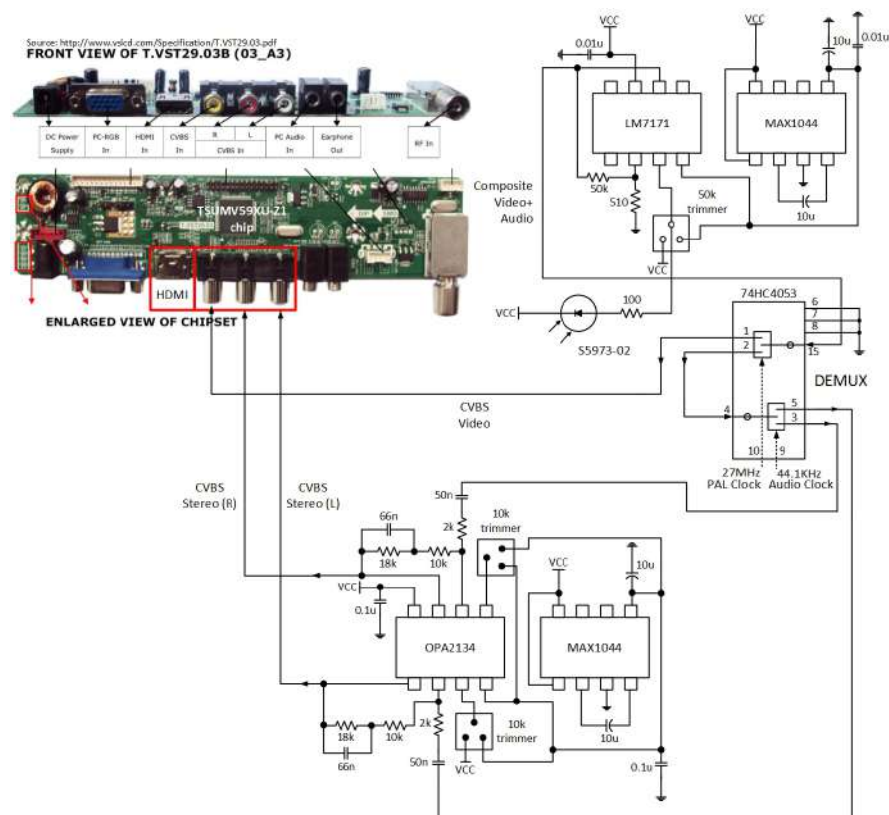
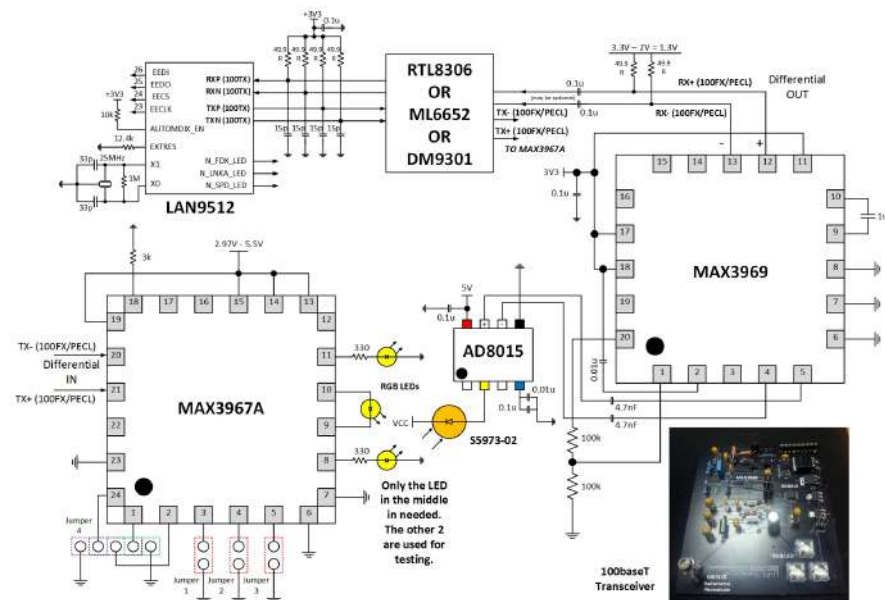


Figure 10.10 VLC audio/video receiver integration circuit with T.VST29.



**Figure 10.11** VLC Ethernet transceiver integration circuit with LAN9512. N. B.: The S5973 photodiode has three pins, namely CATHODE, ANODE, and GND.



**Figure 10.12** VLC Ethernet transceiver (100baseT). The pins (top right corner) are designed to replace the optical fiber transceiver of the media converter.

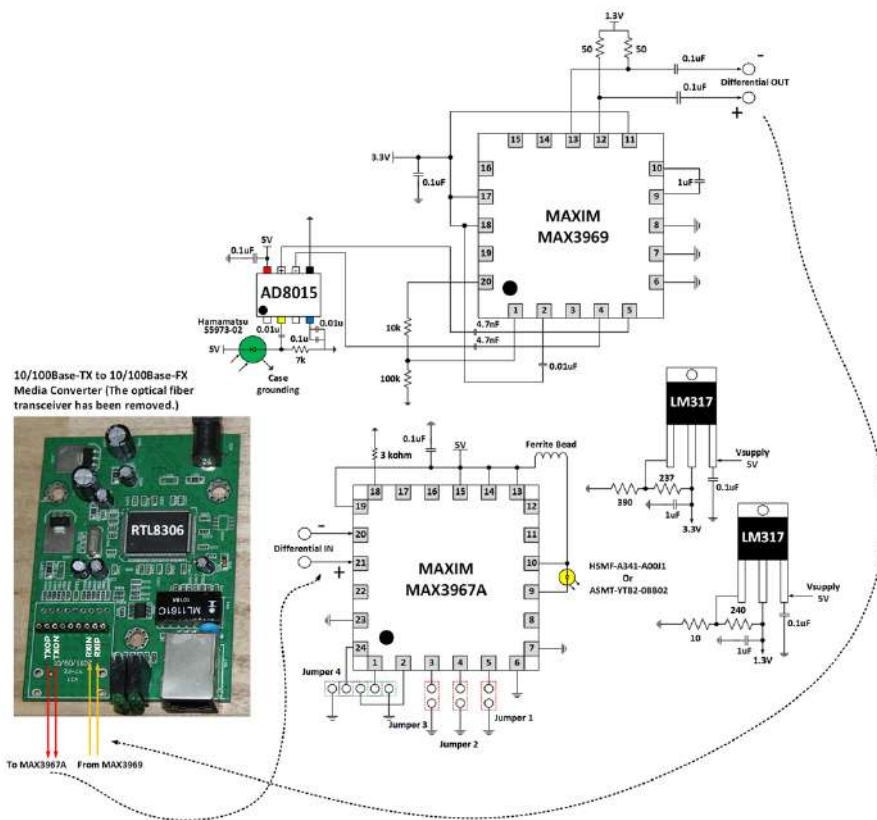
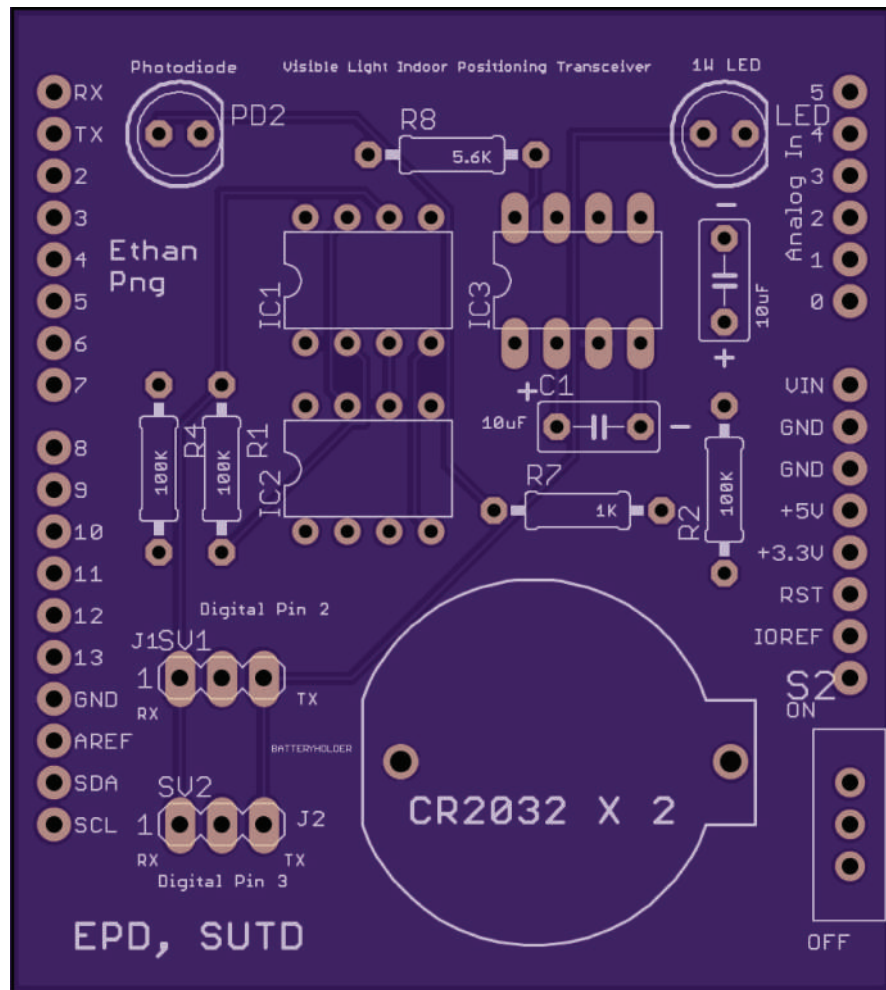


Figure 10.13 Integration with optical fiber TX-FX media converter.



**Figure 10.14** Top view of the Version 3 transceiver design (under fabrication). Two LF357 op-amps and a negative voltage converter MAX1044 are used. We found that CA3140 is a more stable op-amp, but it consumes more power.

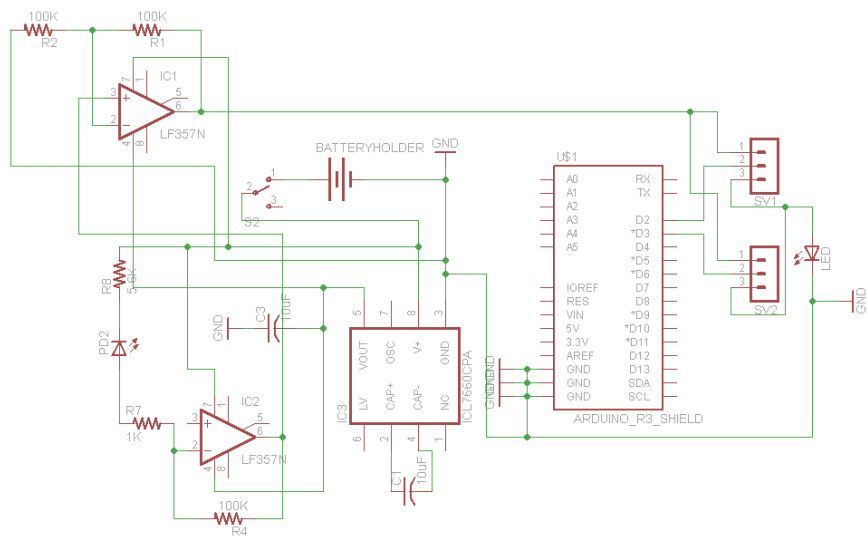
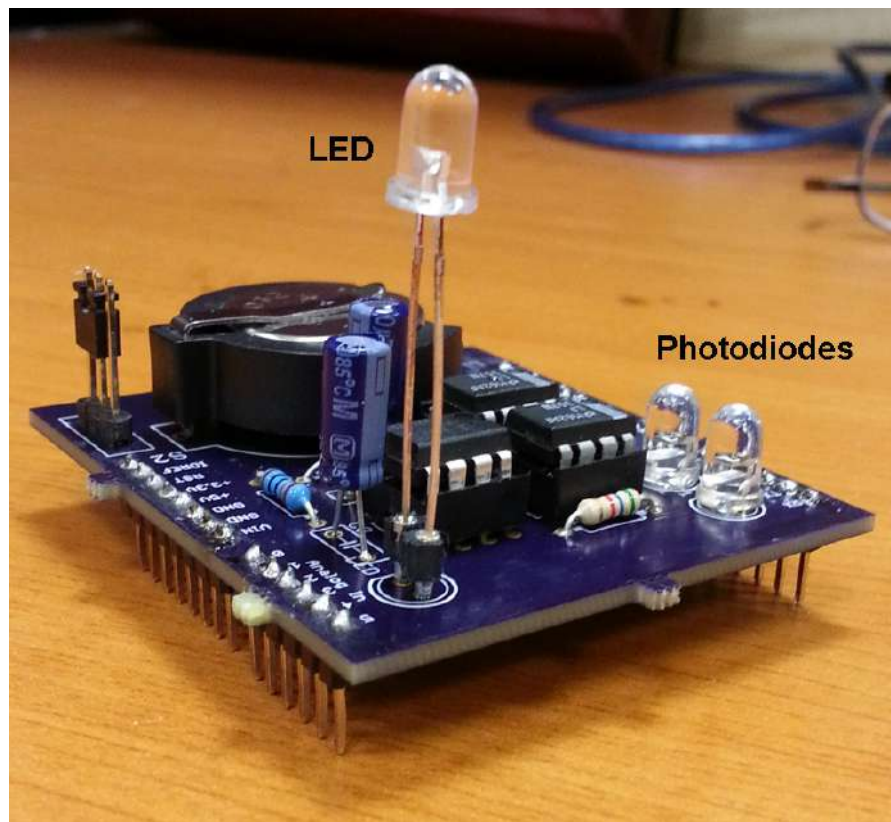
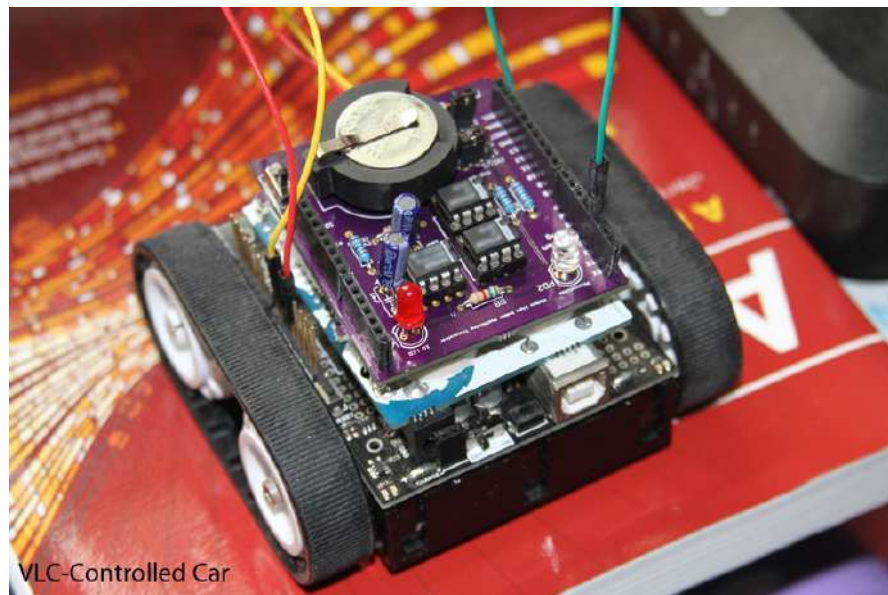


Figure 10.15 Eagle schematic diagram of the pcb.



**Figure 10.16** Version 2 transceiver showing the installation of the transmitter (LED) and the receiver (photodiode).



**Figure 10.17** A Zumobot utilizing VLC indoor navigation for remote control.



**Figure 10.18** Version 2 transceiver with the initial app: (left) UMFT311EV's pinout is slightly different from Arduino's pin layout. The TX and RX pins have to switch position; (right) USBDroid has no such problem. The Version 3 pcb design is an improved version made to accommodate both bridge modules.



**Figure 10.19** The improved app with indoor map and position marker.



# Chapter 11

## Designs of VLC Video and Audio Transceivers for Desktop HDMI Applications

In this project, we built an HDMI VLC transmitter and receiver (Fig. 11.2). Real HDMI signals are very high in frequency, so we reduce this frequency by putting the HDMI signals through converters. This makes the signals easier to manage.

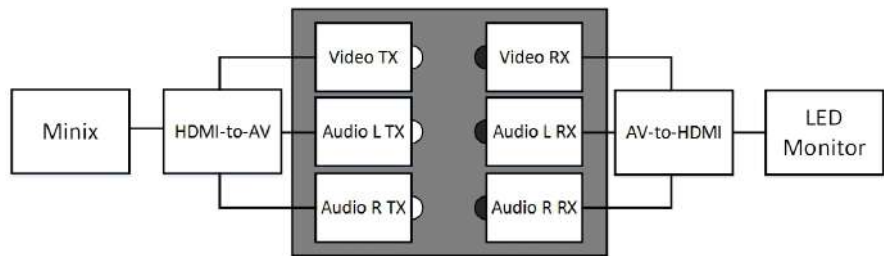


**Figure 11.1** Block diagram of the setup: transceiver for VLC HDMI-converted signals.

### 11.1 HOW IT WORKS

We use the MINIX Dual Core Pocket PC (Fig. 11.2) as the video source for transmission. Then we use the HDMI-to-AV converter (Fig. 11.4 top) to convert

HDMI video and audio signals to AV (or RCA) format. Next, these three RCA signals (yellow (video), white (L), red (R)) are passed to the LED transmitter circuit. After reception at the photodiode and receiver, we convert AV (RCA) video and audio signals back to HDMI format using the AV-to-HDMI converter (Fig. 11.4 bottom). This converter output is connected to the LED monitor. The MINIX Neo G4 Dual Core pocket-sized PC is a good HD video source for our HDMI VLC experiment. It has a dual core cortex A9 processor which enables high resolution videos.



**Figure 11.2** The Minix is an Internet movie-viewing gadget via wireless LAN. It runs on Android and outputs movies through its HDMI port (to TV).

## 11.2 ROOM FOR IMPROVEMENTS

Our simple TX and RX circuits (Fig. 11.5) cause lines of disruption (or commonly known as slanting lines or slanting patterns) to appear on the monitor as seen in Fig 11.6. Slanting lines are caused by distortions. The transmitted signals have been distorted during transmission. The video sync separator in the monitor is supposed to extract timing information, including composite and vertical sync and burst/back porch timing. Since the received signal is distorted, it cannot extract the precise clock, thus leading to bad sync separation. We would need a good clock synchronization circuit to enable healthy data transmission between the transmitter and the receiver. Right now the data is sent without a clock.

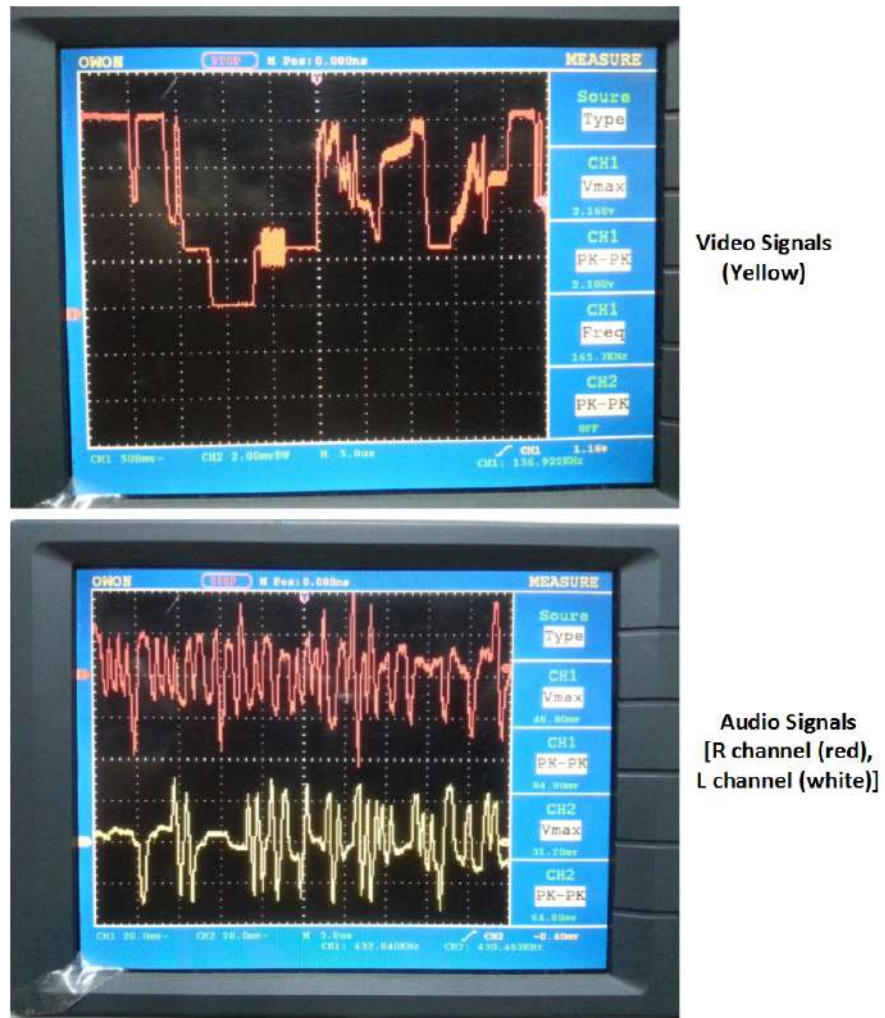
However, including a clock signal into the transmission system would mean more work to do. As this book is just an introduction, we shall leave it at that. Using a video amplifier of higher bandwidth (800 MHz) (e.g. AD8001) rather than LM7171 (240 MHz) may also help to improve the resolution. On the contrary, it would add to the cost and complexity.

## 11.3 CONCLUSION

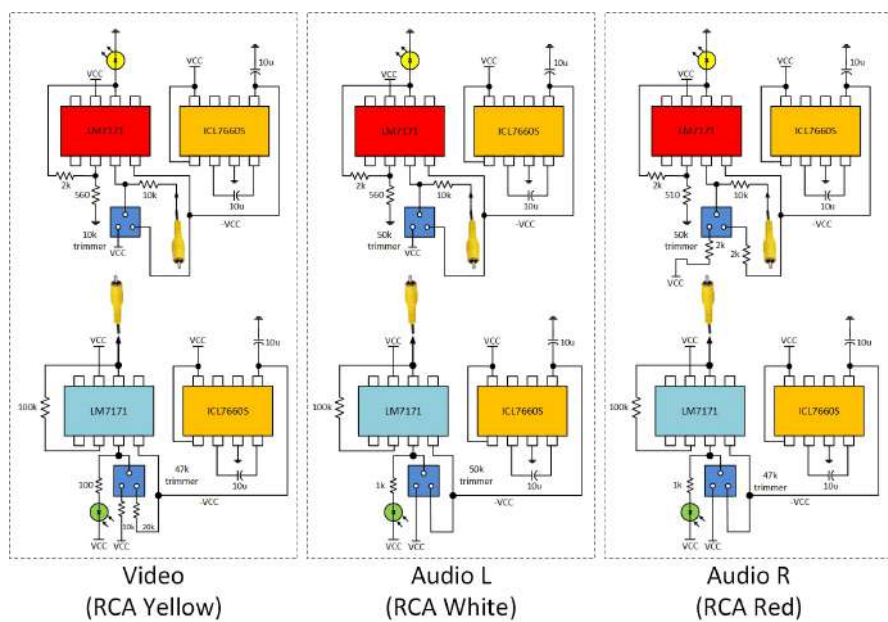
This experiment shows that it is more practical to use converters to build a VLC HDMI transmission system. The signals that come out directly from the HDMI ports are too high in frequency. This makes them hard to handle when designing the transceiver circuit, especially when we are talking about the limitations of present LEDs.



Figure 11.3 Top: HDMI-to-AV converter; bottom: AV-to-HDMI converter.



**Figure 11.4** Top: video waveform captured at the yellow port; bottom: audio waveforms captured at the red (R) and white ports (L) respectively. Note that the L port is not working. Its waveform looks weird.



**Figure 11.5** Schematic of our VLC Video Audio prototype for RCA connection.

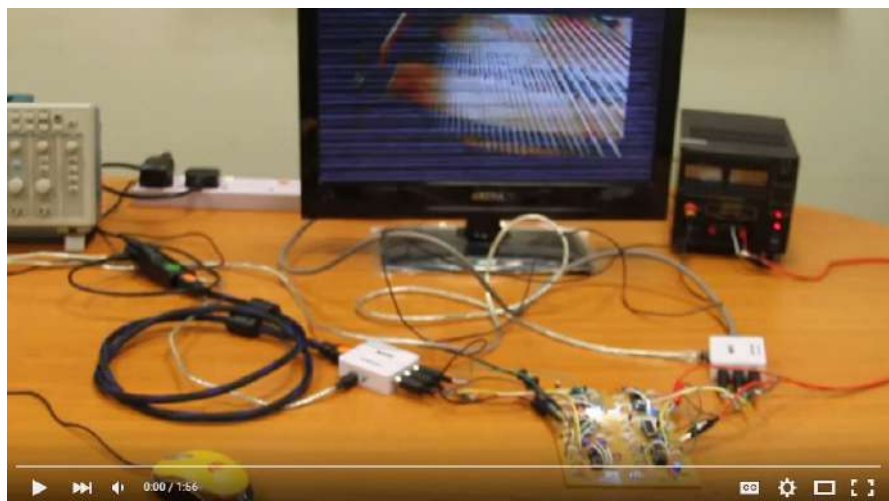


**Figure 11.6** Setup of the prototype for tests.



# **Chapter 12**

## **VLC System Design for Position Detection**

### **12.1 ABSTRACT**

A versatile outdoor and indoor position detection mobile prototype has been successfully constructed and tested. The receiver consists of a GPS module, a visible-light data receiver, and two ultrasonic sensors, all controlled by an Arduino Mega and an Arduino Uno microcontroller. Each ultrasonic sensor detects distance in the X and Y axis respectively. The transmitter system consists of four LED shields each attached to an Arduino Uno which is programmed to transmit a global position relevant to the position of the LED lamp. When a person is outdoors, the GPS module receives global position from the satellite. When a person goes indoors, his or her global position will be given by the LEDs and ultrasound sensors. The location data can be transmitted (a) via XBee to a monitoring system or (b) via a GSM module to a certain cell phone number as sms messages. This system is extremely useful in elderly care service. It ensures specific accuracy in locating senior citizens during cases of emergency inside a house, hospital, or old folks home.

### **12.2 INTRODUCTION**

Visible light communication (VLC) has come to an age where light receivers can also be utilized to detect position. There is not much literature on this topic [69][70]. Basically, two methods can be used to give location: (a) photoreceiver receives location information transmitted by the LED, or (b) position is computed based on light intensity and the angle of reception at the photodiode.

GPS is often only accurate up to 5 meters and worse if you are surrounded by tall buildings. The GPS receiver does not function indoors, although you can still get some signals near the windows. Wi-Fi indoor positioning [71][72][73] shows a promising future, but it is not practical to install Wi-Fi in places where very few people need to access the network.

Sometimes, due to poor weather conditions, GPS signals are weak. For example, if we are standing under a street lamp or a desolated bus stop at night in bad weather, we find that our GPS receiver functions badly. If the street lamp or the lamp at the bus stop is made to transmit GPS position, the place would be safer. The individual can send his/her position to the police or their loved ones during moments of danger.

In an enclosed environment such as an apartment or office, transmitting position by the use of LED lamps becomes more useful. Since every room or every part of the office will at least have one lamp, we are able to capture the precise location of a person if the person happens to faint or have a heart attack.

In this project (Fig. 12.1), ultrasonic sensors are used to complement the visible light positioning system because they can have accuracy up to centimeters. If any of the LED lamps goes off, the ultrasonic sensors can still be used to locate a person.



**Figure 12.1** VLIPS (Visible Light Indoor Positioning System) prototype: receiver device and 4 LED transmitters.

### 12.3 ULTRASOUND AND VLC: HOW IT WORKS

Every LED lamp transmits a unique pair of global coordinates relative to the structure of the building and its global position. The distances in between these LEDs are detected by ultrasound sensors (Fig. 12.2 and Fig. 12.3).

- **Method 1: Boundary mapping**

can pinpoint your rough position.

```
If (x<2 && y<2) //2 meters
{
Lcd.print("Y: 1.322345");
Lcd.print("X:103.343673");
Serial.print("R Corner front door");
}
If you take that corner to be your
reference point (0,0).
```



**Figure 12.2** Determining receiver position using boundary mapping method.

### 12.4 OBTAINING THE POSITION FOR INDOOR ENVIRONMENT

The global position indoors can be determined using this particular tool site: <http://www.mygeoposition.com/> (Fig. 12.4). As we zoom in, we are able to see the perimeter of any office, apartment, or building. Next, when you click on any spot, the pointer will indicate its GIS position. For instance, the global position of my work desk (which is also the global position of the LED light above my seat) is approximately Y: 1.343669, X:103.682324.

In our scaled-down prototype, this position is hardcoded into an Arduino Uno microcontroller, onto which an LED lamp shield is attached. The LEDs will keep sending these coordinates. If the whole office or the entire house is installed with this type of LED lamps, then as long as a person carries a smartphone integrated with such a receiver, global position can be determined. We can even track a person by enabling the received position to be sent to a monitoring system or to another person. This is very useful for monitoring elderly patients at home or at the hospital.

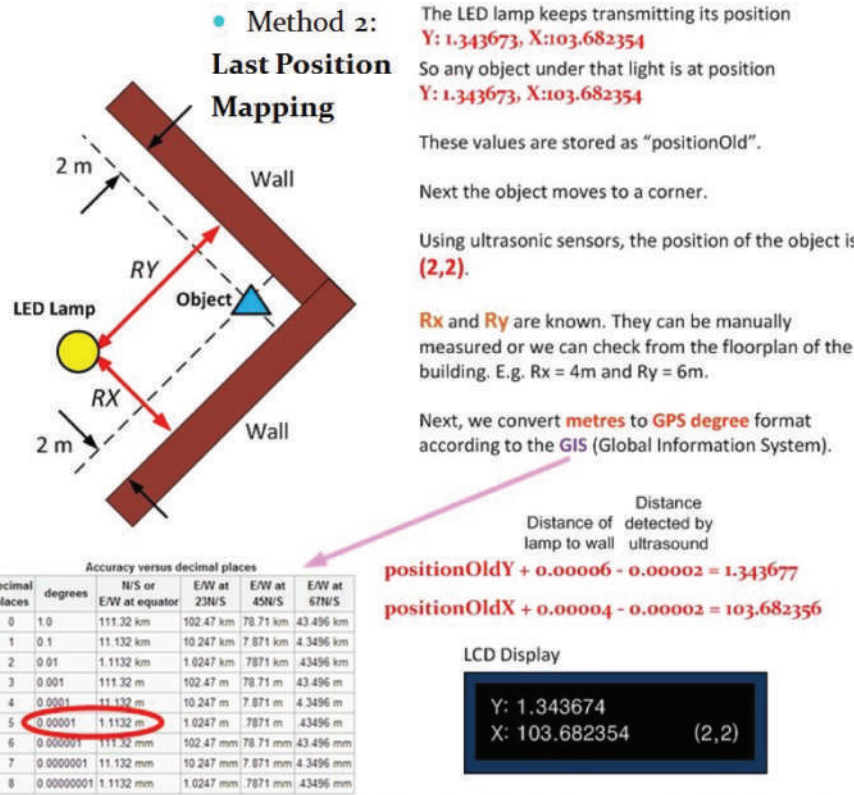


Figure 12.3 Determining receiver position using last position method.

In our prototype, we use a pair of XBee Pro S1 transceivers to link the receiver to the monitoring system on a PC.

## 12.5 TRANSMITTER HARDWARE

The transmitter consists of an Arduino Uno and an LED shield. We have designed four 16-LED shields powered directly by their respective Arduino's 5V supply (Fig. 12.5).

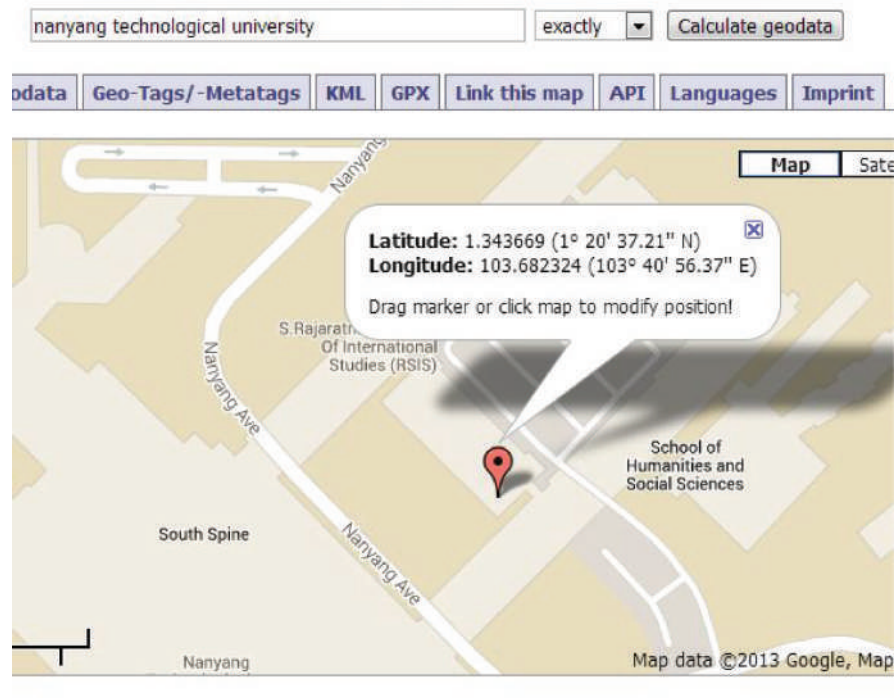
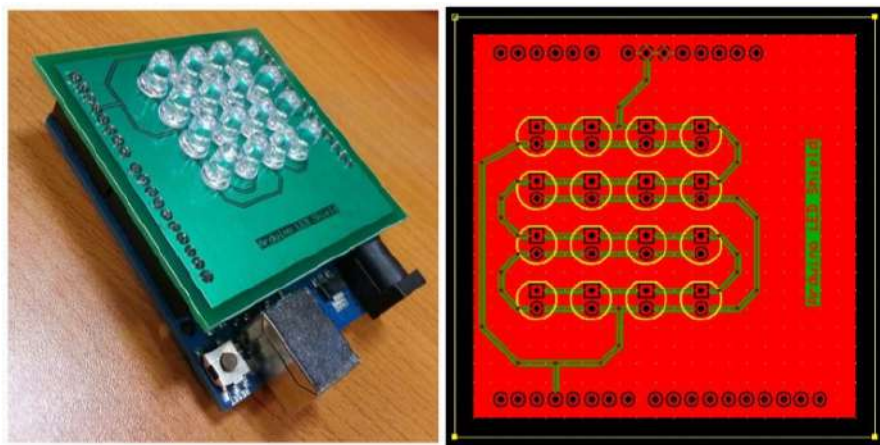


Figure 12.4 Finding transmitter position using *mygeoposition.com*.

## 12.6 ARDUINO CODES FOR TRANSMITTER

The Arduino \*.ino codes are listed below. The baud rate of 38.4kbps and a final delay of not more than 5 ensure that the LEDs do not blink. “H” is used to indicate the start of any message. Commas are used here to separate the coordinate values for easy extraction at the receiver.

```
#include <SoftwareSerial.h>
SoftwareSerial mySerial(2, 3);
void setup()
{
    Serial.begin(38400);
    mySerial.begin(38400);
}
void loop()
```



**Figure 12.5** (Left: Arduino Uno with LED shield attached; right: PCB design of the shield.

```
{
    double value1 = 1.343765;
    double value2 = 103.682265;
    mySerial.print('H');
    mySerial.print(",");
    mySerial.print(value1,DEC);
    mySerial.print(",");
    mySerial.print(value2,DEC);
    mySerial.print(",");
    mySerial.println();
    delay(5);
}
```

## 12.7 RECEIVER HARDWARE

The receiver hardware consists of a pair of ultrasonic rangefinders, a VLC receiver circuit, a GPS module, an XBee Pro S1 transceiver, an Arduino Mega, and an Arduino Uno. Fig. 12.6 is a picture of the receiver and Fig. 12.7 shows its schematic.

## 12.8 ARDUINO CODES FOR RECEIVER

The following are two blocks of *Sketch* codes. The first set is for the Arduino Uno, whereas the second set is for the Arduino Mega.

### 12.8.1 \*.ino Codes for Arduino Uno

This set of codes receives data from the white LEDs and adds or subtracts the values received by the pair of ultrasonic sensors.

```
#include <SoftwareSerial.h>
#include <LiquidCrystal.h>
#include <Wire.h>

float storedY, storedX, vlc_X, vlc_Y;
const int pingPin = 3;
const int pingPin1 = 2;
short LF = 10;

float duration, inches, gpssX, gpssY;
float duration1, inches1;
int cm, cm1;
char charBufX[11];
char charBufY[9];

String lat, lon;
String message;
float latnew;
float longnew;

SoftwareSerial vlcSerial(4, 5);
LiquidCrystal lcd(7,8,9,10,11,12);

void setup() {
    Serial.begin(9600);
    Wire.begin();
    lcd.begin(16, 2);
    vlcSerial.begin(38400);
}

void loop()
{
    delay(300);
    lcd.clear();

    pinMode(pingPin, OUTPUT);
    digitalWrite(pingPin, LOW);
    delayMicroseconds(2);
    digitalWrite(pingPin, HIGH);
    delayMicroseconds(5);
    digitalWrite(pingPin, LOW);
    pinMode(pingPin, INPUT);
    duration = pulseIn(pingPin, HIGH);
    cm = microsecondsToCentimeters(duration);

    lcd.setCursor(13, 1);
    lcd.print('\'');
    lcd.print(cm);
```

```

gpssX = (cm*0.00001)/1.1132;

pinMode(pingPin1, OUTPUT);
digitalWrite(pingPin1, LOW);
delayMicroseconds(2);
digitalWrite(pingPin1, HIGH);
delayMicroseconds(5);
digitalWrite(pingPin1, LOW);
pinMode(pingPin1, INPUT);
duration1 = pulseIn(pingPin1, HIGH);
cml = microsecondsToCentimeters(duration1);

lcd.setCursor(13, 0);
lcd.print('!');
lcd.print(cml);

gpssY = (cml*0.00001)/1.1132;

lcd.setCursor(0, 0);
lcd.print(storedY-gpssY,8);

lcd.setCursor(0, 1);
lcd.print(storedX+gpssX,8);

unsigned long start = millis();

while (start + 1000 > millis()) {

    if (vlcSerial.available() > 0) {

        message = vlcSerial.readStringUntil(LF);
        lon = message.substring(16,26);
        lat = message.substring(3,11);
        lon.toCharArray(charBufX, 11);
        lat.toCharArray(charBufY, 9);
        vlc_X = atof(charBufX);
        vlc_Y = atof(charBufY);

        if (lat.startsWith("1.34")){
            lcd.setCursor(0, 0);
            storedY = vlc_Y;
            float totY = storedY-gpssY;
            lcd.print(totY,8);
            vlcSerial.print(totY,8);
        }

        vlcSerial.print('.');

        if (lon.startsWith("103.68")){
            lcd.setCursor(0, 1);
            storedX = vlc_X;
            float totX = storedX+gpssX;
            lcd.print(totX,8);
            vlcSerial.print(totX,8);
        }
    }
}

```

```

    vlcSerial.println();
    vlcSerial.print('+');

}

long microsecondsToInches(long microseconds)
{
    return microseconds / 74 / 2;
}

long microsecondsToCentimeters(long microseconds)
{
    return microseconds / 29 / 2;
}

```

### 12.8.2 \*.ino Codes for Arduino Mega

These codes mainly collect the GPS and IPS values and output through the GSM module.

```

#include <GSM.h>
#include <TinyGPS.h>
#include <LiquidCrystal.h>
#include <Wire.h>

TinyGPS gps;
void getgps(TinyGPS &gps);
float testfloat = 123.6778;
float storedlat, storedlon;
float latitude, longitude;
#define PINNUMBER ""
const int buttonPin = 4;
char remoteNum[20] = "9XXXXXX"; //mobile no.
short LF = 10;
GSM gsmAccess;
GSM_SMS sms;
LiquidCrystal lcd(5, 6, 8, 9, 11, 12);
int buttonState = 0;

void setup()
{
    pinMode(buttonPin, INPUT); //get ready
    //for button press at pin 4

    Serial.begin(9600);
    Serial1.begin(38400); //VLC
    Serial2.begin(9600); //GPS

    Wire.begin();
    lcd.begin(16, 2);

    boolean notConnected = true;

```

```

while(notConnected)
{
    if(gsmAccess.begin(PINNUMBER)==GSM_READY)
        notConnected = false;
    else
    {
        Serial.println("Not connected");
        delay(1000);
    }
}

Serial.println("GSM initialized");
}

void loop()
{
    String message;
    buttonState = digitalRead(buttonPin);

    if(Serial1.available() > 0) {

        message = Serial1.readStringUntil(LF);

        if(buttonState == HIGH) {
            sms.beginSMS(remoteNum);
            sms.print("IPS:");
            sms.print(message);
            sms.print("GPS:");
            sms.print(storedlat,6);
            sms.print(storedlon,6);
            sms.endSMS();
            lcd.setCursor(0, 0);
            lcd.print("Location Sent.");
            delay(2000);
            lcd.clear();
        }
    }

    if (Serial1.read()=='+') {

        unsigned long start = millis();

        while (start + 10000 > millis()) {

            if (Serial2.available() > 0) {

                char a = Serial2.read();

                if(gps.encode(a)) {

                    gps.f_get_position(&latitude, &longitude);
                    lcd.clear();
                    lcd.setCursor(0,0);
                }
            }
        }
    }
}

```

```
lcd.print("Y:");
lcd.print(latitude, 6);
Serial.print(latitude, 6);
lcd.setCursor(0,1);
lcd.print("X:");
lcd.print(longitude, 6);
Serial.print(longitude, 6);
storedlat = latitude;
storedlon = longitude;

    }
}
}
}
```

## 12.9 SIMPLE VERSION

The simple version can be done easily.

### 12.9.1 Codes

```
Visible Light Communication - Transmitter Codes

#include <SoftwareSerial.h>
SoftwareSerial mySerial(2, 3);
void setup()
{
  Serial.begin(38400);
  mySerial.begin(38400);
}

void loop()
{
  double value1 = 1.343735;
  double value2 = 103.682230;
  mySerial.print('H');
  mySerial.print(",");
  mySerial.print(value1,DEC);
  mySerial.print(",");
  mySerial.print(value2,DEC);
  mySerial.print(",");
  mySerial.println();
  mySerial.print('+');
  delay(5);
}

-----
Visible Light Communication - Receiver Codes

#include <SoftwareSerial.h>
```

```

SoftwareSerial vlcSerial(2, 3);

float vlc_X, vlc_Y;
short LF = 10;
String lat, lon;
String message;
char charBufX[11];
char charBufY[9];

void setup()
{
    Serial.begin(9600);
    vlcSerial.begin(38400);
}

void loop()
{
    if (vlcSerial.available() > 0) {
        message = vlcSerial.readStringUntil(LF);
        lon = message.substring(16,26);
        lat = message.substring(3,11);
        lon.toCharArray(charBufX, 11);
        lat.toCharArray(charBufY, 9);
        vlc_X = atof(charBufX);
        vlc_Y = atof(charBufY);
        if (lat.startsWith("1.34")){
            Serial.println("Latitude: ");
            Serial.println(vlc_Y);
        }
        if (lon.startsWith("103.68")){
            Serial.println("Longitude: ");
            Serial.println(vlc_X);}
```

## 12.10 DIFFERENCE BETWEEN GPS AND IPS

Please read up on the global positioning system. The IPS needs only 3 LEDs, while the GPS needs at least 4 satellites to lock.

```

%Global Positioning System
clear; clc;

%GPS - Global Positioning System - NAVSTAR

%x = distance of the object to the designated x axis (X COORDINATE)
%y = distance of the object to the designated y axis (Y COORDINATE)
%z = distance of the object to the designated z axis (HEIGHT/ALTITUDE)
%cbe = clock bias error

r1 = 1; r2 = 5; r3 = 2; r4 = 4;
x1 = 2; x2 = 1; x3 = 4; x4 = 3;
y1 = 3; y2 = 5; y3 = 7; y4 = 1;
z1 = 2; z2 = 1; z3 = 1; z4 = 1;
```

```

syms ux uy uz cbe

[solutions_x, solutions_y, solutions_z, solutions_cbe] = solve(... 
    (x1-ux)^2 + (y1-uy)^2 + (z1-uz)^2 == (r1 - cbe)^2,... 
    (x2-ux)^2 + (y2-uy)^2 + (z2-uz)^2 == (r2 - cbe)^2,... 
    (x3-ux)^2 + (y3-uy)^2 + (z3-uz)^2 == (r3 - cbe)^2,... 
    (x4-ux)^2 + (y4-uy)^2 + (z4-uz)^2 == (r4 - cbe)^2); 

X = double(solutions_x);
Y = double(solutions_y);
Z = double(solutions_z);
cbz = double(solutions_cbe); %clock error

coordX = real(X(1))
coordY = real(Y(1))
coordZ = real(Z(1))
error = real(cbz(1))

%Indoor Local Positioning

clear; clc;

%Visible Light Indoor Positioning System

r1 = 4; r2 = 5; r3 = 2; r4 = 4;
x1 = 2; x2 = 3; x3 = 4; x4 = 3;
y1 = 3; y2 = 5; y3 = 7; y4 = 1;
z1 = 2; z2 = 2; z3 = 3; z4 = 1;

syms ux uy uz %cbe

%      For indoor positioning systems in buildings, the height from the ceiling to the floor is usually 3
%      or 4 metres, much much shorter than the satellite. Hence the clock bias error is dropped.

[solutions_x, solutions_y, solutions_z] = solve(... 
    (x1-ux)^2 + (y1-uy)^2 == ((z1-uz)*(r1))^2,... 
    (x2-ux)^2 + (y2-uy)^2 == ((z2-uz)*(r2))^2,... 
    (x3-ux)^2 + (y3-uy)^2 == ((z3-uz)*(r3))^2);

%      Use this block if you need a clock biasing error cbe (e.g. deep-space laser transceiver)
%      (x1-ux)^2 + (y1-uy)^2 == ((z1-uz)*(r1 - cbe))^2,... 
%      (x2-ux)^2 + (y2-uy)^2 == ((z2-uz)*(r2 - cbe))^2,... 
%      (x3-ux)^2 + (y3-uy)^2 == ((z3-uz)*(r3 - cbe))^2,... 
%      (x4-ux)^2 + (y4-uy)^2 == ((z4-uz)*(r4 - cbe))^2);

X = double(solutions_x);
Y = double(solutions_y);
Z = double(solutions_z);
%cbz = double(solutions_cbe);

coordX = real(X(1))
coordY = real(Y(1))
coordZ = real(Z(1))
%error = real(cbz(1))

```

## 12.11 MATLAB

Here is something for you to think about.

```
%For the equations, kindly refer to the paper
%L. Zeng et al., "Improvement of Data Rate by using Equalization in an Indoor Visible Light
%Communication System", 2008.
%T. Komine, "Visible Light Wireless Communications and its Fundamental
%Study", 2005.

clear all; clc;
%electron charge (C)
q = 1.60E-19;
%angle of irradiance (half phi)
phi = (25*pi)/180;
%angle of incidence
psi = (15*pi)/180;
%power emitted by LED (mW)
PLED = 30;
%detector area, ARX (or photodiode active area) (cm^2)
ARX = 50/100;
%FOV (field of view) of detector, psi_c
psi_c = (40*pi)/180;
%distance between tx and rx (m)
H = 2.0;

%order of Lambertian emission
m = real(-log(2)/log(cos(phi)));
%Lambertian radiant intensity (or transmitter radiant intensity)
Ro = real(((m+1)/(2*pi))*cos(phi)^m);
%transmitted power, PTX
PTX = PLED*Ro;
%LOS (line of sight) propagation path channel transfer function - HLOS
if (psi>=0) && (psi<=psi_c)
    HLOS = (ARX/H^2)*Ro*cos(psi);
elseif (psi>psi_c)
    HLOS = 0.0;
end;

%number of LEDs per led array - NoLEDs
NoLEDs = 30;
%total power of i LEDs in the directed path - PRXLOS
PRXLOS = NoLEDs*PTX*HLOS;

%photodiode responsitivity
response = 0.4;
%noise power of ambient light
pn = 5840E-6*sqrt(5);
%data rate
Rb = 115200;
%noise bandwidth factor
I2 = 0.562;
```

```

Bn = Rb*I2;
%amplifier bandwidth
Ba = 250E5;
%amplifier noise current
iamplifier = 5E-12*Ba;

%total surface area of room - Aroom
Aroom = 5*5*2 + 5*H*2 + 5*H*2;
Floor_area = 5*5;
Wall1_area = 5*H*2;
Wall2_area = 5*H*2;
Ceiling_area = 5*5;
%average reflectivity - rho
rho = (1/Aroom)*(Floor_area*0.15 + ...
    Wall1_area*0.7 + ...
    Wall2_area*0.7 + ...
    Ceiling_area*0.8);
%the first diffused reflection of a wide-beam optical source emits an
%intensity 'Iprime' over the whole room surface 'Aroom'.
I = rho*PRXLOS/Aroom;
Iprime = I/(1-rho);
%received diffused power 'pdiff' with the photodiode's receiving area ARX
pdiff = ARX*Iprime;

%At the receiver, light passes through the optical filter 'Tf' and
%concentrator gain 'g'.
%Tf is the transmission coefficient of the optical filter.
Tf = 1.0;
%g is the concentrator gain*. The refractive index of plastic is 1.46.
%(My concentrator is a general cheapo plastic lens.
%See the list at http://interactagram.com/physics/optics/refraction/
%*N. Kumar and N. R. Lourenco, "LED-based visible light communication
%system: a brief survey and investigation", J. Engineering and Applied
%Sciences, vol. 5, no. 4, pp. 296-307, 2010.
ri_conc = 1.46;

if (psi>=0) && (psi<=psi_c)
    g = (ri_conc^2)/(sin(psi_c)^2);
elseif (psi>psi_c)
    g = 0.0;
end;

%so the received power prx is
prx = (PRXLOS+pdiff)*Tf*g;
%In fact, there is also the refractive index of the lens/glass/plastic
%covering the photodiode to consider (whose value is about 1.0-1.5);
%however, it is usually ignored.
%shot noise variance - omegashot
omegashot = 2*g*response*(prx+pn)*Bn;
%amplifier noise variance - omegaamplifier
omegaamplifier = iamplifier^2*Ba;
%total noise variance - omegatotal
omegatotal = omegashot+omegaamplifier;
%signal-to-noise ratio SNR
SNR = (response*prx)^2/(omegatotal);
%convert SNR unit to dB

```

```

SNRdb = 20*log10(SNR);

%get radius from height H (between the transmitter and receiver) at
%irradiance angle phi
radius = H/tan(pi-pi/2-phi);
%set grid using radius
[X,Y] = meshgrid(-radius:.1:radius);
%Geometry - get hypotenuse R
R = sqrt((X).^2 + (Y).^2)./cos(pi-pi/2-phi);

%distance between each led array [m]
dist_apart = 1.5;

%translate SNR array to the graph function fx = (sin x)/x.
%Refer to http://press.princeton.edu/books/maor/chapter_10.pdf for
%more info on sin graphs.
Z = SNRdb.*sin(R)./R;

figure(2)
mesh(X+dist_apart,Y,Z,'EdgeColor','black')
xlabel('Length of room [m]')
ylabel('Width of room [m]')
zlabel('SNR [db]')
%axis([-2.5 2.5 -2.5 2.5 0 1])
hold on

mesh(X,Y,Z,'EdgeColor','black')
xlabel('Length of room [m]')
ylabel('Width of room [m]')
zlabel('SNR [db]')
%axis([-2.5 2.5 -2.5 2.5 0 1])
hold on

mesh(X,Y+dist_apart,Z,'EdgeColor','black')
xlabel('Length of room [m]')
ylabel('Width of room [m]')
zlabel('SNR [db]')
%axis([-2.5 2.5 -2.5 2.5 0 1])
hold on

mesh(X+dist_apart,Y+dist_apart,Z,'EdgeColor','black')
xlabel('Length of room [m]')
ylabel('Width of room [m]')
zlabel('SNR [db]')
%axis([-2.5 2.5 -2.5 2.5 0 1])
hold on

title('Communication using White-LED: SNR 3D Plot for Room Illumination')

```

## **12.12 CONCLUSION**

In summary, the VLIPS system works well under present experimental conditions. Efforts are ongoing to integrate it into commercial LED lighting systems for homes and offices. By then, we would have a mature network of position emitting white LEDs that is applicable to old folks homes, hospitals, and open-concept large offices.

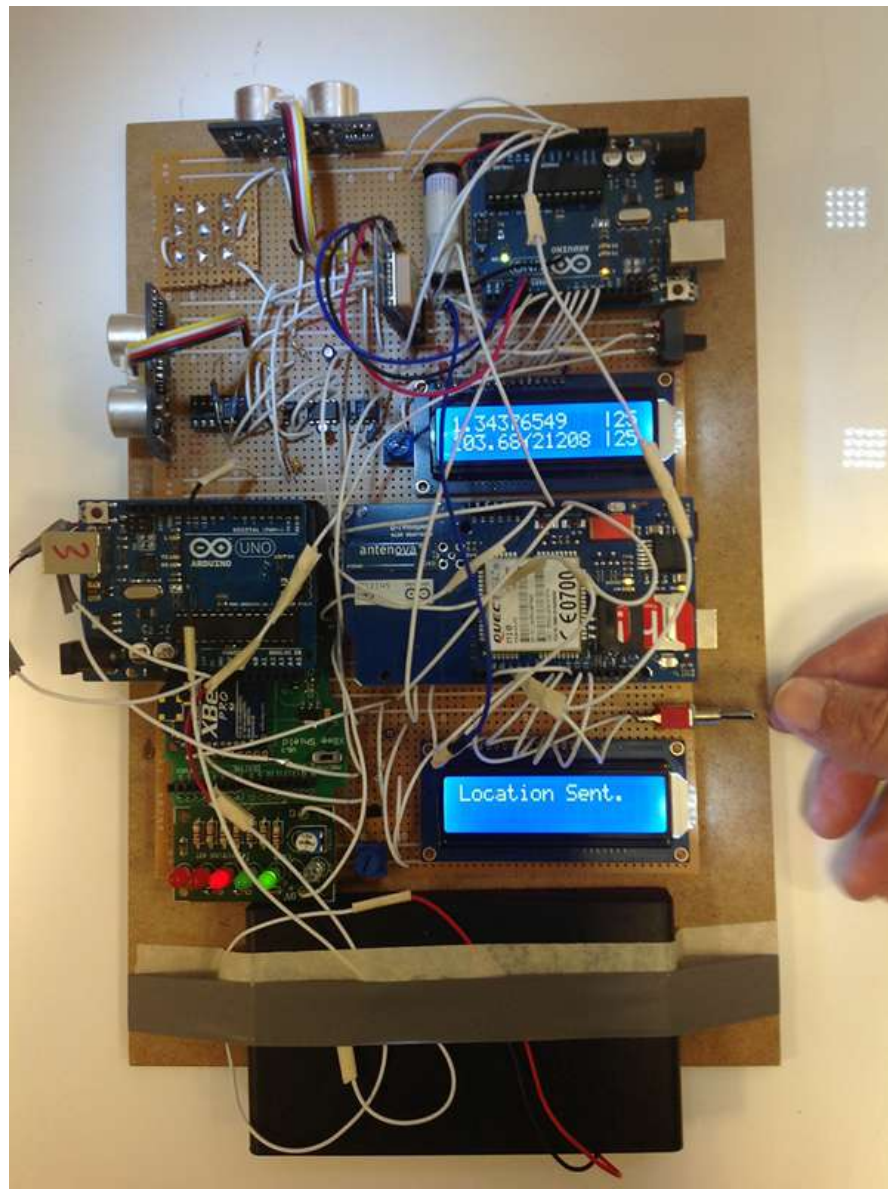


**Figure 12.6** Prototype of the outdoor-indoor positioning receiver.

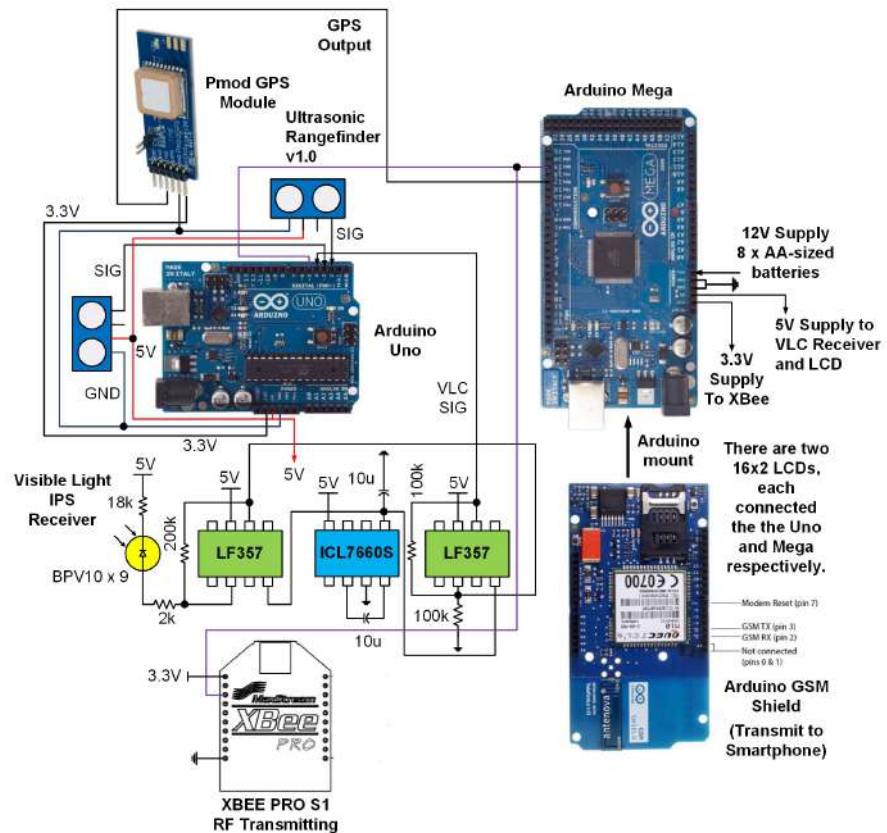


**Figure 12.7** Circuit and connection diagram of the outdoor-indoor positioning receiver.

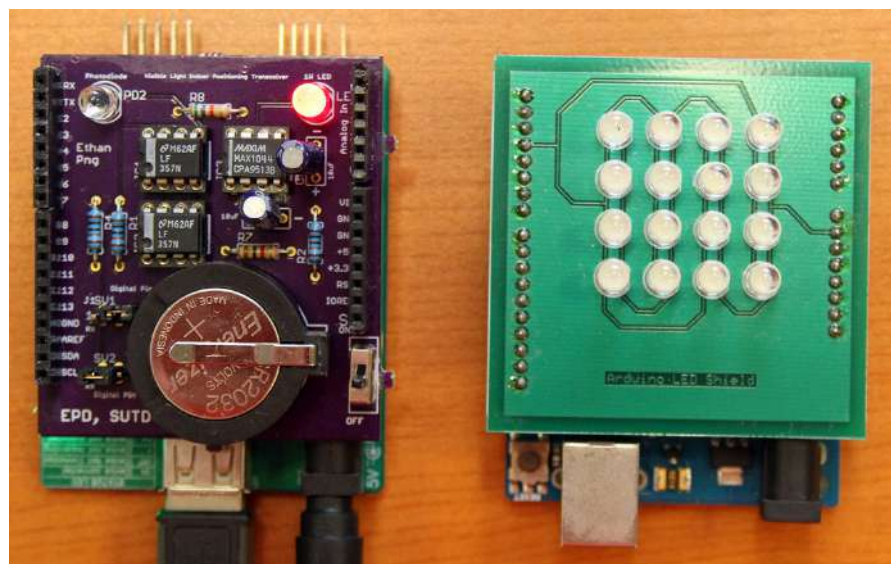
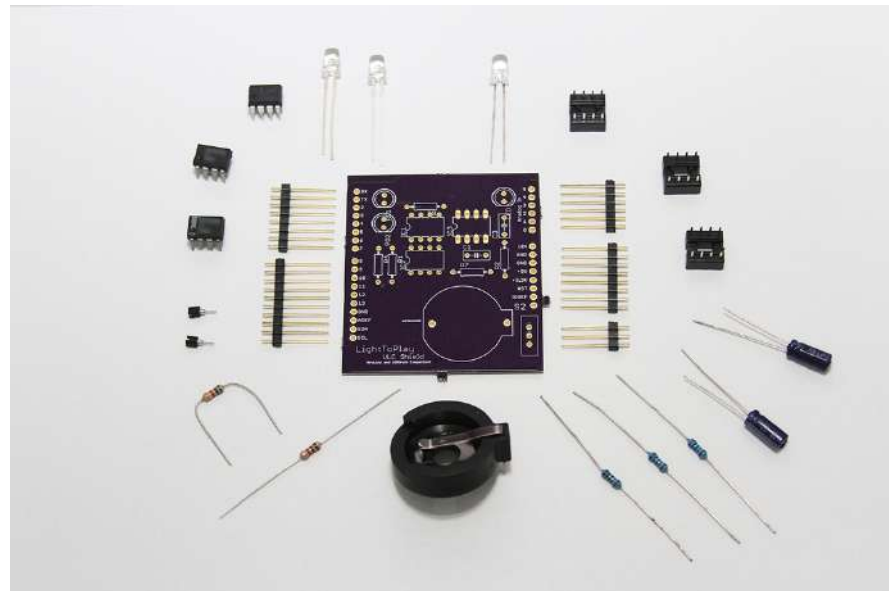


Figure 12.8 VLIPS receiver and transmitter.



**Figure 12.9** Components.

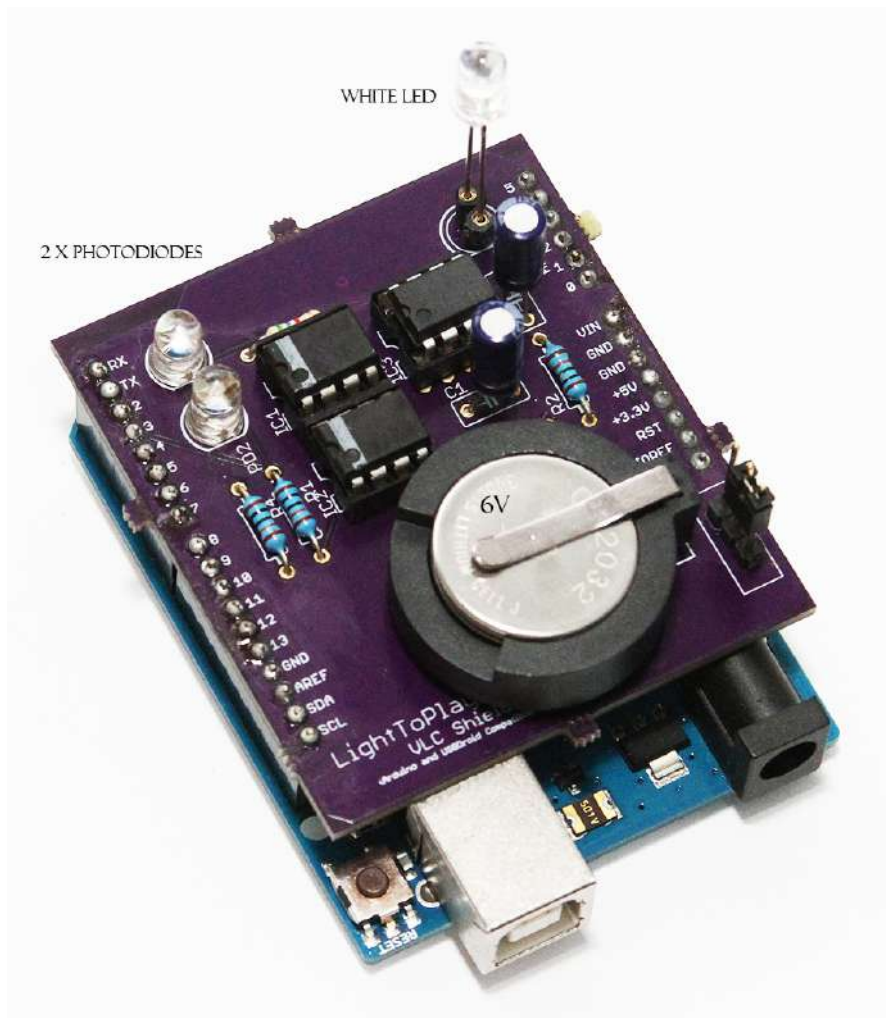
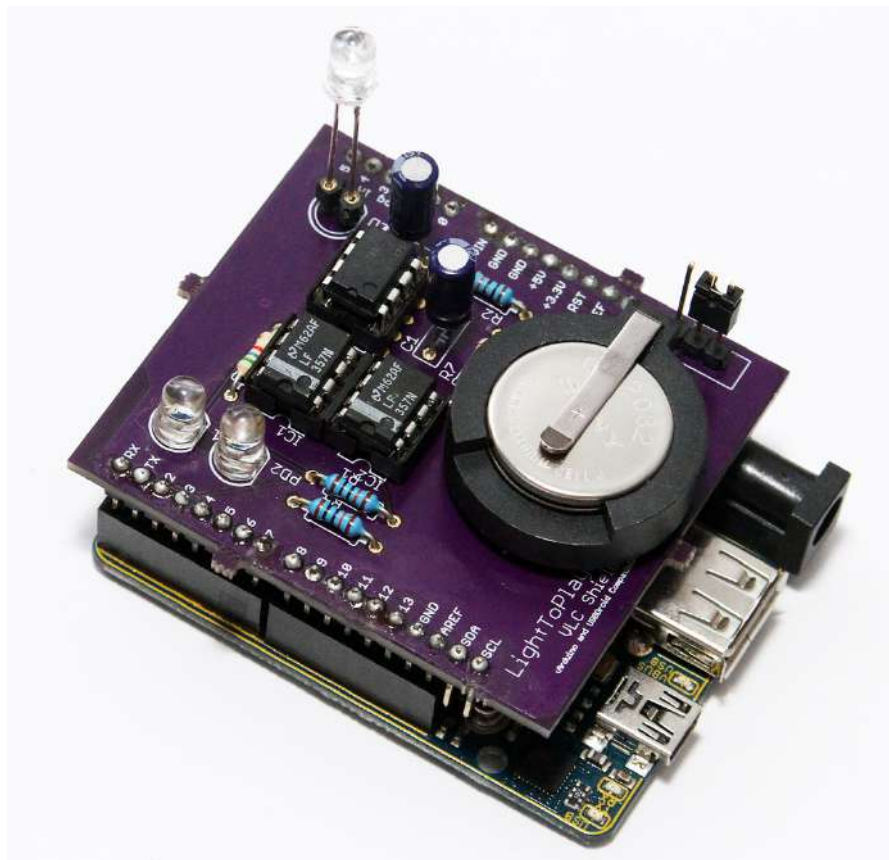
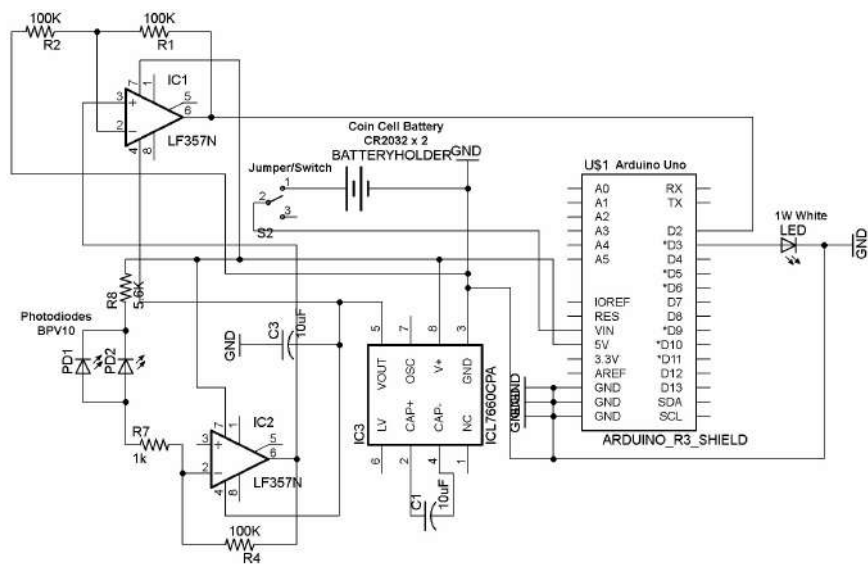


Figure 12.10 Used with Arduino.



**Figure 12.11** Used with USBDroid.



**Figure 12.12** Schematic of IPS Arduino shield.

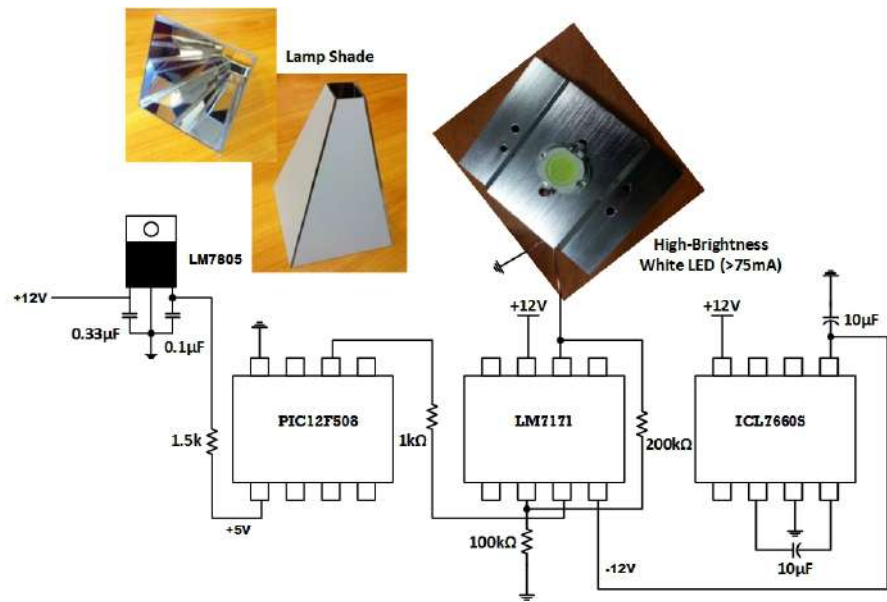
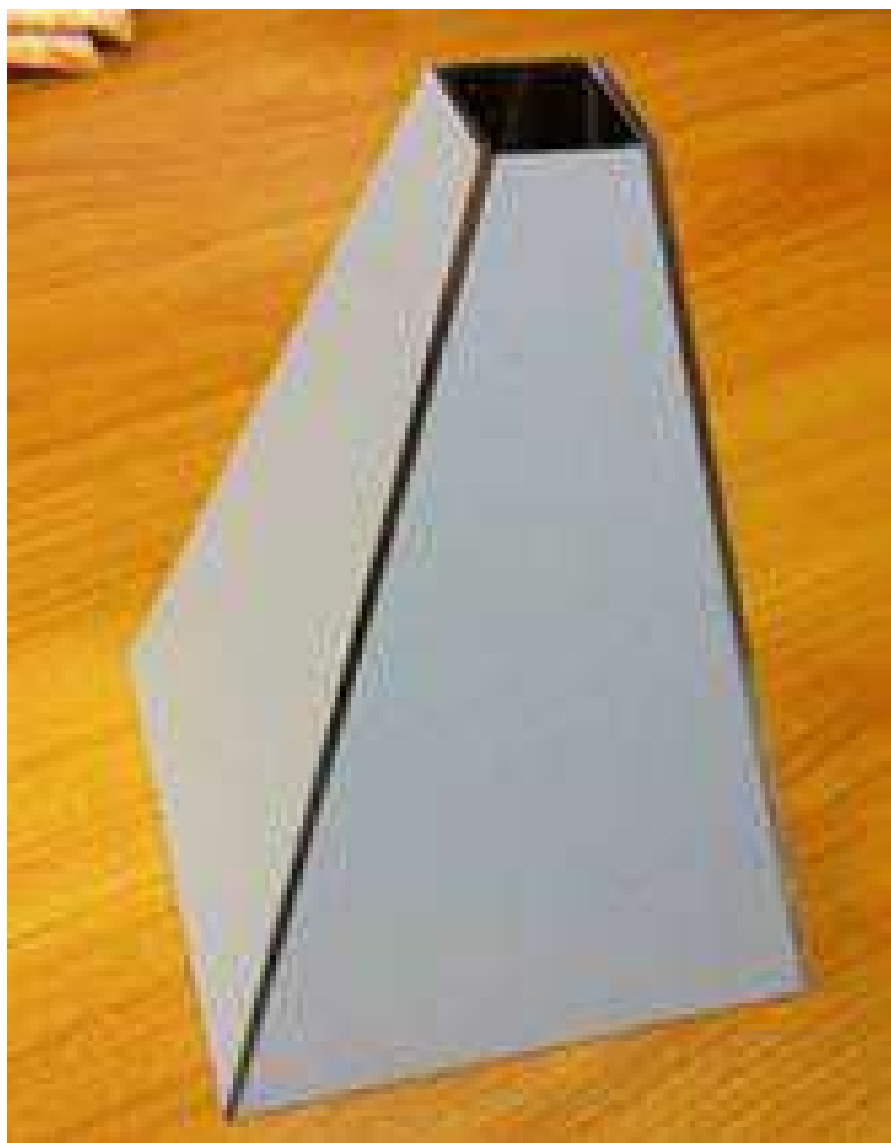


Figure 12.13 Ceiling transmitter circuit.



**Figure 12.14** Customized lamp shade.



**Figure 12.15** Customized lamp shade (bottom view).



# Chapter 13

## Hybrids: Fusion of Visible Light and RF Channels

### 13.1 ABSTRACT

LED lighting has gained wide popularity in recent years. Three Japanese scientists have even been awarded the 2014 *Nobel Prize in Physics* recently for their works in blue LEDs which make the generation of white light possible. Visible light communication (VLC) is expected to become the next alternative medium for indoor high-speed Internet and multimedia access. This proposal aims to investigate by simulations and to discuss the impact of our simulation results on the possibility of a hybrid wireless communication model, where a visible light channel and a radio frequency channel work together to form a MIMO (multiple-input, multiple-output) system. Since optical communication devices can have bandwidths higher than RF, the bit rate can be increased by combining both channels. Such a hybrid system also compensates the awkwardness of lamps. LED lamps will shine down from ceilings (downlink) to deliver data as well as illumination. However, shining lamps upwards (uplink) will produce an uncomfortable glare. RF is not only able to provide the uplink, it is can also improve stability and speed if it operates together with VLC. This research is focused on the indoor environment. For RF, scattering is essential for MIMO channels to improve degrees of freedom. For VLC, it is primarily based on line of sight (LOS); hence, the use of MIMO is mainly for array gain instead of degrees of freedom. There exists a tradeoff between diversity (array) gain and multiplexing gain in such a hybrid system.

### 13.2 INTRODUCTION

VLC [74][75][76] is the application of light in the visible spectrum (380nm to 750nm) as a medium over free space for communication between two devices. The success of IBM's optical processor [77] will revolutionize in the computer industry. If all the Pentium chips were to be replaced by optical chips, we should see an emergence of a whole new generation of optical fiber I/O ports on every PC. Interestingly, these ports can be easily modified to receive free space optical signals by installing visible-spectrum receivers.

The potential for visible light communication is huge [78]. White LEDs have become increasingly popular as illumination sources due to its energy efficiency. The bandwidth of light is virtually unlimited. Local power-line infrastructure can be used as backbone. Depending on the types of LEDs, photodiodes, circuit designs, and IC technologies used, communication can be performed at speeds higher than RF frequencies. Also, light does not penetrate opaque objects, thus preventing eavesdropping.

One of the pressing challenges about VLC is on the uplink. Lights are usually installed on ceilings which provide a natural downlink. This is good for receiving or downloading information. However, to send out information, projecting light towards the ceiling seems impractical and awkward. It also creates glare to the eyes. One of the solutions is to shift the VLC emitter and receiver from the ceiling to the walls, but this would also affect the interior design of the room. The authors thus propose a hybrid communication system to solve this problem: that is, to use RF as the uplink, and VLC and RF as the downlink (Fig. 13.1). Literature on FSO-RF links for outdoor are abundant [79][80][81][82][83][84][85]; however, there are very few literature on indoor VLC-RF modeling.

RF communication has been around for a long time. Currently, the most widely used are Wi-Fi and LTE (Long-Term Evolution) systems. These transceiver chips are easily available on the market which creates an easy opportunity for us to blend both systems. So far, we lack literature on hybrid indoor VLC-RF channel models and its theoretical analyses. This is the central motivation for the paper.

This work focuses mainly on the modeling and simulation of the optical wireless channel and the conventional radio-wave wireless channel. It is highly possible that the future smartphone would include a VLC transceiver. Therefore, a combined mathematical model that utilizes both the VLC and Wi-Fi channels simultaneously to achieve faster information transfer rate is proposed. All the investigations are performed on MATLAB. The hybrid channel model is based on the well-known Gaussian independent parallel channel [86].

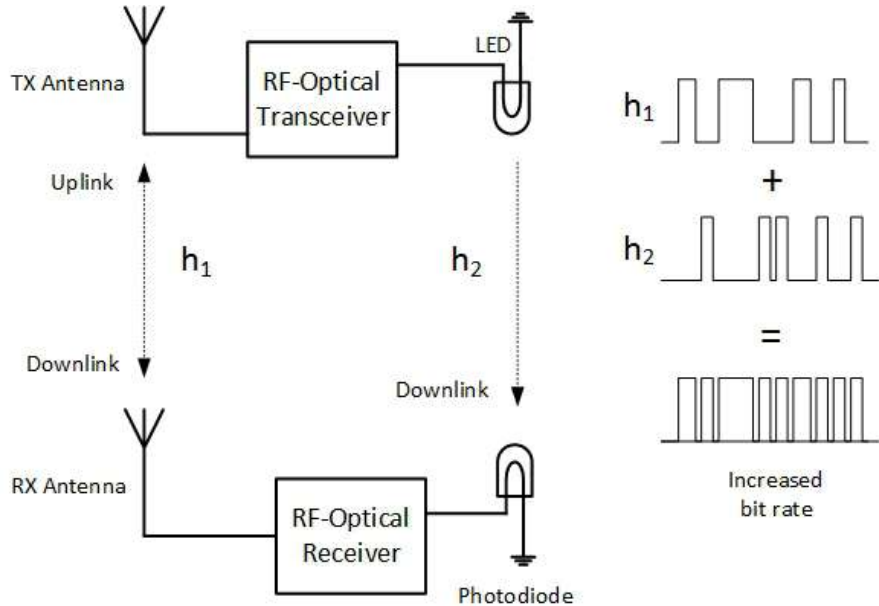


**Figure 13.1** RF-VLC communication system for improved stability and faster bit rate. The RF channel also compensates fading and shadowing problems which can be more serious in VLC.

### 13.3 VISIBLE LIGHT COMMUNICATION CHANNEL

According to [87], the LED optical LOS channel is characterized by the formula

$$h_{ij} = \begin{cases} \sum_{k=1}^K \frac{A_{rx}^j}{d_{ijk}^2} R_o(\phi_{ijk}) \cos(\psi_{ijk}) & 0 \leq \psi_{ijk} \leq \psi_c \\ 0 & \psi_{ijk} \geq \psi_c \end{cases}$$

where  $A_{rx}^j$  is the active area for the  $j^{th}$  receiver;  $d_{ijk}$  is the distance between the  $k^{th}$  LED in the  $i^{th}$  transmitter and the  $j^{th}$  receiver;  $\phi_{ijk}$  is the emission angle;  $\psi_{ijk}$  is the angle of incidence of light at the receiver;  $\psi_c$  is the receiver's field of view;  $R_o(\phi)$  is the transmitter radiant intensity.  $A_{rx}^j$  includes the concentrator gain at the receiver:

$$A_{rx}^j = \frac{n^2}{\sin^2(\psi_c)} A_{PD} \quad (13.1)$$

where  $A_{PD}$  is the photodiode's physical photo-active area and  $n$  is the concentrator's refractive index. The received signal can be written as

$$r_j = \gamma P_{LED} \sum_{i=1}^{i=N_T} h_{ij} t_i + \sqrt{i_{nj}^2} \quad (13.2)$$

$\gamma$  is the photodiode's responsivity which is usually provided in the manufacturer's datasheet.  $i_{nj}^2$  is the mean square noise current at the photodiode output before entering the preamplifier IC. The modeling of the optical wireless channel also includes the diffusion channel which is influenced by the reflectivity of walls and other objects. We will simulate the average reflectivity using Eqn. (13.3) [88]:

$$\langle \rho \rangle = \frac{1}{A_{room}} \sum_i A_i \rho_i \quad (13.3)$$

where  $A_{room}$  refers to the total surface area of the room. The total intensity is finally obtained by summing up the geometrical series:

$$I = I_{init} \sum_{j=1}^{\infty} \langle \rho \rangle^{j-1} = \frac{I_{init}}{1 - \langle \rho \rangle} \quad (13.4)$$

where the individual reflectivities  $\rho$  of walls, windows and other indoor objects are also influenced by their individual areas  $A_i$ . Index  $j$  is the number of reflections.  $\rho_{init}$  is the reflectivity of the region initially illuminated by the transmitter with the optical transmission power  $P_{totalLED}$ . The first diffuse reflection intensity  $I_{init}$  is [89]

$$I_{init} = \rho_{init} \frac{P_{totalLED}}{A_{room}} \quad (13.5)$$

The received diffused power  $P_{diff}$  is therefore

$$P_{diff} = A_{rx} I \quad (13.6)$$

The LOS signal transmitting power (as the major signal component) is formulated as

$$P_{LOS} = P_{LED} \sum_{i=1}^{i=N_T} h_{ij} t_i \quad (13.7)$$

At a particular instant in time, a vector  $T = [t_1, \dots, t_{N_T}]^T$  is transmitted, where  $t_i$  is the convolution of the  $i_{th}$  parallel binary data stream with the LED impulse

response  $h$ . The LOS and diffused components pass through the optical filter and concentrator into the receiver. The final received power is

$$P_{rx} = (P_{LOS} + P_{diff}) T_f(\psi) g(\psi) \quad (13.8)$$

where  $T_f(\psi)$  is the transmission coefficient of the optical filter, and  $g(\psi)$  is the concentrator gain.

### 13.4 RADIO FREQUENCY COMMUNICATION CHANNEL

Considering an indoor environment where emitters and receivers are more or less stationary, the wireless channel can be commonly characterized by [90]

$$h(\tau) = \sum_i a_i \delta(t - \tau_i) \quad (13.9)$$

where  $a_i$  and  $\tau_i$  are the attenuation and propagation delay associated with the  $i^{th}$  multipath component, respectively.  $\delta$  is the delta function.

Cox [91] and Alexander [92] were the first to carefully study indoor path loss in homes and office buildings. Although indoor and outdoor environments are dominated by the same 3 mechanisms (reflection, diffraction, and scattering), indoor conditions are much more variable. For instance, whether the doors are opened or closed do vary signal levels greatly. Wi-Fi antennas mounted at desk level in a partitioned office receive vastly different signals than those mounted on the ceiling. The field of indoor radio propagation is relatively new.

In this work, we will only be investigating the general LOS channel where a Wi-Fi wireless router is located on a wall very close to the ceiling. Since VLC is also a LOS technology, we are looking at ways to theoretically integrate both channels to increase capacity. We will only consider losses by hard partitions (e.g. concrete walls and floors which are part of the building structure). They have physical and electrical characteristics which will affect radio paths. For example [93], a concrete wall has been measured to have about 8-15 dB losses, while a concrete floor has a 10 dB loss. Besides that there is also partition losses between floors. Losses between floors are determined by the external dimensions, the building technology, and the materials of the building. The floor attenuation factor (FAF) usually ranges between 13 dB to 45 dB. For example, the FAF values of the San Francisco PacBell Building from the 1<sup>st</sup> floor to the 5<sup>th</sup> floor are 13.2, 18.1, 24.0, 27.0, 27.1, respectively.

Indoor path loss obeys the distance power law. When there are walls in a direct path between transmitter and receiver antennas, the loss model can be expressed as [94]

$$L(d) = L_0 + 10n \log d + kF_1 + \sum_{i=1}^M A_i \quad (13.10)$$

where  $M$  is the number of partitions between transmitter and receiver antennas.  $A_i$  is the attenuation factor for the  $i^{th}$  partition.  $L(d)$  is the path loss over distance  $d$  from the transmitter.  $L_0$  is the free space propagation attenuation over a reference distance of 1m obtained.  $n$  is the path-loss exponent.  $k$  is the number of floors between transmitter and receiver antennas.  $F_1$  is the single-floor propagation attenuation (floor loss factor).

### 13.5 PARALLEL GAUSSIAN CHANNEL

The VLC-RF channel is basically two SISO channels. Since noise components  $Z_{vlc}$  and  $Z_{rf}$  are independent, the information capacity of the total channel is

$$C = \max_{p(x_{vlc}, x_{rf}): \sum_{j=1}^k P_j \leq P} I(X_{vlc}, X_{rf}; Y_{vlc}, Y_{rf}) \quad (13.11)$$

$$= \max_{\{p_j\} s.t. \sum p_j \leq P} \sum_{j=1}^k \frac{1}{2} \log(1 + \frac{P_j}{\sigma_j^2}) \quad (13.12)$$

which is achieved if  $(X_{vlc}, X_{rf}) \sim \mathcal{N}(0, diag(P_{vlc}, P_{rf}))$ . The power allotment problem reduces to a standard optimization problem which can be solved using Lagrange multipliers.

$$\max_{P_j} \sum_{j=1}^k \log(1 + \frac{P_j}{\sigma_j^2}) \quad (13.13)$$

$$\text{subject to } \sum_{j=1}^k P_j = P, (P_j \geq 0) \quad (13.14)$$

where  $U$  is chosen s.t.  $\sum_j P_j \leq P$ . If we allocate power to channel  $j$ , then its power will be  $P_j = U - \sigma_j^2$ ; otherwise,  $P_j = 0$ . Power is allocated to the channel with

smallest variance and as the power budget increases, we fill up the channels in order of increasing noise variances. At any point, the sum of noise variance and signal power in the channels being used is constant (equal to U).

### 13.6 MODELING WIRELESS INDOOR CHANNEL CONDITION

The indoor channel corresponds to the small coverage areas inside the building, such as an office or a classroom. Since they are completely enclosed by a wall, the power azimuth spectrum (PAS) tends to be uniform (i.e., the scattered components from all directions will be more or less the same power). Further, the channel is relatively static due to extremely low mobility of the terminals inside. The channel condition however may vary with time and location, which still requires a power delay profile (PDP) to represent the channel delays and their average power. In general, a static channel indoor environment means that its channel condition does not change for the duration of data transmission at the given time and location. This is in contrast to a time-varying environment in which the scattered components (objects or people) surrounding the transmitter or receiver are constantly moving even when a terminal is not in motion. A channel condition can be considered static when the degree of time variation is relatively small with respect to the symbol duration. Indoor channels are usually modeled under the assumption that they have either static or quasi-static channel conditions [95].

The IEEE 802.11b Task Group adopts the exponential model to represent a 2.4 GHz indoor channel [96]. Its PDP follows the exponential model. Here, each channel tap is modeled by an independent complex Gaussian random variable with its average power that follows the exponential PDP, while taking the time index of each channel tap by the integer multiples of sampling periods. In other words, the maximum number of paths is determined by the RMS delay spread  $\sigma_\tau$  and sampling period  $T_S$  as follows:

$$p_{max} = \frac{10\sigma}{T_S} \quad (13.15)$$

Assuming that the power of the  $p^{th}$  channel tap has the mean of 0 and variance of  $\sigma_p^2/2$ , its impulse response is given as

$$h_p = Z_1 + j.Z_2, \quad p = 0, \dots, p_{max} \quad (13.16)$$

where  $Z_1$  and  $Z_2$  are statistically independent and identical Gaussian random variables, each with  $\mathcal{N}(0, \sigma_p^2/2)$ .

The power of each channel tap is given as

$$\sigma_p^2 = \sigma_0^2 e^{-pT_S/\sigma_\tau} \quad (13.17)$$

$\sigma_0^2$  is the power of the first tap, which is determined so as to make the average received power equal to one, leading to

$$\sigma_0^2 = \frac{1 - e^{-T_S/\sigma_\tau}}{1 - e^{-(p_{max}+1)T_S/\sigma_\tau}} \quad (13.18)$$

In the IEEE 802.11 channel model, a sampling period  $T_S$  must be at least as small as 1/4. Since the RMS delay spread is relatively small in this example, the power variation in the frequency domain is within at most 15 dB, which implies that frequency selectivity is not that significant.

The RF channel and received power are modeled in this way:

```
%BPSK modulation 0 -> -1; 1 -> 0
data = [0 1 1 1];
s = 2*data-1;
%multiple Eb/N0 values
Eb_N0_dB = [-3:40];
for ii = 1:length(Eb_N0_dB)
    %white gaussian noise, 0dB variance
    n = 1/sqrt(2)*[randn(1,N) + j*randn(1,N)];
    %Rayleigh channel
    hr = 1/sqrt(2)*[randn(1,N) + j*randn(1,N)];
    %Channel and noise Noise addition
    yr = hr.*s + 10.^(-Eb_N0_dB(ii)/20)*n;
    %equalization
    yHat = yr./hr;
    %receiver - hard decision decoding
    ipHat = real(yHat)>0;
    %counting the errors
    nErr(ii) = size(find([ip(ipHat)]),2);
end
```

### 13.7 TOTAL RECEIVED POWER

The total received power is calculated by the sum of the transmitting powers and losses (13.19):

$$P_R(\text{dB}) = P_{RLED}(\text{dB}) + P_{RRF}(\text{dB}) - Loss_{RF}(\text{dB}) \quad (13.19)$$

The received RF power is calculated without including the VLC channel:

$$P_R(\text{dB}) = P_{RRF}(\text{dB}) - Loss_{RF}(\text{dB}) \quad (13.20)$$

where  $P_{RLED}$  is the received power of the LED channel in (13.8);  $P_{RRF}$  is the received power  $yr$  of the RF channel in the code block in the previous section; and  $Loss_{RF}$  is the total loss mentioned in (13.10). Referring back to Fig. 13.1, Eqn. (13.19) is used for the downlink, while Eqn. (13.20) is used for the uplink.

### 13.8 SIMULATION AND ANALYSES

Simulation of the LED channel was conducted first. The model is based on a room which is  $5 \times 5 \times 3$  meters. A white LED lamp (consisting of 4, equally-spaced, high-brightness LEDs) is installed on the ceiling of a room. Fig. 13.2 shows the 3D plot of the light distribution in the room.

The specifications of the component and environmental parameters are as follows:

```
% FOV (field of view) of detector
% in half (Radian)
psi_c = (20*pi)/180;
% Power emitted by LED (W)
PLED = 0.1;
% Detector area, ARX
% (or photodiode active area) (Meter^2)
ARX = 7.8E-7;
% Distance between tx and rx (Meter)
heightLED = 1.48;

% Room Size and reflectivity
% (Meter)
L = 5;
W = 5;
H = 3;
n_floor = 0.15;
n_wall = 0.7;
n_ceiling = 0.8;
% Photodetect concentrator
% refractive index
n_conc = 1.46;
% Gain of lens %
Tf = 10.0;
```

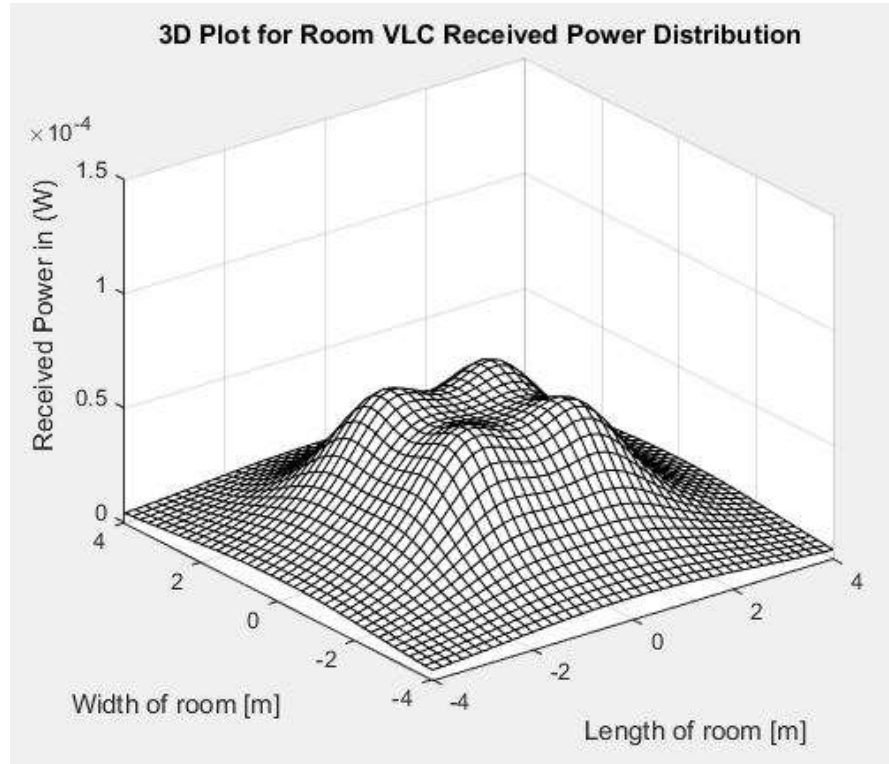


**Figure 13.2** A 3D plot of the illumination intensity in a room.

As illustrated in Fig. 13.3, the spacing between LEDs and radiant angle can be adjusted. This allows us to have a view of the corresponding illumination distribution so that the photo-receiver can be more strategically placed.

We also observe that the amount of loss in the RF signal depends greatly on the walls. Assuming that we are in a 4-room apartment or office separated uniformly by 4 walls (Fig. 13.3), the room diagonally adjacent to the room with a Wi-Fi transceiver will experience the largest loss of 6 dBm. The other 2 adjacent rooms separated by only one wall will experience a lower loss of 3 dBm.

Binary data can be selected in Fig. 13.4 to simulate the transmitted and received signals.

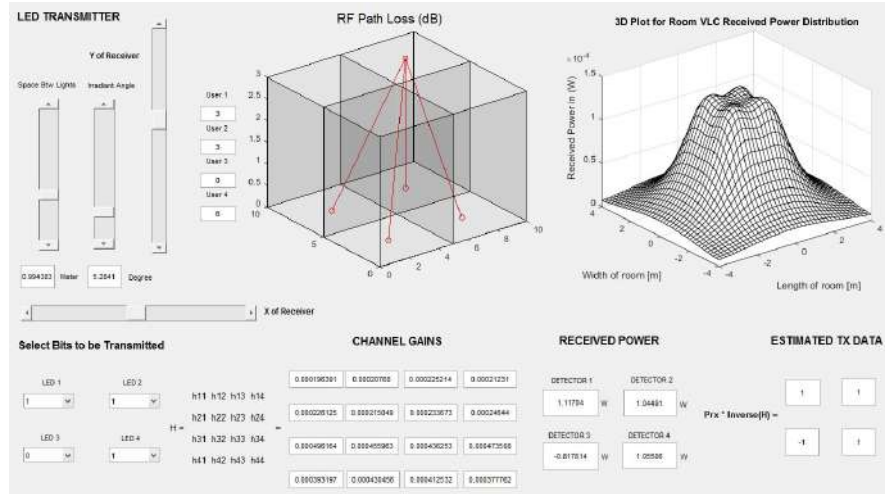


Figure 13.3 Full GUI of the project which includes Benjamin Cizziel's building path loss model [97].

Using only RF wireless channel (13.20), the simulated power is around 0.000057W. We include a random factor to generate different values of path losses (13.10) and find that there are occasional errors in the received bits.

When we implemented the VLC channel in Eqn. (13.19), there is almost no error in the received bits (Fig. 13.6). This is because there is a diversity gain. The SNR for the RF channel is only -12.44 dBm whereas the VLC-RF channel has an SNR of -11 dBm. The diversity channel gain matrix is shown in Fig. 13.7.

Lastly, we want to know more about the VLC-RF transceiver's power allocation and capacity. The parameters for simulation are listed below:

```

nSubChannel = 2; % vlc & rf
totalPower = 0.008; % 9 dBm
channelStateInformation =
    random('rayleigh', 1/0.6552, 1, nSubChannel);
bandwidth = 2.4e9; % 2.4GHz
noiseDensity = 1e-11; % -80 dBm

```

The Shannon capacity generated is 3.4326e9 bps while the powers allocated to the VLC and RF channels are 0.0067W and 0.0013W respectively. The waterfilling power allocation based on noise is illustrated in Fig. 13.8.

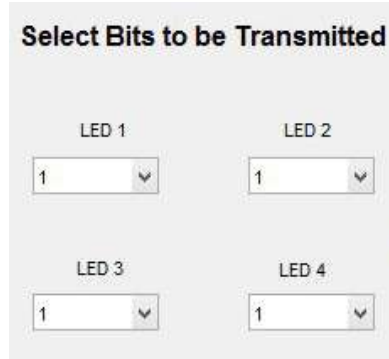


**Figure 13.4** Matlab GUI for selecting binary 1 or 0 for transmission simulation.

### 13.9 COMPARISON BETWEEN INDOOR AND OUTDOOR RF CHANNELS

Indoor and outdoor channels are similar in their basic features: they both experience multi-path dispersions caused by a large number of reflectors and scatterers. They can use the same mathematical model. Also, indoor terminals do not move very rapidly; therefore Doppler shift is negligible. Without distant reflectors, the outdoor rms delay spreads are of the magnitude of several  $\mu s$ . With distant reflectors, it is 10 to 20  $\mu s$ . The indoor channel has excess delays of  $< 1\mu s$  compared to several  $\mu s$  for the outdoor mobile channel. The excess delays can be  $> 100\mu s$  if reflections from distant objects such as hills, mountains, and buildings are taken into account. The indoor rms delay spreads are in the range of several tens to several hundreds of nanoseconds (most often less than 100ns). Thus, for the same level of intersymbol interference, transmission rates can be much higher in indoor environment.

Unlike the empty-room assumption in this work, path loss in an actual indoor environment is bad most of the time, unless you are very near to the wireless router or your computer/notebook is in the line of sight with the router. The real-life indoor environment is cluttered with furnitures and little objects and people moving around. This makes the condition very dynamic and ever-changing over short distances. Simple path loss rules may not be adequate to describe the indoor channel.

### 13.10 CONCLUSION

Light channels have unlimited bandwidth, but this is presently limited by hardware. It is a promising technology that is able to improve the RFCMOS bottleneck. There will come

RECEIVED POWER		ESTIMATED TX DATA	
DETECTOR 1		DETCTOR 2	
0.989529	W	1.09661	W
		$\text{Pr}_x * \text{Inverse}(H) =$	
DETECTOR 3		DETCTOR 4	
1.06665	W	-0.477955	W

**Figure 13.5** Using only RF: occasional error is seen.

a time when the transistor cannot go any smaller and faster. VLC and photonics have to blend in. Therefore, in this paper, we are looking at the raw possibility of achieving VLC and RF integration. The project is able to open up a new way of looking at LED and RF communication. A combined RF and visible light signaling and transmission model is necessary for the next-generation wireless network. We will be able to predict and improve the signal quality and capacity indoors and maximize the usage of all the possible communication devices by integration. The study will also help us select the modulation schemes that are most suitable for MIMO VLC-RF communication. This work suggests that VLC and RF could compensate each other through waterfilling when noise quantity changes. RF problems caused by excessive diffraction, scattering, reflection, and wall, ceiling, and floor losses can be flexibly compensated by LEDs which, if strategically spaced, can give almost error-free transmission for the downlink. On the other hand, RF compensates VLC for the uplink, since LEDs for uplink (i.e. sending data from your desktop terminal or smartphone to the photoreceiver on the ceiling) seems impractical.

RECEIVED POWER				ESTIMATED TX DATA	
DETECTOR 1	1.08659	W	DETECTOR 2	0.846546	W
					1
					1
Prx * Inverse(H) =					
DETECTOR 3	1.08222	W	DETECTOR 4	1.05127	W
					1
					1

Figure 13.6 Using RF and VLC: robust, no error.

CHANNEL GAINS					
	6.26894e-05	6.53649e-05	6.95155e-05	6.65465e-05	
h11 h12 h13 h14					
h21 h22 h23 h24	5.67329e-05	5.42716e-05	5.72651e-05	5.99694e-05	
H =	=				
h31 h32 h33 h34	0.000115815	0.00010768	0.000102944	0.000110467	
h41 h42 h43 h44					
	0.000137165	0.000147583	0.000139579	0.000130077	

Figure 13.7 Using RF and VLC: gain matrix.

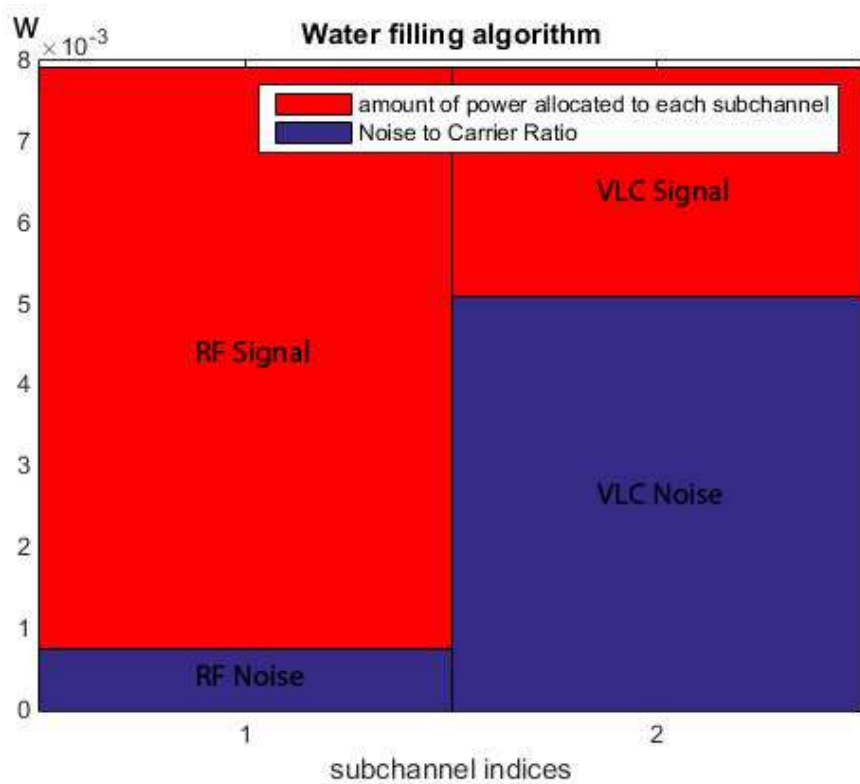


**Figure 13.8** Power allocation based on water filling.



# **Chapter 14**

## **Fusion of VLC and Plasmonics for Clinical Diagnostics**

### **14.1 ABSTRACT**

Healthcare means high cost in many countries. To effectively and affordably diagnose diseases from fluid samples, we need a portable, simple, and easy-to-use device so that they can be distributed and used in remote areas of the world. Deaths can be avoided if patients are able to get their blood samples diagnosed early and receive treatment for their illnesses immediately. There are 2 solutions to this point-of-care (POC) problem by the use of surface plasmonic resonance (SPR): (1) modification of the DVD-R disc to make it suitable for fluid sample test; (2) construction of a portable optoelectronic biosample scanner, possibly to dock to the camera of a smartphone which acts as a photodetector. Based on experiments of protein samples on the DVD-R disc, the authors show the feasibility of such an application.

### **14.2 INTRODUCTION**

The research and development of point-of-care (POC) diagnostic devices started about a decade ago. The objective of such devices is to provide effective, affordable clinical tests and give on-the-spot test results for patients living in remote and under-developed communities [98]. For the middle-class population, such devices should be able to be bought off the shelves at pharmacies and supermarkets to monitor family health at home.

Lab-on-a-DVD technologies vary greatly in terms of the technologies used. These test devices are becoming more attractive recently because they can be ‘near’ the patients due to their portability. They are able to give instant diagnostic results to the patients. Although they are easy to operate, a trained person is still required to conduct a proper test. Hence, at this point in time, this kind of devices are still impossible at ‘village level’. The World

Health Organization's aim is to cut down time and cost by avoiding any test sample to be sent to a far-away hospital or lab. Healthcare in rural societies will considerably improve with the presence of an efficient device which can provide fast diagnoses of contagious and communicable diseases. Timely medical aid can then be activated to bring the diseases under control.

POC diagnostics can be classified into 10 categories: glucose level, blood chemistry and electrolyte, pregnancy and fertility, drug and alcohol, cardiac markers, cholesterol, hemoglobin/hemostasis, urine chemistry and tumor marker. Challenging areas of research include HIV testing, drugs of abuse, and infection diagnosis. However, many POC devices are still expensive and not easy to use. There is still a 'last mile' to conquer to make them easily accessible to everybody. There are 2 feasible ways of achieving this. One way is to modify the DVD-R (digital versatile disc recordable) so that fluid test samples can be deposited on top and then the DVD player is able detect particular cell concentration in the sample. The second method is to build a compact SPR handheld device so that it can be carried anywhere. If need be, it should also connect to the camera on a smartphone since the camera can function as a photosensor.

On the market, the conventional 4.7GB DVD-R disc (which uses silver in the reflective layer) is very cheap. They can be modified and used for a one-time-throw-away sample test. This type of disc is also very easy to be modified into an SPR DVD disc. In contrast, there is also another type of DVD-R disc (called the gold archival disc) which is much more expensive. Because silver can corrode, it adds another layer of gold above the silver to ensure stability and durability. However, since we are aiming at 'one-off' discs, we will focus on the common DVD-R in this work, which is more practical.

### 14.3 SURFACE PLASMON RESONANCE AND DVD

Surface plasmonic resonance (or SPR) is the resonant oscillation of conduction electrons when they are stimulated by incident visible light [99][100]. The resonance condition is established when the frequency of incident photons matches the natural frequency of surface electrons of a metal layer (e.g. silver or gold). SPR is the fundamental principle behind many lab-on-chip, lab-on-DVD, and biosensor applications. A surface plasmon is an electromagnetic wave propagating along the surface of a thin metal layer.

SPR (Fig. 14.1) is used to monitor binding events between the analyte (ranging from ions to viruses) and the ligand (a type of binding chemical). Visible light passes through a prism and hits the gold/silver layer. At a certain incident angle known as the resonant angle, light is absorbed by the gold/silver electrons, causing them to resonate. These resonating electrons are known as surface plasmons. Since light has been absorbed, there is an intensity loss in the reflected beam which appears as a dip in the graph.

The conventional DVD-R disc (Fig. 14.2a) available on the market is usually less than a dollar. The more expensive (and rare) gold archival disc (Fig. 14.2b) is used mainly for permanent backup storage which can last for a century. This was how it got the name 'the

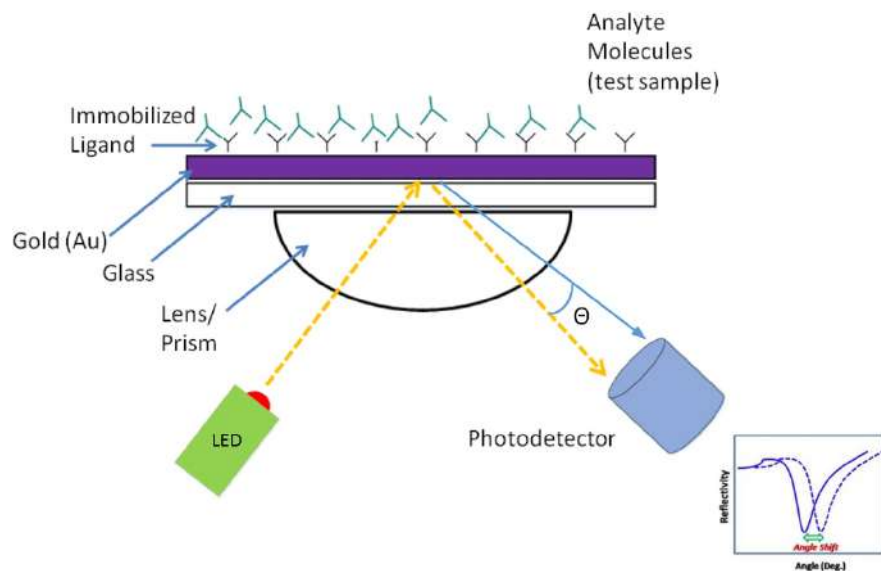


**Figure 14.1** Operation of the typical SPR diagnostic device.

hundred-year disc'. Since a gold layer is added to the silver layer, the reflective layer becomes less likely to corrode. This kind of disc is an equivalent version of the SPR disc or test plate found in lab spectrometers (Fig. 14.1). Many scientists are now trying to modify gold DVD-R for biotests. Gold gives an SPR signal at convenient combinations of reflectance angle and wavelength. In addition, gold is chemically inert to solutions and solutes typically used in biochemical contexts. When the energy of the photon electrical field is just right, it can interact with the free electron constellations on the gold surface. For the sake of affordability, we decided that the typical silver-layered DVD-R will do just fine as an SPR test kit.

#### 14.3.1 SPR DVD-R - How It Works

This section describes how an SPR disc works. This is the implementation in any standard SPR spectrometer. We are only modifying the everyday DVD-R by splitting the disc into two parts (0.6mm thick each) and recombining them again with the test sample sandwiched in between. The basic operation of the concept is shown in Fig. 14.3.

During a sample test, ligand is first coated on top of the gold layer to make it easier to bind with sample molecules or cells. When we place a sample on top of the gold layer, the molecules bind with the surface. During this binding activity, the refractive index at the

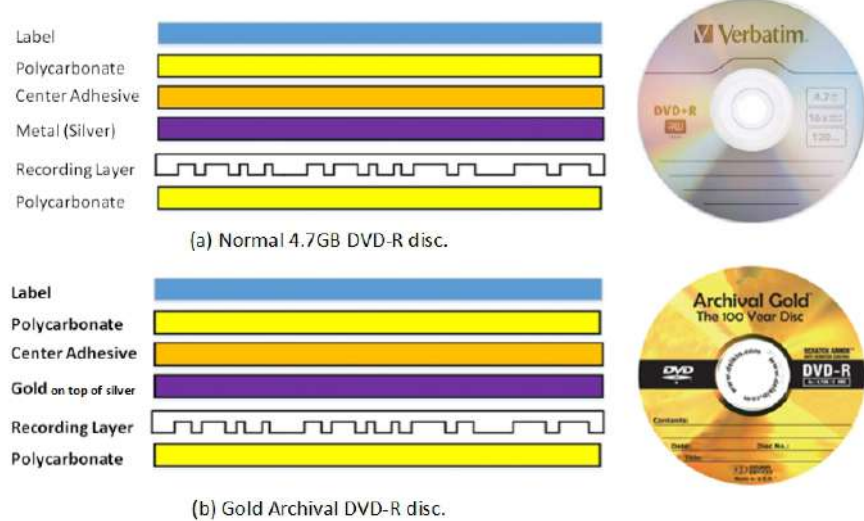


**Figure 14.2** The layer differences between a normal DVD-R disc (top) and a gold archival DVD-R disc (bottom).

gold surface changes, thus altering the angle of reflected intensity from the laser or LED. The original angle of incidence changes by  $\theta$ . Therefore, we see a shift in the position of the reflectance dip along the wavelength axis. The change in SPR angle is proportional to the mass or concentration of the material bound.

It does not matter whether the sample is placed on which side of the metal layer. The principle behind the DVD SPR technique as a biosensor is simply plane-polarized light hitting a metal film under total internal reflection conditions. The best angular accuracy of the goniometer in angular SPR is  $0.001^\circ$ , which corresponds to an optical wavelength shift of 0.6 nm. The observer is able to see a horizontal shift of in the dip in both the angle of incidence plot and the wavelength plot. A full-wavelength standard spectrophotometer can simultaneously observe wavelengths from 400 - 800 nm, and it is more accurate than angle measurements. Nowadays, good spectrometers can range between 200nm to 4000nm, but they are still very expensive and not compact and portable.

DVD and Blu-Ray discs have built-in grooves (carved on the dye layer) which can be used as diffractive gratings. Gratings can be used to further identify samples with very close concentrations. Extra nanopatterns can also be ‘stamped’ onto a flat, transparent polymer disc by nanoimprinting. At the moment, our lab is not able to nanoimprint DVD discs because they will damage the machine (Appendix). Hence we will not discuss nanomiprinting in this paper.

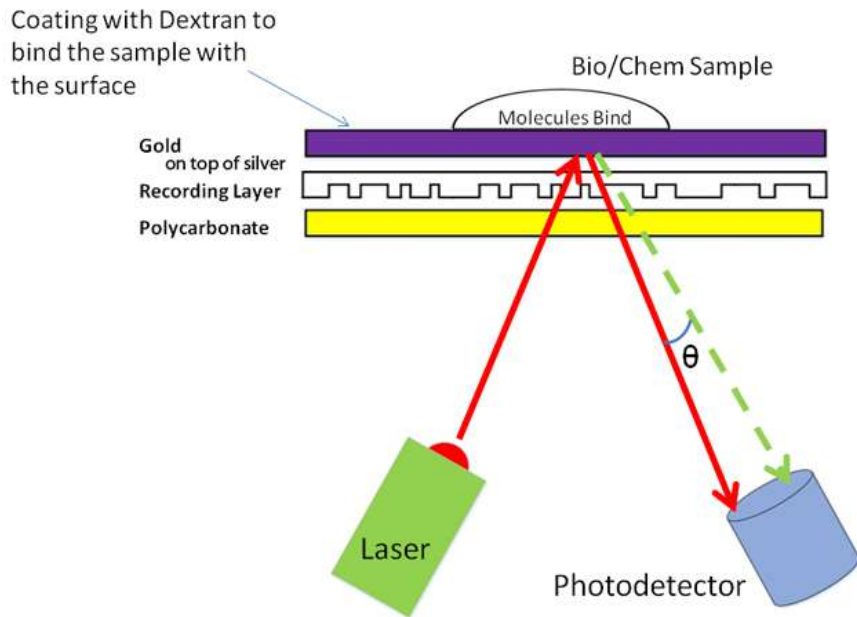


**Figure 14.3** A modified DVD-R in operation. For silver, the plasmonic resonance absorption peak is around 376nm. For gold, the plasmonic resonance absorption peaks at around 920nm.

Dextran can be used as the ligand, but it is not compulsory. It is commonly applied as a stabilizing coating to protect metal nanoparticles from oxidation and improve biocompatibility.

#### 14.4 DVD-R EXPERIMENT ON THE LAB SPECTROMETER

Before the normal DVD-R disc can be tested to pinpoint the absorption peak of silver at resonance, we need to cut down its size and split the disc. This can be done with a metal sheet cutter and a penknife. The processed DVD-R is shown in Fig. 14.4.

The disc should be washed with ethanol alcohol to remove the thin layer of dye. Otherwise, reflectivity from the silver layer will be affected by the dye. Normally, silver nanoparticles gave an absorption peak at 376nm. Our experimental result fits this profile. On the lab spectrometer, we obtained the absorption at 376.65nm (Fig. 14.5).

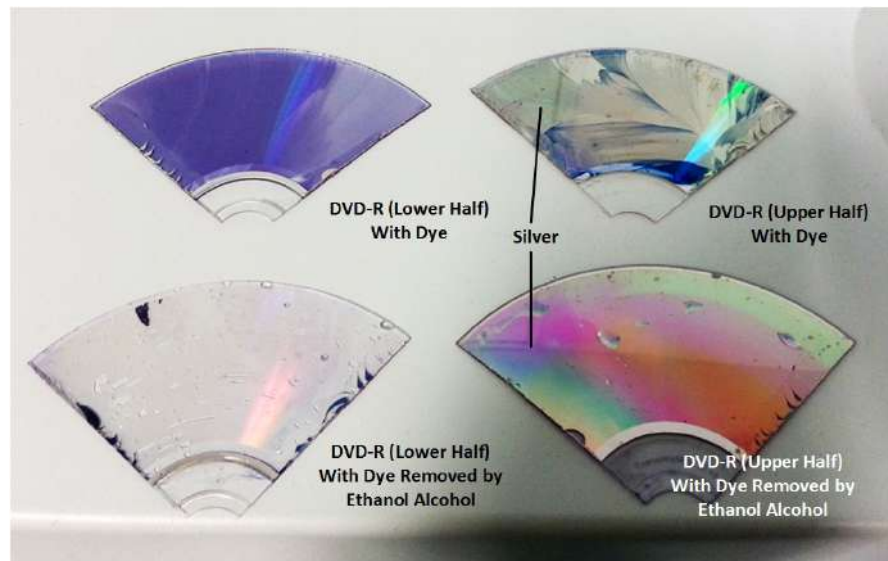


**Figure 14.4** Processed DVD-R disc parts. The piece at the bottom right corner is used for the spectrometer experiment to confirm that the metal layer is silver.

Next, we tested SPR reflectivity on protein concentrations (Fig. 14.6). First, we obtained the reflectance (%R) vs. wavelength plot for a clean disc. Next, we spread a layer of 1xPBS (phosphate buffered saline) and ran the plots. Lastly, we obtained the plots for 1xPBS together with another layer of 1%BSA (bovine serum albumin).

For a clean disc surface, the resonance occurs at 360.23nm. For a 1xPBS, the wavelength is shifted to 358.36nm. For 1xPBS with 1%BSA, the wavelength shifted further back to 356.18nm. This shows that one percent of BSA can be identified with a  $358.36 - 356.18 = 2.18\text{nm}$  wavelength marker in an SPR test. From this experiment, we can also see that the detection range is in the ultraviolet (UV) spectrum. This is good news, since UV products can be cheaply manufactured.

A Blu-Ray Disc Rewritable (BD-RE) is a little different from the DVD-R. On top of the silver layer, there is a layer of zinc sulfide (not gold) to reduce heat. Since zinc sulfide's resonance absorption peak is around 1400nm-1550nm, this will affect the spectrometer reading. Therefore we see that the reflectivity peaks appear at around 1458nm for egg white (Fig. 14.7).

SPR diagnosis using a Blu-Ray is therefore not feasible. It is not only expensive, it also has an inconveniently high resonant wavelength which is normally used in fiber optic cables.

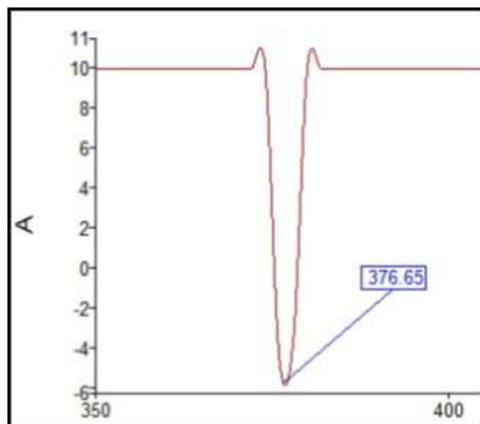


**Figure 14.5** Spectrometer reading: absorption of light in the silver layer at SPR condition. According to [101], we can expect a range of peaking dips between 338nm-376nm in our following experiments.

## 14.5 PORTABLE POC DEVICE DESIGN

From Fig. 14.6, we observe that the values of all the dips occur between 350nm and 370nm generally. This is an ultraviolet (UV) region known as UV-A rays (Fig. 14.8). Since this wavelength does not involve expensive components, it is possible to build a cheap and efficient spectrophotometer. The critical components we need are only an ultraviolet LED and an ultraviolet photodiode. Both are easily available on the market. Most visible spectrum photodiodes are sensitive to the UV-A band. A lot of human-eye mimicking photodiodes have wavelengths ranged between 200nm-800nm. Therefore it is possible to build a simple optoelectronic receiver to receive UV to blue light.

Based on the project in [103], it is possible to build a DIY portable spectrophotometer that docks to a smartphone camera. However, the device is too simple and it does not actually function the way we want it to. We have to come up with our own design (Appendix: Fig. 14.9). The optical receiver circuit is the most important component. It has to capture analog signals so that any microcontroller attached to it is able to generate the intensity values. The LM7171 video amplifier was chosen due to its high slew rate. Fig. 14.10 is a schematic diagram of the receiver. 2 photodiodes receive the reflected light from the silver layer. The first 7171 works as a preamplifier for amplifying light signals, converting current to voltage. The second 7171 works as a comparator to threshold the signals. Fig. 14.11 is a picture of the finished photoreceiver.

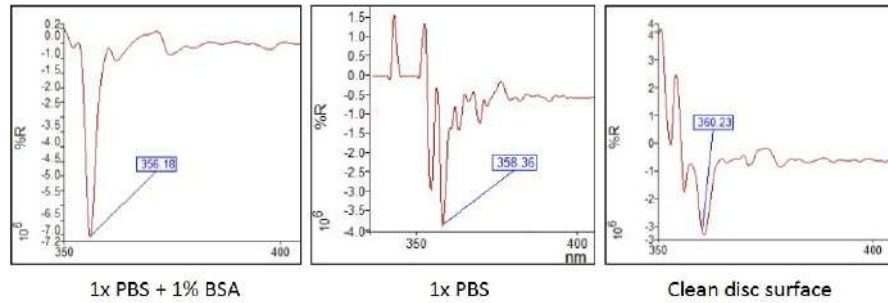


**Figure 14.6** Spectrometer readings for %R vs. wavelength for DVD-R: (left) 1xPBS + 1%BSA, (middle) 1xPBS, (right) clean surface.

#### 14.5.1 Calculation of Absorbance

Although the absorbance graph is usually plotted automatically by the spectrometer system in the lab, the mathematical formula is needed if we were to develop an Android app for the POC device when it docks to our phones. The absorbance  $A$  of a fluid sample or solution at a particular wavelength is described by the *Beer-Lambert Law* [104]:

$$A = -\log_{10}(I/I_0) = \varepsilon c l \quad (14.1)$$

where  $c$  is the sample concentration,  $l$  is the path length of the sample,  $\varepsilon$  is a wavelength-dependent constant characteristic of the sample.  $I_0$  is the incident light intensity and  $I$  is the transmitted light intensity. Absorbance is calculated from voltage. First, we measure the voltage of the receiver output by using a multimeter or oscilloscope for each wavelength (or color). Next,

- determine  $V_{zero}$ , i.e. signal voltage taken when no LED light is shining on the photodiodes,
- determine  $V_{sample}$ , i.e. signal voltage taken after the LED light has been transmitted through the sample,
- determine  $V_{water}$ , i.e. signal voltage taken after the LED light passes through plain water.

Having these readings, we are able to calculate the absorbance ratio of the sample:

$$I/I_0 = I_{sample}/I_{water} \quad (14.2)$$

$$= (V_{sample} - V_{zero})/(V_{water} - V_{zero}) \quad (14.3)$$

The absorbance values can be plotted against wavelength or sample concentration. The most direct way to do an SPR test is to use a professional spectrometer; however, the

spectrometer is expensive and is not available everywhere. This is the reason we have to make POC devices compact and easy to use. Some SPR POC devices are so handy that they can dock to the camera of a smartphone and capture the peaks from the resonance [105]. The Beer-Lambert Law is programmed into an Android app and the smartphone acts as a processing and display terminal.

#### 14.6 CONCLUSION

Experimental tests have been conducted on DVD-Rs and results show that SPR does produce unique identifying wavelengths for particular samples. There is an urgent need around the world for a quick and effective form of virus detection and diagnosis. A set of criteria such as affordability, accessibility, sensitivity, specificity, ease-of-use, speed, and robustness have been listed by WHO as necessary to bring healthcare to developing countries and financially deprived regions. By modifying the DVD-R disc and by building portable spectrophotometers, SPR diagnosis will benefit basic healthcare by reducing cost and time. Since long travels for patients and test samples are avoided, immediate treatment will be available to the sick so that they can have a higher chance of survival.

#### References

- [1] EU Commission Directorate-General for Health & Consumers, "Scientific Committee on Emerging and Newly Identified Health Risks - Light Sensitivity", 2008.
- [2] T. D. C. Little, P. Dib, K. Shah, N. Barraford, and B. Gallagher. "Using LED Lighting for Ubiquitous Indoor Wireless Networking". *IEEE International Conference on Wireless & Mobile Computing, Networking & Communication*, pp. 373-378, 12-14 Oct 2008.
- [3] G. Pang, T. Kwan, H. Liu, and C. H. Chan. "LED Wireless - A Novel Use of LEDs to Transmit Audio and Digital Signals". *IEEE Industry Applications Magazine*, pp. 21-28, Jan/Feb 2002.
- [4] A. B. Sebitosi and P. Pillay. "White LEDs for Rural Lighting". *IEEE Power Engineering Society General Meeting*, pp. 2619-2623, 2003.
- [5] Y. Tanaka, S. Haruyama, and M. Nakagawa. "Wireless Optical Transmission with White Colored LED for Wireless Home Links". *The 11th IEEE International Symposium on Personal, Indoor and Mobile Radio Communications (PIMRC)*, vol. 2, pp. 1325-1329, 2000.
- [6] G. Pang and G. Poon. "A Portable Multimedia Information Device in a Wireless Optical Data Link". *IEEE Trans. on Consumer Electronics*, vol. 47, no. 1, pp. 87-95, 2001.
- [7] G. Pang. "Information Technology based on Visible LEDs for Optical Wireless Communications". *2004 TENCON IEEE Region 10 Conference*, vol. B, pp. 395-398, 2004.
- [8] S. Iwasaki, M. Wada, T. Endo, T. Fuji, and M. Tanimoto. "Basic Experiments on Parallel Wireless Optical Communication for ITS". *Proceedings of the 2007 IEEE Intelligent Vehicle Symposium*, pp. 321-326, 13-15 June 2007.

- [9] G. Pang; T. Kwan, C. H. Chan, and H. Liu. "LED Traffic Light as a Communication Device". *Proceedings of 1999 IEEE/IEEJ/JSAI International Conference on Intelligent Transportation Systems*, pp. 788-793, 1999.
- [10] T. Komine and M. Nakagawa. "Fundamental Analysis for Visible-Light Communication System using LED Lights". *IEEE Trans. on Consumer Electronics*, vol. 50, no. 1, pp. 100-107, 2004.
- [11] E. Chan, D. Koshinz, W. Krug, and H. Hager, "Wireless Optical Links for Avionics Applications", *Proceedings SPIE8026, Photonic Applications for Aerospace, Transportation, and Harsh Environment II*, 80260M, 25 May 2011.
- [12] E. Chan, D. Koshinz, W. Krug, and H. Hager, "Low Cost, High Data Rate White LED (WLED) Transceiver Demonstration", *IEEE Avionics, Fiber-Optics, and Photonics Technology Conference*, pp. 61-62, 30 Sep. - 2 Oct. 2008.
- [13] Airbus, "A380 Aircraft Characteristics Airport and Maintenance Planning", *Airbus SAS, Rev. Dec 01/13*, France.
- [14] IBM, *Made in IBM Labs: Holey Optochip First to Transfer One Trillion Bits of Information per Second Using the Power of Light*, Available: <http://www-03.ibm.com/press/us/en/pressrelease/37095.wss>.
- [15] Intel, *Intel Milestone Confirms Light Beams Can Replace Electronic Signals for Future Computers*, Available: [http://www.intel.com/pressroom/archive/releases/2010/20100727comp\\_sm.htm](http://www.intel.com/pressroom/archive/releases/2010/20100727comp_sm.htm).
- [16] K. -D. Langer and J. Vucic, "Optical Wireless Indoor Networks: Recent Implementation Efforts", *36th European Conference and Exhibition on Optical Communication (ECOC 2010)*, 19-23 September 2010, pp. 1-6.
- [17] K. -D. Langer and J. Grubor, "Recent Developments in Optical Wireless Communications using Infrared and Visible Light", *9th International Conference on Transparent Optical Networks (ICTON 2007)*, 1-5 July 2007, pp. 146-151.
- [18] C. C. Dharmani, *SD/SDHC Card Interfacing with ATmega8/32 (FAT32 implementation)*, Available: <http://www.dharmanitech.com/2009/01/sd-card-interfacing-with-atmega8-fat32.html>.
- [19] G. Pang, K. L. Ho, T. Kwan, and E. Yang, "Visible Light Communication for Audio Systems", *IEEE Trans. on Consumer Electronics*, vol. 45, no. 4, pp. 1112-1118, 1999.
- [20] W. Chen, C. Yu, Y. S. Kwok, and F. Chin, "Video Transmission System based on Visible Light Communication", *2011 International Conference on Information Photonics and Optical Communications (IPOC 2011)*, pp. 1-3, 21-23 Oct 2011.
- [21] J. Rufo, F. Delgado, C. Quintana, A. Perera, J. Rabadan, and R. Perez-Jimenez, "Visible Light Communication Systems for Optical Video Transmission", *Microwave and Optical Technology Letters*, vol. 52, no. 7, pp. 1572-1576, July 2010.
- [22] G. Altunian, *What is Monophonic, Stereophonic, Multichannel and Surround Sound?* (2010). Available: <http://stereos.about.com/od/introductiontostereos/a/soundformats.htm>
- [23] *Sound Systems, Mono versus Stereo*. Available: <http://www.mcsquared.com/mono-stereo.htm>
- [24] R. G. Gupta, *Television Engineering and Video System*, Tata McGraw-Hill, 2006.

- [25] Daycounter, Inc., *Engineering Services*. Available: <http://www.daycounter.com/Filters/Sallen-Key-LP-Calculator.phtml>
- [26] L. C. Png, N. Le Minh, L. Chen, and K. S. Yeo, "Designs of a Free-Space White-LED Mass-Storage Transceiver for SD-Card File Transfer", *IEEE Globecom Workshop 2012: 3rd IEEE Workshop on Optical Wireless Communications (OWC'12)*, 3-7 Dec 2012.
- [27] Open Handset Alliance, Available: <http://www.openhandsetalliance.com>
- [28] National Oceanic and Atmospheric Administration (NOAA). Available: <http://www.tsunami.noaa.gov/>
- [29] B. Truax, *Acoustic Communication*, Greenwood Publishing Group, 2001.
- [30] A. Mehta, "Ultraviolet-Visible (UV-Vis) Spectroscopy - Derivation of Beer-Lambert Law", Apr. 2012.  
Available: <http://pharmaxchange.info/press/2012/04/ultraviolet-visible-uv-vis-spectroscopy-%E2%80%93-derivation-of-beer-lambert-law/>.
- [31] B. Wozniak and J. Dera, *Light Absorption in Sea Water*, Springer, 2007.
- [32] "Research Alert: MIMO Technology", *Datacomm Research Company*, 2005.
- [33] L. B. Zeng, D. C. O'Brien, H. L. Minh, G. E. Faulkner, K. W. Lee, D. W. Jung, Y. J. Oh, and E. T. Won, "High data rate multiple input multiple output (MIMO) optical wireless communications using white-LED lighting", *IEEE Journal in Selected Areas in Communications*, vol. 27, no. 9, pp. 1654-1662, Dec 2009.
- [34] A. H. Azhar, T. A. Tran, and D. C. O'Brien, "Demonstration of high-speed data transmission using MIMO-OFDM visible light communications", *IEEE Globecom 2010 - 1st Workshop on Optical Wireless Communications (OWC'10)*, pp. 1052-1056, 2010.
- [35] K. D. Dambul, D. C. O'Brien, and G. Faulkner, "Indoor optical wireless MIMO system with an imaging receiver", *IEEE Photonics Technology Letters*, vol. 23, no. 2, pp. 97-99, 15 Jan 2011.
- [36] T. Komine, "Visible Light Wireless Communications and its Fundamental Study", *Ph.D. Dissertation*, 2005.
- [37] T. Komine, J. H. Lee, S. Haruyama, and M. Nakagawa, "Adaptive equalization system for visible light wireless communication utilizing multiple white LED lighting equipment", *IEEE Trans. on Wireless Communications*, vol. 8, no. 6, pp. 2892-2900, Jun 2009.
- [38] "Introduction to MIMO: Application Note", *Rohde & Schwarz GmbH & Co. KG*.
- [39] J. R. Barry, *Wireless Infrared Communications*, Kluwer Academic Press, Boston, MA, 1994.
- [40] O. Bouchet, H. Sizun, C. Boisrobert, F. de. Fornel, and P. N. Favennec, *Free-Space Optics Propagation and Communication*, ISTE Ltd, 2006.
- [41] N. Hama, A. Yajima, Y. Yoshida, F. Utsunomiya, J. Kodate, T. Tsukahara, and T. Douseki, "SOI circuit technology for batteryless mobile system with green energy sources," *IEEE Symposium on VLSI Circuits, Digest of Technical Papers (13-15 June 2002)*, pp. 280-283, June 2002.
- [42] Y. Nakamura, T. Nishimura, H. Itoh, and H. Nakashima, "ID-CoBIT: a battery-less information terminal with data upload capability", *The 29th Annual Conference of the IEEE Industrial Electronics Society (IECON '03)*, 2-6 Nov. 2003, vol. 3, pp. 2511-2516, 2003.

- [43] A. B. Sebitosi and P. Pillay, "White LEDS for rural lighting", *Power Engineering Society General Meeting, 13-17 July 2003*, vol. 4, pg. 2623, 2003.
- [44] T. Komine, S. Haruyama, and M. Nakagawa, "Performance evaluation of narrowband OFDM on integrated system of power line communication and visible light wireless communication", *1st International Symposium on Wireless Pervasive Computing, 16-18 Jan. 2006*, pg. 6, 2006.
- [45] T. Komine and M. Nakagawa, "Fundamental analysis for visible-light communication system using LED lights", *IEEE Transactions on Consumer Electronics*, vol. 50, no. 1, pp. 100-107, Feb. 2004.
- [46] C. DeCusatis (editor), *Handbook of Fiber Optic Data Communication*, Academic Press, 2002.
- [47] R. J. Hoss, *Fiber Optic Communications Design Handbook*, Prentice Hall, 1990.
- [48] K. Irie, N. Ohta, M. Morisaki, and H. Tsuji, "Regional PC communication network for residential use supported by fiber-optic access systems", *Proceedings of the 2<sup>nd</sup> International Workshop Community Networking, 'Integrated Multimedia Services to the Home'*, 20-22 June 1995, pp. 9-16, 1995.
- [49] H. Hanrahan, *Network Convergence: Services, Applications, Transport, and Operations Support*, John Wiley & Sons Ltd, 2007.
- [50] R. Wood, *Next-Generation Network Services*, Cisco Press, 2006.
- [51] P. Tomsu and C. Schmutzler, *Next-Generation Optical Networks*, Prentice Hall, 2002.
- [52] S. Kartalopoulos, *DWDM Networks, Devices, and Technology*, IEEE Press and Wiley-InterScience, 2003.
- [53] C. Lam, *Passive Optical Networks*, Academic Press, 2007.
- [54] G. Ellinas and N. Antoniades, *Evolving trends for WDM metro network architectures, The 18th Annual Meeting of the IEEE Lasers and Electro-Optics Society (LEOS'05)*, 22-28 Oct. 2005, pp. 300-301, 2005.
- [55] W. T. Anderson, J. Jackel, G. K. Chang, H. Dai, W. Xin, M. Goodman, C. Allyn, M. Alvarez, O. Clarke, A. Gottlieb, F. Kleytman, J. Morreale, V. Nichols, A. Tzathas, R. Vora, L. Mercer, H. Dardy, E. Renaud, L. Williard, J. Perreault, R. McFarland, and T. Gibbons, "The MONET project - a final report", *Journal of Lightwave Technology*, vol. 18, no. 12, pp. 1988-2009, Dec. 2000.
- [56] Online: <http://mbed.org/cookbook/Ethernet-RJ45>
- [57] Online: <http://electronics.stackexchange.com/questions/27756/why-are-ethernet-rj45-sockets-magnetically-coupled>
- [58] Online: <http://www.es.co.th/Schematic/PDF/HY911103A.PDF>
- [59] A. Eslami, S. Vangala, and H. Pishro-Nik, "Hybrid Channel Codes for Efficient FSO/RF Communication Systems", *IEEE Trans. on Communications*, vol. 58, no. 10, pp. 2926-2938, Oct 2010.
- [60] N. Letzepis, K. D. Nguyen, A. G. i Fabregas, and W. G. Cowley, "Outage Analysis of the Hybrid Free-Space Optical and Radio-Frequency Channel", *IEEE Journal on Selected Areas in Communications*, vol. 27, no. 9, pp. 1709-1719, Dec 2009.
- [61] S. H. Yang and S. K. Han, "VLC based indoor positioning using single-Tx and rotatable single-Rx", *2014 12th International Conference on Optical Internet 2014 (COIN)*, Aug 2014.

- [62] T. Mitsuhiro, "Visible light transmitter, visible light receiver, visible light communication system, and visible light communication method", European Patent (EP2136484 A1), US Patent (20100034540 A1), *Samsung Electronics Co. Ltd*, 2009.
- [63] J. Pederson, "Visible light transceiver glasses", US Patent (8890773 B1), *Federal Law Enforcement Development Services, Inc.*, 2014.
- [64] G. Pang, K. L. Ho, T. Kwan, and E. Yang, "Visible light communication for audio systems", *IEEE Trans. on Consumer Electronics*, vol. 45, no. 4, pp. 1112-1118, 1999.
- [65] W. Chen, C. Yu, Y. S. Kwok, and F. Chin, "Video transmission system based on visible light communication", *2011 International Conference on Information Photonics and Optical Communications (IPOC 2011)*, pp. 1-3, 21-23 Oct 2011.
- [66] T. Matsumura, "10Mbps visible light transmission system", *Nakagawa Laboratories, Inc.*. Available: <https://mentor.ieee.org/802.15/dcn/08/15-08-0171-00-0vlc-10mbps-visible-light-transmission-system.pdf>.
- [67] Z. Ghassemlooy, H. Le Minh, P. A. Haigh, and A. Burton, "Development of visible light communications: emerging technology and integration aspects", *OPTIC 2012 (invited)*, 2012.
- [68] L. Kelion, "Supermarket LED lights talk to smartphone app", <http://www.bbc.com/news/technology-32848763>, Available: <https://youtu.be/uQw-o6bjrec>. May 2015.
- [69] A. Ganick and D. Ryan, "Light Positioning System Using Digital Pulse Recognition", *United States Patent US8248467 B1*, 21 Aug. 2012.
- [70] A. Yoshino, S. Haruyama, and M. Nakagawa, "High-Accuracy Positioning System using Visible LED Lights and Image Sensor", *IEEE 2008 Radio and Wireless Symposium*, pp. 439-442, 22-24 Jan. 2008.
- [71] Y. Chen and H. Kobayashi, "Signal Strength Based Indoor Geolocation", *IEEE International Conference on Communications (ICC '02)*, vol. 1, pp. 436-439, 2002.
- [72] P. Bahl and V. N. Padmanabhan, "RADAR: An In-Building RF-based User Location and Tracking System", *The 19th Annual Joint Conference of the IEEE Computer and Communications Societies (INFOCOM '00)*, vol. 2, pp. 775-784, March 2000.
- [73] K. Dividis, "Design and Prototyping of a Visible Light Indoor Positioning System", *Philips Research Eindhoven (Technical Note TN-2007-00115)*, 2007.
- [74] T. Komine, "Visible Light Wireless Communications and Its Fundamental Study", *PhD Dissertation*, 2005.
- [75] N. Kumar and N. R. Lourenco, "LED-based Visible Light Communication System: A Brief Survey and Investigation", *Journal of Engineering and Applied Sciences*, vol. 5, no. 4, pp. 296-307, 2010.
- [76] O. Bouchet, H. Sizun, C. Boisrobert, F. de Fornel, P-N. Favennec, "Free-Space Optics Propagation and Communication", *ISTE Ltd*, 2006.
- [77] A. Sebastian, *extremetech.com*, Available: <http://www.extremetech.com/computing/121587-ibm-creates-cheap-standard-cmos-1tbps-holey-optochip>, March 2012.
- [78] M. Kavehrad, "Sustainable Energy-Efficient Wireless Applications using Light", *IEEE Communications Magazine*, vol. 48, no. 12, pp. 66-73, December 2010.

- [79] I. E. Lee, Z. Ghassemlooy, W. P. Ng, V. Gourdel, M. A. Khalighi, S. Zvanovec, and M. Ulysal, “Practical Implementation and Performance Study of a Hard-Switched Hybrid FSO/RF Link under Controlled Fog Environment”, *9<sup>th</sup> International Symposium on Communication Systems, Networks and Digital Signal, (CSNDSP 2014)*, pp. 368-373, 2014.
- [80] F. Nadeem, B. Flecker, E. Leitgeb, M. S. Awan, and T. Javornik, “Comparing the fog effects on hybrid network using optical wireless and GHz links”, *Proc. Int. Symp. Commun. Sys. Networks and Digital Signal*, pp. 278282., June 2008.
- [81] H. Wu, B. Hamzeh, and M. Kavehrad, “Achieving carrier class availability of FSO link via complementary RF link”, *Proc. 38th Asilomar Conf. Signals, Systems and Computers*, Oct. 2004.
- [82] Z. Jia, F. Ao, and Q. Zhu, “BER performance of the hybrid FSO/RFattenuation system”, *Int. Symp. Anten., Prop. & EM Theory*, Sep. 2006.
- [83] T. Kamalakis, I. Neokosmidis, A. Tsipouras, S. Pantazis, and I. Andrikopolous, “Hybrid free space optical / millimeter wave outdoor linksfor broadband wireless access networks”, *Proc. Int. Symp. Personal, Indoor and Mobile Radio Commun.*, Aug. 2007.
- [84] S. Vangala and H. Pishro-Nik, “A highly reliable FSO/RF communication system using efficient codes”, *Proc. IEEE Global Commun.Conf.*, 2007.
- [85] H. Wu, B. Hamzeh, and M. Kavehrad, “Availability of airbourne hybrid FSO/RF links”, *Proc. SPIE, 2005*, vol. 5819, 2005.
- [86] T. M. Cover and J. A. Thomas, “Elements of Information Theory”, *Wiley Series in Telecommunications*, 1991.
- [87] L. Zeng, D. C. O’Brien, H. Le Minh, G. E. Faulkner, K. W. Lee, D. W. Jung, Y. J. Oh, and E. T. Won, “High Data Rate Multiple Input Multiple Output (MIMO) Optical Wireless Communications using White LED Lighting”, *IEEE Journal on Selected Areas in Communications*, vol. 27, no. 9, pp. 1654 - 1662, Dec 2009.
- [88] L. B. Zeng, D. O’Brien, H. Le-Minh, K. W. Lee, D. W. Jung, and Y. J. Oh, “Improvement of Data Rate by using Equalization in an Indoor Visible Light Communication System”, *4<sup>th</sup> IEEE International Conference on Circuits and Systems for Communications (ICCS 2008)*, pp. 678-682, 26-28 May 2008.
- [89] V. Jungnickel, V. Pohl, S. Nonnig, and C. von Helmont, “A physical model of the wireless infrared communication channel”, *IEEE Journal on Selected Areas in Communications*, vol. 20, no. 3, pp. 631-640, Apr. 2002.
- [90] D. Tse and P. Viswanath, *Fundamentals of Wireless Communication*, New York, USA: Cambridge University Press, 2005.
- [91] D. C. Cox, R. R. Murray, and A. W. Norris, “Measurements of 800MHz Radio Transmission into Buildings with Metallic Walls”, *Bell Systems Technical Journal*, vol. 62, no. 9, pp. 2695-2717, Nov. 1983.
- [92] S. E. Alexander, “Radio Propagation within Buildings at 900MHz”, *Electronics Letters*, vol. 18, no. 21, pp. 913-914, 1982.
- [93] T. S. Rappaport, “Wireless Communications: Principles and Practice”, *Prentice Hall*, 1996.
- [94] P. Pechac and M. Klepal, “Empirical models for indoor propagation in CTU Prague Buildings”, *Radioengineering*, vol. 9, no. 1, pp. 31-36, Apr. 2000.

- [95] Y. S. Cho, J. Kim, W. Y. Yang, and C. G. Kang, "MIMO-OFDM Wireless Communications with MATLAB", *John Wiley & Sons and IEEE Press*, 2010.
- [96] IEEE (1996), "Tentative Criteria for Comparison of Modulation Methods", P802.11-97/96.
- [97] B. Cizdziel, "Building Path Loss NS-3 and MATLAB Model", University of Washington. Available: <http://students.washington.edu/cizdziel/>
- [98] F. A. Gomez, "The Future of Microfluidic Point-of-Care Diagnostic Devices", *Bioanalysis*, 5(1), pp. 1-3, 2013.
- [99] B. K. Singh and A. C. Hillier, "Surface Plasmon Resonance Enhanced Transmission of Light through Gold-Coated Diffraction Gratings", *Anal. Chem.*, 80, pp. 3803-3810, 2008.
- [100] W. H. Yeh, J. W. Petefish, and A. C. Hillier, "Diffraction-Based Tracking of Surface Plasmon Resonance Enhanced Transmission through a Gold-Coated Grating", *Anal. Chem.*, 83, pp. 6047-6053, 2011.
- [101] P. Kamath C., R. Bhat P, and J. E. Packiyam, "Synthesis of silver nanoparticles from leaf extracts of Wedelia Chinensis (Osbeck) Merrill and Their Antimicrobial Activity", *J. Microbiol. Biotech. Res.*, 3(5), pp. 48053, 2013.
- [102] Available: <http://www.gamonline.com/catalog/uvfilter/UV-protection.php>
- [103] S. J. Tavener and J. E. Thomas-Oates, "Build Your Own Spectrometer", *Education in Chemistry*, pp. 151-154, Sep 2007.
- [104] J. M. Schurr, "Interaction of Light-Pulses with Matter - 1. Derivation of Beer-Lambert Law", *Chemical Physics*, vol. 15, no. 1, pp.1-13, 1976.
- [105] X. Mao and T. J. Huang, "Microfluidic Diagnostic for the Developing World", *Lab Chip*, 12, pp. 1412-1416, 2012.

**With Egg White****Clean: No Egg White**

**Figure 14.7** Spectrometer readings for %R vs. wavelength for BD-RE disc for egg white.

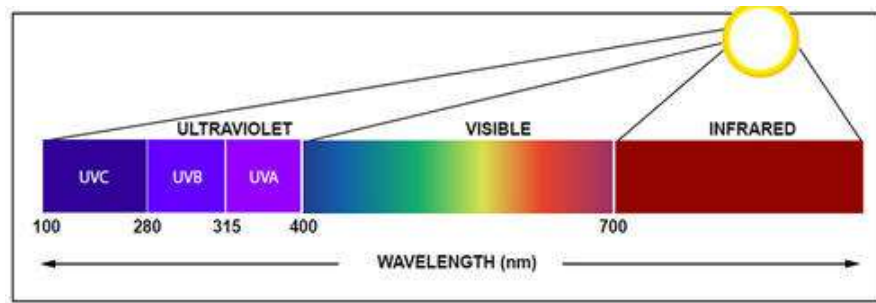


**Figure 14.8** Different parts of the UV spectrum [102]. Notice that only UV-A is applicable to the conventional DVD-R disc.

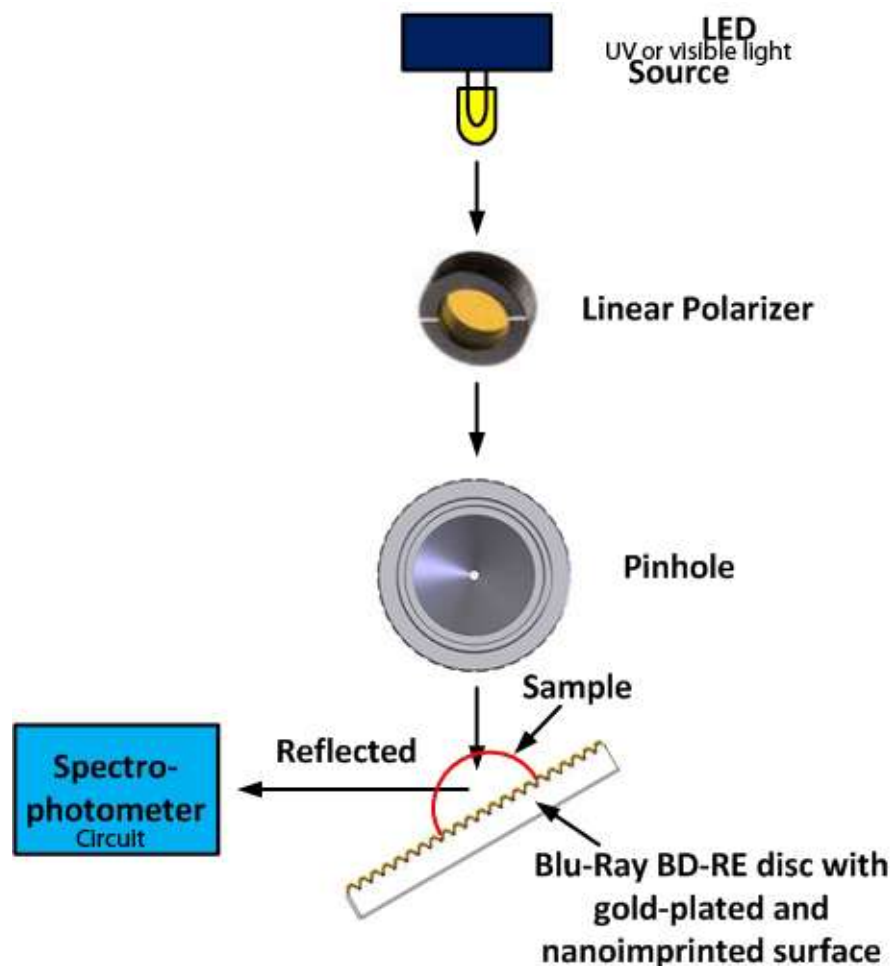


**Figure 14.9** Conceptual design of a compact SPR photometer.

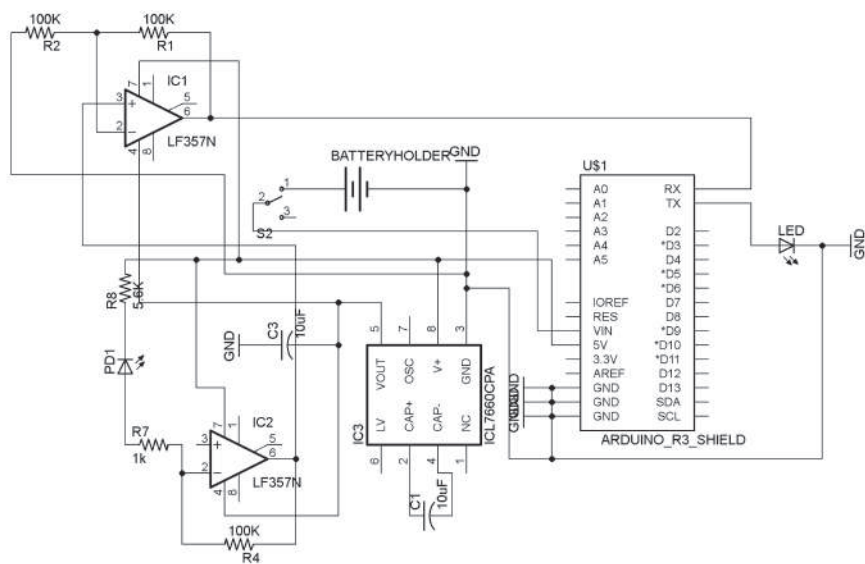


**Figure 14.10** Schematic diagram of the spectrophotometer optical receiver.

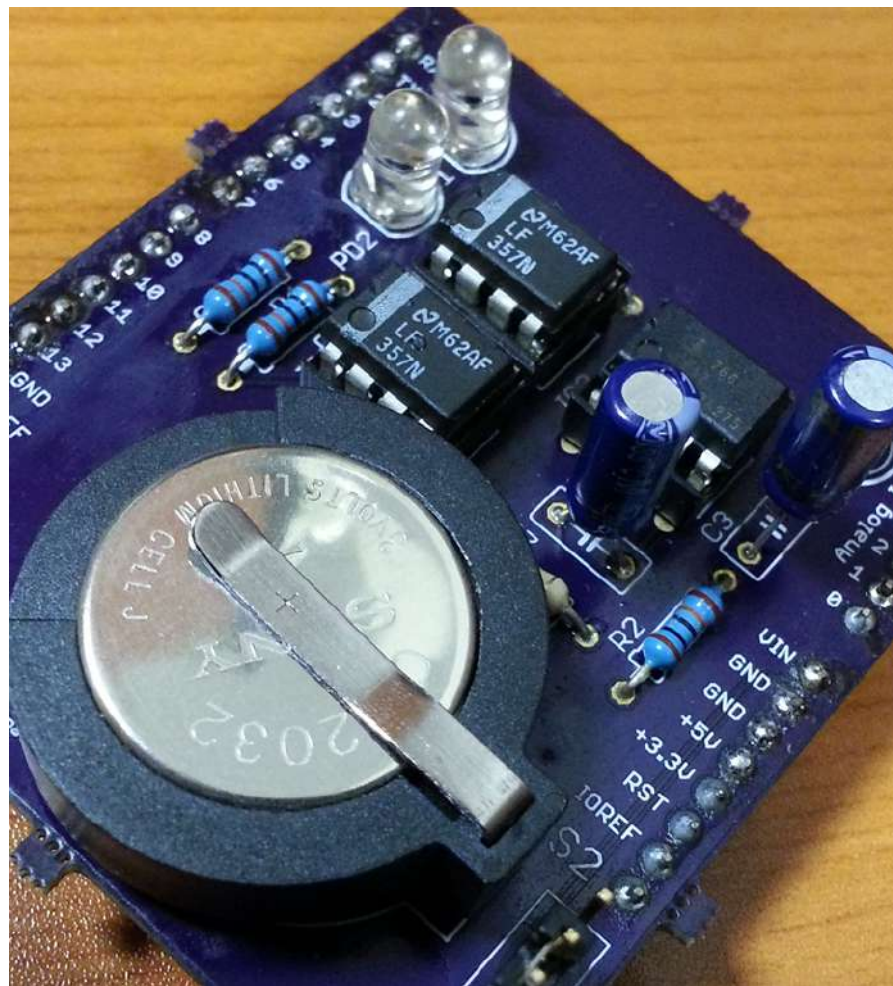


**Figure 14.11** Photograph of the spectrophotometer optical receiver 1. The board is Arduino mountable.

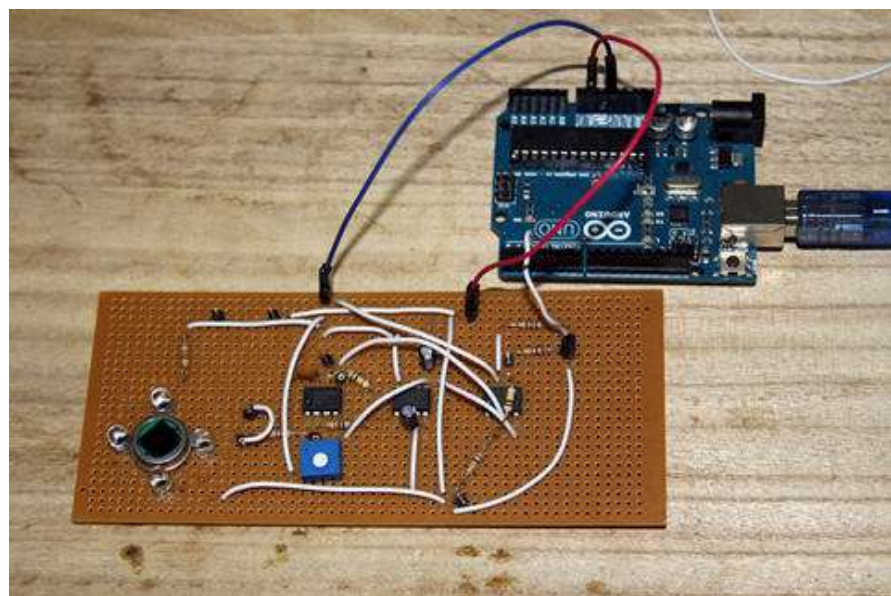


**Figure 14.12** Photograph of the spectrophotometer optical receiver 2.

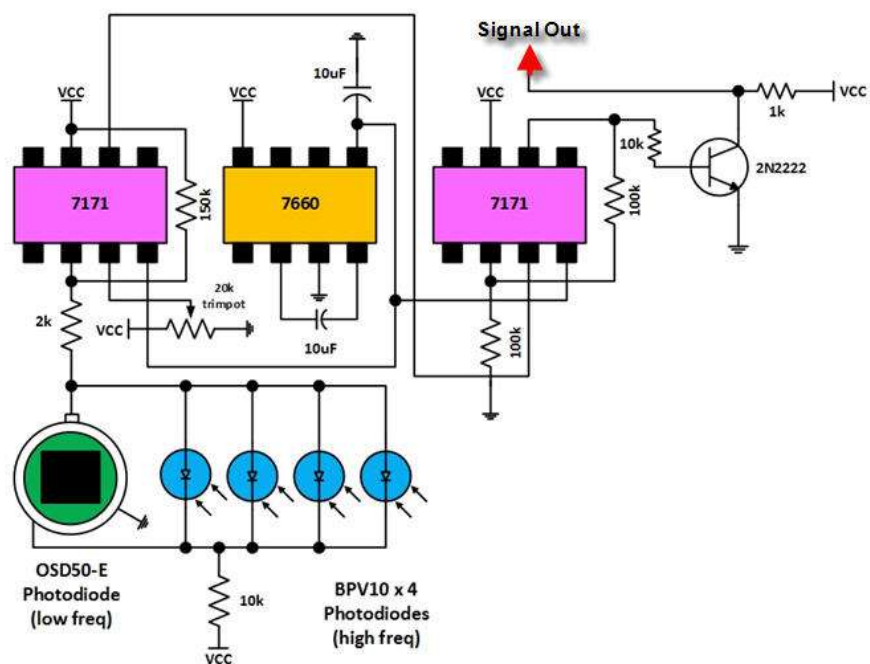


Figure 14.13 Schematic of the spectrophotometer optical receiver 2.